Leibniz-Institut
für Festkörper- und
Werkstoffforschung
Dresden

Annual Report 2010

Contents

Flashback to 2010

The Annual Report of the IFW intends to give an impression of what we consider an overall successful year of the institute's research activities. It addresses our cooperation partners worldwide, friends and all those who are interested in the institute's life and progress within the international materials science community. It presents a cross section of our scientific activities in the past year, highlighting main results in the first part and giving a somewhat more systematic overview of results obtained in our five Research Areas in its second part. It finally informs on the materialized and personalized output and activities, and on how the IFW is organized.

The very first pages of the Annual Report we want to use for a flashback to the institute's life in 2010: highlights, events and important developments beyond scientific results.

In 2010 we hoped to start the construction of the new annex building which will alleviate the severe shortage of office space in our institute. With large efforts we achieved at least the decisive mile stone in that direction: the grant of the building permission in October 2010. Now, we are looking forward to the start of construction and the appearance of the first excavators in spring 2011. Some other infrastructure projects came to a successful completion in 2010: The Helium liquefaction facility that makes the supply of liquid Helium independent from external influences was inaugurated and successfully put into operation in January 2010. In September 2010, we established a room of silence – named Silentium – which is a place for contemplation, meditation and prayer for all members of the IFW regardless of their confession and nationality.

A further successful infrastructure project was the creation of the IFW Chemnitz research site which is going to strengthen the cooperation with the Chemnitz University of Technology, where Prof. Dr. Oliver G. Schmidt holds a chair. We rent a 260 square meter laboratory area in a start-up building of the Chemnitz "Smart Systems Campus" and have equipped it for the development of 3D rolled-up nanomembranes. Since the official inauguration ceremony in October 2010, the cooperation with the Chemnitz University of Technology received a fresh impetus by a number

The State Minister of Science and Fine Arts, Prof. Sabine von Schorlemer, visited the IFW on the occasion of the Annual reception on March 1, 2010

Participants of the "Junior Doctor" event in the IFW

Inauguration ceremony of the IFW Research Site Chemnitz

of joint projects such as the "Center of Excellence for Nanosystem Integration" granted by the German Government and the International Graduate College "Materials and Concepts for Advanced Interconnects and Nanosystems" with the TU Chemnitz and Fudan University Shanghai.

In a similar way the relation between the IFW and the TU Bergakademie Freiberg has been reinforced. In March 2010, an agreement of cooperation between both institutions was signed on the basis of which two group leaders of the IFW were appointed as guest professors in December. Important links to the TU Bergakademie Freiberg are joint projects such as the Excellence cluster "Functional structure design of new high performance materials via atomic design and defect engineering" and the new DFG Research Group on "Molecular Spintronics" with all four Saxon universities (TU Dresden, TU Chemnitz, Leipzig University and TU Bergakademie Freiberg).

Despite the expanded regional networking with the Saxon universities, our main partner in this respect remains the neighboring TU Dresden. In 2010, this close relationship was characterized by large joint efforts to succeed in the second round of the German Universities Excellence Initiative of the German Federal Ministry of Education and Research and the German Research Foundation. The IFW has been strongly involved in the creation of the DRESDEN concept, DRESDEN standing for "Dresden Research and Education Synergies for the Development of Excellence and Novelty". Together with all partners in the DRESDEN concept, we believe in the abilities of this network to succeed also in the third line of funding – namely the institutional strategies required to promote top-level university research, the so-called future concepts.

The training of students and young scientists remains a very important concern of the IFW work. PhD and diploma students are involved in nearly all scientific projects and in the resulting publications. The number of PhD students working at the Institute has increased in the last two years to about 150 on average. Also the number of diploma and master students working for their theses at the IFW has increased significantly during the last years resulting in the record number of 52 diploma or master theses in 2010 which is more than twice as many as in 2009.

Bottling of the first Helium liquefied in our own facility

Getting certified as family friendly institution

Sketch of the new room of silence – the Silentium

As a Leibniz Institute the IFW is budgeted by the federal government and the German federal states in equal parts. However, an important index of quality is the amount of third party project funding, which, in 2010, amounts to 13.4 Mio. Euro – a level at the forefront of the Leibniz Association. Most of this project funding was acquired in a highly competitive mode from the DFG and the EU. In particular the grants of three Emmy Noether Research Groups by the DFG show the competitive capability of the IFW. Further successes in this respect are the start of the new DFG Priority Programs on Fe-pnictides and of the EU network on biocompatible Ti-based structures for orthopaedics, both coordinated by the IFW. As in the previous years the IFW is very successful in initiating EU projects and participating in them. Seven of our 12 EU projects running in 2011 are coordinated by the IFW. Concerning the "Pakt für Forschung" the IFW was also successful with its new project application on "Nano-scaled structures for electrochemical energy storage in autonomous Microsystems". It turns out that the IFW as the only institute in the Leibniz Association has got granted all six projects applications since the beginning of the "Pakt für Forschung" in 2006.

A crucial part of the IFW's identity is its vivid life including the cultivation of the scientific dialogue, family-friendly working conditions and the support of sportive, creative and cultural activities. In 2010 the IFW was re-audited as a family-friendly institution and received the certificate "berufundfamilie". The IFW organizes a series of workshops, colloquia and talks to foster the scientific dialogue and, along the way, allow for social and communication aspects of cooperation. An important meeting for all scientists of the IFW is the yearly two-day program session where all scientists discuss and adjust the research program for the following year. Also the annual IFW Winter School contributes to the scientific communication among all IFW groups and to the training of young scientists in special topics of the IFW research program. In 2010 the topical focus was placed on superconductivity.

The IFW continued its large efforts to make scientific work accessible for the general public and to inspire young people to study science or engineering also in 2010. The IFW took part in many joint actions like the lecture series "Physics on Saturday" or the Summer University of the TU Dresden. The Dresden Long Night of Sciences took place for the eighth time in 2010, and again,

Dr. Jens Freudenberger was awarded the Georg Sachs Prize of the German Society of Material Science

The apprentices of the IFW after a workshop on conflict mamagement

Autumn school for high school girls organized by the IFW for the third time



the IFW offered an ample program which attracted almost 6000 visitors. The greatest attraction in the IFW's program seemed to be the special offers "Chemistry for kids" and "Physics for kids" where the girls and boys could try experiments on their own. An equally large respond of young people as well as of their parents and grandparents was met in the one week event "Science in the shopping center" in advance of the conference of the German Association for the Advancement of Science and Medicine (GDNÄ) in September 2010 in Dresden. In October 2010 we organized the third autumn school for high school girls who wanted to experience scientific work in a research institute at first hand. Besides these big events we organize almost weekly lab-tours for various visitor groups, from school classes through official representatives to guests from foreign organizations.

So we are looking back to a successful year 2010 in the institute's development. We are quite aware that this is due to the sustainable network of colleagues and partners in universities, research institutes and industry, both, on the regional and the international scale. We thank all of them for their constructive cooperation and are looking forward to taking up future challenges together. Special tribute is paid to the members of the Scientific Advisory Board and of the Board of Trustees as well as the funding organizations that continuously support and foster the positive development of the IFW.

Dresden, January 2011

Prof. Dr. Ludwig Schultz
Scientific Director

Dr. h. c. Rolf Pfrengle
Administrative Director

Young visitors of the Dresden Long Night of Sciences

Signing the agreement of cooperation with the TU Bergakademie Freiberg

Best volley ball teams during IFW Summer day

Highlights 2010

Rolled-up nanomembrans form an ultra-compact energy storage element

Born-Oppenheimer molecular dynamics trajectory of $TiSc_2N@C_{80}$

Lorentz trajectories of the conduction electrons in real space for large mean free paths

Cross-section of a MgB_2 superconducting wire with Nb-sheathed filaments

Highlights

Superconductivity without nesting in LiFeAs iron pnictide

S.V. Borisenko, V. B. Zabolotnyy, D. V. Evtushinsky, T. K. Kim, I. V. Morozov,
A. A. Kordyuk, G. Behr, B. Büchner

The particular shape of the Fermi surface can give rise to a number of collective quantum phenomena in solids, such as density wave orderings or even superconductivity. In many new iron superconductors this shape, the "nested" Fermi surface, is indeed observed, but its role in the formation of spin-density waves or superconductivity is not clear. We have studied the electronic structure of the non-magnetic LiFeAs ($T_c \sim 18$ K) superconductor using angle-resolved photoemission spectroscopy. We find a notable absence of the Fermi surface nesting, strong renormalization of the conduction bands by a factor of three, high density of states at the Fermi level caused by a Van Hove singularity, and no evidence for either a static or fluctuating order except superconductivity with in-plane isotropic energy gaps. Our observations set a new hierarchy of the electronic properties necessary for the superconductivity in iron pnictides and, possibly, in other materials.

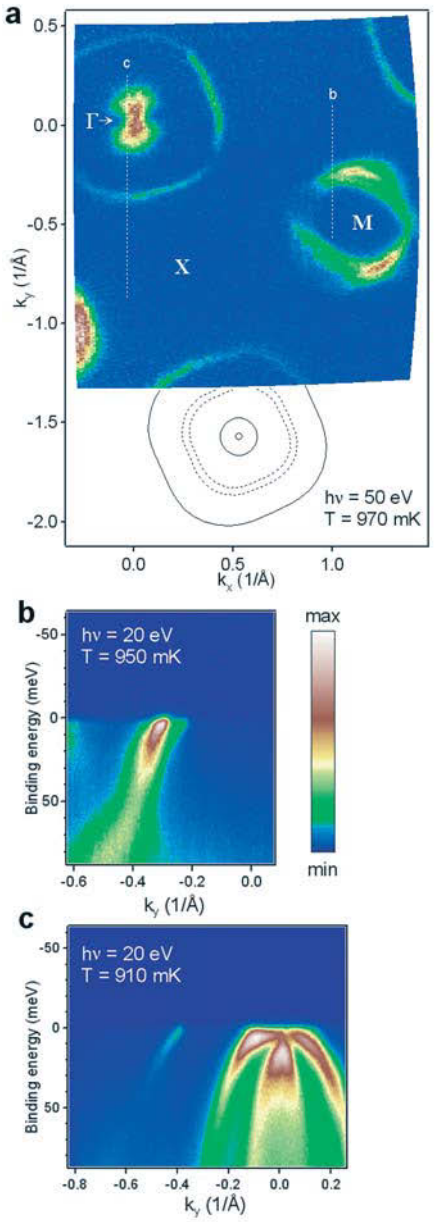

Fig. 1: Fermi surface shape and topology. **a)** Momentum distribution map of the photoemission intensity integrated within 5 meV around the Fermi level. Solid black lines represent Γ-centered Fermi contours, black dashed lines – most pronounced M-centered Fermi contours. **b,c)** Momentum-energy cuts along the vertical directions marked by the white dashed lines in panel a).

The synthesis of another iron superconductor immediately attracted a considerable attention already for several reasons [1-3]. LiFeAs is one of the few superconductors which do not require additional charge carriers and has a considerable T_c approaching the boiling point of hydrogen. Similar to $AeFe_2As_2$ (122) and LnOFeAs (1111) parent compounds, LiFeAs consists of nearly identical $(Fe_2As_2)^{2-}$ structural units and all three are isoelectronic, though the former do not superconduct. The band structure calculations unanimously yield the same shapes of the Fermi surfaces (FS), very similar densities of states and low energy electronic dispersions [4, 5] and even find in LiFeAs an energetically favorable magnetic solution which exactly corresponds to the famous stripe-like antiferromagnetic order in 122 and 1111 systems [5-7], though the experiments show rather different picture. The structural transition peculiar to 122 and 1111 families is remarkably absent in LiFeAs and is not observed under applied pressure of up to 20 GPa [8, 9]. Resistivity and susceptibility as well as μ-spin rotation experiments show no evidence for the magnetic transition [10, 11]. The basic question is therefore why the isoelectronic and nearly isostructural FeAs blocks induce fundamentally different physical properties of the material? We show that this happens due to the important distinctions of the electronic structure and single out those which seem to be indispensable for the superconductivity to occur.

In Fig.1a we show the FS map of LiFeAs which is the momentum distribution of the photoemission intensity integrated within the narrow energy interval around the Fermi level. Three clear features are visible on the map: a high-intensity butterfly-like shape at the Γ-point, a well defined barrel-like FS also centred at Γ, and a double-walled structure with somewhat obscure contours around M-point. Momentum-energy cuts along the selected directions passing near M and Γ points and marked in panel a) by dashed lines are presented in Fig.1b and Fig.1c. While both dispersive features in Fig.1b as well as the left-most one in Fig.1c clearly cross the Fermi level thus supporting a double-walled electron-like FS around M and large hole-like FS around Γ respectively, the other two features from Fig.1c only come close to the Fermi level without clear crossing, at least for the given cut through the momentum space. We have found that for certain excitation energies these features do cross the Fermi level resulting in very small hole-like FSs thus completing the analogy with the FS topolgy of 122 and 1111 systems: there are in total five FSs supported by five bands. The sketch in Fig.1a schematically shows all FS features centered in one point to facilitate the comparison of their sizes. The striking peculiarity of this FS shape is the absolute absence of the (π, π)-nesting peculiar to other pnictides.

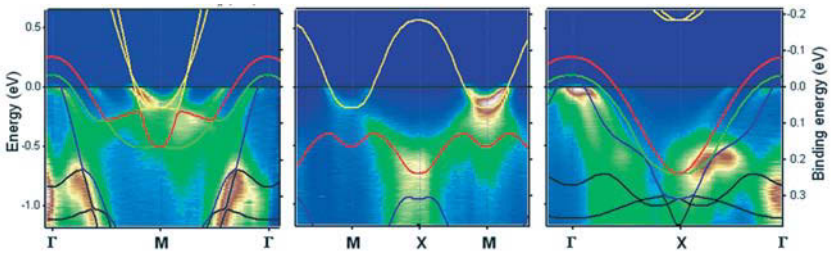

Fig. 2: High-symmetry momentum-energy cuts together with the results of the band structure calculations. Blue, green and red curves are the bands supporting the Γ-centred FSs. Yellow curves – the bands responsible for the electron-like FSs. Black curves – the bands which do not cross the Fermi level. Photon energy is 120 eV for the middle panel and 70 eV for the left and right panels.

According to the band structure calculations the FS of LiFeAs also consists of three hole-like FSs around the Γ-point and two electron-like ones at the corner of the Brillouin zone. In Fig.2 we compare directly the calculated band structure and experimental data along the high-symmetry directions. We made a tight-binding fit to the best defined experimental band which supports the large Γ-barrel and found a remarkable qualitative agreement with the $d_{x^2-y^2}$ originated band from the LDA calculations. The ratio of the bandwidths turned out to be equal to 3.1 (1 eV vs. 0.326 eV). We then applied this renormalization factor to bring the experimental data and the calculated bands to the same energy scale. Overall agreement is very reasonable, taking into account that we have identified all bands in the vicinity of the Fermi level and associated them with the corresponding features in the ARPES spectra. Note that the electron-like pocket at M formed by another band is satisfactorily reproduced as well. As seen from the figure and confirmed by the calculations, a selective shift of the $d_{x^2-y^2}$ band (red curve in Fig. 2) by 150 meV with respect to the others perfectly reproduces the shape of the experimental Fermi surface and dispersion over the whole bandwidth.

This agreement together with the extremely low temperatures at which we carried out our experiments clearly speaks in favor of a non-magnetic ground state realized in LiFeAs. This is supported by the fact that having explored the large portions of the k-space at different experimental conditions, we have not found any typical spectroscopic signatures of commensurate or incommesurate ordering appearing in a form of replica due to Fermi surface reconstruction or suppressed spectral weight due to gap, etc. [12, 13]. What is not captured by the LDA approach, which predicts magnetism in LiFeAs [5, 6], are the actual absence of nesting and renormalization by the factor of ~3. The energy gain from the opening of the gaps at or near the Fermi level due to the FS reconstruction is obviously more significant in a system with 3 times narrower bandwidth. That is probably why the SDW order does not disappear immediately upon doping in 122 and 1111 families of Fe-pnictides. In LiFeAs, where the (π, π)-nesting is absent, static magnetism disappears completely. Our results thus strongly imply the decisive role of nesting in the formation of SDW.

The apparent absence of the magnetism in LiFeAs seems to be not crucial for the superconductivity. We have clearly observed the opening of the superconducting gap in all k_F points with the onset at the nominal T_c of ~18 K. A typical example is presented in Fig. 3a where the crossing of the FS at point A is shown for two temperatures, above and below the transition. Upon entering the superconducting state, the usual BCS-like bending back of the dispersive feature is apparently seen in the lower panel. This is accompanied by the depletion of the spectral weight at the Fermi level with concomitant shift of the leading edge midpoint of the k_F-EDC as seen in Fig. 3b and in zoomed version in Fig. 3c. The typical size of the superconducting gap of the hole-like FSs is estimated to be ~1.5–2.5 meV, while for the electron-like FSs we observed slightly larger values of ~2–3.5 meV implying a multiband superconductivity in LiFeAs. More rigorous estimates based on accurate fitting including the resolution contribution result in the superconducting gap of 3.2 meV on the electron-like pockets.

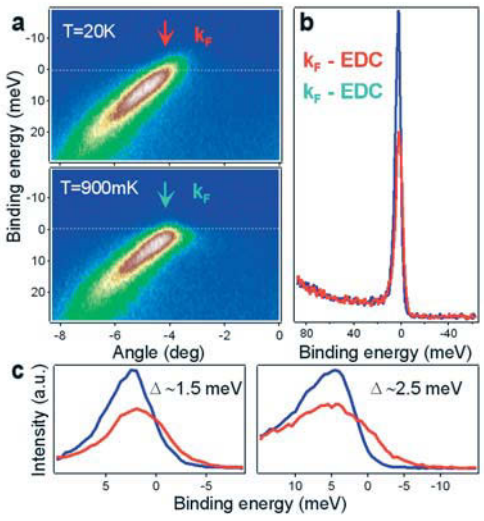

Fig. 3: Superconductivity in LiFeAs. **a)** Fermi surface crossings of the largest hole-like FS (see Fig.1c) taken above and below T_c (~18K). **b)** Energy distribution curves from panels a) corresponding to the k_F. **c)** Energy distribution curves corresponding to Fermi momenta on the largest hole-like electron-like FS measured above (20 K) and below (900 mK) T_c.

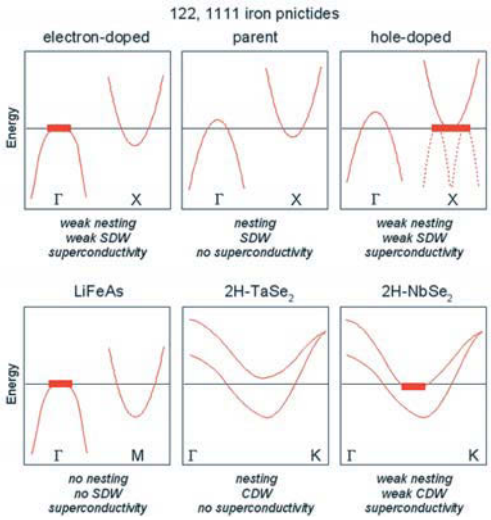

Fig. 4: Van Hove singularities in Fe-pnictides and chalcogenides. Schematic illustration of the main features in the electronic structure of the 122 and 1111 pnictides, LiFeAs, 2H-$TaSe_2$ and 2H-$NbSe_2$. Red curves represent the band dispersions along the high-symmetry directions. Thick red lines represent Van Hove sigularities, i.e. the flat extrema of the corresponding bands or the saddle point.

Disregarding for a moment any relation to other families of Fe-pnictides and thus possible presence of the so far not detected spin fluctuations capable of binding electrons in pairs [14], one may ask why a stoichiometric, nonmagnetic compound with a plane crystal structure is a multiband superconductor with considerable critical temperature and weakly in-plane anisotropic order parameter? The only remarkable property of the electronic structure of LiFeAs which makes it so special and intimately connects it to other superconductors like $NbSe_2$, A15 compounds, MgB_2 and the cuprates is the proximity of the Van Hove singularity to the Fermi level.

In Fig. 4 we suggest a very simple scenario which emphasizes the role of nesting for density wave orders and van Hove singularities for the superconductivity in pnictides and 2H-$NbSe_2$. In the parent compounds and in 2H-$TaSe_2$ the presence of the nesting reconstructs the original Fermi surface and induces the static density wave order resulting in the absence of the superconductivity (or its strong suppression). By doping the holes into the parent pnictide (or substituting Ta by Nb) we destroy the nesting and approach the bottoms of the electronlike bands (or saddle point in 2H-$NbSe_2$) thus bringing high density of states to the Fermi level. As a consequence, the density wave order is strongly suppressed and superconductivity occurs. The same holds for the electron-doped side of the phase diagram. Now the tops of the holelike bands show up at the Fermi level. In this sense LiFeAs appears to be similar to electron-doped pnictides since in this case the top of the holelike band coincides with the Fermi level already in the pristine compound.

The example of LiFeAs suggests that the intriguing presence of the density waves or their fluctuations in many families of the superconductors may turn out to be rather "technical": they neighbour the superconductivity only because, purely from the topological considerations, the nesting is very probable to occur when tuning the system from one Van Hove instability to another by doping in multiband superconductors (see Fig. 4). On the other hand, the non-perfect nesting corresponding to the fading density wave order may result in still larger density of states at the Fermi level thus promoting the superconductivity [15]. However, in view of our present results, the Van Hove singularity close to the Fermi level seems to be a necessary condition for the onset of superconductivity, and not only in the pnictides [16].

[1] X. C. Wang *et al., Solid State Commun.* **148**, 538 (2008).
[2] J. H. Tapp *et al., Phys. Rev.* B **78**, 060505(R) (2008).
[3] M. J. Pitcher *et al., Chem. Comm.* **2008**, 5918 (2008).
[4] I. A. Nekrasov *et al., JETP Lett.* **88**, 621 (2008).
[5] D. J. Singh, *Phys. Rev. B* **78**, 094511 (2008).
[6] Y. F. Li et al., *Eur. Phys. J. B* **72**, 153 (2009).
[7] R. A. Jishi and H. M. Alyahyaei *Advances in Condensed Matter Physics* Volume 2010, Article ID 804343.
[8] S. J. Zhang *et al., Phys. Rev. B* **80**, 014506 (2009).
[9] M. Gooch *et al., EPL* **85**, 27005 (2009).
[10] F. L. Pratt *et al., Phys. Rev. B* **79**, 052508 (2009).
[11] C. W. Chu *et al., Physica C* **469**, 326–331 (2009).
[12] S. V. Borisenko *et al., Phys. Rev. Lett.* **100**, 196402 (2008).
[13] V. B. Zabolotnyy *et al., Europhys. Lett.* **86**, 47005 (2009).
[14] T. Dahm *et al., Nature Physics* **5**, 217 (2009).
[15] V. B. Zabolotnyy *et al., Nature* **457**, 569-572 (2009).
[16] S. V. Borisenko et al., *Phys. Rev. Lett.* **105**, 067002 (2010).

Cooperation: MPI for Solid State Research Stuttgart, Moscow State Univ., Helmholtz-Zentrum Berlin
Funding: DFG (KN393/4, BO 1912/2-1, SPP1458)

Coherent interfacial bonding on the FeAs tetrahedron in epitaxial Fe/Ba-122 bilayers

T. Thersleff, K. Iida, S. Haindl, S. Trommler, M. Kidszun, R. Hühne, F. Kurth, I. Lucas del Pozo, J. Hänisch, D. Pohl, A. Hartmann, I. Mönch, J. Engelmann, J. Scheiter, B. Rellinghaus, L. Schultz, and B. Holzapfel

The production of thin films from the newly-discovered iron-based superconductors is critical to their assessment for applications and the investigation of their fundamental properties. A detailed microstructural investigation of $Ba(Fe_{1-x}Co_x)_2As_2$ thin films fabricated at the IFW suggested that one way to achieve high quality films is through the use of an intermediate iron buffer layer. Films based on this new layer architecture, dubbed "Fe/Ba-122 bilayers," exhibit excellent crystalline and electrical transport properties and additionally open up the route for novel thin film devices potentially suitable for all iron-based superconductors.

Essential to the understanding of key fundamental properties in the newly discovered iron-based superconductors and critical to their assessment for applications and devices is their fabrication into very high quality thin films. Thin films of the $Ba(Fe_{1-x}Co_x)_2As_2$ phase – discovered by Sefat et al. [1] and commonly referred to as "Ba-122"– are particularly interesting since this compound appears to be resilient against oxidation and degradation due to water vapor [2], it is considerably easier to deposit compared to other iron-based superconductors, and it has a relatively high critical temperature. The search for optimal thin film growth parameters for this compound is currently the subject of a number of international research groups. [2–11]. However, difficulties overcoming the poor metal/oxide bond at the interface of many substrates has necessitated the need for significant optimization of the deposition parameters [9,10] as well as the use of various intermediate layers [8] to produce well-textured films. In spite of these efforts, nearly all of these films contain an unintentional amorphous or iron-containing layer at the interface. While the nature of this interface is not yet fully understood, the disruption of local crystallographic ordering associated with it precludes the use of these films for interface-sensitive applications such as multilayers or heterostructures where coherent and chemically inert phase boundaries are required. Moreover, it may be responsible for the challenging growth of epitaxial $Ba(Fe_{1-x}Co_x)_2As_2$ (Ba–122) films in general [7,9] as well as the generation of pinning-active columnar defects observed to originate at this interface in some films [8].

At the IFW, a detailed investigation into the nature of this interface was initiated using the FEI Titan^3 300 kV C_s-corrected transmission electron microscope (TEM) available in-house. This microscope has a point resolution under 1 Å and provides access to a number of high resolution spectroscopic techniques. For Ba-122 deposited on top of bare $(La,Sr)(Al,Ta)O_3$ (LSAT) substrates, it was observed that significant amounts of textured body-centered cubic iron precipitate out at the substrate/film interface [9]. The formation of these iron regions is enabled by the interdiffusion of atomic species between the Ba-122 phase and the oxide substrate, thereby leading to the aforementioned localized

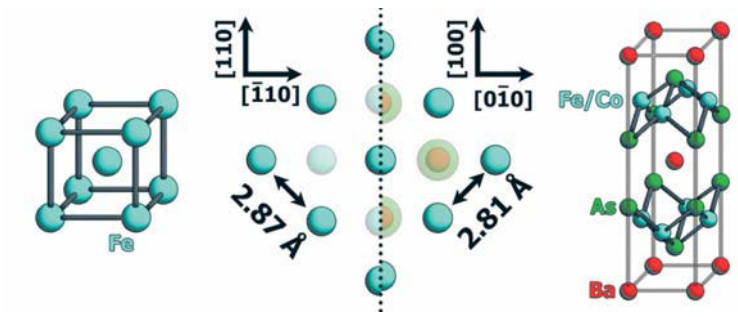

Fig. 1: Schematic model demonstrating that the mismatch between the (001) surface plane of bcc iron (left) and the iron sublayer in the Co-doped Ba–122 unit cell (right) is about 2%. Atomic radii are not to scale.

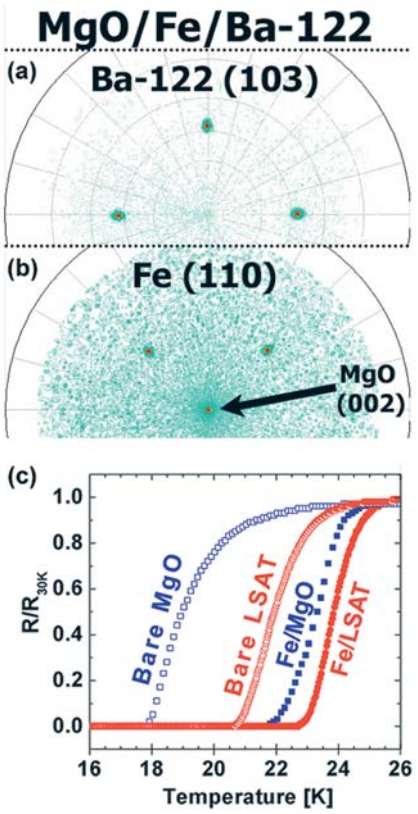

Fig 2: (a) Pole figure of the Ba-122 bilayer grown on an MgO substrate revealing highly textured growth with a $\Delta\varphi$ value of 0.95°. **(b)** Iron grows with a 45° in-plane rotation and exhibits four-fold symmetry. The additional peak in the center arises from the (002) plane of the MgO substrate. Both pole figures are plotted on a square root scale. **(c)** Resistively measured T_c curves for Ba–122 deposited upon bare LSAT and MgO as well as the Fe/Ba–122 bilayers. $T_{c,90}$ is 24.4 K and 24.8 K for the MgO and LSAT bilayers, respectively.

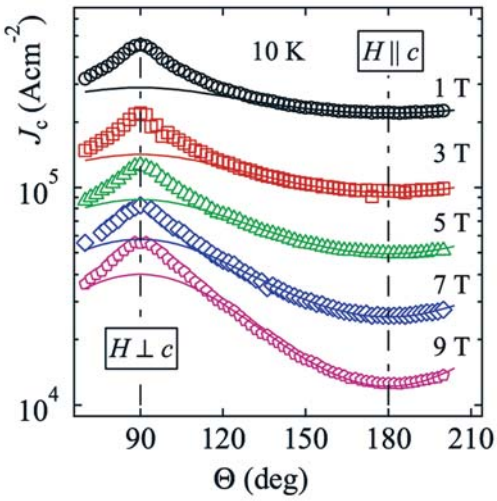

Fig 3: Critical current density of an Fe/Ba-122 bilayer grown on an MgO substrate. Critically, when an externally applied magnetic field H is oriented parallel to the Ba-122 c-axis, no enhancement of J_c can be ascertained. This indicates that there is no correlated network of defects aligned in this direction.

crystallographic disturbance. Furthermore, it was noted that the orientation of these textured iron regions is rotated 45° in-plane to both the substrate and the Ba–122 phase, providing a plausible explanation for the presence of an Fe (002) reflection in x-ray diffraction (XRD) patterns in nearly all Ba-122 films. In this orientation, the (001) surface plane of iron has an approximately 2% lattice mismatch with the square-planar iron sublayer defining the FeAs tetrahedron in the Ba–122 unit cell and thus offers a natural location for coherent interfacial bonding (Fig. 1).

One way to prevent the detrimental interspecies diffusion at the substrate interface is to preemptively deposit textured iron directly on the substrate prior to the deposition of the Ba-122 phase. Since the Fe/Ba-122 bond appears to be more stable than the oxide/Ba-122 bond, the resulting interface should be highly coherent and chemically stable. This new architecture has been dubbed "Fe/Ba-122 bilayers."

Thin layers of textured iron were grown on a number of substrates by our group, as presented in Fig. 2. On each of them, when the iron layer grows in a textured manner, the subsequent epitaxial growth of the Ba-122 phase was observed. The crystalline quality of the Ba-122 phase was of very high quality, exhibiting a sharp texture while retaining good superconducting properties. The presence of a stray texture component in the bilayer grown on the LSAT substrate is due to the growth of iron islands; in every case where an iron (001) facet grew parallel to the LSAT surface, textured Ba-122 was observed. Perhaps the most important criterion for high quality growth of thin films is the amount of current they are capable of transporting – known as the critical current density J_c - particularly when an external magnetic field is applied. The bilayers on MgO exhibit J_c values among the highest reported to date in thin films [8,11,13]. More significantly, however, is the lack of J_c enhancement when the external magnetic field is applied parallel to the Ba-122 c-axis, as depicted in Fig. 3. This indicates that Ba-122 films grown in this manner do not have pinning-active correlated defects oriented along this direction, contrasting the results of other groups [8,11]. Accordingly, these films can be considered suitable for a number of fundamental investigations where the intrinsic anisotropy of the Ba-122 phase is to be probed.

Controlled bilayers of this type lend themselves to an additional investigation of the nature of bonding at the interface. The interface between Fe and Ba–122 was studied using the microscope described above. Figure 4a shows a high resolution scanning transmission electron microscopy (HRSTEM) image obtained with a high angle annular dark field detector. Directly below, higher-resolution data obtained from a different sample region are presented. This image shows a mass-thickness contrast, meaning that atomic columns appear as bright dots. Hence, the location of individual atoms within their unit cell can be elucidated, as indicated in the lower portion of Fig. 4 through the use of artificial colors and a schematic model. The Ba–122 phase is observed to terminate on the upper As sublayer of the FeAs tetrahedron. As an independent confirmation of this analysis, high resolution TEM (HRTEM) was undertaken on a separate sample region and is presented in Fig. 4b. This focus of this image was adjusted such that the atomic columns also appear as white dots. Below it, the atomic positions are identified in the same manner as previously. Combined with the HRSTEM data in Fig. 4a, these observations constitute compelling evidence that the square-planar iron sublayer in the Ba–122 unit cell is directly replaced by the (001) surface plane of the bcc iron layer resulting in a coherent interfacial bond on the FeAs sublattice [12].

These results have opened up a number of new research directions for thin films of the iron-based superconductors. First, as demonstrated by figures 2 and 3, this architecture represents a means by which Ba-122 thin films with a very strong texture and minimal

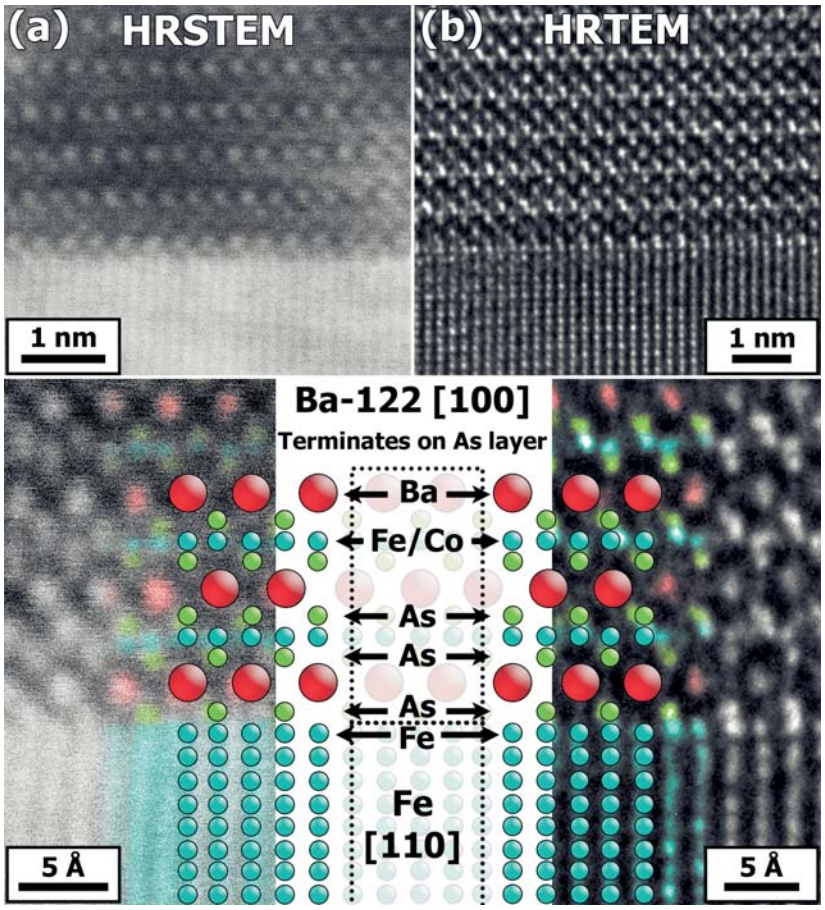

Fig. 4: (a) HRSTEM image of the Fe/Ba–122 interface. Directly below, a higher-resolution image of a neighboring region is shown. **(b)** HRTEM image from the Fe/Ba–122 interface with an enlargement below. In both (a) and (b), the atomic columns appear white and are identified through the use of artificial coloration and a schematic model. The interface is highly coherent and bonding takes place directly on the FeAs sublattice.

defects can be grown without seriously degrading its superconductive properties [13]. This provides researchers with the first thin films representative of the intrinsic Ba-122 phase without being tainted by defects. Second, the bilayer architecture enables the growth of iron-based superconductors on technical substrates such as hastelloy containing an MgO buffer layer that was deposited with Ion Beam Assisted Deposition (IBAD). Our group has produced the first such samples, and the results are shown in Fig. 5. Such thin film designs allow researchers to investigate the influence a grain boundary network exerts on superconductivity and additionally opens the way for in-situ strain investigations [14]. Finally, since the iron buffer layer bonds directly on the one structural feature common to all iron-based superconductors – the iron arsenic tetrahedron – it is likely that this same architecture will work for other families as well.

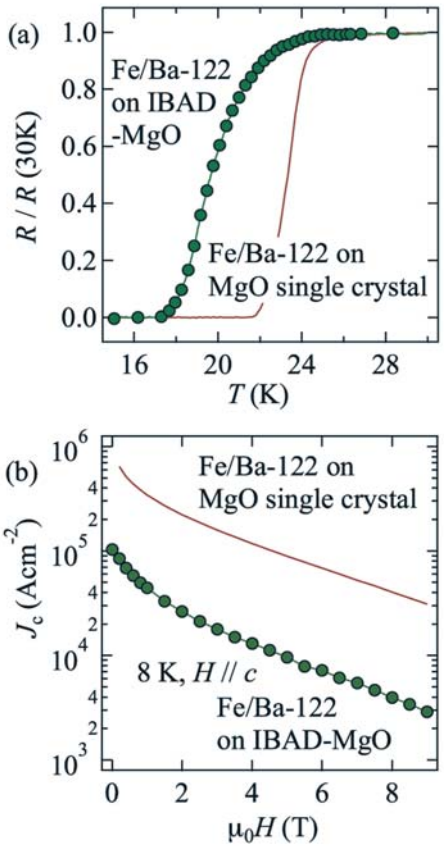

Fig. 5: (a) Normalized resistance of the Co-doped Ba-122 thin film on IBAD-MgO. The data were normalized to the value of 30 K. For comparison, the film on a MgO single crystalline substrate is also plotted. **(b)** J_c-H characteristics for Co-doped Ba-122 thin film on IBAD-MgO at 8K. A self-field J_c of over 10^{-5} A cm^{-2} has been recorded.

The authors acknowledge assistance from R. Heller and V. Mathias.

[1] A. Sefat, et al., Phys. Rev. Lett. **101**, 117004 (2008)
[2] H. Hiramatsu, et al., Phys. Rev. B **80**, 052501 (2009)
[3] H. Hiramatsu, et al., Appl. Phys. Express **1**, 101702 (2008)
[4] E. -M. Choi, et al., Appl. Phys. Lett. **95**, 062507 (2009)
[5] T. Katase, et al., Solid State Commun. **149**, 2121 (2009)
[6] S. Lee, et al., Appl. Phys. Lett. **95**, 212505 (2009)
[7] K. Iida, et al., Appl. Phys. Lett. **95**, 192501 (2009)
[8] S. Lee, et al., Nature Mater. **9**, 397 (2010)
[9] K. Iida, et al., Phys. Rev. B **81**, 100507(R) (2010)
[10] T. Katase, et al., Appl. Phys. Lett. **96**, 142507 (2010)
[11] T. Katase, et al., Appl. Phys. Express **3**, 063101 (2010)
[12] T. Thersleff, et al., Appl. Phys. Lett. **97**, 022506 (2010)
[13] K. Iida, et al., Appl. Phys. Lett. **97**, 172507 (2010)
[14] K. Iida, et al., Appl. Phys. Express **4**, 013103 (2011)

Cooperation: Helmholtz-Zentrum Dresden-Rossendorf, Univ. Stuttgart, Univ. Jena, Karlsruhe Inst. for Technology, Germany; Los Alamos National Laboratory, USA
Funding: EU Marie-Curie RTN NESPA, DFG (SPP 1458 and HA-5934/1-1)

Giant negative domain wall resistance in iron

D. Elefant and R. Schäfer

A domain wall-related magnetoresistance (MR) effect was discovered that may exceed the established MR-effects (Anisotropic MR, Giant-MR, Lorentz-MR etc.) by orders of magnitude. Phenomenologically it is a *negative domain wall resistance* (NDWR), caused by the formation of scattering-induced channels for the charge carriers around domain walls that can "shortcut" the Lorentz-MR (LMR) of magnetic domains. This fundamental influence of walls on the electric transport was not considered so far. The discovery was possible by choosing samples that allowed the separation of all superimposed effects by temperature-dependent resistance measurements and domain control. The samples were bulk single-crystalline iron cylinders (2 – 4 cm long, diameter $D \approx 1 - 4$ mm) [1, 2] with different orientations. They were of high purity and lattice perfection, characterized by residual resistance ratios $RRR = \rho(295\,\mathrm{K})/\rho(T \approx 2\mathrm{K})$ up to 5700, which are the highest values for bulk iron ever published. The domains of the rods were manipulated by small magnetic fields: (i) A circular "self-field" H_{circ}, caused by the (direct) measuring current J along the rods and estimated at the surface to $\mu_0 H_{circ} = \mu_0 J/\pi D \leq 2$ mT, and (ii) an external longitudinal field $\mu_0 H_{long} \leq 100$mT along the rod axis ($\|J$). The domain structure and its field dependence was studied by longitudinal Kerr microscopy [3]. By suspending the rods on a rotation stage the whole surface was accessible. Fields and currents could be applied during imaging. So the resistivity measurements $\Delta\rho(B)$ could be interpreted in terms of the magnetization changes $B = \mu_0 (H+M)$.

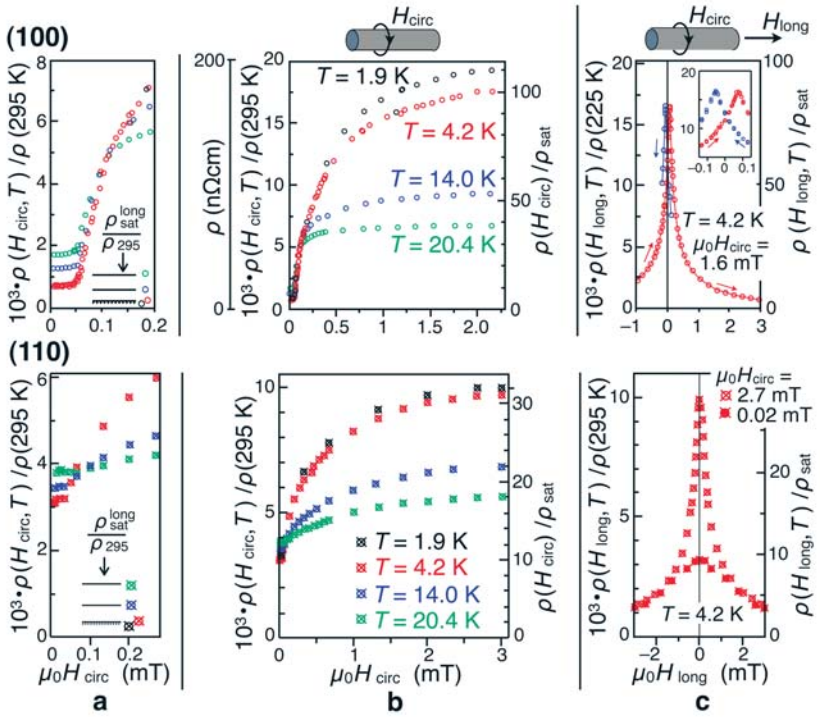

Fig. 1: Two similar sets of resistivity curves, measured on the (100)-crystal (top) and (110)-crystal (bottom). **(a)** Resistivity dependence on small circular self-field H_{circ} for different temperatures. **(b)** Like (a), but for larger circular fields. **(c)** Resistivity dependence on longitudinal field, with circular fields superimposed

In Fig. 1 the field-dependence of resistivity is plotted for the (100)- and (110)-oriented crystals. Reference state is the longitudinally saturated state, the resistance $\rho_{long}^{sat}(T)$ of which is indicated by lines in Fig. 1a. Removing the saturation field, the resistivity rises (compare the $\rho_{long}^{sat}(T)$-lines with the $H_{circ} = 0$ values in Fig. 1a). For increasing H_{circ}, Figs. 1a, b reveal a further resistivity increase — small circular fields of just 2 mT thus cause drastic resistivity changes up to factors of 100 for the (100)- and 30 for the (110)-crystal compared to the reference state (the different factors are primarily due to the different *RRR*). Superimposing then a longitudinal field of the same order of magnitude, nearly all the giant resistivity increase is canceled (Fig. 1c). An interpretation of these effects requires knowledge of the domains.

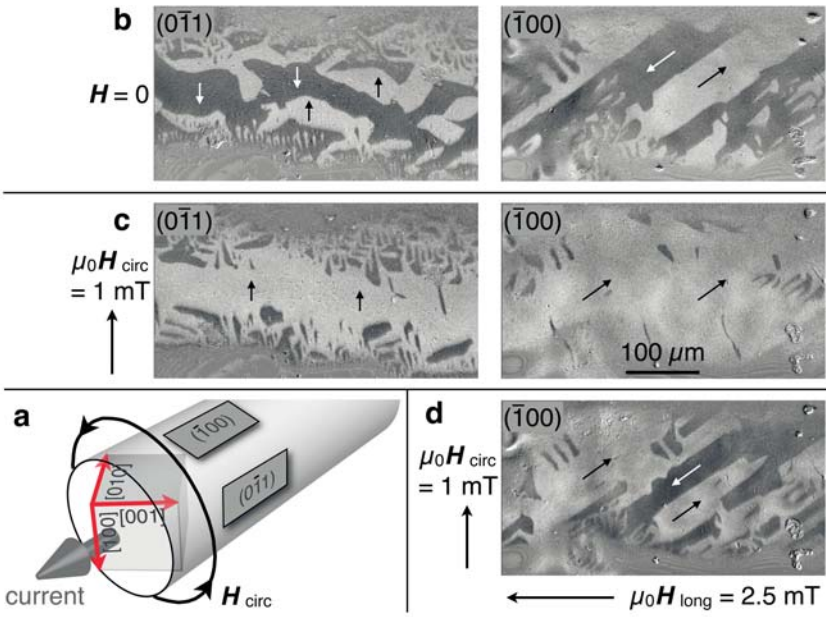

Fig. 2: Surface domains of the (110)-crystal, observed on two surfaces for applied fields as indicated

Figure 2 shows the domains on the (110)-crystal for some states along the curves in Fig. 1. There are 6 easy crystal directions (Fig. 2a): the [100], [-100] directions, called ±90°-directions (relative to the current axis), and the [010], [0-10], [001] and [00-1] directions called ±45°- and ±135°-directions. In an infinite crystal (which roughly applies to our bulk sample) and at zero external field, 1/3 of the volume is occupied by ±90° domains and 2/3 by ±45° and ±135° domains. The occupancy of the two main axes is visible in Fig. 2b. This relative distribution of domain phase volumes also applies to the zero-field state of Fig. 1a, where the resistance was measured with small current, i.e. at $H_{circ} < H_{coercive}$. The resistivity of this multidomain domain state is by a factor of 10 higher than that of the longitudinally saturated state because a substantial transverse LMR is caused by both, the ±90° domains and, to a lower degree, the ±45° and ±135° domains. The ±45°/±135° domains also contribute a longitudinal LMR, which, however, can only play a minor role: Due to their 'short-cutting' effect, the longitudinal LMR of these domains should lead to a total resistance in the same order of magnitude as that of the longitudinally saturated state. As this is not observed, we conclude that the transverse LMR of the ±45°/±135° phase volume dominates the resistance at zero-field.

When a circular field of only 2 mT is applied to this multidomain state, the resistivity strongly rises (Fig. 1b), accompanied by a change in the domain structure (Fig. 2c): domains with magnetization components parallel to H_{circ} grow on expense of antiparallel domains. This leads to a reduction of the wall density at a stable transverse MR situation. The disappearance of domain walls must consequently be responsible for the resistivity rise. A conceivable (though not observed) partial phase transition from ±45° to ±90° domains, which would also lead to an increasing transverse LMR, can only play a marginal role. This fact is supported by the resistivity measurements on (111)-oriented crystals: For such crystals any kind of domain phase rearrangement cannot change the LMR configuration for symmetry reasons (all easy crystal axes have the same absolute angle relative to the current direction). Nevertheless, the resistance change in small magnetic fields (not shown) and the temperature dependence of resistivity have the same characteristics and order of magnitude. Again, there is only the difference in domain wall density left as an interpretation — changes in the longitudinal LMR components can be excluded for (111)-crystals.

If a longitudinal field of 1 mT is added to the circular field, the 180°-walls between the ±45° domains reappear (Fig. 2d) to create a longitudinal ***M***-component. The domain phases are thus rearranged: the +45° (or +135°) volume is partly replaced by –45°

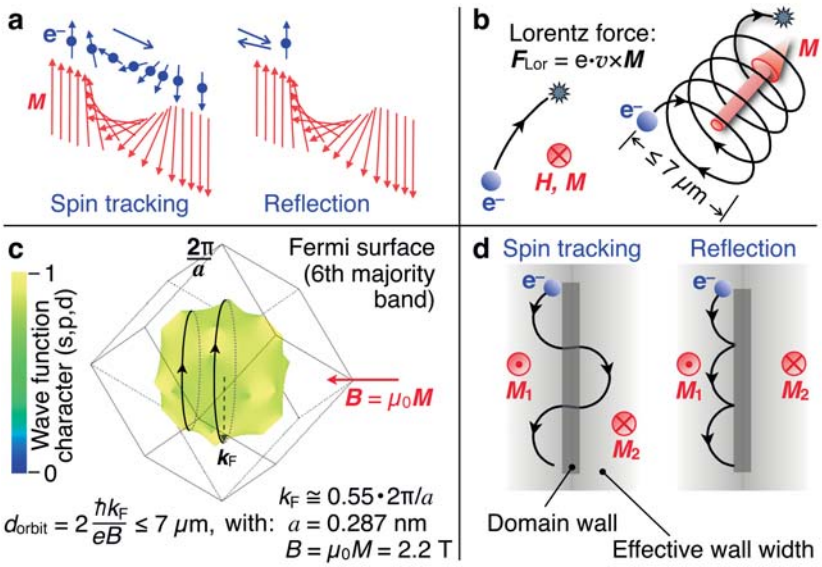

Fig. 3: (a) Interaction of electron (spin and charge e^-) and Bloch wall. Translation with spin tracking is favored for wide walls, reflection with spin conservation for narrow walls. Reflection causes a positive wall resistance. **(b)** Electron trajectories in real space for small (left) and large mean free paths (right). **(c)** Fermi surface sheet of Fe [4, 5] with two cyclotron orbits for large relaxation times caused by the magnetization *M*. **(d)** Lorentz trajectories along domain walls, schematically shown for spin tracking and reflection.

(or –135°) volume, whereas the ±90° phase volume will stay largely unchanged. Again, there is no significant redistribution of the (LMR-relevant) absolute |90°| and |45°|/|135°| phase volumes in the superimposed field. The resistivity, however, drops almost down to that of the longitudinally saturated state (compare Fig. 1b and c)! If the redistributrion of 90° and 45°/135° phases would be responsible for this drop, the resistance should only decrease by a factor $\ll 2$, but not by (at least) an order of magnitude as measured. Again, it must be the domain walls that are responsible for the effect. Domain studies on the (100)-crystal (not shown) lead to the same conclusion.

The key to interpret the huge resistivity changes are the geometrical dimensions of the Lorentz trajectories of the conduction electrons in real space. They can be derived from Fermiology: The conductivity of iron is dominated by the Fermi surface (FS) of the 6th majority band sheet (Fig. 3c). The cyclotron orbits at the FS, caused by the Lorentz force, are transferred to helix-like trajectories around the induction *B* (resp. magnetization *M*) in real space with an average diameter *d* of 5 µm (Fig. 3b). As the mean-free electron path λ in our perfect crystals can be up to 140 µm at low temperature (compared to ~16 nm at room temperature) a spiral trajectory makes several turns *N* before scattering. Thus the so-called "high field limit" $2\pi N = 2\lambda/d_{max} = \omega_c\tau \gg 1$ is realized (ω_c is the cyclotron frequency, τ the relaxation time). Then for $\Delta\rho_{Lorentz}$ theory [6, 7, 8] yields

$$\Delta\rho_{trans}(B,T)/\rho(B=0,T) \propto (\omega_c\tau)^2 \propto B^2/\rho(B=0,T)^2, \quad (1)$$

$$\Delta\rho_{long}(B,T) = c_l\,\rho(B=0,T). \quad (2)$$

These equations for the transverse and longitudinal LMR hold for compensated metals (i.e. equal numbers of electrons and holes) with closed FS sheets, which both applies to iron. According to Eq. 1, ρ_{trans} unboundedly increases with the number of orbits at the FS, which was indeed measured up to $B \sim 20$ T [9, 10]. The temperature dependence of the transverse LMR is determined by $\rho(B=0,T)$ in the denominator of Eq. 1 (the numerator stays constant for a stable domain configuration with total or partial transverse *M*-components). The denominator in Eq. 1 decreases with falling temperature, explaining the negative temperature coefficient (TCR) of the transverse LMR that is measured in Fig. 1b.

Such behavior, however, can only occur if the electron helices propagate within sufficiently wide domains like in Fig. 2c. If a helix interacts with a domain wall, the Lorentz force changes and the spiral trajectory is interrupted. So within an effective width around the wall, given by roughly twice the average helix diameter, full helix turns cannot be

formed. Instead, short Lorentz trajectories, wiggling around the wall, will be generated (Fig. 3d). They are equivalent to highly conductive current channels along the wall, which may 'shortcut' the transverse LMR (and to a lower degree also the longitudinal LMR) if the walls have longitudinal orientational components. For our (110)-crystal this scenario is supported by domain observation: the angles between domain magnetization and electrical current direction stay largely constant in the low- and high-resistivity states (i.e. the last term in Eq. 1 remains unchanged), just the number of walls is different. The huge resistivity changes must consequently be caused by the creation and annihilation of domain walls. Within the channels the negative TCR of Eq. 1 cannot dominate the total resistivity. The TCR thus changes sign from negative to positive (Fig. 1a) when the wall density increases with decreasing circular field (Fig. 2b).

To summarize, our resistivity studies can only be explained conclusively by assuming that domain walls decrease the LMR, thus causing a NDWR. This "channeling" effect of walls, which is due to a change of the Lorentz trajectories and which is therefore a consequence of Fermiology at the end, can drastically exceed any (positive) DWR based on the carrier spin or diamagnetic models [11-14]. It is caused by the electron charge and thus independent of spin/wall interactions, being valid for both, electron transmission with spin tracking [15] or reflection with spin conservation [16]. The NDWR is huge at low temperatures, favored by the electronic structure of iron (compensation and closed FS sheets). The measurable features will be weaker e.g. in Co or Ni and in samples with reduced dimensions (like films) where the surfaces, which act like walls on the Lorentz trajectories [17], are dominating. Also at higher temperatures the effect will be reduced and most likely not be strong enough to be isolated from other MR or DWR effects. Nevertheless it is expected that the NDWR plays a role for all domain walls in any kind of magnetic material. Domain walls generally decrease the LMR, and because the LMR is inherent in every ferromagnet with more or less intensity, a negative domain wall resistance term exists as a matter of principle and has to be taken into account in any resistivity discussion! This effect was overlooked so far. For an extended description see ref. [18].

[1] G. Weise and G. Owsian, Kristall und Technik 11, 729 (1976)
[2] G. Behr, J. Werner, G. Weise, A. Heinrich, A. Burkov, and C. Gladun, Phys. Status Solidi (a) 160, 549 (1997)
[3] A. Hubert and R. Schäfer, Magnetic Domains (Springer-Verlag, Berlin, Heidelberg, New York, 1998)
[4] URL **www.physik.tu-dresden.de/~fermisur/**
[5] P. Zahn, private communication
[6] A. B. Pippard, Cambridge Studies in Low Temperature Physics 2: Magnetoresistance in Metals (Cambridge Univ. Press, Cambridge, 1989)
[7] I. M. Lifshitz, M. Y. Azbel, and M. I. Kaganov, Soviet Physics J.E.T.P.-USSR 4, 41 (1957)
[8] E. Fawcett, Adv. Phys. 13, 139 (1964)
[9] R. V. Coleman, R. C. Morris, and D. J. Sellmyer, Phys. Rev. B 8, 317 (1973)
[10] K. H. Berthel, N. E. Alekseevskij, V. I. Nishankovskij, D. Elefant, and R.-R. Hesske, Proceedings of Colloques Internationaux du CNRS, Paris 242, 387 (1975)
[11] G. G. Cabrera and L. M. Falicov, Phys. Status Solidi (b) 62, 217 (1974)
[12] G. G. Cabrera and L. M. Falicov, Phys. Status Solidi (b) 61, 539 (1974)
[13] Y. I. Mankov, Sov. Phys.-Solid State 14, 62 (1972)
[14] Y. V. Zakharov and L. S. Titov, Physics of the Solid State 46, 303 (2004)
[15] L. Berger, J. Appl. Phys. 49, 2156 (1978)
[16] M. B. Stearns, J. Magn. Magn. Mater. 104, 1745 (1992)
[17] U. Rüdiger, J. Yu, A. D. Kent, and S. S. P. Parkin, Appl. Phys. Lett. 73, 1298 (1998)
[18] D. Elefant and R. Schäfer, Phys. Rev. B **82**, 134438 (2010)

Towards ballistic heat transport of quantum spin excitations

N. Hlubek, P. Ribeiro, R. Saint-Martin[1], A. Revcolevschi[1], G. Roth[1], G. Behr, B. Büchner, C. Hess

Fundamental conservation laws predict ballistic, i.e., *dissipationless* transport behaviour in one-dimensional quantum magnets. Experimental evidence, however, for such anomalous transport has been lacking ever since. Here we provide experimental evidence for ballistic heat transport in a $S = ½$ Heisenberg chain. In particular, we investigate high purity samples of the chain cuprate $SrCuO_2$ and observe a huge magnetic heat conductivity κ_{mag}. An extremely large spinon mean free path of more than a micrometer demonstrates, that κ_{mag} is only limited by *extrinsic* scattering processes, which is a clear signature of ballistic transport in the underlying spin model.

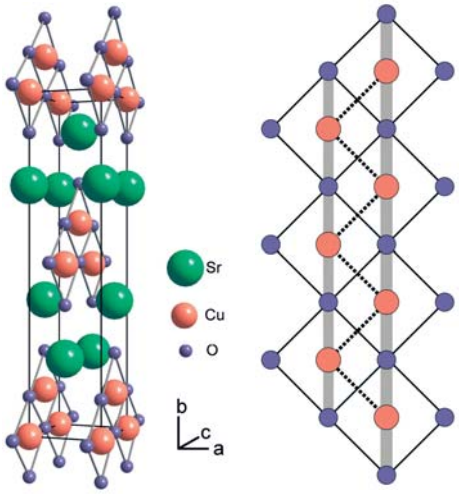

Fig.1: Crystal structure of the spin chain compound $SrCuO_2$. The symmetry is *Cmcm* with lattice constants $a = 3.56$Å, $b = 16.32$Å, $c = 3.92$ Å [16]. The main building block of the crystal, the double spin chain consisting of CuO_2 plaquettes is shown in the right picture.

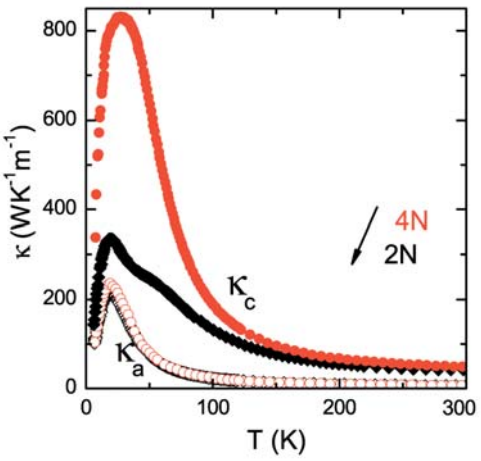

Fig. 2: Thermal conductivities κ_a and κ_c of $SrCuO_2$ for 2N (99%) and 4N (99.99%) purity. Closed (open) symbols represent *c*-axis (*a*-axis) data, circles (diamonds) correspond to 4N (2N) purity.

The integrability of the one-dimensional (1D) antiferromagnetic $S = ½$ Heisenberg chain implies a *divergent* magnetic heat conductivity κ_{mag} at all finite temperatures T [1–4]. Despite this rigorous prediction, experimental evidence for ballistic heat transport in quantum magnets is lacking. Such experimental κ_{mag} is always *finite*, since extrinsic scattering processes due to defects and phonons are inherent to all materials and mask the intrinsic behavior of the chain. A promising large κ_{mag} has been observed in a number of cuprate compounds, which realize 1D $S = ½$ Heisenberg antiferromagnets [5–9]. The compound $SrCuO_2$ is a prominent example [8, 9]. However, a quantitative analysis of κ_{mag} has always been difficult in this compound, since the phononic and magnetic heat conductivities are of similar magnitude at low temperatures. Here we report evidence for ballistic heat transport as a result of a huge enhancement of κ_{mag} upon increasing the samples purity [10].

The main structural element in $SrCuO_2$ is formed by CuO_2 zig-zag ribbons, which run along the crystallographic *c*-axis, as shown in Fig. 1. Each ribbon can be viewed as made of two parallel corner-sharing CuO_2 chains, where the straight Cu-O-Cu bonds of each double-chain structure result in a very large antiferromagnetic intrachain exchange coupling $J/k_B \approx 2100-2600$ K of the $S = ½$ spins at the Cu^{2+}sites [11, 12]. The frustrated and much weaker interchain coupling $|J'|/J \approx 0.1-0.2$ [11] and presumably quantum fluctuations prevent three-dimensional long range magnetic order of the system at $T > T_N \approx 1.5-2\text{K} \approx 10^{-3}J/k_B$ K [13, 14]. Hence, at significantly higher T the two chains within one double chain structure can be regarded as magnetically independent, which is consistent with results by inelastic neutron scattering [12].

Fig. 2 presents our results for κ_a and κ_c of $SrCuO_2$ for both 99% (2N) and 99.99% (4N) purity as a function of T. We first describe the data for 2N purity, which are in good agreement with earlier results by Sologubenko et al. [9]. A pronounced low-T peak is found for $\kappa_{a,2N}$, perpendicular to the chains. This peak and a $\sim T^{-1}$-decrease at $T \gtrsim 150$ K towards a small value at room temperature, represent the characteristic T-dependence of phonon-only heat conductivity κ_{ph}. A similar low-T peak is also present for $\kappa_{c,2N}$, parallel to the chains. It is however larger and exhibits a distinct shoulder at $T \gtrsim 40$ K. $\kappa_{c,2N}$ decreases at higher T, but remains much larger than $\kappa_{a,2N}$ even at room temperature. The apparent large anisotropy, together with the unusual T-dependence of $\kappa_{c,2N}$, is the signature of a large magnetic fraction of $\kappa_{c,2N}$ over a large T-range [8, 9].

We now turn to the new data which have been obtained for the high-purity compound. The heat transport perpendicular to the chains ($\kappa_{a,4N}$) is slightly enhanced as compared to $\kappa_{a,2N}$. This reflects a somewhat reduced phonon-defect scattering. However, a much more drastic and unexpected large effect of the enhanced purity is observed in the heat transport parallel to the chains, $\kappa_{c,4N}$. Instead of a narrow low-T peak and a shoulder, as observed in $\kappa_{c,2N}$, a huge and broad peak centered at ~28 K is present in $\kappa_{c,4N}$. This peak exceeds $\kappa_{c,2N}$ at $T \lesssim 70$ K by more than a factor of 2. For 70K $\lesssim T \lesssim$ 200 K we observe $\kappa_{c,4N} > \kappa_{c,2N}$ and interestingly both curves approach each other. At $T \gtrsim 200$ K both curves

exhibit almost the same T-dependence and $\kappa_{c,4N}$ is still larger than $\kappa_{c,2N}$, although only by a factor of 1.2.

Without further analysis some clear-cut conclusions can be drawn. First, the extraordinary enhancement of κ_c upon the improvement of the materials purity in contrast to a concomitantly negligibly small one in κ_a, straightforwardly implies that the enhancement primarily concerns the magnetic heat conductivity κ_{mag}, which is present in κ_c only. Second, at low-T, the extreme sensitivity to impurities of κ_{mag} suggests, that spinon-defect scattering is the dominating process, which relaxes the heat current in this regime. Third, at larger T, the spinon-defect scattering is increasingly masked by a further scattering process, which leads to $\kappa_{c,2N}$ and $\kappa_{c,4N}$ being very similar at $T \gtrsim 200$ K. The most reasonable candidate for this process is spinon-phonon scattering, since the only thinkable alternative, i.e. spinon-spinon scattering, is negligible [1, 2, 5, 15] in this T-regime.

An estimate for the magnetic thermal conductivity can be obtained by $\kappa_{mag} = \kappa_c - \kappa_a$. The results for the 2N and the 4N samples are shown in Fig. 3. κ_{mag} of the 4N sample exhibits a sharp peak at ~37 K with an extraordinary maximum value of about 660 $Wm^{-1}K^{-1}$, which is more than a factor of 3 higher than the largest reported κ_{mag} [9]. The peak is followed by a strong decrease upon raising T. Similar to the typical T-dependence of a clean phononic heat conductor, the overall T-dependence of κ_{mag} suggests, that, in a simple picture, two competing effects determine κ_{mag}. These are at low-T the scattering of spinon on defects and for higher T spinon-phonon scattering. κ_{mag} of the 2N sample is qualitatively very similar. However, the absolute value at the peak is much lower (~ 172 W/mK) and the position of the peak is shifted to a higher T (~ 55 K).

We analyze κ_{mag} quantitatively by extracting the spinon mean free path l_{mag} according to [5, 6, 9]

$$l_{mag} = \frac{3\hbar}{\pi N_s k_B^2 T}\ \kappa_{mag}, \qquad (1)$$

where $N_s = 4/ab$ is the number of spin chains per unit area. As can be inferred from Fig. 4, l_{mag} of both samples shows a strong decrease with increasing T, which directly reflects spinon-phonon scattering becoming increasingly important. Both curves are very similar, but clear differences are present at low-T, where l_{mag} of the 2N sample is somewhat lower, in accordance with a higher spinon-defect scattering. We evoke Matthiesen's rule to model the T-dependence of l_{mag} and to account for both scattering processes viz. $l_{mag}^{-1} = l_0^{-1} + l_{sp}^{-1}$. Here, l_0 describes the T-independent spinon-defect scattering whereas $l_{sp}(T)$ accounts for the T-dependent spinon-phonon scattering. For the latter, we assume a general Umklapp process with a characteristic energy scale $k_B T_u^*$ of the order of the Debye energy, which is commonly used in literature [7, 9]. We thus have

$$l_{mag}^{-1} = l_0^{-1} + \left(\frac{\exp(T_u^*/T)}{A_s T} \right)^{-1}, \qquad (2)$$

which can be used to fit the data with l_0, A_s and T_u^* (A_s describes the coupling strength) as free parameters. We find an excellent agreement between such fits and the experimental l_{mag}, as shown in Fig. 4. Inspection of the fit parameters [17] yields two remarkable aspects, which corroborate our previous qualitative findings. First, the parameters A_s and T_u^*, which determine the spinon-phonon scattering are practically the same for both samples. In fact, a good fit is obtained if the same T_u^* is used for both curves. Note that the extracted $T_u^* \sim 200$K is of the order of the Debye temperature Θ_D of this material and thus leads to the conjecture, that mostly acoustic phonons are involved in this scattering process. Second, the spinon-defect scattering length l_0, which represents a lower bound for the low-T limit of l_{mag} and which should significantly depend on the samples purity turns out to be drastically different for both cases. To be specific, we find $l_0 \approx 300$ nm for the 2N compound and an extraordinary $l_0 \approx 1.6$ μm for the 4N sample. These distances correspond to more than 750 and 4100 lattice spacings, respectively.

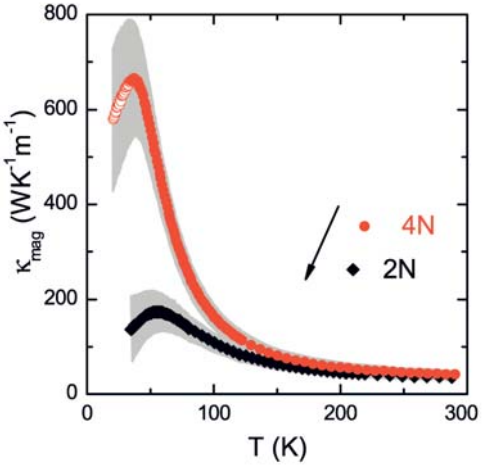

Fig. 3: κ_{mag} of $SrCuO_2$ for different purities. Open symbols represent low-T κ_{mag}, which is disregarded in the further analysis. The shaded areas show the uncertainty of the estimation of κ_{mag} due to the phononic background.

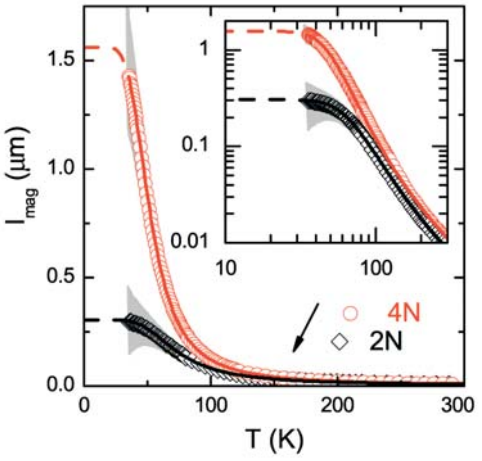

Fig. 4: Magnetic mean free paths of $SrCuO_2$ for different purities. The solid lines were calculated according to Eq. 2. The shaded area illustrates the uncertainty from the estimation of the phononic background. The inset shows the same set of curves on a double logarithmic scale.

These findings provide a further confirmation, that for 2N and 4N purity, κ_{mag} is determined by the same spinon-phonon scattering process and that the difference between the two curves can be described by the different defect density only.
A major outcome of our study is the unambiguous identification of the *extrinsic* scattering processes as the only relevant ones. *Intrinsic* spinon-spinon scattering, on the other hand, plays no role in our analysis, even in the case of the very clean sample. The strong enhancement of κ_{mag}, upon a reduced number of impurities, thus appears as the manifestation of ballistic heat transport of the underlying spin model, where κ_{mag} is rendered finite by extrinsic scattering processes only. A simple analysis reveals a remarkable lower bound for the low-temperature limit of the spinon mean free path l_{mag} of more than a micrometer. This renders $SrCuO_2$ an intriguing candidate for future spin transport experiments.

[1] F. Heidrich-Meisner, A. Honecker, D. C. Cabra, and W. Brenig, Phys. Rev. B **68**, 134436 (2003).
[2] A. Klümper and K. Sakai, J. Phys. A: Math. Gen. **35**, 2173 (2002).
[3] X. Zotos, Phys. Rev. Lett. **82**, 1764 (1999).
[4] X. Zotos, F. Naef, and P. Prelovsek, Phys. Rev. B **55**, 11029 (1997).
[5] C. Hess, Eur. Phys. J. Special Topics **151**, 73 (2007).
[6] C. Hess, H. ElHaes, A. Waske, B. Büchner, C. Sekar, G. Krabbes, F. Heidrich-Meisner, and W. Brenig, Phys. Rev. Lett. **98**, 027201 (2007).
[7] T. Kawamata, N. Takahashi, T. Adachi, T. Noji, K. Kudo, N. Kobayashi, and Y. Koike, J. Phys. Soc. Jpn. **77**, 034607 (2008).
[8] P. Ribeiro, C. Hess, P. Reutler, G. Roth, and B. Büchner, J. Mag. Mag. Mater. **290-291**, 334 (2005).
[9] A. V. Sologubenko, K. Giannò, H. R. Ott, A. Vietkine, and A. Revcolevschi, Phys. Rev. B **64**, 054412 (2001).
[10] N. Hlubek, P. Ribeiro, R. Saint-Martin, A. Revcolevschi, G. Roth, G. Behr, B. Büchner, and C. Hess, Phys. Rev. B **81**, 020405(R) (2010).
[11] N. Motoyama, H. Eisaki, and S. Uchida, Phys. Rev. Lett. **76**, 3212 (1996).
[12] I. A. Zaliznyak, H. Woo, T. G. Perring, C. L. Broholm, C. D. Frost, and H. Takagi, Phys. Rev. Lett. **93**, 087202 (2004).
[13] M. Matsuda, K. Katsumata, K. M. Kojima, M. Larkin, G. M. Luke, J. Merrin, B. Nachumi, Y. J. Uemura, H. Eisaki, N. Motoyama, et al., Phys. Rev. B **55**, R11953 (1997).
[14] I. A. Zaliznyak, C. Broholm, M. Kibune, M. Nohara, and H. Takagi, Phys. Rev. Lett. **83**, 5370 (1999).
[15] F. Heidrich-Meisner, A. Honecker, and W. Brenig, Phys. Rev. B **71**, 184415 (2005).
[16] L. Teske and H. Müller-Buschbaum, Z. anorg. allg. Chem. **379**, 234 (1970).
[17] For the 4N compounds we get $l_{0,4N} = (1.56 \pm 0.16)$ µm, $T^*_{u,4N} = (204 \pm 11)$ K, $A_{s,4N} = (59 \pm 5)\ 10^{-6}$ 1/mK. Setting $T^*_{u,2N} = T^*_{u,4N} = 204$K gives $l_{0,2N} = (320 \pm 13)$ nm and $A_{s,2N} = (72 \pm 5)\ 10^{-6}$ 1/mK for 2N. The errors account for the accuracy of the fit.

Cooperations: Laboratoire de Physico-Chimie de L'Etat Solide, ICMMO, UMR8182, Université Paris-Sud, 91405 Orsay, France, Institut für Kristallographie der RWTH, D-52056 Aachen, Germany

Funding: EuropeanCommission NOVMAG project (FP6-032980),DFG Forschergruppe-FOR912 (grantHE3439/8) and DFG grant HE3439/7.

Exploring a new field of nanoscience: endohedral electrochemistry

A. A. Popov, L. Zhang, S. Klod, P. Rapta[1], F. Lipps, C. B. Chen[2], S. F. Yang[2], L. Dunsch

Endohedral metallofullerenes (EMFs) – i.e. fullerenes encapsulating one or more metal atoms or a cluster in their inner space – are characterized by a high degree of internal electron transfer between the encaged metal and the host carbon cage. The vast majority of EMFs is limited to encaged metals of group I - group III. As a rule these metals are found in their highest oxidation states in such EMFs. The frontier molecular orbitals (MOs) of EMFs are thus essentially carbon cages' MOs, and therefore electrochemical activity of EMFs is mainly determined by the properties of the carbon cage. The situation is similar for the large group of nitride clusterfullerenes (NCF),[1] i.e. the EMFs with three metal atoms bonded to a central nitride ion inside the fullerene cage, which are the most stable endohedral fullerene structures available so far.

The electronic state of the endohedral metal atoms remains thus barely constant irrespective of the charge of the whole EMF molecule. Therefore any electrochemical reaction does not change the redox state of the encaged species. One of the notable exclusions from this rule is $Sc_3N@C_{80}$, which has Sc-localized LUMO.[2] Both the chemical and the electrochemical reduction of $Sc_3N@C_{80}$ leads to the change of the valence state of all three Sc atoms which can be especially well observed in the ESR spectrum of the anion-radical, which exhibits large ^{45}Sc hyperfine coupling constant (hfc) and shift of g-factor from the free-electron value.[2, 3] So far, all other metallic-nitride clusterfullerenes (NCFs, the EMFs with composition of $M_3N@C_{2n}$, where M is Sc, Y and lanthanides, while 2*n* can vary from 68 to 100) have carbon cage-based frontier orbitals, and hence the valence state of endohedral metal atoms in NCFs cannot be manipulated by chemical and electrochemical techniques.

The world of NCFs has been severely enlarged by the development and implementation of the procedures for the synthesis and separation of mixed-metal NCFs (i.e. NCFs with two different metal atoms in one M_3N cluster). To get isolated mixed-metal nitride cluster fullerenes (MMNCFs) of high isomeric purity, the application of high level recycling chromatography is required. The change in the metal composition of the endohedral species opens the way to EMFs with unprecedented electronic properties.[4, 5] By this approach, it is now possible to synthesize and isolate MMNCFs with those metal atoms which do not form homometallic M_3N clusters. For instance, $Ti_3N@C_{2n}$ NCFs cannot be synthesized up till now,[6] but the MMNCF with mixed Sc-Ti cluster, $TiSc_2N@C_{80}$, is readily available in the arc burning process. Besides, in the MMNCFs the single metal atom combined with two others can exhibit specific properties, which are not available in the homometallic clusters. This has been demonstrated in the recent study for the valence state of a metal ion which can be tuned electrochemically in certain MMNCFs.

Searching for MMNCFs with unexpected properties of the encapsulated metal atoms the case of $CeLu_2N@C_{80}$ is of special importance opening the route to a new redox reaction at EMFs.[7] NMR spectroscopic studies have shown that Ce in this MMNCF is in the III valence state with a single localized 4f electron (its spin can be followed by the characteristic temperature dependent shift in ^{13}C NMR spectra). All previous electrochemical studies of Ce(III)-containing EMFs in comparison to their La and lanthanide analogues (including $M@C_{82}$, $M_2@C_{72,78,80}$, $M_3N@C_{88,92,96}$) have not revealed any special redox behaviour of endohedral Ce. That is, redox potentials of Ce-based endohedral metallofullerenes were always close to those of the non-Ce analogues. However, for $CeLu_2N@C_{80}$ we have found that its oxidation potential is shifted by 0.6 V from the values of all other $M_3N@C_{80}$ NCFs (Fig. 1).[7] Such a strong shift of the redox potential indicates that

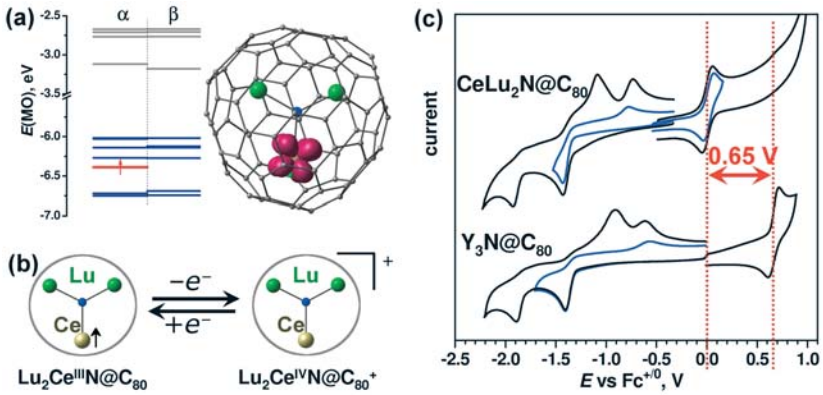

Fig. 1: (a) Kohn-Sham MO levels and spin density distribution in $CeLu_2N@C_{80}$ (computed at the PBE0/SVP level of theory); **(b)** schematic description of the reversible single-electron oxidation of $CeLu_2N@C_{80}$; **(c)** cyclic voltammetry curves of $CeLu_2N@C_{80}$ in comparison to that of $Y_3N@C_{80}$. Strong shift of the oxidation potential is denoted by red arrow

its origin is not based on changes of the carbon cage MOs of the EMF but is obviously grounded in the change of the valence state of the Ce atom in the encaged cluster. Indeed, DFT calculations have shown that the removal of the 4f electron from Ce atom in $CeLu_2N@C_{80}$ is 0.43 eV more favorable than oxidation of the carbon cage. Thus, $CeLu_2N@C_{80}$ is the first Ce-based endohedral metallofullerene exhibiting redox activity of endohedral Ce(III), which can be reversibly oxidized into the Ce(IV) state. In this way a new type of redox reactions at fullerenes is described being the matter of a new branch in electrochemistry, called *endohedral electrochemistry*. Moreover, $Ce^{IV}Lu_2N@C_{80}^+$ cation is the first EMF with the tetra-valent cerium atom.

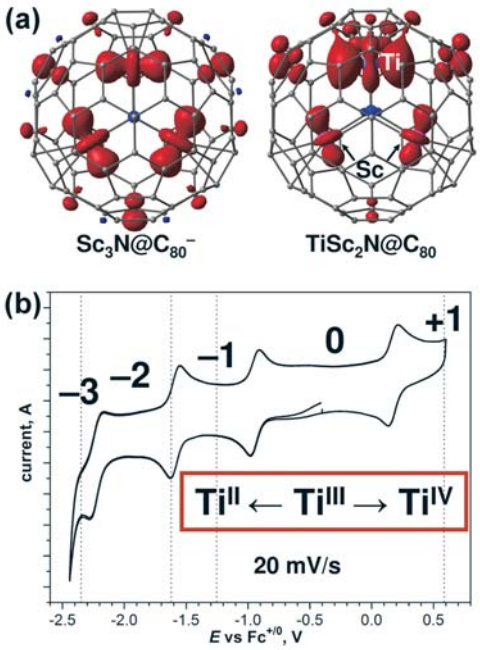

Fig. 2: (a) Spin density distribution in $TiSc_2N@C_{80}$ in comparison to the isoelectronic $Sc_3N@C_{80}^-$ (B3LYP/6-311G*). **(b)** cyclic voltametry of $TiSc_2N@C_{80}$, charge of the molecules and the valence state of Ti atom are also indicated

The existence of the $Ce^{IV}Lu_2N@C_{80}^+$ cation is by no means a single case of endohedral electrochemistry in action. Unprecedented electrochemical properties of endohedral fullerenes were also revealed for the MMNCF $TiSc_2N@C_{80}$.[8] This MMNCF is paramagnetic and ESR spectroscopic as well as DFT computational studies have shown that Ti is in the III-valence state in the neutral form of the MMNCF. Single-occupied MO (SOMO) and hence the spin density as well are to a large extent localized on the Ti atom (Fig. 2). Unlike all other $M_3N@C_{80}$ NCFs either with a homometallic or a mixed-metal nitride cluster, which exhibit electrochemically irreversible (but chemically reversible) reductions, the $TiSc_2N@C_{80}$ has three electrochemically reversible reductions and one reversible oxidation step (Fig. 2). The redox behaviour which is different from all other known NFCs is caused by the new route of endohedral electrochemistry. Both reduction and oxidation of $TiSc_2N@C_{80}$ proceed through the change of the valence state of Ti atom: from Ti(II) in the $TiSc_2N@C_{80}^-$ anion through Ti(III) in the neutral state to Ti(IV) in the $TiSc_2N@C_{80}^+$ cation. $TiSc_2N@C_{80}$ is the first example of EMF with metal-only redox system in which endohedral metal is electrochemically active in both reduction and oxidation.

It is to be mentioned that exohedral derivatization can also significantly alter the properties of NCFs. The studies of $Sc_3N@C_{80}(CF_3)_2$ have shown that addition of only two CF_3 groups drastically changes dynamics of the cluster and electrochemical properties of $Sc_3N@C_{80}$ core.[3] $Sc_3N@C_{80}(CF_3)_2$ exhibits two single-electron oxidation and three single-electron reduction steps, all of them are electrochemically reversible even at low voltammetric scan rates. High stability of the charge states in solution enabled an *in situ* ESR spectroscopic characterization of the electrochemically generated charged paramagnetic states (cation, anion, and trianion; $Sc_3N@C_{80}(CF_3)_2^{3-}$ is the first trianion of any EMF ever characterized spectroscopically). Analysis of the ^{45}Sc hyperfine structure of the anion and trianion has shown that exohedral addition of two CF_3 groups hinders rotation of the Sc_3N cluster (in $Sc_3N@C_{80}$ the cluster rotates freely). The study also revealed a mixing of the fullerene and cluster states in the frontier orbitals of the derivative and, as a result, the mixed cage-cluster distribution of the spin density in the derivative with the exceptionally high spin population on one Sc atom in the trianion.

Localization of the spin density in EMFs on the endohedral cluster and fast dynamics of the endohedral clusters raises the question of their mutual influence. Detailed DFT studies have shown that spin density distribution in such EMFs is very flexible; even slight reorientation of the cluster results in considerable changes of the spin populations of the metal atoms.[2, 8] This conclusion was further corroborated by the DFT-based Born-Oppenheimer molecular dynamics, which provided details of the spin density dynamics (dubbed as the spin flow). Fourier transformation of the time dependencies of the spin populations resulted in the spin-flow vibrational spectra, which reveal the major spin-flow channels. In particular, for $TiSc_2N@C_{80}$ it is shown that the cluster-cage spin flow is selectively coupled to one vibrational mode.[8]

In general, the judicious choice of synthetic and separation techniques and target EMFs opens the way to compounds with chemically and electrochemically tuneable valence states of the endohedral species. In the studies of such EMFs, the new field of electrochemistry, endohedral electrochemistry, is emerging. An interesting question still to be addressed in more details is the mechanism of the electron transfer to and from endohedral species through the formally inert carbon cage. The first studies of the electron density distribution[2, 8] have revealed that the formal change of the valence state of the endohedral atoms is accompanied by the spatial spin-charge separation.

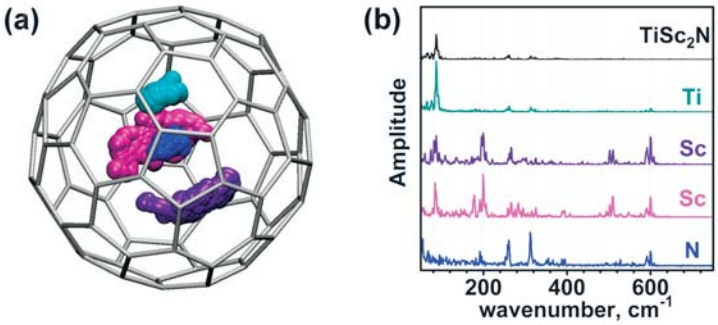

Fig. 4: (a) Born-Oppenheimer molecular dynamics trajectory of $TiSc_2N@C_{80}$ (10 ps at 300 K, displacements of carbon atoms are not shown); **(b)** spin-flow vibrational spectra of $TiSc_2N@C_{80}$ (note that the scale for Ti is an order of magnitude higher than the scale for Sc and N atoms).

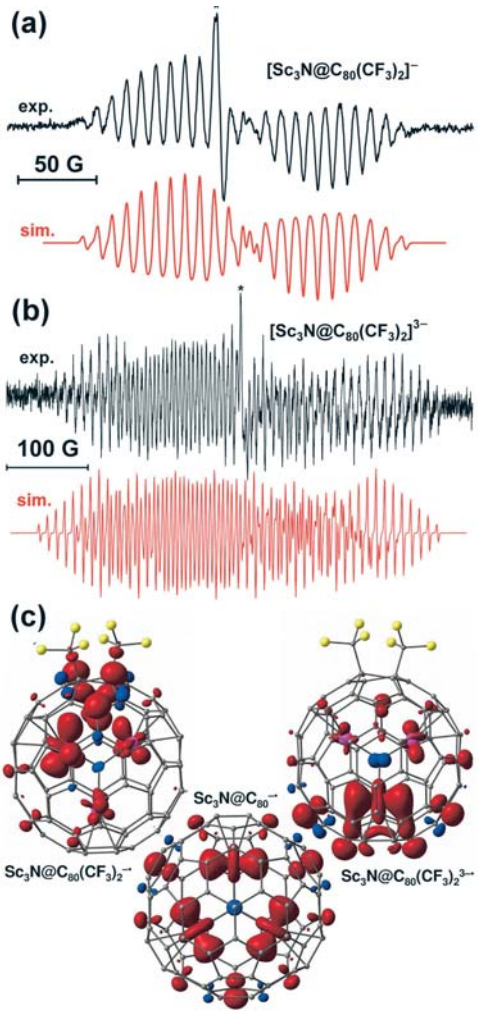

Fig. 3: (a–b) Experimental and simulated ESR spectra of (a) $Sc_3N@C_{80}(CF_3)^-$ and (b) $Sc_3N@C_{80}(CF_3)^{3-}$; **(c)** spin density distribution in $Sc_3N@C_{80}(CF_3)^-$, $Sc_3N@C_{80}(CF_3)^{3-}$, and $Sc_3N@C_{80}^-$.

[1] L. Dunsch, S. F. Yang, *Small* **2007** *3* (8), 3067–3081
[2] A. A. Popov, L. Dunsch, *J. Am. Chem. Soc.* **2008,** *130* (52), 17726-17742; Jakes, P.; Dinse, K. P. *J. Am. Chem. Soc.* **2001,** *123* (36), 8854-8855.
[3] Popov, A. A.; Shustova, N. B.; Svitova, A. L.; Mackey, M. A.; Coumbe, C. E.; Phillips, J. P.; Stevenson, S.; Strauss, S. H.; Boltalina, O. V.; Dunsch, L. *Chem.-Eur. J.* **2010,** *16* (16), 4721-4724.
[4] Yang, S. F.; Kalbac, M.; Popov, A.; Dunsch, L. *ChemPhysChem* **2006,** *7* (9), 1990-1995.
[5] Yang, S.; Popov, A. A.; Chen, C.; Dunsch, L. *J. Phys. Chem. C* **2009,** *113* (18), 7616-7623.
[6] Yang, S.; Chen, C.; Popov, A.; Zhang, W.; Liu, F.; Dunsch, L. *Chem. Commun.* **2009**, 6391-6393.
[7] Zhang, L.; Popov, A. A.; Yang, S.; Klod, S.; Rapta, P.; Dunsch, L. *Phys. Chem. Chem. Phys.* **2010,** *12*, 7840-7847.
[8] Popov, A. A.; Chen, C.; Yang, S.; Lipps, F.; Dunsch, L. *ACS Nano* **2010,** *4* (8), 4857-4871.

Cooperation: [1]Hefei National Laboratory for Physical Sciences at Microscale & Department of Materials Science and Engineering, Hefei (China); [2]Institute of Physical Chemistry and Chemical Physics, STU Bratislava (Slovakia); Colorado State University, Fort Collins (USA); University of Southern Mississippi, Hattiesburg (USA)

Funding: Alexander von Humboldt foundation and Chinese Scholarship Council

Towards controlled graphene properties: Direct synthesis on dielectrics and Tuning via stress

F. Ding, J. X. Ji, Y.F. Mei, K. Dörr, A. Rastelli, O. G. Schmidt, M. H. Rümmeli, A. Bachmatiuk, A. Scott, G. Cuniberti, B. Büchner

Interest in graphene since its isolation in 2004 has rapidly escalated. It has been described as nature's thinnest elastic material and its exceptional mechanical and electronic properties make it an extremely exciting material. Within the realm of electronics, it is its one atoms thickness, planar geometry, high current-carrying capacity and thermal conductivity and potential to open a gap when existing as a narrow ribbon that hold particular promise. These features make it ideally suited for further miniaturizing electronics to form ultra-small devices and components for future semiconductor technology.

In order for graphene to realize its potential in electronics various obstacles need to be overcome. One of the more important aspects is its actual synthesis. Various routes exist to synthesize graphene; however, most are not best suited for integration into current silicon technology. The primary routes are through graphite exfoliation, epitaxial graphene, graphene oxide and chemical vapor deposition. Most of these routes require the graphene to be transferred onto a dielectric or, as in the case of SiC, require high temperatures. To use graphene as the basis of field-effect transistors at room temperature one needs to modify graphene's semi-metallic nature so as to open a band gap. When existing as narrow strips (nanoribbons) quantum confinement effects lead to band gap formation. Most band gap engineering routes use multiple lithographic steps to fabricate a graphene device. This leads to contamination and disorder to the flake. Dry lithography-free techniques can help, nonetheless technical difficulties still remain. Another approach is chemical modification, for example, graphene oxide in which hydroxyl and other chemical groups attach to graphene. Although the technique is able to lift the degeneracy of the π band at the Fermi level of graphene, it is difficult to control its electronic properties and avoid defect formation.

A more attractive route to control graphene's properties is through mechanical strain engineering which modifies graphene's geometrical structures. For example, substrate-induced sublattice symmetry breaking in expitaxially grown graphene can give rise to energy gaps; scanning tunneling microscopic studies show evidence for strain-induced spatial modulations in the local conductance of graphene on SiO_2; strain with triangular symmetry induces strong gauge field that effectively act as a uniform magnetic field exceeding 10 T. However most of these experiments are based on graphene layers with fixed static strain. Thus, new techniques allowing for *strain on demand* are quite important in order to intentionally tune and understand the interplay between geometry and electronic properties of graphene.

Uniaxial strain on graphene has been experimentally controlled by bending graphene on a plastic substrate, and using Raman spectroscopy to probe its phonons. However, this bending-substrate geometry is not practical for many experiments. Moreover, uniaxial strain moves the relative positions of the Dirac cones and induces a significant influence in the intervalley double-resonance processes. Thus, biaxial strain, which ensures a planar-substrate geometry and avoids complicate perturbations to the Dirac cones, would be more suited to control the graphene's properties.

Recently we developed a method by utilizing a piezoelectric substrate to control the properties of micro-/nanostructures. [1-2] The same approach has been successfully applied to the strain engineering of single layer graphenes (SLG). [3] We use a 300 μm $[Pb(Mg_{1/3}Nb_{2/3})O_3]_{0.72}$ - $[PbTiO_3]_{0.28}$ (PMN-PT) substrate overgrown with a thin ($\sim$ 20 nm) epitaxial layer of $La_{0.7}Sr_{0.3}MnO_3$ (LSMO) acting as top contact, see Fig. 1. The backside is coated with gold. A bias voltage *V* applied to the PMN-PT results in an out-of-plane electric field *F* which leads to an in-plane strain $\varepsilon_{||}$. After the deposition of a 1 μm-thick SiO_2

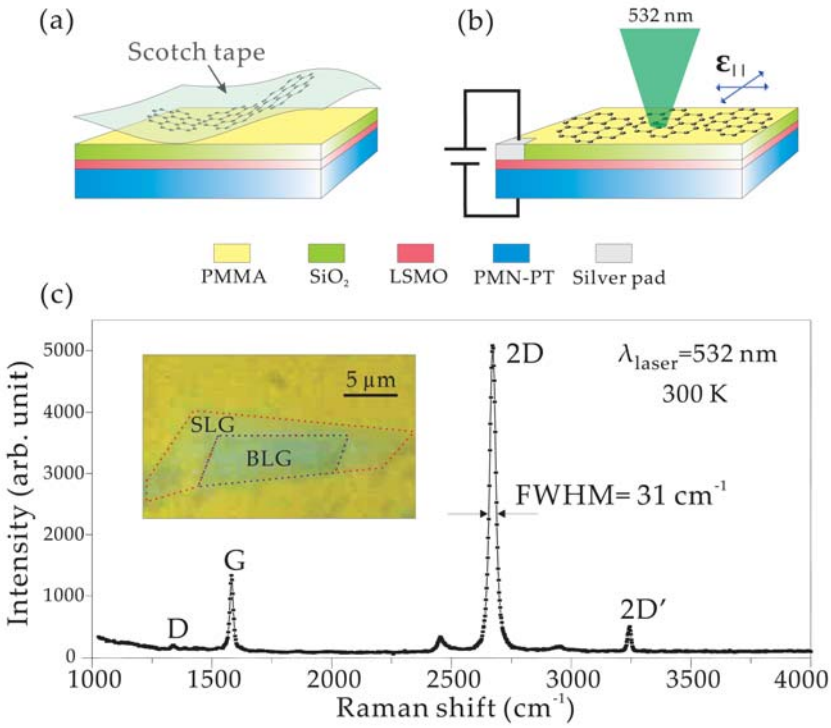

Fig.1: (a) Mechanical cleavage technique with a scotch tape is used to fabricate graphene which is then transferred, using a thin layer of PMMA as glue, onto a SiO_2/LSMO covered PMN-PT substrate. **(b)** Schematic drawing of the electro-mechanical device used to apply in-plane biaxial strain to the graphene. **(c)** Typical Raman spectrum (measured at 300 K) of SLG that is transferred onto a piezoelectric substrate. The inset is an optical microscopy image of the SLG as well as of a BLG (bilayer graphene), indicating the good optical contrast.

layer, the substrate is spin-coated with a 60 nm-thick PMMA (polymethyl methacrylate) layer. We fabricate the graphene samples from highly ordered pyrolytic graphite (HOPG) by mechanical cleavage with the scotch tape technique. The tape is then placed onto the substrate followed by a baking process at 120 °C for 10 min [Fig. 1(a)]. The glue-like PMMA layer becomes solid and the graphene layers are transferred onto the piezoelectric actuator [Fig. 1(b)]. The thickness of the interfacial SiO_2/PMMA layers has been carefully optimized to visualize the SLGs under an optical microscope.

Figure 1(c) shows the typical Raman spectrum (measured at 300 K) of a SLG after transfer onto the piezoelectric substrate. The characteristic Raman features are the so-called *D*, *G*, 2*D*, and 2*D′* peaks, which locate at 1339 cm^{-1}, 1581 cm^{-1}, 2671 cm^{-1}, and 3245 cm^{-1}, respectively. Many of the measurements on graphene need to be performed at low temperature. The advantage of using PMN-PT crystal is that it is capable of exerting either compressive or tensile stresses at very low temperature. Figure 2(a) presents the color-coded intensity map of the Raman peaks of one SLG sample as a function of the voltage *V* applied to the PMN-PT actuator (measured at 15 K). *V* is swept several times between -550 ~ V and 1100 ~ V with steps of 20 ~ V, to demonstrate the reversibility of the strain tuning technique. The maximum voltage is only limited by our power supply, in fact, with a thinner PMN-PT substrate it is possible to achieve the same out-of-plane electric field *F* (therefore, the same in-plane strain $\varepsilon_{||}$ with much smaller voltage. For $V<0$ the graphene experiences an in-plane tension (T) and the Raman peaks show roughly a linear shift to lower frequency, as reported before. In-plane compression (C) on the graphene is also feasible with this piezoelectric actuator, just by applying a positive voltage $V>0$ to the substrate. From Fig. 2(a) we do not see any hysteresis over multiple compressing/stretching cycles.

The Grüneisen parameters describe the strain sensitivity of the phonon frequencies, and are thus an important fundamental set of parameters for graphene. There have been

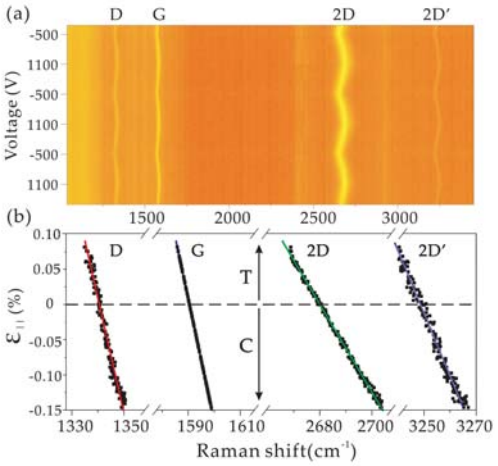

Fig. 2: (a) Color-coded intensity map of the Raman peaks of one SLG sample as a function of the voltage applied to the PMN-PT actuator. The Raman spectra measured at different strain are fully reproducible over multiple compressing/stretching cycles without hysteresis **(b)** D, G and 2D peaks plotted as a function of the biaxial strain $\varepsilon_{||}$, the solid lines are linear fits. Both tensile strain (T) and compressive strain (C) are feasible with the piezoelectric actuator.

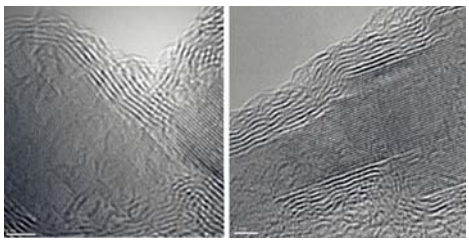

Fig. 3: Multilayer graphene synthesized over MgO from cyclohexane at 775 °C and 100 mbar. The attachment of graphene layers to the (100) oxide step edges can be observed.

several attempts to measure the Grüneisen parameters under uniaxial strain or hydrostatic strain. As discussed before the *D*, and 2*D* peaks are zone-boundary phonons activated by intervalley double resonances, the relative movement of the Dirac cones changes the phonon wave vector we are probing. Therefore, it would be more suitable to measure the *D* mode Grüneisen parameter under biaxial strain. After the strain calibration by the movement of *G* mode,[3] we can plot the strain-dependent shifts of all Raman peaks in Fig. 2(b). All peaks show smooth and linear shifts with biaxial strain, indicating that neither slippage nor corrugation of the graphene occurs during the experiment. Linear fits of all data (under either compressive or tensile strain) yield the Grüneisen parameters $\gamma_D = 1.8$, $\gamma_D = 2.30$, $\gamma_{2D} = 2.98$, and $\gamma_{2D'} = 1.73$. Our results are in good agreement with values derived from first-principles calculations for graphene, and experimental values for carbon materials under hydrostatic pressure (for example, carbon fibers and graphite), suggesting that graphene has similar strain dependencies of the Raman frequencies with graphite. There are some differences between our results and the values derived from uniaxial experiments, which might be explained by the reasons stated above. In the experiments we found different strain sensitivities of the *D* mode and its overtone 2*D* mode, i.e., different Grüneisen parameters. This peculiar phenomenon has been theoretically predicted for two-dimensional graphite. Our experimental studies [3] suggest that the defect-activated *D* mode is in fact associated with intervalley double-resonance scattering with two different phonon processes. The inelastic scattering by a phonon and the elastic scattering by a defect can happen at reversed time sequences, thus involving phonons with different wavevectors. The 2*D* mode, however, does not need defects for its activation and only involves the elastic scattering process. The linewidth analysis of the *D* and 2*D* modes at different applied strain supports this conclusion.[3]

Although we have shown the potential of graphene strain engineering via piezoelectric actuation there exists a technical drawback, similar to the for graphene based FETs, namely the need to transfer the material onto the piezoelectric material (or gate dielectric in the case of FETs). Transferring graphene generally leads to damage and impurity deposition which can adversely affect its performance. For example the PMMA gluing layer in aforementioned technique can be a drawback when performing STM analysis. Thus, the fabrication of graphene devices with atomically uniform dielectrics which can provide a uniform electric field and/or uniform stress induction across the active region is attractive. To this end we are developing thermal CVD techniques to deposit graphene directly on dielectrics at temperatures below 500°C. In Fig. 3, a variety of micrographs are seen which show we are able to grow graphene flakes on the surface of magnesium oxide and tune the growth from single to multi layers. The multi layers shown in the overview of Fig. 3(a) are grown from cyclohexane at 775°C and 100 mbar. With these conditions, the reaction stops when the catalyst is fully encapsulted by graphitic layers. We found that the number of layers can increase up to nine. In Fig. 3(c) we highlight the closely spaced parallel lattice fringes of the crystals are those of (100) planes on top of which there is epitaxial graphitic carbon. Furthermore, as indicated by the arrow, the multilayers are ubiquitously anchored into step edges on the (100) surfaces. We propose that, similar to observations in silicon carbide growth, these step sites initiate the growth of graphitic layers. We argue that these step sites are not only nucleation sites, but also growth sites because growth appears to stop once the particle is fully encapsulated. In this regard, this work corroborates previous studies suggesting the cooperative role of oxide supports in the growth of multiwalled carbon nanotubes. We also investigated zirconium oxide to further elucidate the atomic surface structure required for graphitic synthesis on oxides. This catalyst has recently been extensively explored for the synthesis of carbon nanotubes. In our case, the synthesis of graphitic layers is performed on nanocrystallites which following the reaction are in the baddeleyite form and the graphitic layers are anchored on a face with (020) at its surface normal.

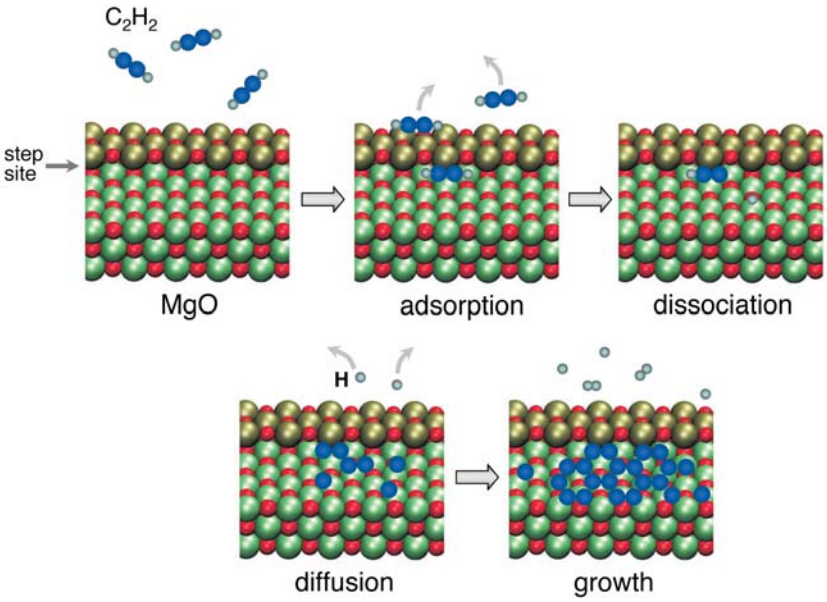

Fig. 4: Proposed growth processes for graphene at step sites on oxides. C_2H_2 is preferentially adsorbed at step sites, where it dissociates, therafter H diffuses away and finally carbon addition leads to graphene growth. (Blue = carbon, gray = hydrogen, red = oxygen, green/gold = Mg).

Preliminary first principles density functional theory investigations using MgO (100) surfaces with step sites as a model system for oxides show acetylene does not easily adsorb on the surface but does so more readily at steps sites. More over, acetylene dissociation on the surface is shown to be endothermic whilst at a step site the process is exothermic. Complimentary diffusion studies show a diffusion barrier of ca. 0.38 eV for C and 0.2 eV for H over an oxygen atom on the MgO (100) surface. This points to C remaining on the surface whilst H simply flies away. We propose a graphene formation mechanism involving four distinct sub-process; the adsorption of the carbon feedstock molecules on the substrate surface, dissociation of hydrogen from the precursor, surface diffusion and addition of carbon atoms to the network. These sub-processes are shown in Fig. 4.

Conclusions

In conclusion we have achieved several milestones towards the controllable modification of the graphene properties. First, we demonstrate that tunable modification of the graphene Raman modes can be realized by applying external biaxial strains. The experiment utilizes a newly developed piezoelectric actuator-based technique. The key mechanical characteristics of graphene, i.e., the Grüneisen parameters, are studied under biaxial strain. Combining graphene with the piezoelectric actuator promises new opportunities to study and control the strain-related behaviors of graphene, such as the ballistic conductance, the basal-plane hydrogenation, and the thermal conductivity, with unprecedented details. Second, we are aiming at the direct synthesis of graphene on dielectric substrates, which could avoid the use of PMMA gluing layer and provide a uniform electric field and/or uniform stress induction across the active region. Regards the thermal CVD investigations, our experimental and theoretical data indicate high *K* dielectrics have potential for the catalytic formation of graphene via thermal CVD at temperatures below 500°C.

[1] T. Zander *et al.*, Optics Express **17**, 22452 (2009).
[2] F. Ding *et al.*, Phys. Rev. Lett. **104**, 067405 (2010).
[3] F. Ding *et al.*, Nano Letter **10**, 3453 (2010)

Cooperation: TU Dresden, Oxford Univ., Chinese Academy of Sciences, MPI für Festkörperforschung. We acknowledge Andreas Herklotz, J. D. Plumhof for fruitful discussions.

Funding: DFG RU 1540/11-1, CAS-MPG Joint Scholarship, NSFC China (60625402), Alexander von Humboldt Foundation.

Transformations in glassy CuZr-based alloys

S. Pauly, S. Gorantla, T. Gemming, U. Kühn, L. Schultz, and J. Eckert

Monolithic bulk metallic glasses (BMGs) are known to be extremely prone to shear localisation upon mechanical loading. Macroscopically, this behaviour reflects in the formation of so-called shear bands, which have characteristic thicknesses of tens of nanometres [1]. The operation of shear bands becomes apparent once their propagation creates a shear step on the surface of the specimen. Even though the strain within these shear bands is surprisingly high ($\varepsilon \approx 10$) [2] the low shear band density leads to catastrophic failure without detectable plastic strain, especially under tensile loading conditions. In order to exploit the unique combination of mechanical properties like high strength, large elastic limit and low Young modulus for instance in structural applications, the deformation behaviour of BMGs has to be understood and ways have to be found to overcome their intrinsic brittleness.

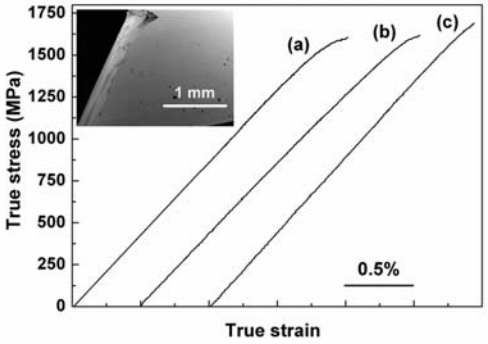

Fig. 1: Room temperature true stress-strain curves in tension and surface of the material after fracture. **(a)** $Cu_{47.5}Zr_{47.5}Al_5$, **(b)** $Cu_{47}Zr_{47}Al_6$ and **(c)** $Cu_{46}Zr_{46}Al_8$ alloys tested at a strain rate of 1×10^{-4} s^{-1}. Next to a marginal ductility the samples show work hardening. The inset displays the typical sample surface after fracture. No shear steps can be seen.

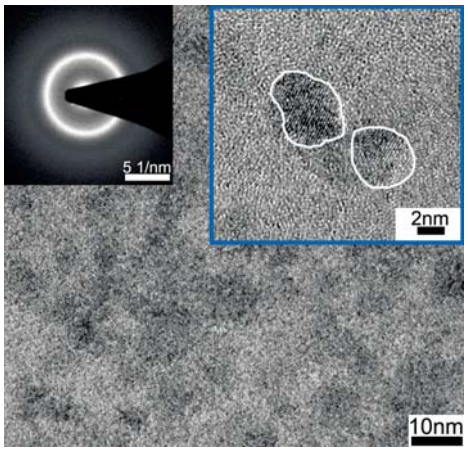

Fig. 2: Microstructure of an as-cast $Cu_{46}Zr_{46}Al_8$ specimen. The cloud-like contrast in this low-resolution TEM micrograph may arise from the microstructural heterogeneity of this alloy family. Electron diffraction gives no hint for the presence of crystalline phases (left inset). However, at high magnification 2 – 5 nm large, scattered lattice fringes become apparent (right inset).

In principle there are two stages of shear localisation at which one can interfere in order to postpone fracture: either at the early stage of shear band evolution or at a later stage during propagation of existing shear bands. The latter approach has been successfully implemented for BMG matrix composites, in which a crystalline phase is embedded in a glassy matrix [3]. Blocking, deflection and substantial branching of shear bands has been shown to significantly enhance the plastic strain in these composites [3]. However, to date no mechanisms are known, which could impede and retard the generation of shear bands in monolithic BMGs at the early stages of their nascence.

The current understanding of how shear bands evolve in BMGs is based on the concept of so-called shear transformation zones (STZs). These entities consist of up to several hundreds of atoms [4] and represent the fundamental units of plasticity [5]. Upon shearing, the atoms of a given STZ rearrange in a cooperative manner passing through a transition state. The latter configurational state becomes "jammed" and thus renders this rearrangement irreversible –or plastic [6]. The formation of a shear band is the result of the percolation of STZs in each others' direct vicinity [6] and their lateral expansion [7].

Surprisingly, in the case of certain $(Cu_{0.5}Zr_{0.5})_{100-x}Al_x$ bulk metallic glasses (e.g. x = 5, 6, 8) there is a clear deviation from linearity at high stresses upon tensile deformation, which is in contrast to the typical brittleness of BMGs (Fig. 1). As the inset of Fig. 1 shows, this small ductility is not accompanied by shear steps, which means shear bands do not appear to be the carriers of plastic deformation in the present case. Instead, transmission electron microscopy (TEM) reveals that in these alloys, which are glassy apart from sparse nanocrystals with diameters around 2-5 nm (Fig. 2), nanocrystals precipitate and substantially grow during deformation (Fig. 3 (a)). Furthermore, some of these crystals exhibit a contrast reminiscent of twinning. The Fast-Fourier-Transformation (FFT) of high-resolution TEM images clearly reveals that the nanocrystals consist of the B2 CuZr phase (Pm-3m) (Fig. 3 (c)). The larger nanocrystals undergo twinning, which is corroborated by the occurrence of additional diffraction spots in the corresponding FFT (Fig. 3 (b)). It is noteworthy that the B2 CuZr phase is thermodynamically stable only at temperatures above 988 K and should not precipitate at room temperature [8].

In the following, this unique deformation mechanism is discussed in the framework of the potential energy landscape (PEL) theory [9,10]. The potential energy function of BMGs is relatively complex and consists of broad minima, so-called inherent states and smaller undulations, which are separated by low-energy barriers (Fig. 4 (a)) [11]. Upon loading, the external elastic stress field is superimposed on the potential energy function of the system (Fig. 4 (a)). This effectively reduces the potential energy barrier, E_a, between two inherent states and biases flow of the material in the respective direction (Fig. 4 (a)). Moreover, simulations show that elastic energy flattens out the minima [12]

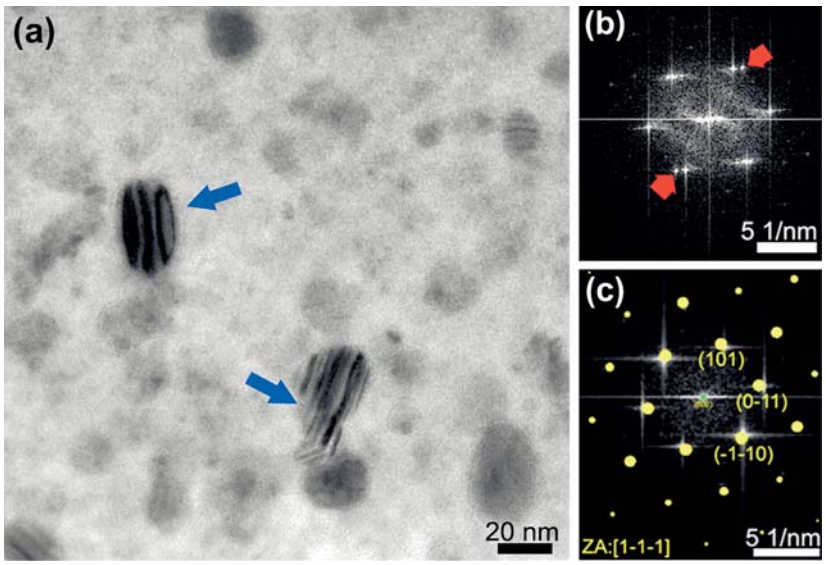

Fig. 3: Microstructure of a $Cu_{47.5}Zr_{47.5}Al_5$ specimen deformed to fracture. **(a)** The low-resolution TEM micrograph reveals the abundance of nanocrystals with sizes between 10 – 50 nm after fracture. Some of these nanocrystals show a diffraction contrast typical of twins. **(b)** The FFT of the twinned region produces additional diffraction spots corroborating the presence of twins. **(c)** In the un-twinned regions the FFT can be indexed assuming the B2 CuZr phase (zone axis [1-1-1]).

and thus reduces the energy barrier height (Fig. 4 (b)), which has a strong impact on the elastic constants of the material as will be shown below. The simplest function to capture the potential energy landscape is a sinusoidal function, similar to a Frenkel landscape [13]:

$$\frac{\phi}{\phi_0} = \sin^2\left(\frac{\pi\gamma}{8\gamma_c}\right), \tag{1}$$

where Φ is the potential energy, Φ_0 is the amplitude of the energy function, γ is the shear strain and γ_c is a critical shear strain limit. The second derivative of the potential energy with respect to the shear coordinate (representing the curvature of the potential energy function at $\gamma = 0$) yields the instantaneous shear modulus, G:

$$\left.\frac{d^2\phi}{d\gamma^2}\right|_{\gamma=0} = G = \left(\frac{\pi^2}{8\gamma_c^2}\right)\phi_0, \tag{2}$$

This means the flattening out of the inherent states during loading represents a decrease of the shear modulus, which facilitates structural rearrangements or flow. The total barrier height, which has to be surmounted to initiate structural rearrangements, $\Delta F(T)$, is the product of the amplitude of the potential energy function, Φ_0, and the size of the cooperatively rearranging zone, Ω [14]:

$$\Delta F(T) \equiv \phi_0\,\Omega = \frac{8\gamma_c^2}{\pi^2}\,G\Omega, \tag{3}$$

Viscosity, η, can be expressed as [13]:

$$\eta = \eta_0 \exp\left\{\frac{\Delta F(T)}{k_B T}\right\}, \tag{4}$$

the pre-exponential constant η_0 being the viscosity at infinite temperature, $\Delta F(T)$ being the temperature dependent activation energy, k_B being the Boltzmann constant and T being the temperature. Inserting eq. (3) into eq. (4) establishes a link between the flow behaviour (viscosity) and the shear modulus. In short, the elastic energy imposed onto the system reduces the shear modulus of the BMG and biases structural rearrangements and thus reduces the viscosity.

The structural rearrangements can now lead to two competing processes, namely the formation of STZs and, as in the present case, to the precipitation of B2 CuZr nanocrystals (Fig. 3 (a)). The fact that the thermodynamically unstable B2 phase forms instead of the equilibrium phases $Cu_{10}Zr_7$ and $CuZr_2$ implies that kinetics play the crucial role. Since the B2 phase is polymorphous to the composition of the glass there might be a similar coordination in the glass as in the B2 phase itself. Consequently, only marginal atomic

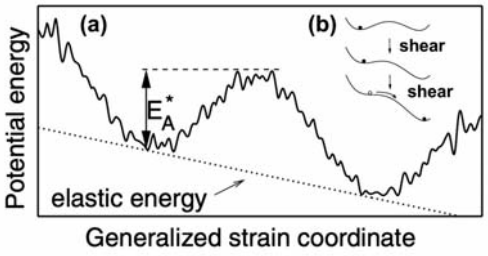

Fig. 4: Influence of shearing a simulated glass on the topography of its PEL. **(a)** Elastic energy tilts the PEL and thus decreases the potential energy barrier, E_a, separating two inherent states (IS). Taken from Ref. [17]. **(b)** Shearing furthermore flattens out some IS and with it reduces the energy barrier. Structural rearrangements are biased towards more stable states. Taken from Ref. [12].

rearrangements are required to precipitate B2 CuZr crystals during deformation, which rivals the minor atomic rearrangements disemboguing in STZs. The volume change associated with the crystallisation and the differences in the elastic properties most likely reduce the stress concentrations in the glass, which would otherwise lead to the evolution of additional STZs in their vicinity. As a consequence the amount of STZs, which form in the course of deformation, is effectively reduced. Besides, the nanocrystals represent obstacles for the propagation of a shear band at the later stages of deformation and hence fracture is postponed. A similar effect is achieved by the twinning process, which is found in the larger nanocrystals. The volume changes during this diffusionless transformation also interact with the stress fields in the matrix and impede the generation and subsequent percolation of STZs into shear bands.

B2 CuZr is a shape memory alloy exhibiting a reversible martensitic transformation [15]. However, due to the small grain size, the confinement by the rigid glassy matrix and due to the dissolved Al atoms the B2 phase is distorted and the deformation-induced phase transformation rather proceeds in form of twinning. Since both precipitation of nanocrystals and twinning consume energy, the formation of STZs and with it the formation of detrimental shear bands is retarded and macroscopic plasticity combined with work hardening can be measured during tensile deformation [16].

The development of glassy alloys derived from shape memory phases such as the present Cu-Zr-Al BMGs, could open up an alloy design strategy for the development of advanced BMGs with an increased tolerance towards failure.

[1] C. A. Schuh et al., Acta Mater. **55** (2007) 4067.
[2] T. Masumoto et al., Acta Metall. **19** (1971) 725.
[3] J. Eckert et al., Adv. Eng. Mater. **9** (2007) 443-453.
[4] D. Pan et al., PNAS **105** (2008) 14769.
[5] A. S. Argon, Acta Metall. **27** (1979) 47.
[6] M. L. Falk et al., Phys. Rev. E **57** (1998) 7192.
[7] S. Pauly et al., J. Appl. Phys. **106** (2009).
[8] K. J. Zeng et al., J. Phase Equilibria **15** (1994) 577-586.
[9] F. H. Stillinger, Science **267** (1995) 1935.
[10] P. G. Debenedetti et al., Nature **410** (2001) 259-267.
[11] J. S. Harmon et al., Phys. Rev. Lett. **99** (2007) 135502.
[12] D. L. Malandro et al., J. Chem. Phys. **110** (1999) 4593.
[13] W. L. Johnson et al., MRS Bull. **32** (2007) 644.
[14] W. L. Johnson et al., Phys. Rev. Lett. **95** (2005) 195501.
[15] Y. N. Koval et al., Scripta Metall. Mater. **27** (1992) 1611.
[16] S. Pauly et al., Nature Mater. **9** (2010) 473-477.
[17] S. G. Mayr, Phys. Rev. Lett. **97** (2006) 195501.

Cooperation: Xi'an Jiaotong Univ. (China), Yonsei Univ. and Sejong Univ. (South Korea), HASYLAB at DESY Hamburg.

Funding: The Global Research Laboratory Program of the Korean Ministry of Education, Science and Technology and the program "Promotionsförderung des Cusanuswerks".

Damascene light weight metals

T. Marr, J. Freudenberger, A. Kauffmann, J. Scharnweber[1], U. Siegel, D. Seifert, T. Wolf, H. Klauß, M. Frey, H.-P. Trinks, S. Neumann, C. Rodig, D. Geißler, U. Kühn, U. Martin[2], C.-G. Oertel[1], W. Skrotzki[1], J. Eckert and L. Schultz

In a broad field of applications, as e.g. for mobile applications, transport systems and the required components as well as for optimised light weight design elements, there is a huge demand for materials with a high specific strength (strength divided by the mass density). One possible way to improve strength is to refine the materials microstructure. A variety of such ultra-fine grained (ufg) or even nanocrystalline (nc) materials is available in laboratory scale, however, useable semi-finishes products with the right property combination are commonly not yet available. Research on nc materials has been found to reveal some exciting combinations of properties. In this context, magnetic, superconducting, biomedical as well as mechanical properties are strongly affected by a nc microstructure. For example, the saturation magnetisation as well as the Curie temperature [1] of Ni can be reduced significantly when the microstructure becomes nanocrystalline. An increase in cell proliferation by more than one order of magnitude has been observed for commercially pure Titanium when the grain size is reduced from 4,5 μm to 200 nm [2]. The mechanical properties also undergo a remarkable change when the microstructure is refined to the nc range. In particular, some nc materials exhibit a high ultimate tensile strength while retaining a reasonable elongation [3, 4], which is essential for their applicability. Deforming bulk, coarse grained materials to very high strains is one possibility to reaching a nc, or an ultra-fine grained microstructure [5]. Severe plastic deformation allows to build large quantities of ufg materials without impurity issues, as it is the case for compacting nc powders to dense work pieces.

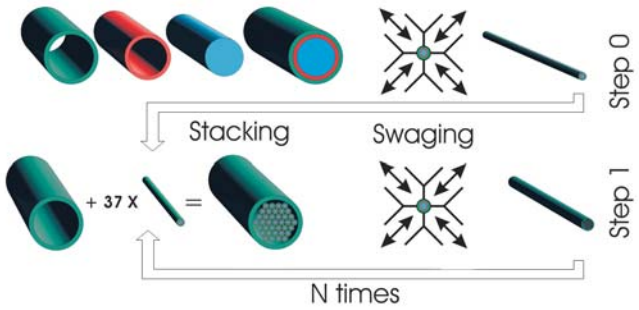

Fig. 1: Repeatable swaging and bundling processing route for composite materials, here: Ti tube (green), Nb tube (red), Al rod (blue).

The presently used technology allows to producing semi-finished parts in the shape of wires with tuneable density and high specific strength [6]. In this respect, use is made of the good mechanical properties of ufg microstructures, which is combined with the ability to produce a common semi-finished product. One further goal is to improve the specific strength, which is of great interest in constructive light weight design. This already suggests the use of common light weight metals such as Ti, Al or Mg for processing. Fig. 1 shows the processing technique for a macro composite consisting of a Ti tube (green), a Nb tube (red) and an Al rod (blue), which is repetively swaged up to a logarithmic strain of $\eta = 8.4$. The composite is cold deformed to $\eta = 4.3$, cut into 37 pieces, bundled and stacked in a Ti tube and swaged again. The process is theoretically arbitrarily repeatable. It reminds on the production of the so called damascene steel in past centuries. However, the two-dimensionality of stacking and the application to light weight metals are rather new.

The heavy cold work causes a strong grain refinement of the starting materials (see Fig. 2). In the processed composite, Niobium acts as a diffusion barrier. Consequently,

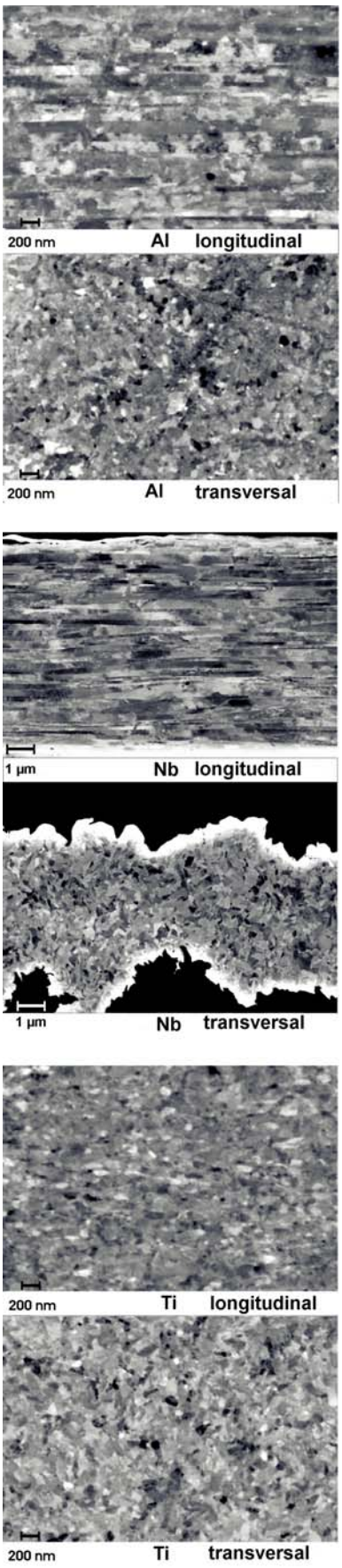

Fig. 2: Microstructure of the constituents after deformation up to $\eta = 8.4$. Grain sizes in cross section: Al: ~0.2 μm, Nb: ~0.2–0.5 μm, Ti: ~100 nm.

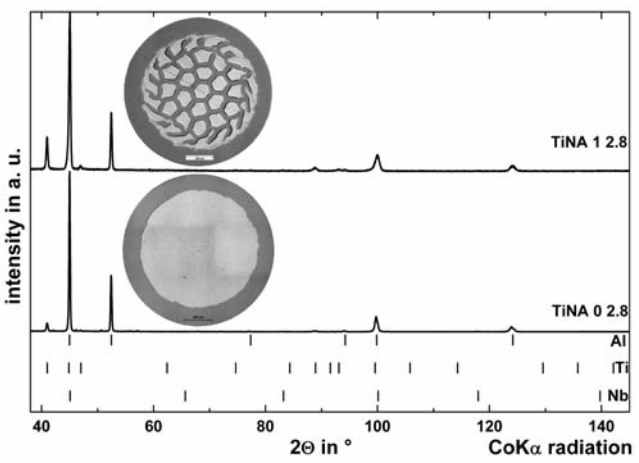

Fig. 3: X-Ray diffraction analysis of the processed wires after $\eta = 4.3$ and $\eta = 8.4$. All reflections can be identified by the starting materials and no formation of intermetallic phases can be detected.

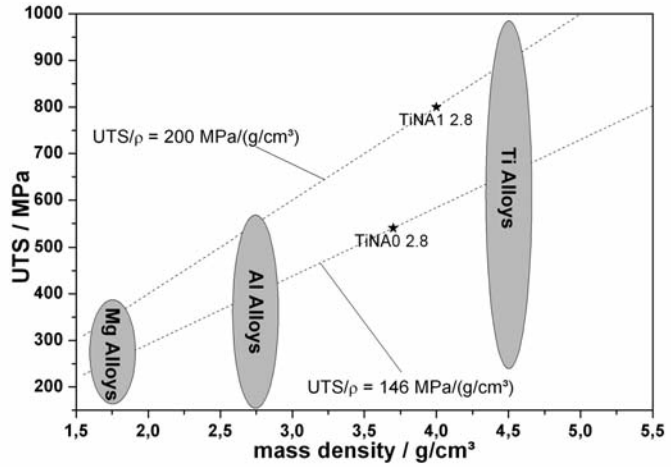

Fig. 4: UTS of different materials including the present composite wires. The strength after deformation up to $\eta = 8.4$ is equivalent to a specific strength of 200 MPa/(g/cm^3).

no intermetallic phase formation of Ti and Al can be detected by X-Ray diffraction after deformation (Fig. 3). The mechanical properties of the wires are shown in Fig. 4 in comparison to other materials. After being deformed to a logarithmic strain of $\eta = \ln\left(\frac{A_0}{A_E}\right) = 8.4$ (where A_0 and A_E are the starting and final cross sectional area), the wires show an ultimate tensile strength of 790 MPa, whereas 540 MPa were obtained after deformation up to $\eta = 4.3$. These values are shown in Fig. 4 with respect to their absolute mass density. The obtained strength of 790 MPa is equivalent to a specific strength of 200 MPa/(g/cm^3). This value is comparable to the upper limits of conventional Ti, Al or Mg alloys (refer to the upper dashed line in Fig. 4) and is therefore in direct competition with the conventional high strength alloys of the different classes. These values are promising, since the used Ti, Nb and the Al alloy are easily available. Furthermore, there is potential of optimisation with respect to e.g. reduction of the grain size, an increase of the frequency of high angle grain boundaries due to re-bundling and during further cold working, as well as the possible introduction of heat treatments during or after processing.

There are a number of properties that are changed intrinsically by the used processing route, such as: dislocation density, mass density, elastic constants, texture, grain size and distribution, the frequency of high and low angle grain boundaries as well as the total amount of internal interfaces. These properties interact in a rather complex way. Although the bulk properties are easily accessible, their individual character as well as their interaction is yet not well understood. Forthermore, the characterisation of the microstructure of the processed wires is a challenging task. One main goal for future activities deals with the characterisation of the mentioned features, including their distinctness, as well as the characterisation of their interactions. This understanding of the mechanisms will allow a further improvement of the specific strength.

[1] R.Z. Valiev et al., Phil Mag B, 75(6) (1997) 803
[2] Y. Estrin et al., J Biomed Mater Res 90A, (2009) 1239
[3] H. Gleiter, Progr Mat Sci, 33, (1989) 223
[4] C.C. Koch et al. J Mater Sci 45, (2010) 4725
[5] Bulk nanostructured materials, Eds. Michael J. Zehetbauer, Yuntian T. Zhu, WILEY-VCH Weinheim, 2009
[6] T. Marr et al., Adv Eng Mater 12 ,(2010) 1191

Cooperation: [1]TU Dresden, [2]TU Bergakademie Freiberg
Funding: European Union and the Free State of Saxony

Energy storage elements based on hybrid organic/inorganic nanomembranes

C. C. Bof Bufon, J. D. C. Gonzales, D. J. Thurmer, D. Grimm, M. Bauer and O. G. Schmidt

In this work we demonstrate the fabrication of three-dimensional ultra-compact hybrid organic/inorganic energy storage elements, manufactured in parallel on a single chip. The inorganic version of our elements exhibit capacitances per footprint area higher than their state-of-the-art planar counterparts and specific energy comparable with supercapacitors (~0.55 Wh/kg). In addition, the electronic properties of these devices were precisely controlled by incorporating self-assembled molecular layers.

The evident progress in the miniaturization of electronic devices and circuits as well as the substantial reduction of their power consumption gave rise to the concept of Energy Autonomous Systems (EAS). EAS by definition is an electronic system that has been designed to operate as long as possible in any environment providing, elaborating and storing information without being connected to a power grid. Such a system could potentially operate in external natural or industrial environments as well as for in-vivo applications in the diagnostic and therapeutic area. Regarding to the nowadays status-of-the-art, EAS should have the ability to operate with less than hundreds of μW of power within less than some cubic centimeter. Examples of such systems are nomadic devices operating at ultra low power (wireless sensor networks, in-vivo sentinels and actuators, ambient intelligence devices, "smart dust"). EAS can be divided in 4 basic modules: the energy harvester, the energy storage element, the operation module and communication interface.

Over the past decade a lot of research has been dedicated to create new ways for efficient energy harvesting (vibrational, thermal, photovoltaic and RF energy based systems), circuit power management and low power RF modules. However, the available solutions for energy storage are still based on electrochemical batteries which occupy large foot print areas. Several approaches have been described for the development of micro batteries, however, none of them are fully suitable for EAS since criteria like small foot print ($<1 cm^2$), life time (>10 years), high number of charge-discharge cycles (several thousands) and short charging time (1-10) has still not been achieved. As an alternative to batteries, electrostatic storage elements like solid-state capacitors can be an approach to supply energy to EAS. Being an electrostatic element, capacitors have the capability to deliver high power densities for a short period of time in conventional electronic circuits but also supply sufficient energy densities (0.01-1Wh/Kg) for EAS. Due to the nature of the dielectric used, capacitors can be charged very fast (1-60s), perform several thousand charge-discharge cycles and have a life time longer that 10 years. Nevertheless, to reach a minimum level of energy density to operate an EAS, the capacitor has to be made larger than the acceptable criteria for EAS.

Nowadays, self-assembly is widely accepted as a standard technique to generate complex structures on many length scales [1]. One of such self-assembly processes was reported 100 years ago when Stoney noticed that strained metal layers spontaneously "curl up into beautiful close rolls" once they detach from their host substrate[2]. It was not until a decade ago however, that the great potential of this phenomenon was recognized as appropriate for exciting new perspectives and applications in micro- and nanotechnology [3]. The self-rolling of patterned thin layers elegantly combines top-down and bottom-up approaches to generate ordered micro- and nanostructured building blocks of almost arbitrary material combinations on a single chip [4]. Applying the self-rolling phenomenon, however, we achieve an approach that is fully integrative on a chip, and components can be fabricated in parallel using well-established semiconductor processing technologies (see the fabrication scheme in Fig. 1).

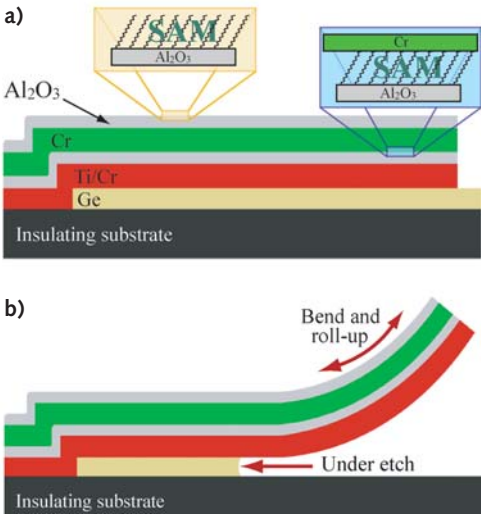

Fig. 1: Fabrication process: **(a)** Deposition of the multi-stack layer. **(b)** The selective etching of the sacrificial layer releases the hybrid nanomembrane to form the roll-up device. **(c)** Illustration of a parallel array of ultra-compact energy storage elements (after [5]).

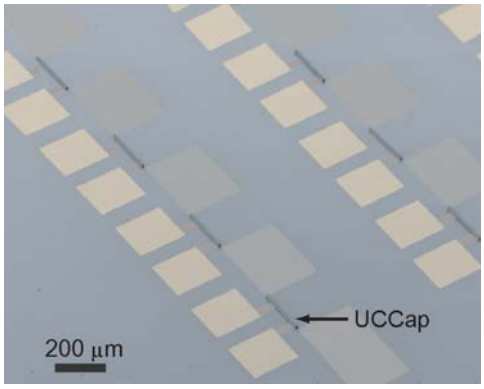

Fig. 2: Typical SEM images of nanomembrane-based UCCaps highlighting the high reproducibility of the process (after [5]).

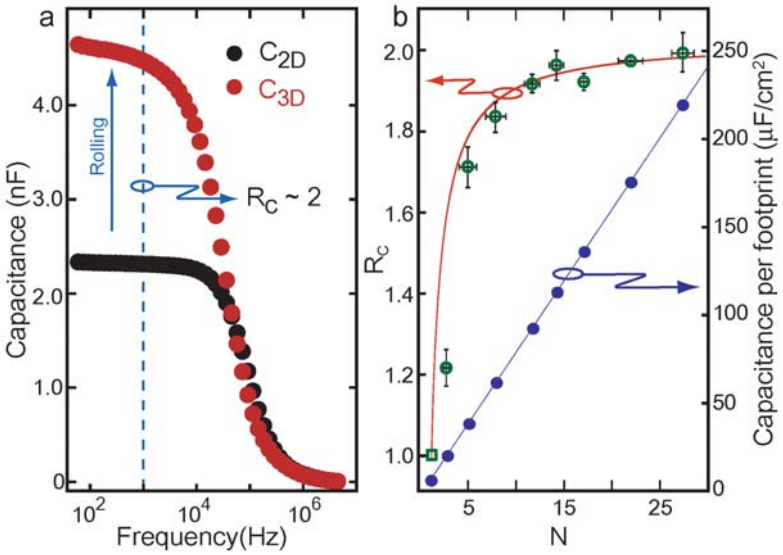

Fig. 3: (a) Increase of the capacitance going from 2D to 3D structures. **(b)** Shows the increase of the capacitance per footprint area (right-axis) and R_c with number of windings N (left-axis), which indicates good agreement with the estimated values. (red solid line). For N>>1, the graph further highlights the convergence $R_C \rightarrow 2$ (after [5]).

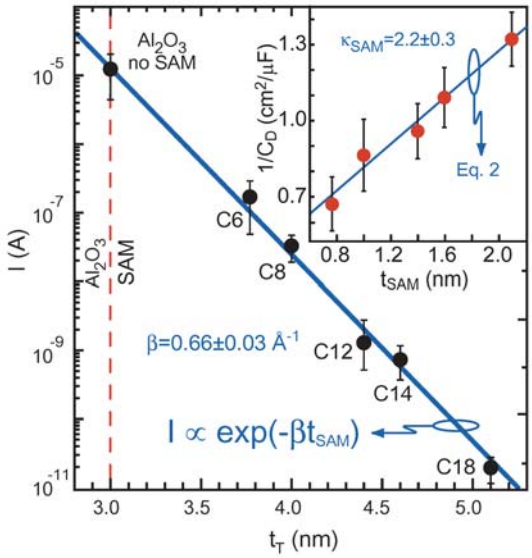

Fig. 4: The control of the UCCaps electrical properties is demonstrated by the dependence of leakage current with the SAM chain length (t_{SAM}). The total dielectric thickness is $t_T = t_{OX} + t_{SAM}$. Upper inset: the device capacitance decreases with increasing SAM chain length (after [5]).

Here, we demonstrate that self-assembly methods combined with standard top-down approaches are suitable for fabricating three-dimensional ultra-compact hybrid organic/inorganic electronic devices, such as self-wound capacitors (UCCaps), manufactured in parallel on a single chip (Fig. 2) [5]. In addition to reducing the device footprint by the rolling process, the bottom metallic plate (red strip in Fig. 1) mechanically touches the top oxide layer so that the final active capacitor area increases. For a large number of rotations (N), this effect is equivalent to connecting two unrolled capacitors in parallel. Figure 3 shows the capacitance increase due to the rolling. To the best of our knowledge, the inorganic UCCaps, based on Al_2O_3 thin layers, exhibit capacitances per footprint area (see Fig. 3b) higher than their state-of-the-art planar counterparts [6] and specific energy comparable with supercapacitors (~0.55 Wh/kg). While their small size may limit their application range to low power systems, apart of being suitable for EAS, we believe that rolled up supercapacitors with high specific energy could find many uses in stand-alone microelectronic systems where other supercapacitor structures would be far too bulky. Additionally, the incorporation of solid-state-electrolytes could lead to ultra-compact batteries extending the application range to system where shorter life time and longer charging periods are acceptable.

Due to the synthetic tailorability of molecular systems, their incorporation in inorganic elements gives rise to novel devices with almost limitless chemical and biological functionalities. To demonstrate this advantage, we have self-assembled phosphonic acid anchor groups (SAM) into the inorganic capacitor structure (Fig. 1) [5]. The integration of organic molecules provides further free parameters to tune the properties and extend the range of applications of the final self-wound device (Fig. 4). Replacing the phosphonic acids by magnetic molecules may represent a route towards organic spin-electronics in the near future.

[1] G. M. Whitesides and B. Grzybowski Science **295** (2002) 2418.
[2] G. G. Stoney Proc. R. Soc. Lond. A **82** (1909) 172.
[3] O. G. Schmidt and K. Eberl Nature **410** (2001) 168.
[4] Y.F. Mei et al. Adv. Mater. **20** (2008) 4085.
[5] C. C. Bof Bufon et al. Nano Letters **10** (2010) 2506.
[6] P. Banerjee et al. Nature Nanotech. **4** (2009) 292.

Cooperation: H. Klauk, MPI for Solid State Research, Stuttgart, Germany
Funding: Nanett-BMBF and AFOSR-MURI

Precise control of thermal conductivity at the nanoscale via individual phonon scattering barriers

P. Chen, F. Pezzoli, M. Stoffel, J. Schumann, I. Mönch, Ch. Deneke, A. Rastelli, O.G. Schmidt

The ability to precisely control the thermal conductivity (κ) of a material is fundamental in the development of on-chip heat management or energy conversion applications. Nanostructuring permits to dramatically reduce κ of single-crystalline materials, as recently demonstrated for silicon nanowires. However, silicon-based nanostructured materials with extremely low κ are not limited to nanowires. By engineering a set of individual phonon scattering nanodot-barriers we have accurately tailored the thermal conductivity of a single-crystalline SiGe material in spatially defined regions as short as ~15 nm. Single barrier thermal resistances between $2\text{-}4\times10^{-9}$ m^2 K/W were attained, resulting in a room temperature κ down to about 0.9 W/m-K, in multilayered structures with as little as 5 barriers. Such low thermal conductivity is compatible with a totally diffuse mismatch model for the barriers, and it is well below the amorphous limit.

Tailoring the thermal conductivity of nanostructured materials with high spatial resolution is a fundamental challenge for micro and nanoelectronics heat management, and for micro/nano scale energy conversion on a chip [1-4]. Previous work on nanoscale thermal transport has demonstrated that in some cases nanostructuring can reduce the thermal conductivity of a material below that of its disordered alloy counterpart [5-7], and can even beat the amorphous limit [8], which for a long time was believed to represent a bound to the minimum attainable thermal conductivity of a material with a given composition [9]. In dislocation-free SiGe/Si multilayered materials however, it has not been clear how low the thermal conductivity can be pushed. A plausible lower bound when the SiGe layers are very thin would be given by a model in which ballistic Si layers are separated by interfaces, or phonon barriers (the thin SiGe regions), where phonons are scattered in a completely diffusive way. This is the diffuse mismatch model, DMM, in the particular case of no acoustic mismatch between the two sides of the interface [10]. In general, however, previous works only showed a weakly diffusive behavior of the interfaces, with layer resistances lower than those predicted by the DMM. This raises the question: is it possible to achieve highly diffusive interfaces in SiGe/Si systems? Besides, most previous measurements were performed on systems above 1 μm thick and comprising over a hundred periods. Thus, it was unclear whether much thinner systems would still preserve the individually additive character of the single interface resistance, or whether ballistic effects across multiple periods might occur, rendering the concept of thermal conductivity inadequate for such thin regions [11].

We have answered the two questions above, and showed that: (1) highly diffusive interfaces can be achieved in dislocation-free SiGe/Si nanodot systems; and because of this, (2) a well defined thermal conductivity can be accurately tailored for material regions as short as ~15 nm, comprising just a small number of periods.

The studied structures (see sketch in Fig. 1a) consist of 5 and 11 layers of epitaxial Ge nanodots separated by Si spacers with thickness t_{Si}. The first island layer was obtained by deposition of about 6 monolayers (ML) Ge leading to the formation of small {105} faceted islands on top of a 3-4 ML thick wetting layer (Fig. 1c). Dots have an average height of 1.2 ± 0.2 nm and a surface density of $\sim8\cdot10^{10}$ cm^{-2}, with a fractional area coverage of about 70%. In the upper layers, the Ge coverage was reduced in order to prevent the occurrence of misfit dislocations. In comparison with most of the previous works [7,12-14], our multilayers were grown at lower substrate temperature (500°C),

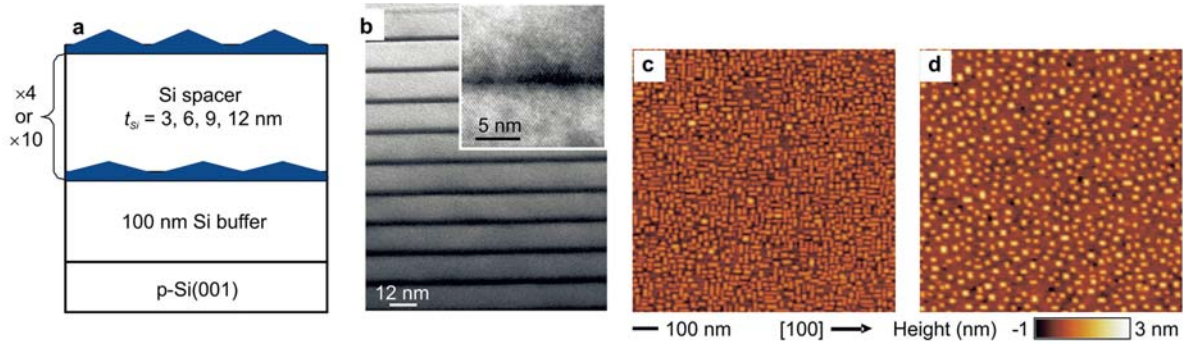

Fig. 1: Sample structure. **a)** Sketch of the self-assembled nanodot multilayers fabricated by molecular beam epitaxy. **b)** Bright field TEM image of a sample with t_{Si} = 12 nm. Dark areas correspond to the Ge layers. The inset shows a high-resolution TEM of a nanodot. **c)** AFM image of a single Ge/Si(001) dot layer prior to overgrowth with Si. d) AFM image of the topmost layer of a sample with t_{Si} = 3 nm.

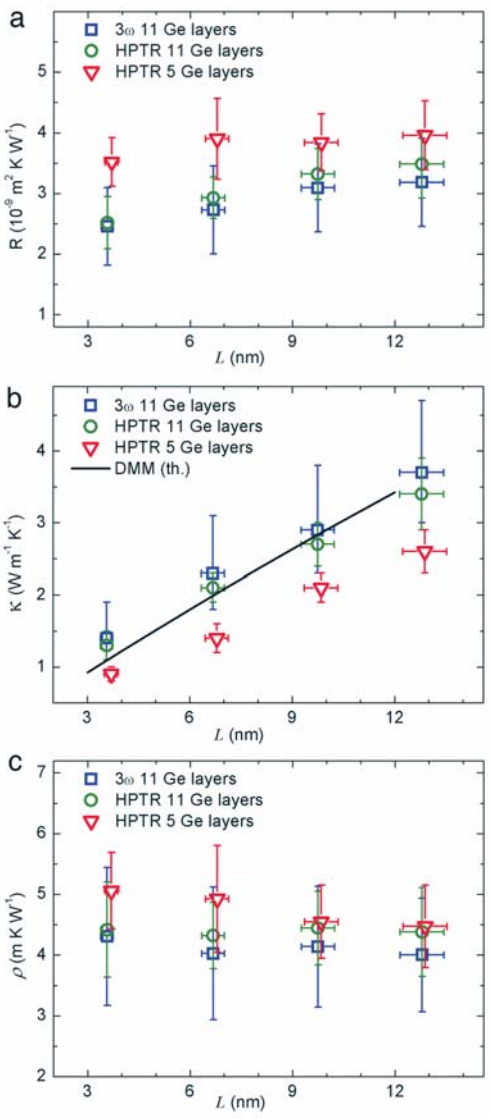

Fig. 2: Thermal response of the Ge nanodot multilayers. **a)** Experimental thermal resistance divided by the number of layers, for the 5 and 11 layer systems, measured by HPTR, and the 11 layer system measured by the 3ω technique, as a function of the average distance between layers, *L*. **b)** Experimental thermal conductivities corresponding to the systems in Fig. 2(a). The solid line is the result of the diffuse mismatch model. **c)** Thermal resistance per barrier, normalized by average amount of Ge in the barrier (given as an effective length), for the systems of Fig. 2(a).

resulting in smaller dots ("hut-" instead of "dome-" and "pyramid-" shaped clusters) with higher Ge content and higher surface densities.

In order to characterize the cross-plane thermal conductivity, κ, of the samples, HPTR measurements were carried out at the University of Bordeaux on the samples with 5 and 11 Ge layers, and independent 3ω measurements were carried out at IFW Dresden on samples with 11 Ge layers, yielding results consistent with those from HPTR. The results are shown in Fig. 2, where the cross-plane thermal resistance per interface *R* (Fig. 2a) and the thermal conductivity of all the samples (Fig. 2b) are plotted as a function of multilayer period thickness *L*. (*L* is estimated as the sum of t_{Si} and the average amount of Ge per dot layer t_{Ge}.)

It is illuminating to normalize the thermal resistance values of Fig. 2a by the average amount of Ge contained in each interface, given in terms of its thickness t_{Ge}. When this is done, one obtains a nearly constant thermal resistivity, of about 4.5 m K W^{-1} for a single layer, independent on the period (Fig. 2c). This strongly suggests that transport through the Si regions is ballistic, and resistance is produced by the independent nanodot layers: each layer acts as an individual barrier, and the total thermal resistance is the sum of the individual barrier resistances. Such a picture is consistent with the fact that the average phonon mean free path in Si is larger than a hundred nm [15]. The phonon mean free path is thus determined by scattering with the SiGe nanodots, which are arranged in individual layers, perpendicular to the direction of heat propagation, and separated by a distance *L* between each consecutive layer. In an overly simplistic view, a fully diffusive barrier will have equal transmission and reflection probabilities of ½, yielding the limit $\lambda \sim L$ for the mean free path. The thermal conductivity can now be evaluated as an integral over frequencies [16], obtaining the DMM limit shown by the solid line in Fig. 2b. The measured thermal resistance associated to one individual interface is around $2.5\text{-}4 \cdot 10^{-9}$ m^2K/W. This is close to the DMM value in the totally diffuse case (see Fig. 2b), and it is 2-3 times larger than the values reported in Refs. [6, 7].

The above implies that a very precise control over the thermal conductivity value of the nanostructured material can be achieved by varying the period length. As a result of the highly diffusive character of the interfaces, we are able to reach the very low thermal conductivity value of (0.9±0.1) W/m-K when using periods of ~3.7 nm (5 nanodot layers separated by 4 Si spacings, with a total thickness of 15.5 nm and an average barrier resistance of $3.5 \cdot 10^{-9}$ m^2K/W in this case). This thermal conductivity is the lowest reported so far for bulk-like Si or SiGe samples, and it is well below the amorphous Si

limit of 2.5 W/m-K [17]. A smaller thermal conductivity of 0.76 W/m-K was reported only for 10-nm-wide Si nanowires [18]. A value of 1.2 W/m-K was independently reported on rough Si nanowires [19].

The additive character of the individual interface thermal resistances allows us to engineer regions with accurately defined values of κ, with good spatial resolution down to the 10 nm level. In our samples, the shortest measured region was ~15 nm thick, consisting of 5 interfaces [20]. This demonstrated ability to tailor thermal conductivity with 1W/m-K precision and a spatial resolution below the 20 nm range is very relevant to the development of integrated miniaturized energy harvesting or thermal management devices, fully compatible with silicon nanoelectronics. The highly diffusive interfaces achieved permit the precise control of thermal conductivity at the local level, via the sole distance between interfaces. A similar approach could be used with other materials, thus extending the range of thermal conductivities available, and possibly being able to simultaneously tailor electronic properties as well.

[1] D. G. Cahill *et al. J. Appl. Phys.* **93** (2003) 793.
[2] A. Shakouri *Proceedings of IEEE* **94(8)** (2006) 1613.
[3] I. Chowdhury *et al. Nature Nanotechnology* **4** (2008) 235.
[4] G. Zeng *et al. Appl. Phys. Lett.* **88** (2006) 113502.
[5] W. Kim *et al. Phys. Rev. Lett.* **96** (2006) 045901.
[6] S. M. Lee *et al. Appl. Phys. Lett.* **70** (1997) 2957.
[7] M. L. Lee *et al. Appl. Phys. Lett.* **92** (2008) 053112.
[8] C. Chiritescu *et al. Science* **315** (2007) 351.
[9] D. G. Cahill *et al. Phys. Rev. B* **46** (1992) 6131.
[10] E. T. Swartz *et al. Rev. Mod. Phys.* **61** (1989) 605.
[11] M. Highland *et al. Phys. Rev. B* **76** (2007) 075337.
[12] J. L. Liu *et al. J. Cryst. Growth* **227-228** (2001) 1111.
[13] J. L. Liu *et al. Phys. Rev. B* **67** (2003) 165333.
[14] Y. Bao *et al. J. Electrochem. Soc.* **152** (2005) G432.
[15] G. Chen *Phys. Rev. B* **57** (1998) 14958.
[16] N. Mingo *Phys. Rev. B* **68** (2003) 113308.
[17] D. G. Cahill *et al. Phys. Rev. B* **50** (1994) 6077.
[18] A. Boukai *et al. Nature* **451** (2008) 168.
[19] A. I. Hochbaum *et al. Nature* **451** (2008) 163.
[20] G. Pernot, M. Stoffel, I. Savic, F. Pezzoli, P. Chen, G. Savelli, A. Jacquot, J. Schumann, U. Denker, I. Mönch, Ch. Deneke, O.G. Schmidt, J. M. Rampnoux, S. Wang, M. Plissonnier, A. Rastelli, S. Dilhaire, and N. Mingo, Nature Materials 9, 491 (2010)

Cooperation: CEA Grenoble, University of Bordeaux-CNRS, Fraunhofer-IPM Freiburg, MPI-FKF Stuttgart

Funding: EU (Nano-thermoelectrics, IRG 39302), ANR (Thermaescape, ANR-06-NANO-054-01, Accatone), (EThNA, ANR-06-NANO-020),(OCTE, ANR-06-BLAN-129), the Conseil Régional d'Aquitaine (projet Photon et Phonons, 2007), the DFG (SPP1386, RA 1634/5-1), the European Regional Development Fund (n. 4212/09-13) and the State of Saxony.

Catalytic and Biocatalytic Microbots

S. Sanchez, A. A. Solovev, S. Schulze, S. M. Harazim, Y. F. Mei and O. G. Schmidt

Introduction

The development of useful micro- or nanomachines which could one day be manipulated inside the human body, remains a challenging dream in nanotechnology and biomedicine [1]. Over the last five years, there has been substantial interest in the use of chemistry to propel tiny engines in a similar fashion that nature uses biochemistry to power biological motors [2,3].

Motor proteins powered by chemical fuel have inspired scientists to design hybrid and synthetic nano/micromachines which efficiently generate locomotion (propulsion power) autonomously from their surroundings (chemical). In eukaryotic cells, kinesin motors convert chemical energy from adenosine triphosphate (ATP) into mechanical energy to move intracellular cargo along microtubules where they "walk" [4]. These impressive molecular motors have inspired scientists to search for versatile nanomachines which can swim in diverse conditions while transporting cargo in a controlled manner.

There are three main challenges that researchers try to conquer when engineering artificial nanomachines: i) efficient *self-propulsion*, demonstrated by the catalytic breakdown of H_2O_2 by Pt [3,5], Ni [6,7] catalysts and catalase enzyme [8] contained in nanomotors; ii) *motion control*, achieved by the incorporation of Ni or Fe segments and subsequently using external magnetic fields to orient the nanomotors [9,10] and; iii) the *development of useful task* such as the transport of cargo in fluid [11].

Rolled-up microtubes containing a Pt catalyst [10] or catalase enzyme [8] in their inner layer can trigger the breakdown of the hydrogen peroxide fuel wherein they are immersed. The hollow structure generates a thrust of oxygen microbubbles in their interior released from one of the tubular openings. The motion of laminar fluid through the interior of the microtube sucks the cargo towards its front opening, permitting a large variety of microobjects to be easily transported without the need of functionalization [7].

Here we describe our recent advances on the controllable manipulation of microbots in microfluidic channels and the transport of biological material such as cells. Moreover, the coupling of catalytic biomolecules such as enzymes and artificial nano/microdevices are a promising alternative to the first generation of catalytic nanomotors containing Pt metal as a catalyst towards the finding of higher efficiency conversion, versatile configurations, more physiological conditions and biocompatible fuels.

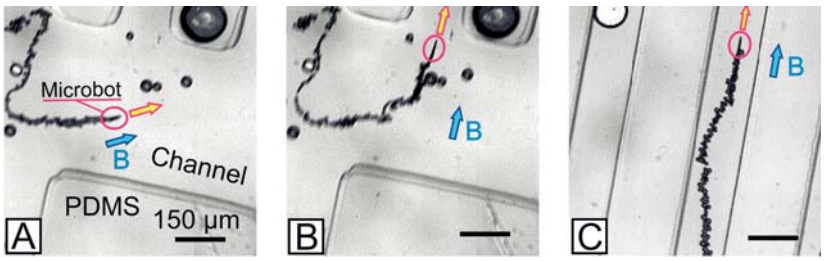

Fig. 1: (A-C) Optical sequence of microbot "swimming" into the microchannels of a PDMS chip. Blue arrow represents the direction of the magnetic field. **(D)** Schematics of the fabricated microchip used for the transport of microparticles.

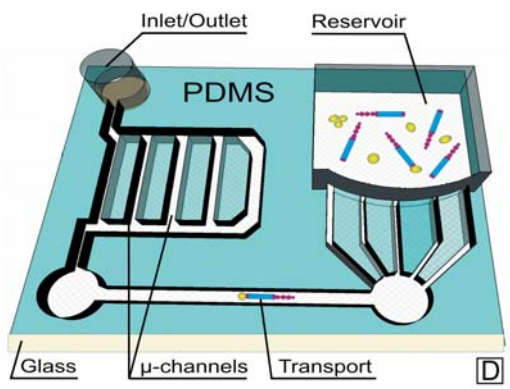

Microbots swimming in microfluidic channels

The easy loading and delivery of cargo within a lab-on-a-chip microchannel network remains a big challenge for this class of nanomotors, motivating the search for versatile nanomachines which can swim in diverse conditions while transporting cargo in a controlled manner.

The accurate stirring of autonomous microbots swimming within PDMS microfluidic channels is shown in Fig. 1. First, the Ti/Fe/Pt microbots were suspended along with polystyrene microparticles (5 µm diameter) into a reservoir chamber (1 cm^2) containing hydrogen peroxide solution (8.75 % v/v) and soap (5 % v/v). Immediately, the microbots

start to self-propel by the oxygen released from one of the openings of the microtubes as described before. The optical images in Fig. 1 depict the microbot travelling and being directed from the wide microfluidic channel (Fig. 1.A) towards the narrower areas (Fig. 1.B and Fig. 1.C) wherein microparticles are ultimately loaded and transported. As an example, a microbot against a flow of 73 μm s^{-1} travels at 78 μm s^{-1}. This speed significantly overcomes Brownian motion, proving a high power output from the rolled-up microbots into the fabricated microchannels. The microbot's motion is controlled by a magnetic field generated by a small NdFeB magnet bar placed underneath the microfluidic chip. The ability of artificial micromachines to swim against a continuous flow is of particular interest for future applications since living systems contain moving fluids rather than static ones (Fig. 2).

In addition, the transport of spherical particles in the flowing streams of microchips is achieved (Fig. 1.D)[12].

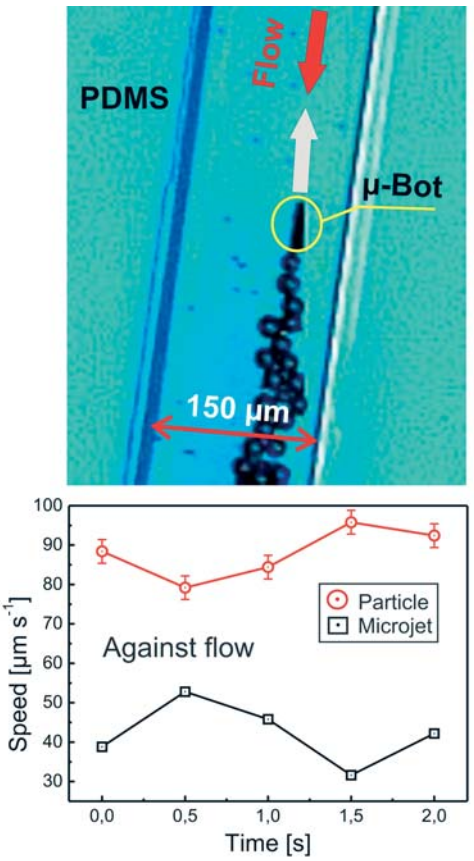

Fig. 2: Microbots swimming against the continuous induced flow of fuel into the microchannels. Plots at the bottom depict the speed of the tracer particles (n=5) and the microbots in absolute values.

Transport of animal cells

The controlled transport of cells is of significant importance since it is clearly the next step towards the use of artificial nanomachines in future biomedical applications. Animal cells can be transported within a fluid in a controllable manner by using artificial microbots [13]. The Ti/Fe/Pt rolled-up catalytic microbot is guided towards a specific cell, which is moved to a desired location where it is released (Fig. 3, A-C). Its motion is coordinated by an external magnetic field, which –once is turned rapidly–, enables the release of the loaded cell at a desired target (small insets of Fig. 3 A-C).

We describe the pick-up, transport and release, of multiple neuronal CAD cells (Catecholaminergic cell line from the central nervous system) in fluid by using catalytic microbots. Although "large" cells are loaded at the front end of the microbots (diameters ranging from 10 to 15 μm), their motion is not totally halted. One would expect that microbots with diameter larger than 15 μm will suck the cell through the tube body due to the fluid pumping, whereas microbots with a very small size will not be suitable for the manipulation of very large cell. Therefore, we optimized the fabrication parameters to produce microbots with diameters from 6 to 10 μm (see SEM image in Fig. 3, D).

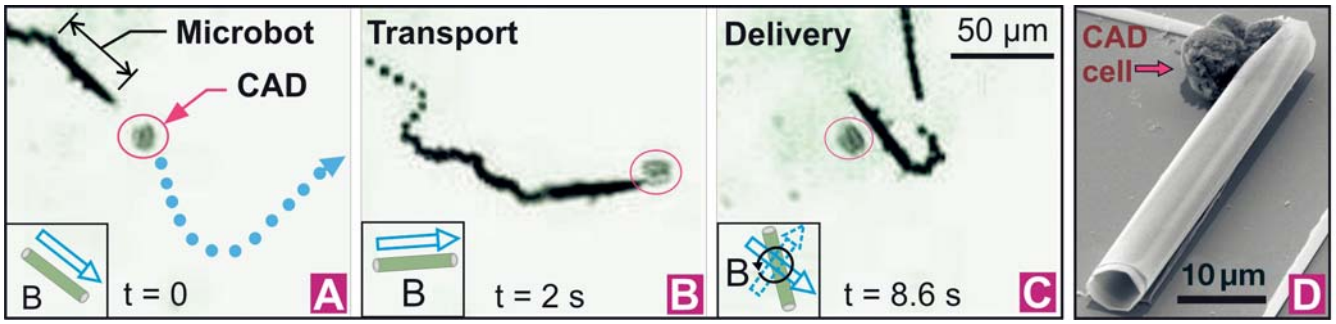

Fig. 3: Controlled manipulation of CAD cells by using catalytic microbots. The motion of the microbot is aligned by an external magnetic field (schematic insets) provided by a small magnet which is placed underneath the sample containing the cells and microbots. **A)** Microbot directed towards the CAD cell, its transport **(B)** and delivery in a desired location by a quick rotation of the magnet **(C)**. SEM **(D)** image of Ti/Fe/Pt rolled-up μ-tubes with CAD cells.

Sophisticated micromachines are required for the performance of multiple tasks. For instance, the consecutive loading of several cells is beneficial for complex applications such as cell sorting. Therefore, high power output and easy loading mechanisms are demanded for this purpose.

Biocatalytic microbots, increasing the power

The versatile rolled-up technique allows on-demand fabrication of microtubes by deposition of different materials [14]. Therefore, we fabricate rolled-up microtubes containing Au as inner layer instead of Pt (i.e. Ti/Au), and modify them with an enzyme which decomposes peroxide, catalase, in a very efficient manner. By using low concentration of hydrogen peroxide (1.5 % v/v), the hybrid microengines move at 10 body length sec^{-1} at the air-water interface compared with 1 body length sec^{-1} from the Pt based-microengines. The high efficiency of these microengines is of significant importance

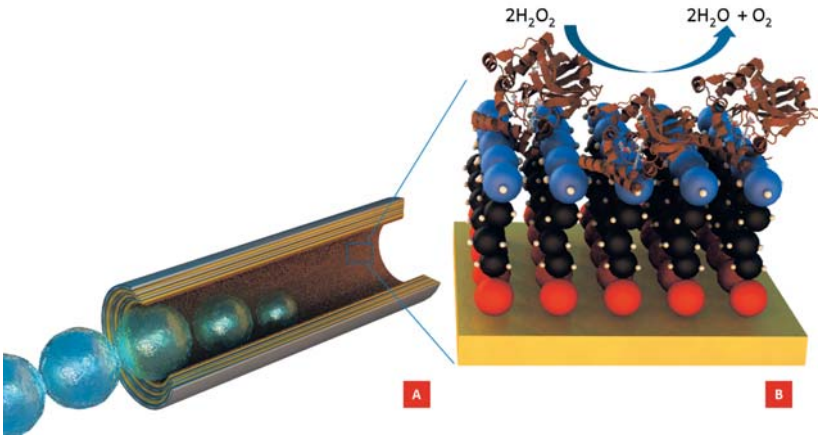

Fig. 4: A) Open view of the hybrid biocatalytic microengine. **B)** Surface modification of inner Au layer and enzymatic decomposition of peroxide fuel

towards the design of more powerful nanomachines. In order to bind the enzyme to the inner layer of the microtubes., we functionalized the thin Au layer with self assembled monolayers (SAM) of 3-mercaptopropionic acid (3-MPA) where the enzymes covalently bond (Fig. 4).

This was the first report on the effective use of enzymes as catalysts in self-propelled microengines [8]. Moreover, as a proof of concept, the specific enzyme-binding into the microtubular structures demonstrates that new configurations can be used for autonomous motion towards the finding of more biocompatible fuels, e.g. glucose.

In summary, our work clearly indicates that our microbots could be suitable in the near future for the development of bioanalytical and biomedical applications using different kind of cells.

For instance, the microbots can be used for cell sorting or to move one single cell into an analytical device (e.g, lab-on-a-chip) to analyse the changes in biochemistry, physiology or metabolism of the single cell.

On the other hand, the hybrid biocatalytic microengines pave the way to other chemical configurations to induce motion and towards the finding of biocompatible fuels and why not, to biochemically sense their environment. This novel approach leads to faster, more powerful and more efficient microengines compared with those based on a Pt catalyst, as well as using lower concentrations of peroxide fuel.

All together, the integration of "smart and powerful" microbots with different microchip schemes can lead to multiple functions in Lab-on-a-chip devices such as the separation and sorting of drugs or cells, and also biosensing. Other visionary tasks could be the translocation of stem cells on-demand to build up new tissues or to replace disease cells or tissues.

[1] T. E. Mallouk and A. Sen, Sci. Am., 300 (2009) 72; G. A. Ozin, et al, Adv. Mater. 17, (2005) 3011.
[2] T. Mirkovic, et al, Small 6,(2010) 159;
[3] M. Pumera, Nanoscale 2 (2010) 1643; W. Paxton, et al, Angew. Chem. Int. Ed., 45, (2006) 5420; S.Sanchez, M. Pumera, Chem. As-J. 4 (2009) 1402.
[4] Van den Heuvel, M. G. L.; Dekker, C. Science 317 (2007)333.
[5] W. F. Paxton, et al, J. Am. Chem. Soc. 126 (2004) 13424
[6] S. Fournier-Bidoz, et al, Chem. Commun. (2005) 441.
[7] N. S. Zacharia et al, Chem Commun, (2009) 5856.
[8] S. Sanchez, et al, J. Am. Chem. Soc. 132 (2010) 13144
[9] T. R. Kline, et al, Angew. Chem. Int. Ed. 44 (2005) 744;
[10] A. A. Solovev, et al, Small 5 (2009) 1688.
[11] K. M. Manesh, et al, ACS Nano, 4 (2010) 1799.
[12] S. Sanchez et al. , J. Am. Chem. Soc (2011)Dx.doi.org/10.1021/ja109627w
[13] S. Sanchez et al, Chem Commun. 47(2011) 698
[14] O. G. Schmidt and K. Eberl, Nature 410, (2001) 168.

Funding: VW–Stiftung

Direct alignment of rolled-up tubes in a fluid suspension by surface acoustic waves

X. H. Kong, Ch. Deneke, H. Schmidt, and O. G. Schmidt

Rolled-up micro-/nanotubes cover a wide range of potential on-chip applications such as optofluidic components [1], ultra-compact capacitors [2], and meta material fiber optics [3]. Apart from on-chip integration, free floating rolled-up tubes have been engineered to create self-propelling catalytic microjet engines [4]. Control over position and motion has been exerted by means of magnetic fields or confinement into small channels, but a rigorous control over whole ensembles of tubes is still challenging. Meanwhile, surface acoustic waves (SAWs) have been employed to align and control single as well as ensembles of micro-objects in a fluid [5].

Here, we demonstrate that SAWs can be used as a versatile tool to align metallic rolled-up tubes suspended in a fluid. Using carefully designed interdigital transducers (IDTs), SAWs are excited on a $LiNbO_3$ surface. A droplet of the tube suspension is deposited between the IDTs – in the first case a two-port device, in the second case a four-port device – and tube alignment was monitored. We find that tubes can be aligned periodically, where the periodicity is defined by the wavelength of the SAW. Furthermore, tubes can be rotated and in this way manipulated by the four-port device offering rigorous control over these micro-objects in the fluid environment [6,7].

Figure 1(a) shows a schematic diagram of the two-port SAW devices in our experiments. The devices were fabricated on 128° rotated Y-cut single-crystal $LiNbO_3$ substrates with SAW propagation along the X axis. A pair of opposing IDTs composed of Cr/Au (20/70 nm) layers were patterned on each device using optical lithography and electron-beam evaporation. The acoustic path length between the split-finger IDTs was 3.6 mm with an IDT finger-width of 16.2 μm. The IDT finger pitch was roughly 130 μm which defines the SAW wavelength λ_{SAW} according to the formula $\lambda_{SAW} = v_{SAW}/f$, where v_{SAW} is the acoustic velocity and f is the high-frequency of the applied signal. The as-designed IDT device launched SAWs with a wavelength of 130 μm at a corresponding frequency of about 30 MHz. Signal powers were added to the IDT device by two signal generators for the tube alignment experiments where each signal generator provided a 0 - 13 dBm output power at 30 MHz.

Rolled-up Cr microtubes with lengths of 30, 50, and 80 μm were used in our study (tube layer thickness and tube diameter were 10 nm and 7 ~ 9 μm, respectively). For the experiments, one drop of PC-solvent (propylene carbonate) followed by a drop of tube suspension were placed in the capillary gap between the $LiNbO_3$ substrate and a glass cover, as illustrated in Fig. 1a. The PC-solvent was applied to decrease the liquid evaporation. The glass cover was pressed onto the tube suspension parallel to the substrate surface with a spacing of 50 μm or less in order to create a microfluidic channel. SAW induced motion of the microtubes was monitored by an optical microscope connected to a high speed camera.

At the start of each experiment, the rolled-up microtubes in the fluid are randomly dispersed on the $LiNbO_3$ substrate, as shown in Fig. 1b. When two rf-signals of 30 MHz with equal power are applied to the two IDT ports simultaneously, a standing SAW pattern forms on the $LiNbO_3$ surface. Under this condition, the rolled-up metallic Cr microtubes are aligned in one direction, with their axis parallel to the propagation direction of the SAWs, as seen in Fig. 1c. Furthermore, it is observed that Cr tubes are located in equispaced columns perpendicular to the SAW propagation direction, similar to particle alignment reported previously. These columns are marked by the green dashed lines in Fig. 1c. The space between the columns is around 65 μm, close to $\lambda_{SAW}/2$, corresponding to the separation of the SAW standing wave nodes.

Interestingly, Cr tubes are able to link together and form bridges by increasing the tube concentration. As shown in Fig. 1d, linked Cr tubes appear as shorter or longer micro

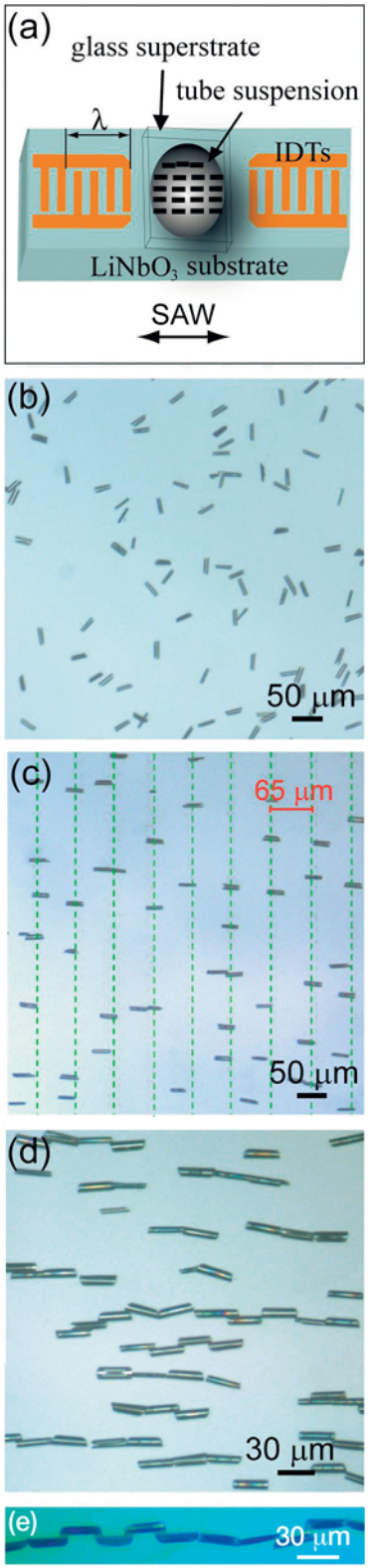

Fig. 1: (a) Schematic of a two-port device and the tube alignment regarding the device. The double side arrow indicates the SAW propagation direction. **(b)** Cr rolled-up tubes after dispensing the solution on the SAW device **(c) – (e)** Tube ensembles after application of SAWs.

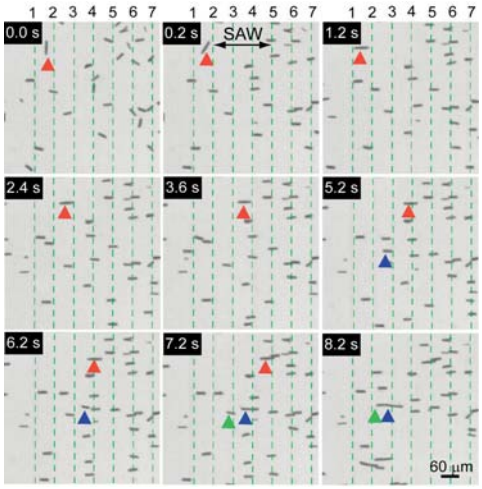

Fig. 2: Sequential optical images obtained during the tube ordering process. The process is initiated by applying SAWs and the formation of "tube-chains" is observed.

chains, parallel to the SAW propagation direction. Up to 17 Cr tubes can be linked together (Fig. 1e), forming a long tube-chain.

A set of sequential optical images obtained from a video is depicted in Fig. 2 to display the dynamic process of the tube-chain formation. Once the rf-signal power is activated, the randomly dispersed Cr tubes are immediately (in 0.2 s) aligned parallel to the SAW propagation direction. Only those tubes strongly adhering to the substrate need more time to be aligned, such as the one pointed at by the red triangle (1.2 s). Once aligned, the tubes are in a thermodynamically metastable state and oscillate inside well defined columns (green dashed lines) due to a microfluidic background flow and mechanical vibration forces caused by the SAWs. When the instability of a tube's position is too large, the tube moves to a neighboring column. As shown in Fig. 2, the tube marked by the red triangle originally oscillates around column 2 for about 1.2 s. It hops to column 3 (2.4 s) and later to column 4 after leaving its initial equilibrium position. Subsequently, it leaps to column 5 (7.2 s) and attaches to another tube there. Finally, the two tubes are linked together and oscillate as a whole entity. Similar behavior is observed for the tube marked by the blue triangle in Fig. 2. It oscillates around column 3 originally, then jumps to column 4 and connects with another tube. Afterwards the two merged tubes connect with a third tube (marked by the green triangle) and form a small tube-chain. Longer tube-chains are formed in a similar way.

By systematically tuning the experimental conditions, we find out that the percentage of microtubes aligned by SAWs at a certain frequency depends on the size of the tubes and the applied signal power. Cr tubes with equal layer thicknesses and diameters, but with lengths less than $\lambda_{SAW}/2$ are easier aligned than those being longer than $\lambda_{SAW}/2$. Additionally, tubes align faster when the applied rf-signal power is increased.

To obtain further control over the microtubes in solution, a four port device is used. In this case, two IDT pairs are perpendicular to each other allowing for exciting the SAW field along both major directions of the substrate parallel to the edges.

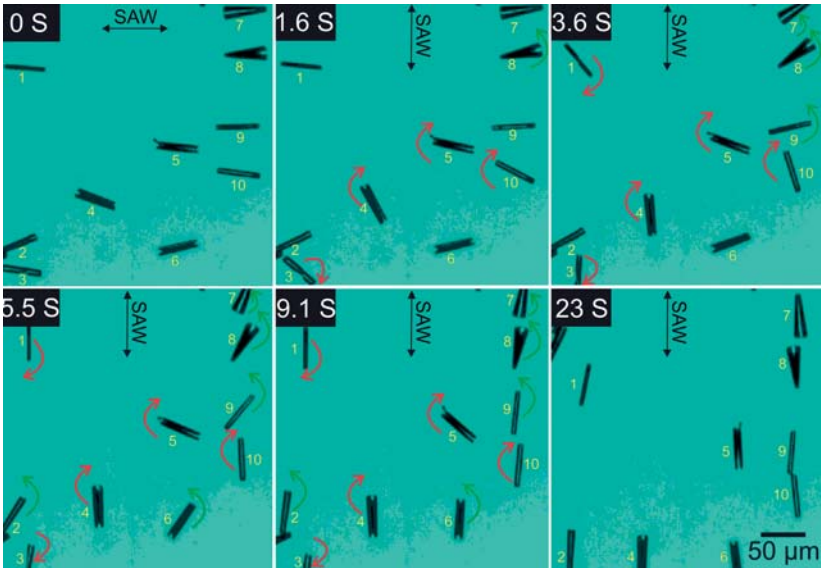

Fig. 3: Sequence of optical images demonstrating a 90° rotation process by altering the SAW propagation direction.

In Fig. 3 the 90° rotation process of Cr tubes by a single switching of SAW propagation direction is demonstrated. At the beginning (0 s) tubes are aligned in the x -direction due to the SAW propagation along this direction. Then the signal power for the x-directed IDT is turned off and the y-propagating SAW is activated. Consequently, tubes begin to rotate gradually. The adhesive force from the substrate and a cover slip as superstrate is the main resistance for the tube rotation. Some tubes with less adhesion to the environment can be rotated easier (e.g. No. 3, 4, 5, 10). Most tubes can be finally rotated with time going on. Of the ten tubes shown in Fig. 3, five tubes (No. 1, 3, 4, 5, 10) rotate clockwise while the other five (No. 2, 6, 7, 8, 9) rotate counter-clockwise. The tube

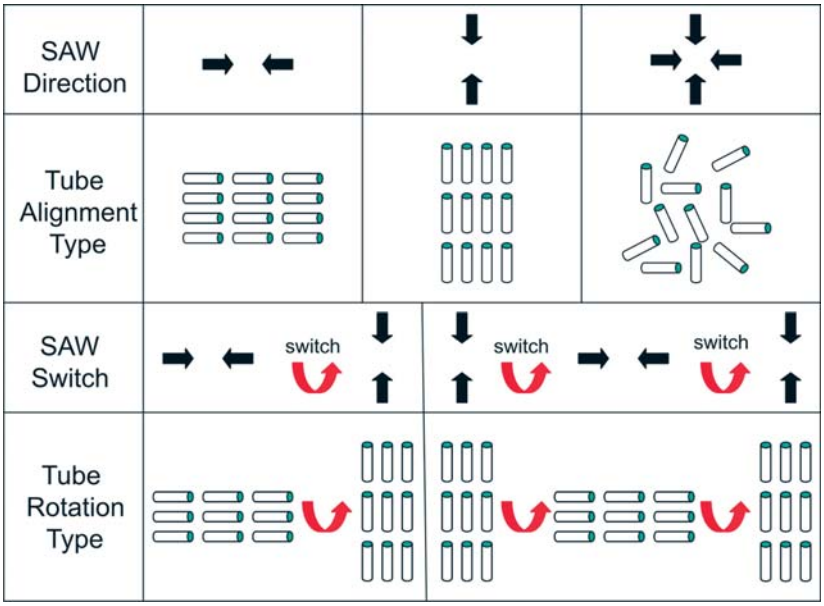

Fig. 4: Relation of the tube alignment and rotation in relation to the SAW propagation direction.

rotation direction is determined by the balance of moments from dielectrophoresis [6] and the viscosity of the tube solution at the beginning of SAW propagation. In this SAW-based operation, the angular tube orientation is manipulated at certain places by the formation of a proper piezoelectric field distribution only, whereas the lateral tube location can be only affected by the fluidic flow caused by SAW-induced acoustic streaming.

The different kinds of relationships between rotational tube alignment and corresponding SAW propagation are summarized in Fig. 4. The basic operation modes are illustrated by the upper three cases: If SAW (counter-)propagate along one direction, metallic tubes can be aligned with their axis parallel to the SAW direction due to the presence of a well-defined piezoelectric field. But if SAW propagate along two or more directions (for example, if power signals were applied to all four ports simultaneously), the tubes will not be aligned. If the SAW propagation direction is switched after proper tube alignment, the tubes will rotate accordingly until their axes are parallel to the current SAW propagation direction. This behavior can be repeated many times, as far as the dielectrophoretic force is strong enough to overcome the tube adhesion to substrate and cover slip, respectively (Fig. 4, lower cases).

The SAW-based dielectrophoretic manipulation of rolled-up metallic microtubes in a microfluidic system was demonstrated. Within this setup, the SAW-induced piezoelectric fields act as contactless tweezers for sensitive manipulation of the angular tube orientation as well as of their lateral location. In this sense, SAW-controlled microtube manipulation opens up new perspectives for on-chip microfluidic applications.

[1] A. Bernardi *et al., Appl. Phys. Lett.* **93**, 094106 (2008)
[2] C. C. Bof Bufon *et al., Nano Lett.* **10**, 2506 (2010)
[3] E. J. Smith *et al., Nano Lett.* **10**, 1 (2010)
[4] A. A. Solovev et al., *Small* **5**, 1688 (2009)
[5] C. J. Strobl, *Appl. Phys. Lett.* **85**, 1427 (2004)
[6] X. H. Kong et al., *Appl. Phys. Lett.* **96**, 134105 (2010)
[7] H. Schmidt et al, *IEEE* NEMS **2011** (submitted)

Funding: Volkswagen Foundation, BMBF (InnoProfile 03IP610)

Technological impact

MgB_2 superconducting wires with high critical current density for MRI magnets

W. Häßler, M. Herrmann, C. Rodig, M. Schubert, A. Kario, J. Scheiter, K. Nenkov, H. Prescher, B. Holzapfel, L. Schultz

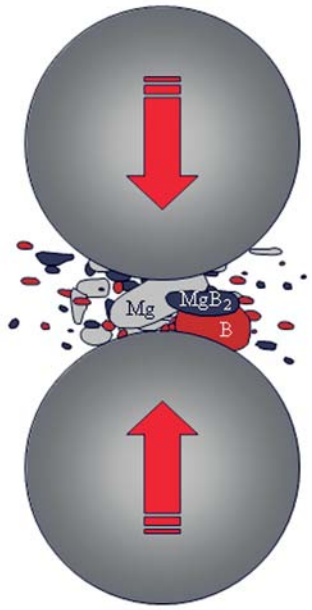

Fig. 1: Principle of mechanical alloying in a planetary ball mill. Extreme pressure and temperature conditions in the collision-zone lead to grain refinement and a solid state formation of MgB_2.

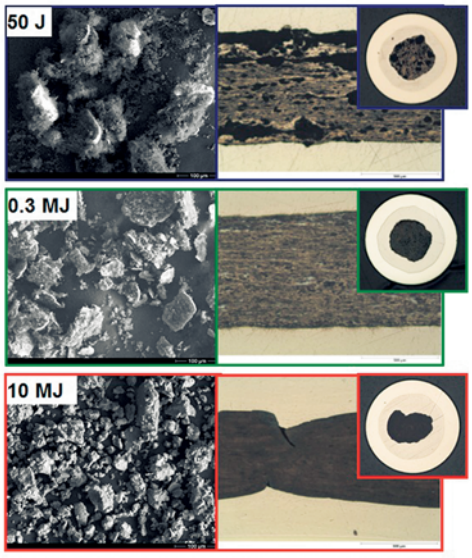

Fig. 2: SEM micrographs of the as milled precursor powder with different amounts of imparted energy (left) showing all stages of a mechanical alloyed ductile-brittle powder system and longitudinal resp. cross-sectional micrographs of the subsequently prepared wires (right).

MgB_2 was found to be superconducting with a critical temperature T_c of 39 K, the highest value found amongst the common metallic compounds. Therefore the potential operating temperature range is between the one of low temperature superconductors like NbTi or $NbSn_3$ and high temperature superconductors like YBCO and BSCCO. Two properties are recognized to be crucial for potential applications: the lack of weak-link behaviour and the capability of the microstructure of MgB_2 to allow for an effective flux pinning. Whereas the applicability of NbTi and $NbSn_3$ is limited to operating temperatures around 4 K, MgB_2 can be operated even at temperatures above 10 K and is therefore cost-effectively useable in cryogen-free systems (refrigerator cooling).
Already reported high upper critical fields and large critical current densities [1,2] as well as the low cost of the constituent elements makes the material a candidate for superconductor applications including MRI-magnets [3]. Prototypes such as current leads in a Japanese satellite and a liquid Hydrogen level sensor [4] have been presented already.
The material is in an early stage of commercialization. Two pre-commercial prototype producers of MgB_2-wires are on the market, Columbus Superconductors in Italy [5] and Hypertech in the USA [6]. In this context, IFW is cooperating in the development of MgB_2 wires with Bruker EAS in Hanau, one of the world leading producers of superconductors [7].

The IFW has a long standing experience in the preparation and characterization of MgB_2-wires in the laboratory scale [8-10]. The distinctive feature of our technology is the usage of mechanically alloyed precursor powders.
Mechanical alloying is an excellent technique to adjust the microstructure in the MgB_2 precursor powder. The basic principle of this method is shown in Fig. 1. The resulting nanocrystalline particle size serves for a high amount of grain boundaries acting as pinning sites and therefore is beneficial to obtain high critical current densities in the material.
Facing the challenge of introducing MgB_2 wires and tapes into application, it is also essential to adapt its preparation to the industrial scale. Only a reasonable interplay of both key parameters, current carrying capability and an appropriate preparation route, will allow for a widespread use of MgB_2 conductors. To allow for a reliable production of MgB_2 wires on the kilometer scale, it is indispensable to make use of a precursor which can be deformed properly within the sophisticated architecture of a conductor as required for all different aspects of the application.

The deformability of the precursor strongly depends on the powder morphology, which can be tailored by the imparted energy during ball milling. Fig. 2 (left side) shows a series of SEM micrographs of the as milled precursors with varying milling energy from gently mixed powders (50 J) to extreme processing conditions (10 MJ), an intermediate energy level (0.3 MJ) is shown also.
All stages of a mechanically alloyed ductile-brittle powder system are present. With increasing imparted energy, from mixing to high energy mechanical alloying, an ongoing refinement of the powder can be observed. Additionally, an increasing homogeneity and also a higher densification of the precursor powder can be obtained, as can be seen from the longitudinal images of the as prepared wires in Fig. 2 (right side). At the same time

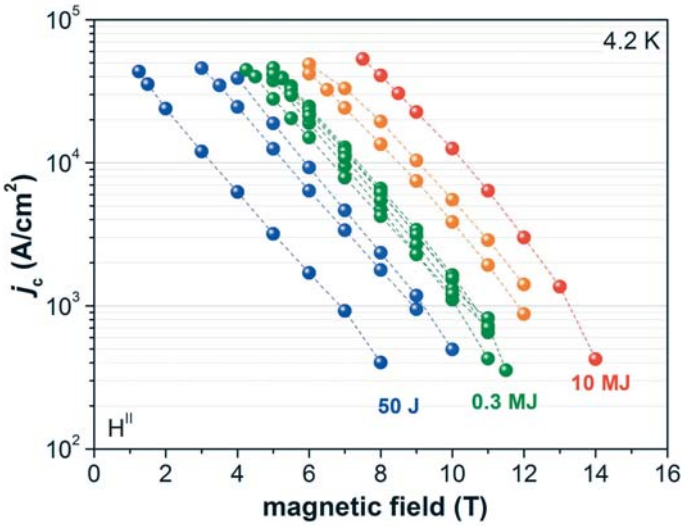

Fig. 3: Critical current density j_c of tapes with precursor powders of different imparted energies. Same color code corresponds to comparable energy input, but different processing parameters.

the flowability of the powder within the sheath material and therefore the deformability of the conductor as a whole will deteriorate when used in the conductor preparation. This is also shown by the misshaping of the filament cross-section and the formation of shear-bands in the filament of the wire with the precursor of the highest imparted energy (10 MJ).

The critical current density of tapes prepared from precursors with varied milling treatment show clearly that an increasing imparted energy results in a higher ampacity of the conductor (Fig. 3). This is explained by the declining crystallite size due to the intensification of the mechanical alloying resulting in an increasing number of grain boundaries acting as pinning sites in the material. Furthermore it is shown that independently from the set of processing parameters, the total amount of imparted energy transferred is determining the critical current density of the MgB_2. This is shown by the j_c-curves of tapes prepared with an imparted energy of approximately 0.3 MJ, but clearly different processing parameters in terms of milling time, speed and ball-powder-ratio.
The used standard preparation setup (250 rpm, 50 h, ball-powder-ratio of 36) equals an imparted energy of around 5 MJ, representing a compromise of high performance and adequate deformability at the same time.

Wires were prepared using the powder-in-tube-technique (PIT). As sheath materials for the monofilamentary wires a double tube of Nb as diffusion barrier in an ODS-Cu-tube is utilized. The filled tube is deformed by swaging. For the preparation of multifilamentary tapes 21 monofilamentary wires were stacked in an outer Monel-tube.
This compound is deformed further. First deforming steps are carried out by swaging. Starting at a diameter of about 7 mm the deformation is switched to wire drawing. It has to be mentioned that interstage annealing has to be applied in the temperature range of 300°C to 500°C in Ar atmosphere to reduce work hardening respectively to decrease mechanical stresses in the sheath. The final diameter of the wire is 0.85 mm, a typical cross-section of such a multifilamentary wire is shown in Fig. 4.
Wire drawing of such a compound material with nanocrystalline precursor powder is a sophisticated process, because the precursor powder is already reacting to MgB_2 at temperatures > 500°C. Thus an increasing hardness of the filaments is degrading the drawing ability of the conductor. Therefore the drawing process has to be optimized by applying an optimal cycle of deformation/annealing steps using an appropriate lubricant.
The final heat treatment for the complete formation of MgB_2 is carried out in Ar at temperatures between 550°C and 700°C. With the best combination of peak temperature,

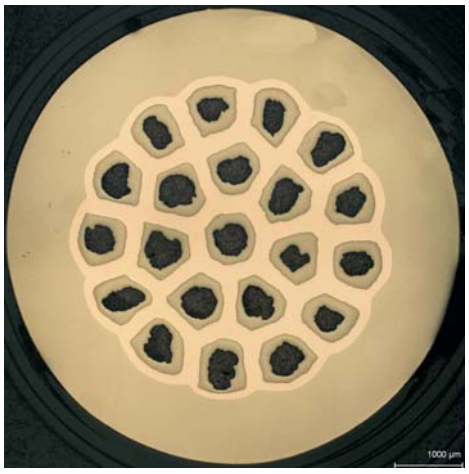

Fig. 4: Cross-section of a 21-filament wire. The sheath system consists of Nb-sheathed filaments in a GlidCop® ODS-Cu-matrix with a Monel®(NiCu) outer sheath.

Fig. 5: Final single piece multifilament wire in batch size exceeding 1000 m (Bruker EAS).

dwell time and heating/cooling rates engineering critical current densities j_e of 170 A/mm² at short samples could be realized. Medium length samples obtained j_e-values of 120 A/mm^2 in a magnetic field of 5 T at 4.2 K. At 20 K a critical current density of about 50 A/mm² was found at fields of 3 T. The n-value at 4.2 K is about 40 for magnetic fields ≤ 5 T.

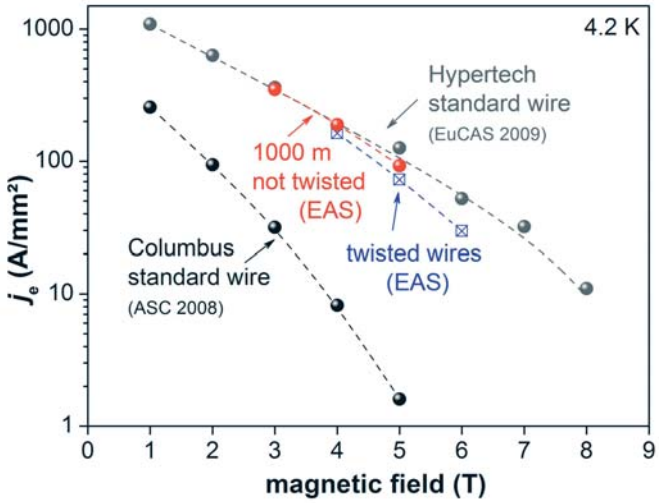

Fig. 6: Comparison of the engineering critical current density j_e of the Bruker-IFW wires with commercial wires.

The collaboration with Bruker EAS succeeded in the preparation of a single piece multifilamentary wire exceeding a 1000 m in length (Fig. 5) with a j_e of up to 91 A/mm^2 at 4.2 K and 5 T. In Fig. 6 the $j_e(B)$-curves of a wire with 21 filaments at 4.2 K are shown in comparison to commercial wires.

This conductor, using a mechanically alloyed in-situ MgB_2 precursor prepared at the IFW, was manufacturedly under industrial production conditions at Bruker EAS. The wire was already successfully twisted for reducing the AC-losses and the thermal stabilization was improved by the wire-in-channel-technique (soldering of the wire into a Cu-profile). One focal point of further development of wires is the increasing of the filling factor from 10 % to about 20 % to further increase the engineering critical current density.

[1] M. Eisterer, *Supercond. Sci. Technol.* **20**, R47 (2007)
[2] E.W. Collings et al., *Supercond. Sci. Technol.* **21**, 103001 (2008),
[3] T.C. Cosmus and M. Parizh, *IEEE Trans. Appl. Supercond.*, to be published (2010)
[4] S.I. Schlachter et al., *Cryogenics* **46**, 201 (2006)
[5] http://www.columbussuperconductors.com/mgb2.htm, Dec. 22nd (2010)
[6] http://www.hypertechresearch.com/page3.html#D, Dec. 22nd (2010)
[7] http://www.bruker-est.com/pr091207.html, Dec. 22nd (2010)
[8] W. Haessler et al., in: E.H. Peterson (Ed.), *Superconductivity Research Horizons*, Nova Science Publishers, Chapter 7, 193 (2007)
[9] W. Häßler et al., *Supercond. Sci. Technol.* **21**, 062001 (2008)
[10] M. Herrmann et al., *Appl. Phys. Lett.* **91**, 082507 (2007)

Cooperation: Bruker EAS GmbH (Hanau), Slovak Academy of Science - Institute of Electrical Engineering (Bratislava)

Funding: Bruker EAS GmbH, DAAD, NESPA

Application Laboratory for Metastable Alloys

W. Pfeiffer, U. Kühn

Leibniz application laboratories stand for a new technology transfer initiative of the Leibniz Association. They represent a platform permitting potential customers and cooperation partners from industry and public areas to receive information on application-oriented research results, and to prepare the transfer of such results to practical applications in the form of projects and joint ventures.

IFW Dresden operates the Leibniz application laboratory "Amorphous Metals". Considering the unique properties of amorphous metals, also known as "metallic glasses", they can be advantageously used in a wide range of applications. The recognition of the research results achieved so far in this field – they were awarded the 2009 Leibniz Prize – reflects the great expectations of the industry regarding the utilization of these results. Therefore, it is the purpose of an IFW project initiated under the "industry meets science" research program, to apply and improve in industrial applications manufacturing technologies that have so far been primarily oriented toward scientific research and communication, and to create and present multi-faceted practicable application schemes for amorphous metals by using the IFW plant and equipment existing in a Leibniz application laboratory as is detailed below.

In particular, the equipment added in previous years for doing research work on these innovative materials - for example special melting and casting equipment, rapid solidification as well as modern rapid prototyping equipment - is planned to be efficiently used also for making prototype products. In this context, the project will focus on the addition to previously applied technologies of a hot-rolling process for amorphous sheet metals and an impact extrusion process for complex amorphous components. What is most important, however, is the establishment of an application centre, e.g. in the form of an exhibition area, which aims at improving communication with the industry and uses specific marketing activities to this end.

The funding received for the implementation, and carrying out the work required in the project phase of approx. 2 years (July 2009 – June 2011) amount to kEUR 360. The persons financed in connection with the technology transfer project work in close cooperation with the scientists in the field so as to ensure the proper implementation of the work schedule.
Essential activities within this project were the enlargement of the presentation area and the provision of more exhibits as a basis for the permanent establishment of the application laboratory for the purpose of permitting especially small and middle sized companies the access to research and development technologies as well as production resources that are mature to be used in practical applications. This goal was reached in October 2010, and the show and advisory service space so created can now be made use of by the scientists.

Under aspect of an economic utilisation of the technologies the research fields and work teams have been subdivided into following development lines:
>> Casting of amorphous metal alloys
>> Thermoplastic forming
>> Selective laser melting (SLM)
>> High-strength iron base alloys

The objective of the **"casting of amorphous metal alloys"** development line is to translate the current know-how of massive metallic glasses in such a way that it can be used in the two technologically oriented development lines „thermoplastic forming" and „3D laser melting" for the development of marketable semi-finished products and prototypes. In the process, the characteristic properties of amorphous metal alloys, such as high hardness, near-net-shape castability, elastic formability and/or good corrosion behaviour shall be maintained or even improved. Another objective is the optimisation of the alloy systems in dependence of the economic and ecological requirement profile.

The **"thermoplastic forming"** line aims at transferring for the first time production methods known from the plastics and glass industry to the processing of massive metallic glasses, thus permitting metallic glass components to be produced economically and in large quantities. This approach is based on the particularity that in a certain temperature range metallic glasses can be processed in the same way as conventional (oxidic) glass or polymer materials. It is the goal of the research team to develop automatable manufacturing processes in which, starting from a suitable semi-finished product (granulate), a component can be manufactured in a few production steps and in large numbers.
It is the purpose of the „3D laser melting" line to transfer this technology from conventional metallic alloy systems to massive moulded bodies of metallic glass. Using conventional metal powders, this 3D laser melting process is meant to allow the manufacture of components featuring complex structures on the one hand, and offer new potentials for the economical production of prototypes and small batches of metallic glass components on the other.

The **"high-strength iron base alloys"** line is designed to develop innovative iron-based materials with extreme mechanical properties, and to lay the foundation for their use in practical applications. This class of materials is characterized by high hardness, high strength, high wear resistance, a high energy absorption potential and good plasticity, and is therefore ideal for a wide range of applications. First tests carried out in industry, in which these materials were used for cutting tools and wearing parts of building machinery (digging teeth), showed that their tool life was up to ten times longer than that of conventional materials.

As a result of the project, it will be possible to manufacture and design a much greater range of simple components and semi-finished products of metallic glass which will facilitate the transfer of the technology for industrial applications.

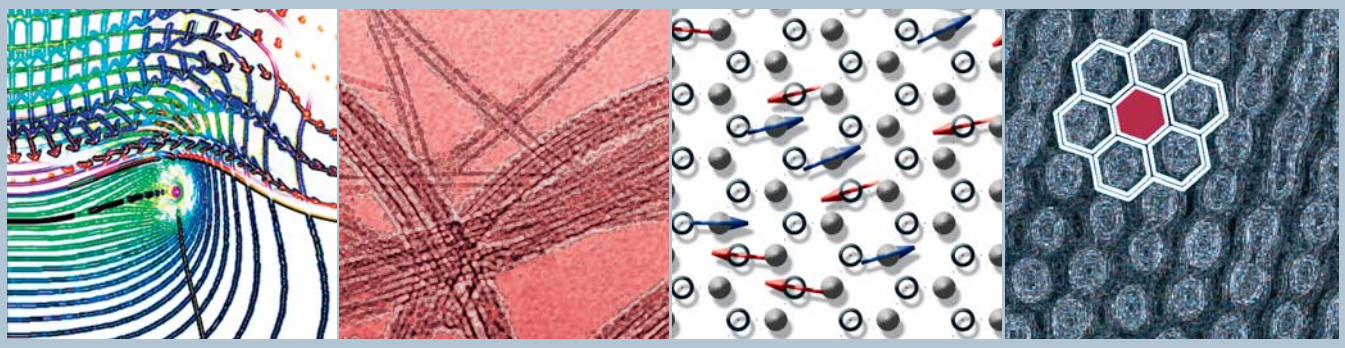

Reports from Research Areas

Numeric simulation of electrodeposition in high gradient magnetic fields

Bundles of single-wall carbon nanotubes

Snapshot of Monte-Carlo simulation

High resolution TEM micrograph of graphene

Research Area 1
Superconductivity and superconductors

Studies on the influence of strain on superconducting properties using piezoelectric single crystals

R. Hühne, S. Trommler, P. Pahlke, K. Iida, S. Haindl, J. Hänisch, F. Kurth, B. Holzapfel, L. Schultz

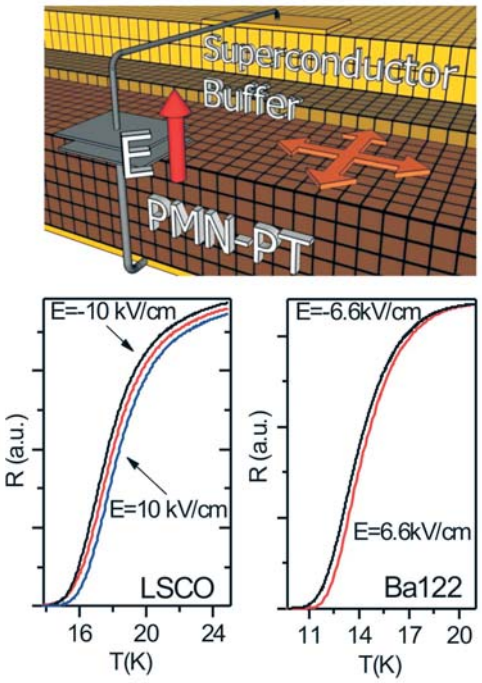

Fig.: Top: sketch of the film architecture; **Bottom:** shift of the transition temperature with applied electric field for LSCO and Ba122

The application of piezoelectric substrates is a promising alternative to static pressure experiments for the investigation of strain-dependent properties of functional materials. The applied strain can be changed continuously and reversibly by using an electric field on such substrates due to the inverse piezoelectric effect. Therefore, superconducting $YBa_2Cu_3O_{7-x}$ (YBCO), $La_{1.85}Sr_{0.15}CuO_4$ (LSCO) and $BaFe_{1.8}Co_{0.2}As_2$ (Ba122) layers were grown on buffered single crystalline (001) oriented $Pb(Mg_{1/3}Nb_{2/3})_{0.72}Ti_{0.28}O_3$ (PMN-PT) substrates using pulsed laser deposition. X-ray measurements revealed an undisturbed epitaxial growth of these materials on the piezocrystals and verified the strain transfer from the substrate to the superconductor under an applied electric field. The applicable strain values at low temperatures were determined by a Pt strain gauge deposited on the buffered PMN-PT substrates to enable a correlation between the change of the superconducting properties and the applied electrical field. A reversible shift of the superconducting transition temperature T_c of 0.4 K for LSCO and 0.2 K for Ba122 was observed on applying biaxial strains of 0.022% and 0.017%, respectively (Fig.) [1]. The change of the transition temperature is almost one order of magnitude smaller for optimally doped YBCO [2]. The observed T_c shift in LSCO is in good agreement to literature data, which confirms the suitability of the piezocrystalline approach for the study of strain-dependent properties in superconductors.

[1] S. Trommler et al., New J. Phys. **12**, 103030 (2010)
[2] R. Hühne et al., Supercond. Sci. Technol. 21, 075020 (2008)

Funding: DFG

J_c scaling and electronic mass anisotropy in F-doped LaFeAsO thin films

J. Hänisch, M. Kidszun, S. Haindl, T. Thersleff, A. Kauffmann, K. Iida, J. Freudenberger, L. Schultz and B. Holzapfel

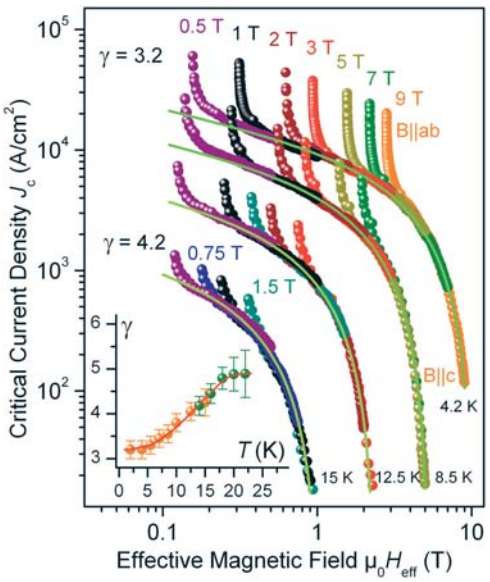

Fig. 1: Scaling of the angular dependent J_c data according to [2], green lines: contribution of random pinning, inset: temperature dependence of the electronic mass anisotropy γ, red line: guide to the eye.

We have successfully fabricated the first high-quality superconducting $LaFeAsO_{1-x}F_x$ thin film using an ex–situ phase formation process. A precursor is deposited by pulsed laser deposition at room temperature and afterwards annealed at 950 °C in an evacuated quartz ampoule, where the phase formation takes place.[1] This thin-film preparation method leads to an extremely clean microstructure of the superconducting layer without any correlated defects perpendicular to the film plane, as transition electron microscopy investigations have shown. In such samples, the anisotropic critical current density, J_c, is predominantly determined by flux pinning at randomly distributed and isotropic pinning centres. According to Blatter, Geshkenbein and Larkin,[2] J_c can then be scaled by an effective magnetic field which is the product of the applied field and the Ginzburg-Landau anisotropy term, which contains the electronic mass anisotropy γ and the angular information. This scaling is shown for four different temperatures in the figure. Fits (shown as green lines) according to the Kramer model denote the contribution of random pinning. The deviations from these fits are caused by intrinsic pinning due to the layered crystal structure and the short coherence length of this compound. The scaling of J_c reveals a temperature dependent γ, see inset in Fig. (yellow data points). This is a direct consequence of the multi-band superconductivity in the

oxypnictides. At high temperatures, where J_c values are not available due to the low irreversibility field, γ was determined from the ratio of the upper critical fields from magneto-resistance measurements in pulsed magnetic fields up to 45 T (green data points). Both data sets for γ overlap at around 15 K.

The J_c scaling approach is a powerful method to determine the electronic mass anisotropy in temperature regions where the upper critical fields are too high to be measured.[3]

[1] M. Kidszun et al., Supercond. Sci. Technol. **23**, 022002(2010), M. Kidszun et al., EPL **90**, 57005 (2010)
[2] G. Blatter, V. B. Geshkenbein, and A. I. Larkin, Phys. Rev. Lett. **68**, 875 (1992)
[3] M. Kidszun et al., arXiv:1004.4185v1

Funding: DFG

Nanoscale Electronic Order in Iron Pnictides

G. Lang, H.-J. Grafe, F. Hammerath, D.Paar, K. Manthey, J. Werner, G. Behr, B. Büchner

A striking feature of the iron-based superconductors is the proximity of superconductivity and static magnetism in their phase diagram. While there have been numerous, sometimes contradicting studies on the issue of ground-state coexistence, it remains unclear whether intrinsic electronic inhomogeneities can show up as in related transition metal oxides such as cuprates and manganites. Using nuclear quadrupole resonance (NQR) at the arsenic sites, we investigated the local charge distribution in „1111" pnictides ($(La,Sm)O_{1-x}F_xFeAs$), where dopant disorder effects are minimized [1,2]. While undoped and optimally-doped/overdoped samples show a single type of charge environment, underdoped samples feature systematically two different local charge environments, irrespective of the ground state (see the spectra in the Figure). Spin-lattice relaxation measurements show that the electronic spin susceptibility is similar for both environments, pointing at their coexistence at the nanoscale. Also considering the quantitative variations of the spectra with doping, the picture of an intrinsic local electronic order emerges, which is likely to impact the interplay of static magnetism and superconductivity. While a possible candidate for this order would be the nanoscale mixing of low- and high-doping-like regions, an intriguing possibility would be orbital effects, in line with the frequently-argued role of orbital physics at low doping.

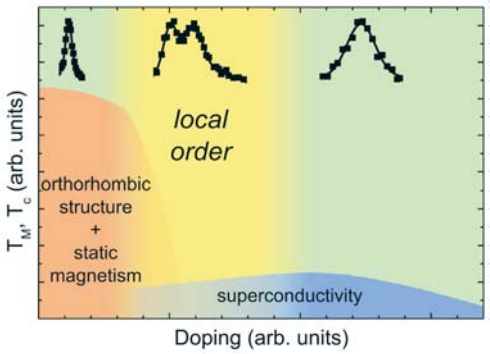

Fig.: Electronic phase diagram for the 1111 pnictides. T_M,T_c denote the magnetic and superconducting transition temperatures. A local electronic order develops in the underdoped region, with superconductivity being favored over static magnetism. At the top are shown typical NQR spectra. At very low and high doping levels a single resonance line indicates electronic homogeneity, whereas for intermediate doping levels two resonances are found indicating two different local charge environments.

[1] G. Lang *et al.*, Phys. Rev. Lett. **104**, 097001 (2010)
[2] H.-J. Grafe *et al.*, New J. Phys. **11**, 035002 (2009)

Cooperation: MPI for Chemical Physics of Solids, Dresden; Department of Physics, Univ. of California, Davis, USA
Funding: DFG, Forschergruppe 538, SPP 1458, Alexander von Humboldt Stiftung

YBCO coated conductor architectures based on IBAD-TiN

R. Hühne, R. Gärtner, J. Hänisch, T. Thersleff, R. Kaltofen, S. Oswald, B. Holzapfel, L. Schultz

Ion Beam Assisted Deposition (IBAD) is one of the major approaches to realise highly textured templates for $YBa_2Cu_3O_{7-x}$ (YBCO) coated conductors. Whereas IBAD-MgO is mostly used so far in such architectures, TiN is a suitable alternative as it is showing a similar textured nucleation required for fast processing. Therefore, a new robust buffer layer architecture based on IBAD-TiN was developed and applied on electropolished Hastelloy as well as on polished stainless steel tapes using an amorphous $Ta_{0.75}Ni_{0.25}$ bed layer. Cube textured TiN layers have been prepared by ion beam assisted pulsed laser

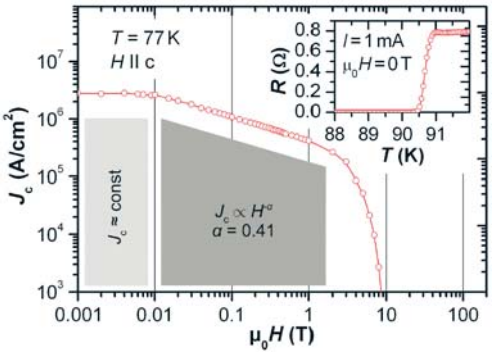

Fig.: Dependence of the critical current density J_c on the applied magnetic field for a 200 nm thick YBCO layer grown on stainless steel using a $Ta_{0.75}Ni_{0.25}$/IBAD-TiN/homoepi-TiN/$SrZrO_3$ buffer architecture investigated by transport measurements in tape direction on a 300 μm wide bridge. The inset shows the superconducting transition temperature in self-field.

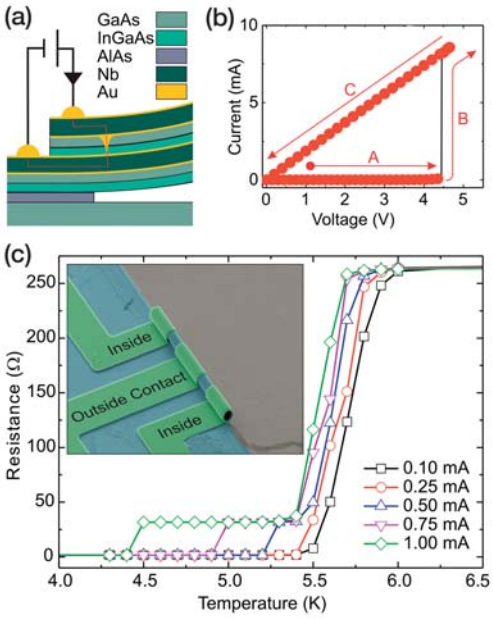

Fig. 1: (a) Schematic of the semiconductor breakdown and electromigration of gold filaments. **(b)** I-V trace of the gold filament formation process. **(c)** Current dependence of the Nb-Au-Nb hybrid superconducting junction (Inset: SEM of a rolled-up device).

deposition on these substrates. The biaxial texture was preserved to a higher thickness using homoepitaxial growth at elevated temperatures and transferred to a second $SrZrO_3$ buffer layer [1]. Consequently, highly textured YBCO layers were obtained with an in-plane and out-of-plane alignment of less than 6° and 3°, respectively, using this buffer layer stack. Dense layers with sharp interfaces were observed in cross sectional micrographs. Typically, superconducting transition temperatures above 89 K were obtained indicating a high film quality and sufficient diffusion barrier properties of the developed architecture. A maximum critical current density of about 2.9 MA/cm^2 was measured at 77 K in self field for a sample prepared on a stainless steel substrate [2]. Additionally, this layer showed an improved J_c(H)-behaviour compared to standard YBCO films on single crystalline substrates.

[1] R. Hühne et al., Supercond. Sci. Technol. **23**, 014010 (2010).
[2] R. Gärtner et al., IEEE Trans. Appl. Supercond. **21** (2011) accepted.

Cooperation: Los Alamos National Laboratory, Bruker HTS GmbH

Nanomembrane hybrid superconducting heterojunctions

D. J. Thurmer, C. C. B. Bufon, Ch. Deneke, O. G. Schmidt

Nowadays, instead of relying on solely top-down or bottom-up approaches, clever combinations of both have lead to many interesting new methods for fabricating novel devices on a micro- and nanoscale. Using simple optical lithography in combination with inherently strained rolled-up nanomembranes and the intrinsic roughness of metal films, we are able to fabricate nanomembrane based hybrid superconducting junctions. Here, two separated contacts are rolled up such that they overlap and have a semiconductor nanomembrane sandwiched in between them. Afterward, the naturally occurring roughness of a gold film is used to concentrate current pathways and create a local breakdown of the semiconductor. Simultaneously, a diffusion of gold into the semiconductor occurs. In Fig. 1a, the breakdown schematic is shown. An applied voltage between the separated Au/Nb/Au films causes a breakdown and electromigration of gold into the semiconductor layer creating Au-filaments, as schematically indicated. This breakdown characteristic is also seen in I-V curves as shown in Fig. 1b. Initially, the nanomembrane exhibits a Shottky behavior (Region A) before a voltage is reached where a drastic increase in current is seen (Region B). Afterward, a linear ohmic response is seen (Region C). These Nb-Au Filament-Nb hybrid structures were measured at low temperature as shown in Fig. 1c. An SEM image of a rolled-up device is shown in the inset. While the Nb leads transition into a superconducting state at the same temperature (~5.6K), the intermediate Au region transition is highly dependent on the applied current. This current sensitivity could make such devices useful for radiation detection.

Funding: BMBF (Nanett [FKZ: 03IS2011])

Photoemission and surface states in iron pnictides

K. Koepernik, A. Lankau, E. van Heumen[1], M. S. Golden[1], H. Eschrig, J. van den Brink, S. Borisenko, B. Büchner

The recent development in highly accurate angle resolved photoemission experiments (ARPES) opens an unprecedented possibility for comparison of experimental data with band structure theory. This allows to test the validity of density functional theory (DFT) but also to analyze experimental data based on theoretical results. In order to differentiate the surface effects from the bulk signal in ARPES experiments we investigated the

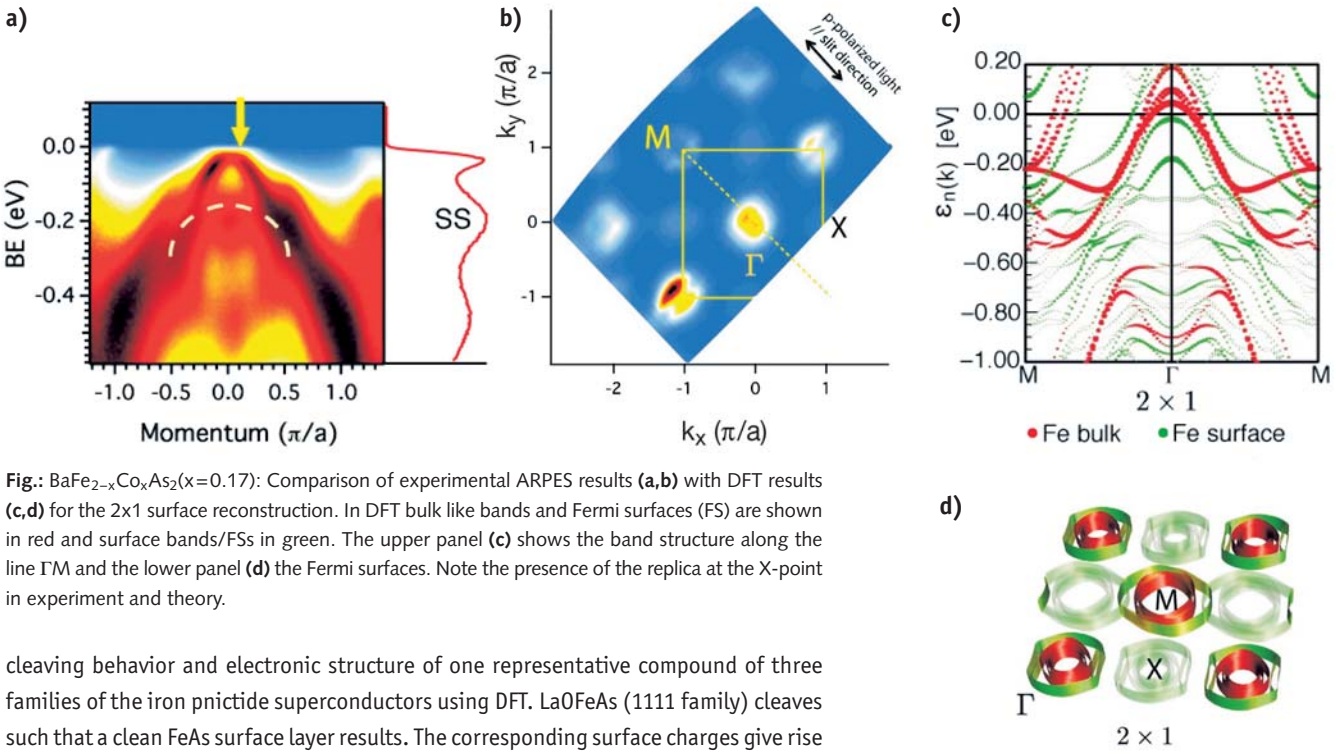

Fig.: $BaFe_{2-x}Co_xAs_2$(x=0.17): Comparison of experimental ARPES results **(a,b)** with DFT results **(c,d)** for the 2x1 surface reconstruction. In DFT bulk like bands and Fermi surfaces (FS) are shown in red and surface bands/FSs in green. The upper panel **(c)** shows the band structure along the line ΓM and the lower panel **(d)** the Fermi surfaces. Note the presence of the replica at the X-point in experiment and theory.

cleaving behavior and electronic structure of one representative compound of three families of the iron pnictide superconductors using DFT. LaOFeAs (1111 family) cleaves such that a clean FeAs surface layer results. The corresponding surface charges give rise to a clearly developed surface state, which has been seen in ARPES experiments. On contrary LiFeAs (111) cleaves between two Li layers avoiding pronounced surface recharging. The resulting absence of surface states makes LiFeAs an ideal compound for investigation by ARPES and other surface sensitive probes. The most complicated behavior is shown by (Co-doped) $BaFe_2As_2$(122), which cleaves such that a 50% Ba layer forms the surface. This opens the possibility for various types of surface reconstruction. In combination with low energy electron diffraction (LEED) we concluded that these ½ Ba surface superstructures also deform the subsurface FeAs triple layer, giving rise to surface states and replica. The close proximity of the surface-related states to the bulk bands leads to broadening of the ARPES results and excludes the use of this compound for accurate determination of self-energies using ARPES.

Cooperation: [1]Univ. of Amsterdam, van der Waals - Zeeman Institute

Fermi surface of $Ba_{1-x}K_xFe_2As_2$ from combined magnetotransport and photoemission measurements

D. V. Evtushinsky[1], A. A.Kordyuk[1], V. B. Zabolotnyy[1], T. K. Kim[1], B. Büchner[1], and S. V. Borisenko[1]

As it became clear soon after discovery of high temperature superconductivity (HTSC) in iron arsenides, the Fermi surface (FS) of these materials consists of two sets of sheets—one at the center of the Fe_2As_2 Brilloiun zone (BZ), and second at the corner [1]. The behavior of electronic bands at the BZ center is well established—three bands exhibit hole-like dispersion [2], and the variation for different ferropnictide HTSC consists merely in sizes of the formed roundish hole-like FS sheets. At the same time the nature of the FS at the BZ corner appeared to be more complicated and less universal. Thus, angle-resolved photoemission spectroscopy (ARPES) experiments on nearly optimally doped $(Ba,K)Fe_2As_2$ revealed an unexpected propeller-like structure at the corner of BZ [3] [see Fig. 1(a)], while in ARPES measurements for cases of $Ba(Co,Fe)_2As_2$ [4], $BaFe_2(As,P)_2$ [5], and LiFeAs [6] a double-walled electron-like FS was found. A combi-

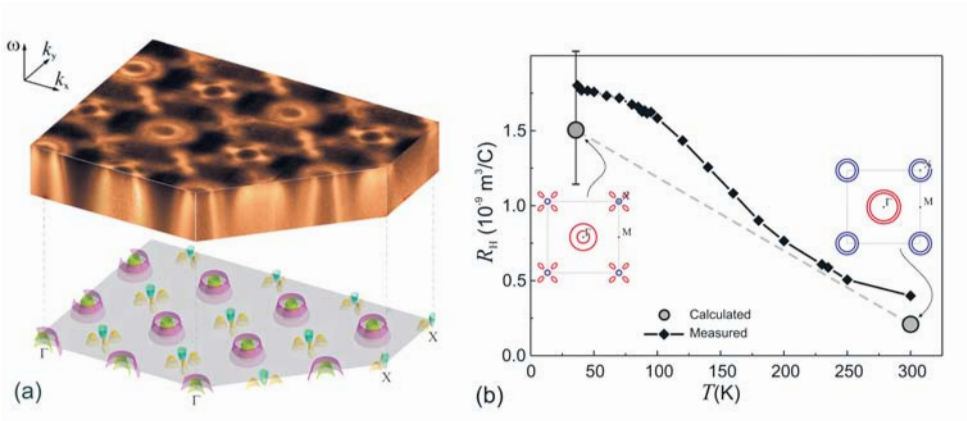

Fig. 1: (a) Three-dimensional representation of low temperature $Ba_{1-x}K_xFe_2As_2$ ARPES data, shown for the energy range of approximately -50..0 meV and band dispersion, extracted from fitting of ARPES spectra [7]. **(b)** The Hall coefficient (RH) for nearly optimally doped $Ba_{1-x}K_xFe_2As_2$ as calculated on the basis of the band structure and as measured experimentally. Insets show the high and low temperature FSs for $Ba_{1-x}K_xFe_2As_2$.

nation with an independent probe of the electronic states at the Fermi level seems helpful for distinguishing the FS shape more precisely and confidently. Therefore results, obtained for $(Ba,K)Fe_2As_2$, were compared to the Hall effect measurements of the same material [see Fig. 1(b)]: photoemission data were used to derive the electronic dispersion relation, which was taken as basis for calculation of the Hall coefficient, R_H. Good agreement between photoemission and magnetotransport was found: both methods reveal temperature-dependent electronic structure, and, found in ARPES, evolution to the propeller-like FS topology at low temperatures appeared quantitatively consistent with measured R_H.

[1] S. Raghu et al., Phys. Rev. B **77** 220503(R) (2008).
[2] A. N.Yaresko *et al.*, Phys. Rev. B **79**, 144421 (2009).
[3] V. B. Zabolotnyy *et al.*, Nature (London) **457**, 569 (2009).
[4] C. Liu *et al.*, Nat. Phys. **6**, 419 (2010).
[5] T. Yoshida *et al.*, arXiv:1008.2080.
[6] S. V. Borisenko *et al.*, Phys. Rev. Lett. **105**, 067002 (2010).
[7] D. V. Evtushinsky *et al.*, New J. Phys. **11**, 055069 (2009).

Cooperation: MPI FKF, Stuttgart and IOP, Beijing
Funding: DFG under grants No. KN393/4 and BO1912/2-1.

Investigation of the Electronic Structure of $LaAlO_3$ - $SrTiO_3$ Heterointerfaces by Soft X-ray Spectroscopy

A. Koitzsch, J. Ocker, M. Knupfer, M. Dekker, K. Dörr, B. Holzapfel, B. Büchner, and P. Hoffmann[1]

Fascinating and counterintuitive phenomena have been observed previously at the interface of $SrTiO_3$ and $LaAlO_3$. The most important is the appearance of metallic conductivity between two firm insulators [1]. Intriguingly the interface remains insulating as long as no more than three layers of $LaAlO_3$ are deposited on top of $SrTiO_3$ but switches to metallic with the fourth layer. Also superconductivity was found below $T_C = 0.2$ K and even magnetism [2]. The picture of the polar catastrophe has been invoked early on to explain the metallic conductivity: the $SrTiO_3$ substrate consists of neutral SrO and TiO_2 layers, whereas the LaO^+ and AlO_2^- layers making up $LaAlO_3$ are charged. Stacking of LaO and AlO_2 layer by layer on top of $SrTiO_3$ leads to an divergent electrostatic potential which is compensated by a charge transfer of 0.5 e to the interface per unit cell for the case of LaO deposited on TiO_2. These charge carriers are responsible then for metallicity at the interface.

We investigated $LaAlO_3$ -$SrTiO_3$ heterointerfaces grown either in oxygen rich or poor atmosphere by soft x-ray spectroscopy. Resonant photoemission across the Ti $L_{2,3}$ absorption edge of the valence band and Ti 2p core level spectroscopy directly monitor the

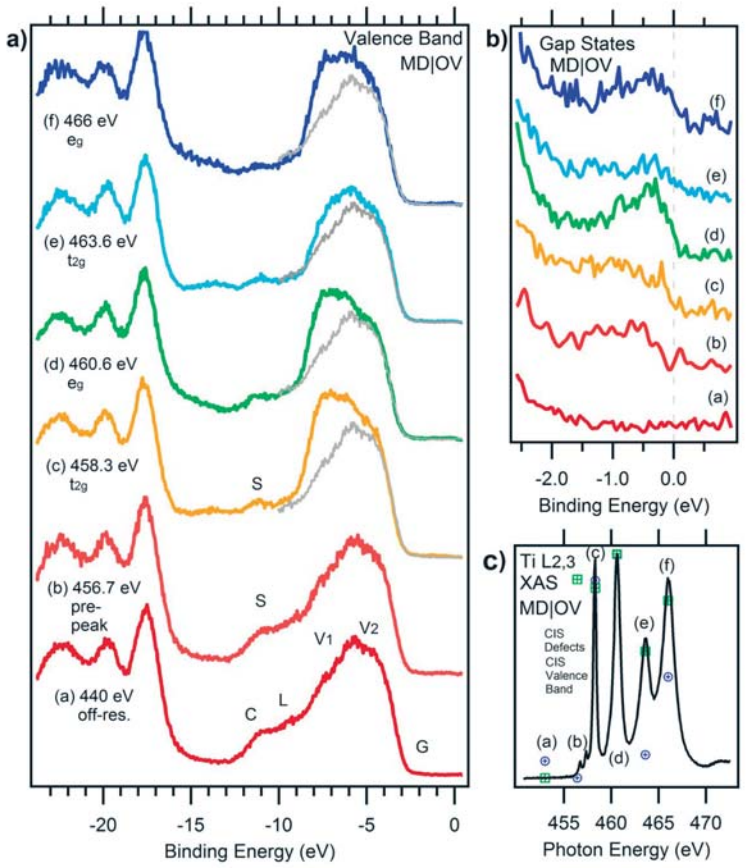

Fig.: Valence band photoemission of $LaAlO_3$ - $SrTiO_3$ **a)** Ti 2p - 3d resonant photoemission valence band obtained by varying the photon energy through the Ti $L_{2,3}$ absorption threshold. The grey lines show the enhancement of Ti 3d derived states by comparison with off- resonant spectra at $\hbar\omega = 440\,eV$. **b)** Expanded view on the spectra shown in (a) near E_F. **c)** Ti $L_{2,3}$ absorption edge taken in total electron yield mode. Letters indicate the photon energy for the valence band spectra.

impact of oxygen treatment upon the electronic structure. Two types of Ti^{3+} related charge carriers are identified. One is related to the filling of the $SrTiO_3$ conduction band and appears for low oxygen pressure only. The other one is probably related to Ti defects and independent of the growth condition. It is shown that low oxygen pressure is detrimental for the Ti - O bonding. The results are consistently explained by extrinsic electron doping due to the formation of oxygen vacancies depending on growth condition.

[1] A. Ohtoms *et al.*, Nature 427, 423 (2004).
[2] N. Reyren *et al.*, Science 317, 1196 (2007).

Cooperation: [1]Helmholtz - Zentrum Berlin

Research Area 2
Magnetism and magnetic materials

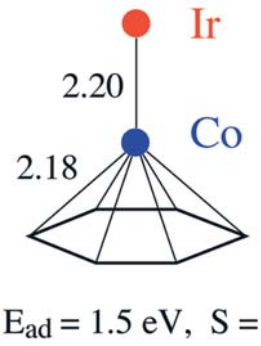

Fig.: The dimer adsorption energy (E_{ad}) and the metal-metal and metal-carbon bond lengths in Å for the ground-state geometry and spin (S) state of the $CoIrC_6H_6$ complex. The hexagon indicates the benzene ring.

Cobalt-carbon complexes with magnetic anisotropies larger than 0.2 eV

Ruijuan Xiao, M. D. Kuz'min, K. Koepernik, M.Richter

We recently reported a density-functional study of the heteronuclear CoIr dimer adsorbed on benzene or graphene [1]. In either case, CoIr prefers an upright position above the center of a carbon hexagon with the Co atom next to it (Fig.). The Ir atom stays away from the carbon ring and thus preserves its free-atom-like properties. This results in a very large magnetic anisotropy of more than 0.2 eV per dimer. So high a value might suffice for long-term data storage at the temperature of liquid nitrogen, using one single magnetic molecule for each bit. In comparison with our earlier prediction for homonuclear Co dimers [2], the *lower estimate* for the magnetic anisotropy becomes five times higher by replacing one Co atom by Ir [1].

[1] Ruijuan Xiao at al., Appl. Phys. Lett. **97** (2010) 232501.
[2] Ruijuan Xiao et al., Phys. Rev. Lett. **103**, (2009) 187201.

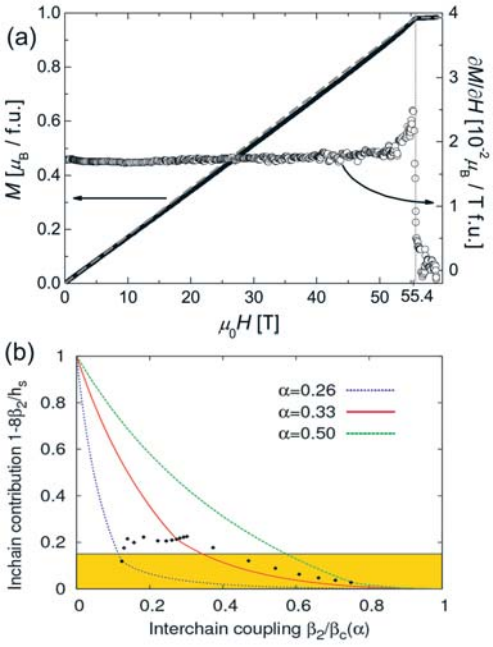

Fig.: (a) Magnetization $M(H)$ for field along the hard b-axis for Li_2CuO_2. The saturation field is obtained from the high field anomaly in $\partial M / \partial H$.
(b) In-chain exchange contribution to the saturation field $h_s = H_{sat}/|J_1|$ from SWT vs. main interchain coupling β_2 for various frustration ratios α and a diagonal exchange interchain coupling scheme. Dots represent the transition to magnon bound state for lower β_2. The shade region marks predominant influence of β_2 on h_s. For Li_2CuO_2, $\beta_2/\beta_c \approx 1.1 > 1$ and $h_s = h_s(\beta_2)$.

Precise determination of the weak interchain interaction of frustrated ferromagnetic spin-chain compounds by saturation field measurements

W.E.A. Lorenz, S. Nishimoto, S.-L. Drechsler, R.O. Kuzian, J. van den Brink and B. Büchner

We have studied the influence of interchain couplings onto the saturation field for a class of frustrated quasi-one-dimensional S= ½ magnets [1]. The materials under consideration are characterized by a ferromagnetic (fm) interaction $\boldsymbol{J}_1$ between nearest neighbors in the chain, which is frustrated by a next-nearest neighbor antiferromagnetic (afm) interaction $\alpha|\boldsymbol{J}_1|$. These dominant interactions are accessible by a number of methods, including L(S)DA calculations and fits to $\chi(T)$ data. However, knowledge about the weak interchain couplings (ICC) which eventually determine the magnetic ground state is often missing.

One of the generic aspects of fm-afm frustrated magnets is attractive interaction between magnons due to the fm in-chain interaction, which gives rise to a rich phase diagram in near saturation magnetic fields. Employing spin-wave theory (SWT) as well as DMRG on interacting spin-chains we have shown that even weak ICC are decisive for the value of the saturation field H_{sat}. Moreover, for $\beta_2 = |\mathrm{ICC}/\boldsymbol{J}_1|$ larger than a critical value β_c we find that H_{sat} is exactly independent of the strong in-chain interactions. This situation is given e.g. in the representative material Li_2CuO_2, such that H_{sat} constitutes a precise measure of the ICC. Indeed, the value determined by our pulsed field magnetization measurements is in excellent agreement to results of inelastic neutron scattering studies [2]. Moreover, we succeeded to show that even if $\beta_2 < \beta_c$, H_{sat} depends only weakly on the frustrated in-chain interactions. In conclusion, we propose a new, efficient and precise measurement of the ICC in such materials being of current interest.

[1] S. Nishimoto *et al.*, arXiv:1004.3300v2 (2010).
[2] W.E.A. Lorenz *et al.*, Europhys. Lett. **88**, 37002 (2009).

Cooperation: Univ. Magdeburg, FZ-Dresden-Rossendorf, Univ. of Heidelberg
Funding: DFG, PICS program and EuroMagNET

Heat conductivity of the spin-Peierls compounds TiOCl and TiOBr

N. Hlubek, M. Sing[1], S. Glawion[1], R. Claessen[1], S. van Smaalen[2],
P. H. M. van Loosdrecht[3], B. Büchner, and C. Hess

We have studied the heat conductivity κ of the $S = ½$ spin chain compounds TiOBr and TiOCl for temperatures 5 K < T < 300 K and magnetic fields up to 14 T [1]. These compounds are considered as good realizations of $S = ½$ spin chains with rather high magnetic exchange coupling J(Cl) ≈ 676 K and J(Br) ≈ 375 K. The compounds undergo two phase transitions T_{c1} and T_{c2}, where the lower one, at T_{c1}, leads to a nonmagnetic dimerized state which is accompanied by a doubling of the unit cell. These features thus render the Ti oxyhalides the second (besides $CuGeO_3$) type of inorganic compounds which undergoes a spin-Peierls transition. In the intermediate regime between T_{c1} and T_{c2} an incommensurate superstructure is present, and above T_{c2} the system is in a pseudo-spin-gap regime up to a characteristic temperature T^*. Surprisingly, we find no evidence of a significant magnetic contribution to κ, which is in stark contrast to recent findings in spin chain cuprates. Despite this unexpected result, the thus predominantly phononic heat conductivity of these spin-Peierls compounds exhibits a very unusual behavior (see Fig. for the case of TiOBr). In particular, we observe strong anomalies at the phase transitions T_{c1} and T_{c2}, and an overall but anisotropic suppression of κ in the intermediate phase which extends even to temperatures higher than T_{c2}. An external magnetic field causes a slight downshift of the transition at T_{c1} and enhances the suppression of κ up to T_{c2}. Our findings provide strong evidence for significant spin-phonon coupling and phonon scattering arising from spin-driven lattice distortions.

[1] N. Hlubek et al., Phys. Rev. B **81**, 144428 (2010)

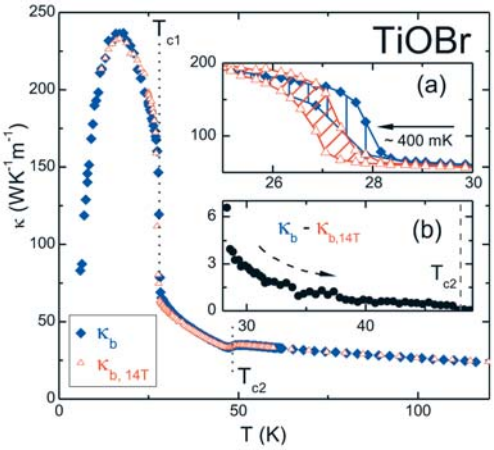

Fig.: Thermal conductivity along the b-axis (κ_b) of TiOBr as a function of temperature T with and without an applied magnetic field of 14 T along the chain direction. Inset **(a)** illustrates the shift of $T_{c1} = 28$ K towards lower temperatures in the presence of a magnetic field. Inset **(b)** shows the decreasing influence of the magnetic field on κ_b in the intermediate regime, i.e. $T_{c1} \leq T \leq T_{c2} = 48$ K. Figure taken from [1].

Cooperation: Experimentelle Physik 4, Universität Würzburg, 97074 Würzburg, Germany; Laboratory of Crystallography, Universität Bayreuth, 95440 Bayreuth, Germany; Zernike Institute for Advanced Materials, University of Groningen, 9747 AG Groningen, The Netherlands
Funding: DFG, European Commission (NOVMAG project, Grant No. FP6-032980)

Oxygen superstructure and electric polarization in multiferroic YMn_2O_5

J. Geck, S. Partzsch, H. E. Hamann-Borrero, J. P. Hill, G. A. Sawatzky, E. Schierle, D. Souptel, H. Wadati, E. Weschke, S. Wilkins, and B. Büchner

The discovery of transition metal oxides (TMOs) with strongly coupled magnetic and ferroelectric properties was greeted with excitement, because these multiferroics have prospects for novel technological applications. For basic research, however, the complex microscopic mechanisms that actually cause this multiferroicity are a major challenge. Prevalent in the current discussion are ionic displacements that optimize the superexchange energy of the magnetic system. But in contrast to this ionic description, correlated TMOs are notorious for their complexity which involves not only lattice and spins but also charges, orbitals and strong covalency. This raises the question whether ionic models are sufficient to capture the main mechanisms of multiferroicity in the TMOs.
To address this question for YMn_2O_5, we performed state-of-the-art resonant soft x-ray diffraction experiments at the HZB in Berlin and the NSLS in Brookhaven. YMn_2O_5 displays a sequence of antiferromagnetic ordering transitions upon cooling, which goes from incommensurate (IC) over commensurate (C) to low-temperature incommensurate (LTIC). Interestingly, the corresponding magnetic superlattice reflections were observed not only at the Mn L_{23}-edge, where the magnetic sensitivity is large. We also detected a surprisingly high intensity at the O K-edge. This observation is direct proof of a spatial modulation of the oxygen valence states, which tracks the periodicity of

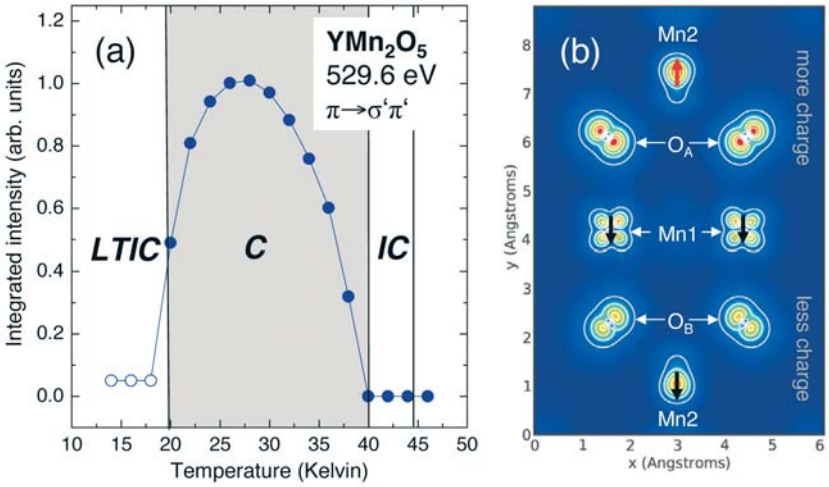

Fig.: (a) Temperature dependence of the oxygen superstructure in YMn_2O_5. **(b)** LSDA+U charge density. Mn1 and Mn2 are octahedral and pyramidal sites, respectively. Local spins are indicated by red and black arrows. The charge density and spin density (not shown) on oxygen depends on the relative orientation of Mn1 and Mn2 spins. The spin dependent hybridization yields a broken inversion symmetry, i.e., a electric dipole moment.

the magnetic order. Most importantly, the temperature dependence of the O K-intensity (Fig. (a)) closely follows the macroscopic electric polarization [1]. These results reveal an electronic contribution to the electric polarization, imply that the Mn-O hybridization plays a central role for the multiferroicity (Fig. (b)) and provide stringent constraints for theoretical models.

[1] Y. Nada, J. of the Korean Phys. Soc. 42 (2003) 1192

Cooperation: Helmholtz-Zentrum Berlin für Materialien und Energie, Germany; Brookhaven National Lab., USA; Univ. of Tokyo, Japan; Univ. of British Columbia, Canada
Funding: DFG (Emmy-Noether program)

Modulated Martensite: Why it forms and why it deforms easily

S. Kaufmann R. Niemann, T. Thersleff, U. K. Rößler, O. Heczko, J. Buschbeck, B. Holzapfel, L. Schultz and S. Fähler

Fig.: Paper model illustrating the incompatibility at a mesoscopic twin boundary formed in modulated martensite. Instead of the gap visible in this simplified model, a diffuse mesoscopic twin boundary forms, exhibiting high mobility.

Diffusionless phase transitions are at the core of the multifunctionality of (magnetic) shape memory alloys, ferroelectrics and multiferroics. Giant strain effects under external fields are obtained in low symmetric modulated martensitic phases. We outline the origin of modulated phases, their connection with tetragonal martensite and consequences for their functional properties by analysing the martensitic microstructure of epitaxial Ni-Mn-Ga films from the atomic to macroscale.

Geometrical constraints at an austenite-martensite phase boundary act down to the atomic scale. Hence a martensitic microstructure of nanotwinned tetragonal martensite can form as an adaptive martensite. Coarsening of twin variants can reduce twin boundary energy, a process we could follow from the atomic to the millimetre scale. Coarsening is a fractal process, proceeding in discrete steps by doubling twin periodicity. The collective defect energy results in a substantial hysteresis, which allows retaining modulated martensite as a metastable phase at room temperature. In this metastable state elastic energy is released by the formation of a 'twins within twins' microstructure which can be observed from the nanometre to millimetre scale. This hierarchical twinning results in mesoscopic twin boundaries which are diffuse, in contrast to the common atomically sharp twin boundaries of tetragonal martensite. We suggest that observed extraordinarily high mobility of such mesoscopic twin boundaries originates from their diffuse nature which renders pinning by atomistic point defects ineffective.

Cooperation: Institute of Physics Praha, Czech Rep.
Funding: SPP 1239

Peculiar high-field quantum magnetism in the frustrated $s = 1/2$ spin chain cuprate linarite

A. U. B. Wolter, M. Schäpers, S.-L. Drechsler, S. Nishimoto, F. Lipps, V. Kataev, B. Büchner

One current interesting direction in the field of one-dimensional (1D) quantum magnetism concerns highly fascinating magnetic field-induced phases. Here, one relevant example is presented by frustrated $s = 1/2$ chains with ferromagnetic nearest-neighbor (J_1) and antiferromagnetic next-nearest-neighbor (J_2) interactions, where it has recently been shown that the ground state of the 1D Hamiltonian has an instability towards field-induced multipolar Tomonaga-Luttinger-liquid (TLL) phases. In this context, the natural mineral linarite $PbCuSO_4(OH)_2$ has been proposed to represent such a frustrated quasi-1D magnet with $J_1 = -30$ K and $J_2 = 15$ K along the chain [1], giving rise to pronounced frustration effects as well as to possible field-induced multipolar TLL phases.

In order to shed light on the magnetic phase diagram of linarite, we started a combined experimental and theoretical analysis in external fields up to saturation. It includes magnetization, ESR and NMR studies as well as theoretical simulations using the DMRG technique for quasi-1D isotropic spin models and a corresponding analysis within the L(S)DA+U approach. As a result we arrive at new values for these exchange interactions, which are surprisingly significantly higher as determined previously [1]. Furthermore, a manifold of field-induced phases are probed in the magnetization measurements, from which we draw a preliminary phase diagram. Notably, a qualitative different dependence of $1/T_1(T)$ in fields below and above 6.5 T and at $T > T_N$ seems to be an intriguing feature, whose origin is not clear yet, but which might be related to a magnetic multipolar spin liquid phase transition as recently predicted [2].

[1] M. Baran, *et al.*, phys. stat. sol. (c) **3**, 220 (2006).
[2] M. Sato, T. Momoi, A. Furusaki, Phys. Rev. B **79**, 060406(R) (2009).

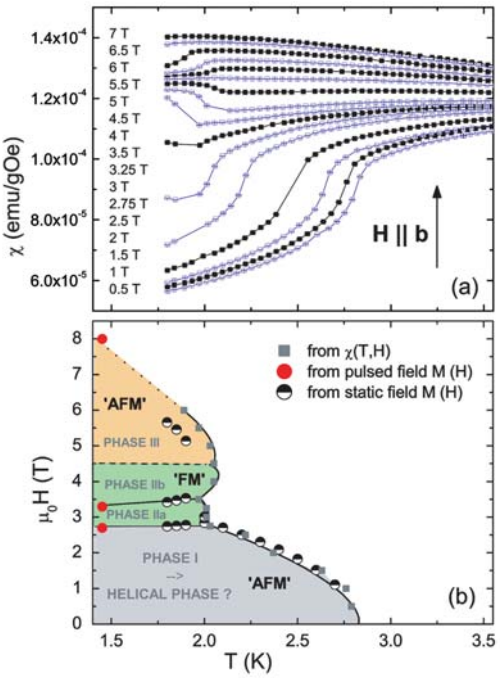

Fig.: (a) Low temperature magnetic susceptibility of $PbCuSO_4(OH)_2$ for different external magnetic fields between 0.5 - 7 T applied || b (Cu chain direction). **(b)** Preliminary phase diagram of linarite for H || b as obtained from susceptibility (grey squares) and magnetization experiments (red and black/white circles). Phase I and III are devoted to an antiferromagnetic downturn in the susceptibility at low temperatures, while Phase II shows a ferri-/ferromagnetic upturn in χ.

Cooperation: Forschungszentrum Dresden-Rossendorf; MPI Chemische Physik fester Stoffe Dresden; Helmholtz Zentrum Berlin für Materialien und Energie; TU Braunschweig; TU Bergakademie Freiberg
Funding: DFG

Quantitative interpretation of flux lines arrangement in Fe-pnictides

H. Stopfel, T. Shapoval, V. Neu, U. Wolff, S. Haindl, J. Engelmann, B. Holzapfel, D. S. Inosov, J. T. Park, D. L. Sun, C. T. Lin, V. Hinkov, and L. Schultz

In superconducting non-ideal single crystals the distribution of magnetic flux quanta is affected by existing defects. This interplay between repulsive vortex-vortex interaction and attractive pinning results in a strongly disordered vortex arrangement. Visualization of flux lines with low temperature magnetic force microscopy (LT-MFM) followed by the quantitative analysis of data offers direct insight into pinning on a local scale. We have performed a quantitative analysis of MFM images of a single crystalline $BaFe_{2-x}Co_xAs_2$ sample. In the whole range of magnetic fields up to 9 T, vortex pinning precludes the formation of an ordered Abrikosov lattice. Instead, a vitreous vortex phase with a short-range hexagonal order is observed. Statistical processing of MFM data allows us to directly measure its radial and angular distribution functions and to extract the radial correlation length. In contrast to predictions of the collective pinning model, no increase in the correlated volume with the applied field is observed when compared with different experimental methods. This suggests that the vortices remain in the single-vortex pinning limit [1].

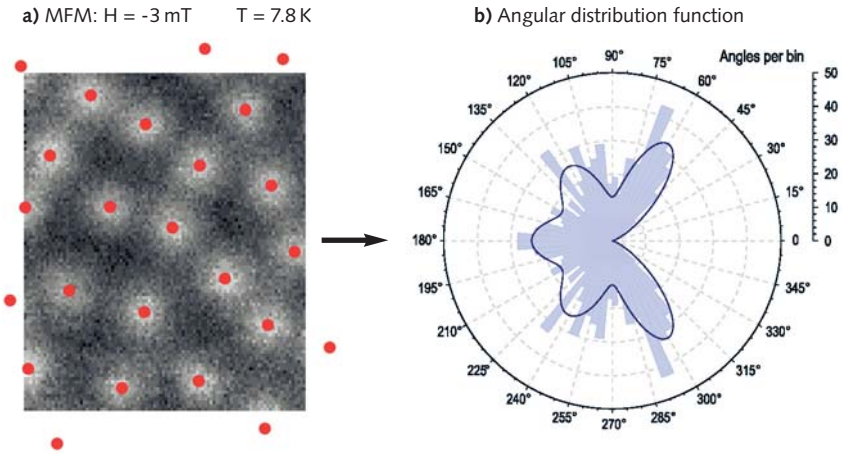

Fig. 1: a) Magnetic force microscopy image of a single crystalline $BaFe_{2x}Co_xAs_2$ sample: red dots from monopole fitting, **b)** the angular distribution reveals the hexagonal coordination of the lattice, as indicated by the pronounced peak located at 60° followed by a dip at 90°. This lets us conclude that the vortex glass phase can be considered as a highly disordered triangular lattice.

Other activities of the MFM group cover investigations of domains in complex magnetic multilayers ([Co/Pt]/Ru [2], Co/CoO [3]), visualization of the phase separation in $Ba_{1-x}K_xFe_2As_2$ superconductors [4] and vortex pinning in NbN thin films as well as the quantitative interpretation of magnetic force microscopy measurements [5].

[1] D.S. Inosov et al. PRB **81** (2010) 014513
[2] C. Bran et. al., PRB **79** (2009) 24430
[3] S.Y. Suck et. al., APL **95** (2009) 162503
[4] J.T. Park et. al., PRL **102** (2009) 117006
[5] S. Vock et. al., APL **97** (2010) 252505

Cooperation: MPI for Solid State Research, Stuttgart, Germany; San Jose Research Center, Hitachi Global Storage Technologies, San Jose, USA; Institut Néel, Grenoble, France

Crystal growth of the intermetallic compounds Pr_2PdSi_3 and Nd_2PdSi_3

Y. Xu, W. Löser, F. Tang, M. Frontzek, C.G. F. Blum, L. Liu, G. Behr, S. Wurmehl, B. Büchner

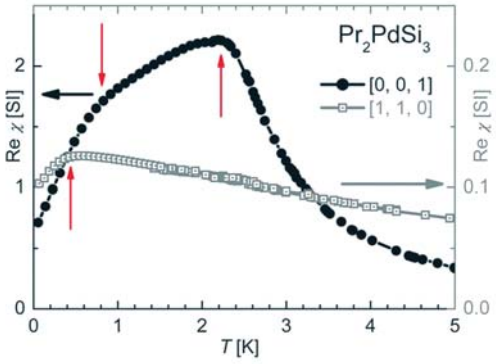

Fig.: Magnetic susceptibility χvs. T for the low temperature range. The curves represent the [0 0 1] (left axis) and the [1 1 0] (right axis) direction, respectively. The Néel temperature, $T_N = 2.17$ K, and two additional transitions at 0.25 and 0.62 K are marked by arrows.

Single crystals of R_2PdSi_3 intermetallic compounds with the light rare earths R = Pr and Nd were grown by a vertical floating zone method with radiation heating at a zone travelling rate of 3 mm/h. Both compounds exhibit congruent melting behaviour at 1790°C (Nd_2PdSi_3) and 1770°C (Pr_2PdSi_3), respectively. Similar to other R_2PdSi_3 compounds the actual crystal compositions are slightly Pd-depleted compared to the nominal stoichiometry. Therefore, the gradual accumulation of Pd in the travelling zone led to a decrease of the operating temperature during the growth process, which was controlled by *in situ* measurements with a two-colour pyrometer using a unique stroboscopic method. Single crystalline Pr_2PdSi_3 samples exhibit a huge anisotropy due to the crystal electric field effect and order antiferromagnetically below the Néel temperature $T_N = 2.17$ K [1]. The [1 1 0] orientation was identified as the magnetic easy axis at room temperature. At lower temperature (≈ 20 K) magnetic easy and hard axes interchange with each other. Two additional magnetic phase transitions are observed at temperatures below 1 K (Fig.). By contrast, Nd_2PdSi_3 is the only compound in this class of intermetallics, which exhibits ferromagnetic order below the Curie temperature $T_C = 15.1$ K [2]. The [001] orientation was identified as the magnetic easy axis.

[1] Y. Xu *et al.*, J. Crystal Growth **312** (2010) 1992–1996.
[2] Y. Xu, *et al.*, Cryst. Res. & Technol., **46** (2011) 135–139

Cooperation: NPU Xian, TU Dresden, TIRF Mumbai, ORNL
Funding: China Scholarship Council

Metamagnetic transition in a novel class of synthetic metamagnets

N. S. Kiselev, C. Bran, U. Wolff, L. Schultz, A. N. Bogdanov, O. Hellwig, V. Neu, U. K. Rößler

Ferromagnetic (FM) multilayers with antiferromagnetic (AF) interlayer exchange coupling are widely used in spin valves and various other spin-electronics devices, and they are considered as promising materials for thermally stable high-density recording technologies. Antiferromagnetically coupled multilayers with strong perpendicular anisotropy ([Co/Pt]/Ru, [Co/Pt]/Ir and others) represent a novel and intensively investigated class of synthetic metamagnets. The magnetization processes in such multilayers strongly depend on the type of the ground state: FM stripe domain state or AF single domain state. We have experimentally investigated $\{[Co(4\ Å)/Pt(7\ Å)]_{X-1}/Co(4\ Å)/Ru(9\ Å)\}_N$ multilayers with AF single domain ground state. We have also provided theoretical description for the magnetic-field-driven evolution of the metamagnetic domains appearing during the magnetization processes. Direct in-field observation of multidomain states confirms the theoretical description of this evolution. Our theoretical approach based on the phenomenological theory of magnetic domains allows one to understand the experimentally observed magnetization processes in [Co/Pt]/Ru superlattices as well as to derive the equilibrium parameters of metamagnetic stripe and bubble domains and to calculate magnetic phase diagrams. These diagrams for the field-driven equilibrium states can also provide the basis for future investigations of the hysteretic processes induced by coercivity and the dynamics at the various magnetic phase transitions in these multilayer systems.

[1] N. S. Kiselev et al. Phys. Rev. B **81**, 054409 (2010).

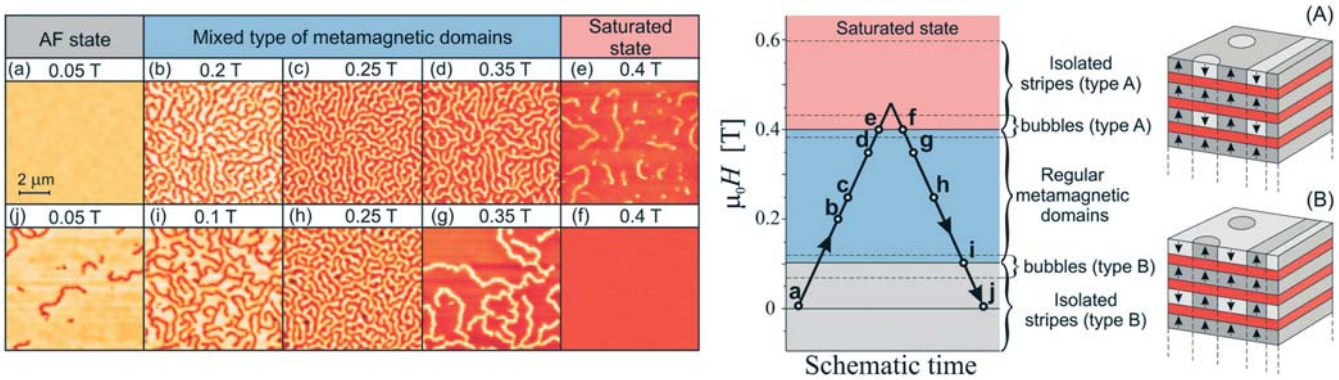

Fig.: Left: domain images of $[\{[Co(4\ Å)/Pt(7\ Å)]_{X-1}/Co(4\ Å)/Ru(9\ Å)\}_N$ multilayers with X=8 and N=18 measured by MFM in a magnetic field. **Right:** theoretical phase diagram and schematic representation of two types of isolated stripe and bubble domains about the saturation field (A) and in remanence (B). A set of points from (a) to (j) on the phase diagram corresponds to the succession of MFM images. Shaded areas indicate the regions for equilibrium states: AF single domain state (gray), metamagnetic regular domains (blue) and FM saturated (pink). Within the equilibrium states isolated ferromagnetic stripes and bubble domains can exist as metastable structures (see MFM images (e) and (j)). Isolated stripe of type B can exist everywhere in the AF single domain state.

Cooperation: Hitachi Global Storage Technologies, San Jose Research Center, USA
Funding: DFG (SPP1239, A8)

Local formation of a Heusler structure in CoFe-Al alloys in CPP-GMR spin valves

S. Wurmehl, P. J. Jacobs[2], J. T. Kohlhepp[2], H. J.M. Swagten[2], B. Koopmans[2], S. Maat[3], M. J. Carey[3], and J. R. Childress[3]

The magnetotransport properties of current-perpendicular-to-the plane giant magnetoresistance (CPP-GMR) devices consisting of ferromagnetic Co-Fe alloys have recently been shown to be significantly improved by addition of up to 28% Al [1]. In order to further optimize CoFe-Al spin-valves, it is important to understand the impact of the Al alloying on the local and electronic structure. Nuclear magnetic resonance (NMR) is able to reveal the next neighbouring shells of the ^{59}Co nuclei in the Co-Fe-Al magnetic films. Its sensitivity to small changes in the local (magnetic and electronic) environment makes NMR an ideal method to determine the local modifications upon addition of Al to the Co-Fe alloy. In our present NMR study, we demonstrate the local formation of a Heusler-like structure by addition of Al to the Co-Fe alloy in CPP-GMR multilayers. The observed local formation of a highly spin-polarized Heusler compound may be correlated to the observed enhancement of the GMR effect [2].

[1] S. Maat *et al.* J. Appl. Phys. **101**, 093905 (2007).
[2] S. Wurmehl *et al.* Appl. Phys. Lett. **98**, 012506 (2011).

Cooperation: [2]Eindhoven Univ. of Technology, The Netherlands; [3]San Jose Research Center, Hitachi GST, USA
Funding: DFG (Emmy Noether project WU595/3-1)

Electrodeposition in high gradient magnetic fields

K. Tschulik, M. Uhlemann, J. Koza, R. Süptitz, K. Hennig, A. Gebert

Patterned metal deposits of Cu, Fe, Co and CoFe alloys were obtained from aqueous electrolytes in superimposed high magnetic gradient fields using arrays of magnetized iron wires. Structuring showed a strong correlation to the magnetic gradient field and to the ion concentration. It was observed that with increasing metal ion concentration the structuring effect decreases despite the increasing paramagnetic properties of the electrolyte. An explanation of this effect is based on local convection induced by the magnetic field gradient force which is dependent on the concentration gradient established during the deposition. Superimposed effects of Lorentz force driven convection were observed only for high Cu^{2+}-ion concentrations decreasing the patterning effect. The Lorentz force caused a smearing of the pattern (Fig. b). Numerical simulations (in cooperation with the TU Dresden) prove that the major influence is due to the action of the magnetic field gradient force and that the action of the Lorentz force would not reproduce the deposit structure. A model based on the impact of the gradient force and the necessity of a concentration gradient was developed, showing the induced convective phenomena in the vicinity of the electrode (Fig. c). The gradient force generates a jet flow normal to the electrode increasing the mass transfer to the electrode, whereas the Lorentz force leads to an electrode-parallel azimuthal flow. This model was qualitatively confirmed by first velocity measurements performed in cooperation with the Bundeswehr University Munich.

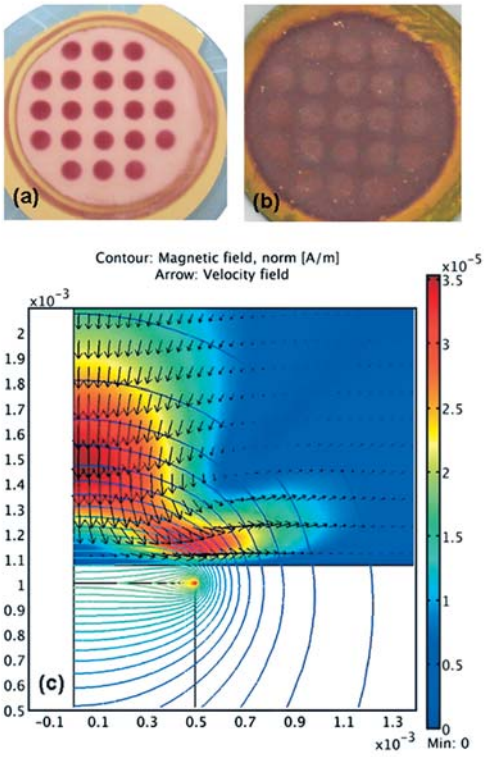

Fig.: Cu deposition from **(a)** 0.01 M $CuSO_4$ and **(b)** 0.3 M $CuSO_4$, **(c)** numeric simulation of the velocity field over a single dot

Cooperation: TU Dresden, FZ Dresden-Rossendorf, Univ. der Bundeswehr München
Funding: DFG / SFB 609, Studienstiftung des deutschen Volkes

The fate of high-field exotic multipolar quantum phases in quasi-1D frustrated spin-chain compounds

S. Nishimoto, S.-L. Drechsler, R. O. Kuzian, and J. van den Brink

We have studied theoretically the influence of various realistic antiferromagnetic (AFM) interchain couplings (ICC) onto the phase diagrams at $T=0$ and high magnetic fields near the saturation field H_s for strongly frustrated quasi-one-dimensional $s=1/2$ magnets with ferromagnetic (FM) nearest neighbor (NN) and AFM next-nearest neighbors (NNN)-inchain couplings $\boldsymbol{J}_1$ and $\boldsymbol{J}_2$, respectively, applying such powerful tools as the DMRG and the Green's function hard-core boson techniques [1]. As a main result (see Fig., [2]) we found that even a relatively weak AFM ICC may remove exotic multipolar phases derived from multi-magnon bound states (MBS) as suggested recently by studies of corresponding 1D models [3]. The reason for this remarkable behavior is the additional repulsion for single magnons provided by the AFM ICC. Among the considered well-known edge-shared chain cuprates, only $LiVCuO_4$ seems to be a promising candidate for a quadrupolar (nematic) phase deri-ved from 2-MBS. Even more exotic octupolar (derived from 3-MBS) or hexadecapolar (4-MBS) phases, located closer to the 1D critical point between a FM and a helical ground state, in principle possible for such systems as $LiZrCuO_4$, are killed by a tiny ICC with a strength < 1% (in units of $|J_1|$). To summarize, our *exact* calculations provide an important step to the understanding of real quasi-1D and 3D strongly frustrated cuprates modelled here within spin isotropic models and arbitrarily strong ICC. For a final assignment the account of weak spin anisotropy, FM ICC, and finite T are necessary.

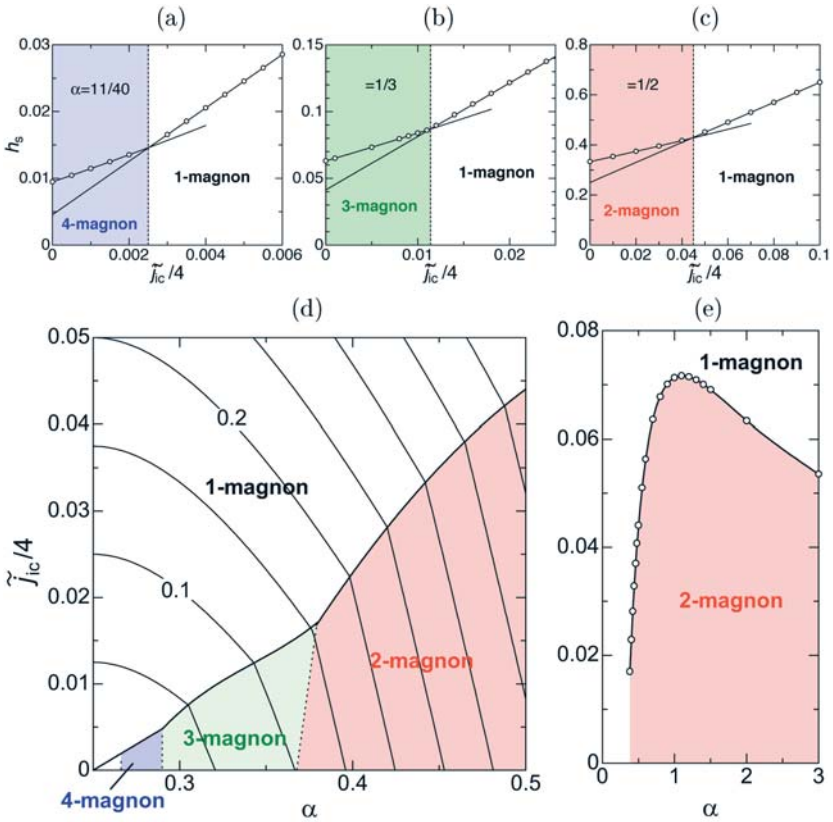

Fig.: Upper **(a-c)**: Dimensionless saturation field h_s (in units of $|J_1|$) *vs.* ICC; lower: critical ICC for the 3D case with perpendicular ICC $j_{ic}=N_{ic}J_{ic}/|J_1|$ *vs.* inchain frustration $\alpha=J_2/|J_1|$. $N_{ic}=4$ is the number of NN interchain neighbors. The phase boundaries are constructed from the 'kinks' in the h_s-plots like in (a-c). The contour lines in **(d)** show the values of h_s for a 3D square lattice of chains. The 2D case with $N_{ic}=2$ is shown in **(d,e)** (dotted lines).

[1] R. Kuzian and S.-L. Drechsler, Phys. Rev. B **75**, 024401 (2007)
[2] S. Nishimoto *et al.*, arXiv:1005.5500v2. (2010)
[3] R. Kecke *et al.* , Phys. Rev. B **76**, 060407 (2007)

Cooperation: Univ. Magdeburg
Funding: DFG

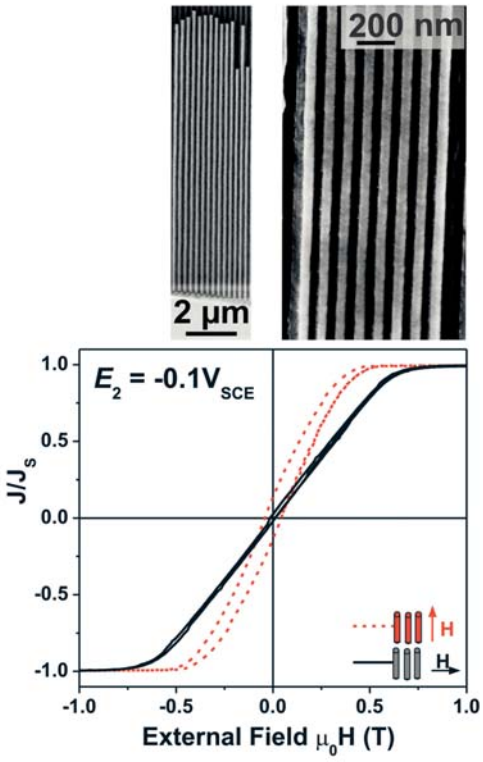

Fig.: Top: Cross sectional HR-SEM micrographs showing the continuity and length of the nanowires and the defect-free microstructure.
Bottom: Magnetization curves of Fe-Pd nanowire arrays in alumina template deposited at optimized E_2. Measurements are shown for both field directions, along and perpendicular to the wire axis.

$Fe_{70}Pd_{30}$ nanowires by pulsed electrodeposition

V. Hähnel, S. Neitsch, C. Mickel, S. Fähler, H. Schlörb, L. Schultz

$Fe_{70}Pd_{30}$ alloys are of particular interest for micro- and nanoactuators and sensors as they show both the thermal and magnetic shape memory effects. Besides thin films nanowires are expected to be beneficial for highest maximum strains and actuation frequencies. Nanowires can be most efficiently grown by electrodeposition within nanoporous templates.

A highly stable plating bath for the electrodeposition of Fe-Pd nanowires into nanoporous alumina templates has been developed [1]. By using an ammonia-sulfosalicylic complexed solution and exchanging Fe^{2+} by Fe^{3+} the chemical reduction of Pd and, therefore, undesirable deposition can be avoided. A pulse potential mode was shown to avoid major inhomogeneities caused by strong hydrogen evolution. Whereas the nanowire composition is mainly determined by the first pulse (deposition) potential, the second pulse ("off") potential E_2 was identified to be the key parameter for continuous defect-free nanowires. The adjustment of the "off" potential to more positive values does not change the nanocrystalline bcc $Fe_{75}Pd_{25}$ structure of the as-deposited alloy but avoids local composition variations such as Pd rich areas, constrictions, short wire fragments and partially empty pores. The magnetic behaviour is dominated by shape anisotropy along the axis of the nanowires but the reduced number of defects increases magnetostatic interactions between neighbouring nanowires [2].

[1] V. Haehnel et al. Electrochem. Commun. **12** (2010) 1116.
[2] V. Haehnel et al. J. Phys. Chem. C **114** (2010) 19278.

Funding: DFG

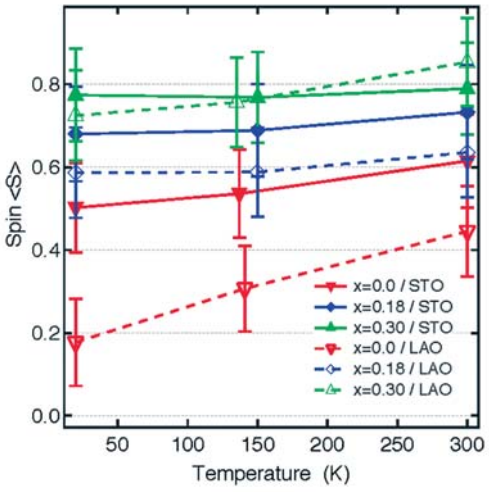

Fig.: Summary of the temperature dependent spin values for all films. A clear temperature dependence is observable for the compressed and undoped LCO/LAO sample only (LAO – $LaAlO_3$, STO – $SrTiO_3$).

Spin state evolution of strained $La_{1-x}Sr_xCoO_3$ thin films

T. Kroll, G. Vankó[1], A. D. Rata, J. Geck, S. Huotari[2], M. Knupfer, B. Büchner

The perovskite cobaltates $La_{1-x}Sr_xCoO_3$ (LSCO) have attracted considerable attention in the last decade due to several puzzling phase transitions induced by changes in temperature doping and hydrostatic pressure. Most of these phase transitions seem to be strongly related to the spin state degree of freedom of Co^{3+} and Co^{4+} ions.

At low temperatures, the parent compound $LaCoO_3$ (LCO) is a nonmagnetic insulator with a low-spin configuration. However, for T > 90 K higher spin states become populated; a phenomenon whose nature is still under debate. The latest available experimental and theoretical results are rather contradictory, suggesting either an additional high-spin or an intermediate-spin state contribution of the Co 3d electrons at higher temperatures.

We investigated hole doped LSCO films epitaxially grown under compressive ($LaAlO_3$ substrate) and tensile ($SrTiO_3$) strain in a wide doping range. The local electronic structure of Co and the macroscopic magnetic properties are studied employing x-ray emission spectroscopy at the Co Kβ line together with SQUID measurements, respectively. We find a dependence of the local magnetic moment on three factors: epitaxial strain, doping and temperature. While compressed LSCO thin films behave similar to bulk samples, clear differences have been observed when applying tensile strain. We conclude that the itinerant double exchange picture generally assumed for bulk LSCO, still builds the basis of the electronic structure of the films. The metal–insulator transition observed for different strains at 30 % hole doping, is explained by a narrowing of the conduction band due to the lattice distortions.

Cooperation: [1]KFKI Research Institute for Particle and Nuclear Physics, Budapest; [2]European Synchrotron Radiation Facility, Grenoble
Funding: DFG, EU, OTKA

Magnetic Materials in Sustainable Energy

O. Gutfleisch, T. Woodcock, J. Thielsch, K. Güth, K. Skokov, M. Krautz, J. Moore, M. Mohr, J. Liu, K. Löwe, M. Richter, R. Schäfer, D. Lindackers, K.-H. Müller, L. Schultz

A new energy paradigm, consisting of greater reliance on renewable energy sources and increased concern for energy efficiency in the total energy lifecycle, has accelerated research in energy-related technologies. Due to their ubiquity, magnetic materials play an important role in improving the efficiency and performance of devices in electric power generation, conversion and transportation. Magnetic materials are essential components of energy applications (i.e. motors, generators, transformers, actuators, etc.) and improvements in magnetic materials will have significant impact in this area, on par with many "hot" energy materials efforts (e.g. hydrogen storage, batteries, thermoelectrics, etc.).

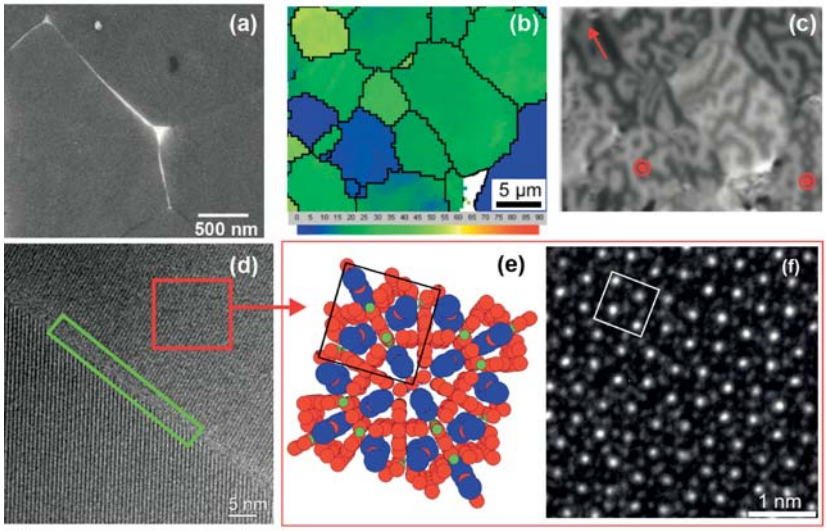

Fig.: Multiscale characterization of sintered NdFeB commercial magnets: **(a)** Backscattered electron SEM image showing the hard magnetic 2-14-1 matrix grain well-separated by a thin Nd-rich intergranular phase (white contrast), **(b)** EBSD image showing quantitatively the local variation in orientation of the different grains, **(c)** optical Kerr microscopy showing the corresponding magnetic domain structure of the same area, **(d)** TEM image showing the amorphous Nd-rich intergranular phase of about 1 nm thickness (green box), (e) and (f) showing schematically and in atomic resolution the 2-14-1 matrix phase.

Our work focuses on the state-of-the-art hard magnets and magnetocaloric materials with an emphasis on their optimization for energy applications. Specifically, the impact of hard magnets on electric motor and transportation technologies, of soft magnetic materials on electricity generation and conversion technologies, and of magnetocaloric materials for refrigeration technologies, is analysed.

The synthesis, characterization, and property evaluation of the materials, with an emphasis on structure-property relationships, is examined in the context of their respective markets as well as their potential impact on energy efficiency.

Finally, considering future bottle-necks in raw materials and in the supply chain, options for recycling of rare-earth metals are being developed.

Ref.: O. Gutfleisch et al. Magnetic Materials and Devices for the 21st Century: Stronger, Lighter, and More Energy Efficient (review), Adv. Materials, DOI: 10.1002/adma.201002180.

Cooperation: CNRS Grenoble, France; Toyota Motor Corporation, Japan; Tohoku Univ. Sendai, Japan; Univ. of Texas, USA; Vacuumschmelze GmbH, D; Nat. Institute of Materials Science, Tsukuba, Japan; Imperial College London, UK; Istituto Nazionale di Ricerca Metrologica Torino, I; Univ. de Barcelona, E; Ames National Labs, USA; Univ. de Zaragoza, E; Cambridge Ltd., UK

Funding: Toyota, Hans L. Merkle Stiftung, Bosch, Aichi-Steel, Forschungsvereinigung Antriebstechnik (FVA), EU (Solid State Energy Efficient Cooling - SSEEC), Pakt 2010

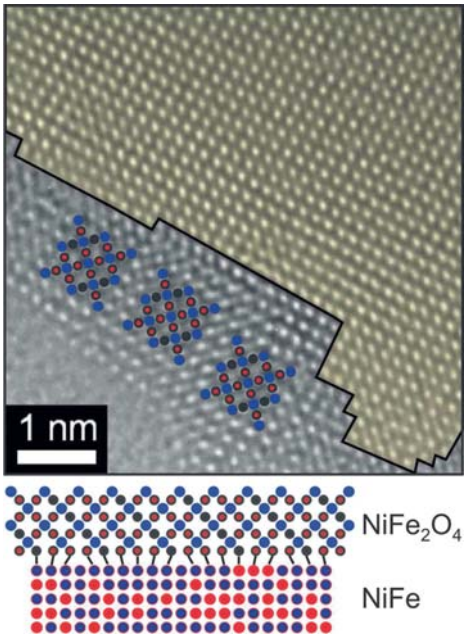

Fig.: Top: Aberration-corrected HRTEM image of the interface between the $NiFe_2O_4$ oxide shell and the metallic core (shaded in yellow) in an oxidized FeNi nanoparticle in [100] zone axis orientation.
Bottom: Model structure of the metal-oxide interface as derived from the HRTEM analysis and supportive EELS measurements.

The impact of oxygen on the surface-near lattice structure in FeNi nanomagnets

B. Bieniek, D. Pohl, A. Hartmann, L. Schultz and B. Rellinghaus

As a consequence of the augmented impact of the surface free energy due to a largely enhanced surface-to-volume ratio, binary metallic alloy nanoparticles frequently experience a segregation of one of the alloy constituents toward the particle surface. Such segregation phenomena were investigated in binary FeNi nanoparticles with close to equi-atomic composition by means of a combination of aberration-corrected high resolution transmission electron microscopy (HRTEM) and molecular dynamics (MD) simulations. It was also studied if and to which extend a (partial) oxidation of the particles affects the surface-near lattice structure. FeNi nanoparticles which are less noble and thus more sensitive to oxidation than previously studied FePt particles were prepared by means of inert gas condensation in order to provide clean, uncovered surfaces. Transport of the particles under a protective atmosphere in a dedicated transfer holder prevented the particles from oxidation prior to their examination and thus allowed for a comparison of oxidized and un-oxidized particles. HRTEM investigations and local electron energy loss spectroscopy (EELS) show that segregation also occurs in FeNi particles. Here, Fe is enriched at the surface which leads to the formation of a (Fe-rich) $NiFe_2O_4$ shell around a metallic core as soon as the particles are exposed to air (c.f. Fig.). The surface-near lattice structure of the metal (or the metallic core), however, remains largely unaffected by the oxidation. This in turn renders the surface-near lattice dilation a fingerprint of segregational phenomena in alloy nanoparticles.

Research Area 3
Molecular nanostructures and molecular solids

Tailor-made carbon nanotubes by fixed bed CVD

M. Ritschel, A. Leonhardt, B. Büchner

Different application fields of carbon nanotubes (CNT) require nanotubes with defined diameters, lengths, numbers of shells and this in large quantities. For example, only single-walled (SW) CNTs are appropriate as membranes in the desalination of sea water. For the embedding in polymers or metals multi-walled (MW) CNTs with a high aspect ratio show the best results. The mechanical strength in composites will be improved only by CNTs with a few numbers of shells. In contrast, MWCNTs with low defect density and with a shell number not more than 20 show a high electrical conductivity.
By using the so-called "fixed bed CVD" these tailor-made CNTs can be synthesized in dependence on the loading of MgO powder with metals like Fe, Co, Mo and Cr. Within a BMBF project we created special catalyst materials for SW-, double (DW)- and MWCNTs. Regarding the reproducibility of the synthesis process and the yield of CNTs methane (for SW/DW) and ethylene (for MW) are the most suitable hydrocarbons. Yields (related to 1 g assigned catalyst) of 1.4 g for SW, 12 g for DW and 17 g for few-walled CNT (till 7 shells) could be achieved. For almost structurally perfect MWCNTs with an averaged diameter of 12 ± 3 nm yields higher than 500 g (99 % purity) are possible. These enormous differences are caused by the strong dependence of the shell numbers on the catalyst particle size on the support MgO. Our detailed investigations show that SW/DW- CNTs are only formed till particle sizes < 2 nm, this corresponds to a loading of MgO with max. 2 wt % metal (Fe, Co, Mo, Cr). Higher loading rates lead to larger particles and therefore to MWCNTs. All catalysts are usable in an industrial "fluidised bed reactor", where CNTs were produced in the kg-scale/day.
Cooperation: Bayer MaterialScience AG, Fritz-Haber-Institut Berlin,
Ruhr-Univ. Bochum. Univ. Erlangen-Nürnberg, TU Ilmenau
Funding: BMBF „InnoCNT"

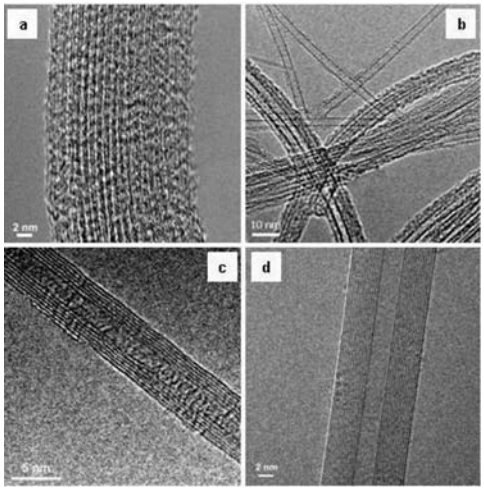

Fig.: CNT-structures in dependence on the metal-loading of MgO; **a:** SW- bundles (< 1 wt% metal); **b:** SW/DW-mixture (< 1–4 wt % metal); **c:** MW with 7 shells (3–8 wt % metal); **d:** MW with 13 shells (~20 wt % metal)

Oxide graphitisation catalysts for carbon nanotubes and graphene

M. H. Rümmeli, A. Bachmatiuk, F. Börrnert, I. Ibrahim

For the most part, the synthesis of carbon nanotubes (CNT) and graphene revolves on the use of 3d valence transition metals such as Fe, Ni and Co. More recently several groups have grown CNTs from noble metals such as Au, Ag and Cu and poor metals, *e.g.* Pb, In. However, metals are not best suited for microelectronics because they can diffuse within chip reducing its lifetime. Moreover, in the case of graphene, the use of a metal catalyst requires the graphene be transferred for device fabrication. This process can damage the graphene and also leave impurities on it. Thus, the ability to form CNT and graphene from materials compatible with Si technology is attractive. To this end we are developing oxide catalyst systems carbon nanostructure formation. For example, we have successfully shown the use of SiO_2 as a graphitisation material for CNT & carbon fibre formation [1] and graphene (see Fig.). The studies show SiO_2 undergoes a carbothermal reduction to SiC. We are also developing the use of non-reducible high dielectric constant, *k*, catalysts, again for CNT and graphene [2]. Of particular interest are the use of high K dielectrics such as magnesia, alumina and zirconia.
[1] A. Bachmatiuk et al. *ACS Nano*, 2009, 3, 4098-4104.
[2] M.H. Rümmeliet al. *ACS Nano* 4, 4206 (2010)
Cooperation: Technical University Dresden and Oxford University
Funding: DFG RU 1540/11-1

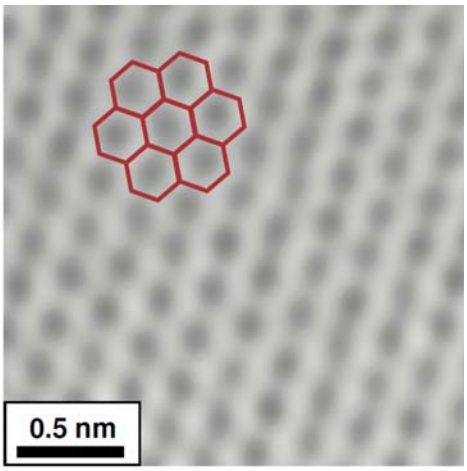

Fig.: HRTEM micrograph of graphene section

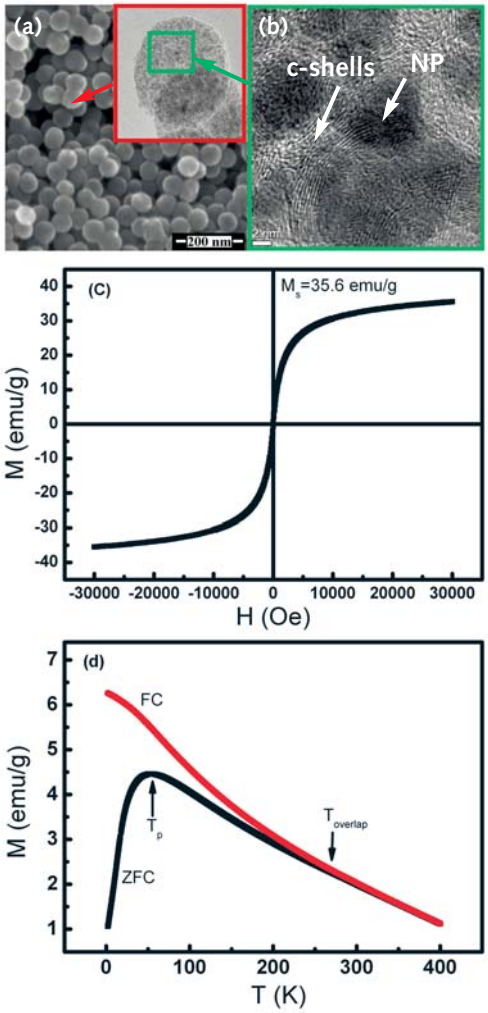

Fig.: (a) SEM image of the synthesised particles. The inset shows HRTEM image for one nanoball. **(b)** HRTEM image at higher magnification showing the morphology of one nanoball surface. **(c)** and **(d)** M vs. H at room temperature and M vs. T at 100 Oe respectively, for the nanoballs.

Synthesis of superparamagnetic nanoparticles dispersed in geometrically perfect spherical shape carbon nanoballs

E. M. M. Ibrahim, S. Hampel, J. Thomas, A. U. B. Wolter, V. O. Khavrus, C. Täschner, A. Leonhardt, B. Büchner

The main challenge for producing superparamagnetic nanoparticles (with size lower than the domain dimension) using chemical vapour deposition technique is avoiding the particles agglomeration due to Oswald ripening and sintering process. The use of radio frequency (rf) plasma for pre-decomposition of ferrocene leads to electrostatic charging of the produced particles and therefore decreases the particle agglomeration. Scanning and high resolution transmission electron microscopy investigations (Fig. a) show that the synthesised material consists of carbon nanoballs with a geometrically perfect spherical shape and a nearly unique diameter of 70±2 nm. Fig 1b shows the detailed morphological structure of an individual nanoball, the metal (Fe) nanoparticles appear as dark spots embedded in the carbon nanoballs. Their size is about 5-10 nm with a quite narrow size distribution. Both the X-ray diffraction and electron energy loss spectroscopy analyses indicate that the embedded nanoparticles are composed of either Fe_3O_4 or γ-Fe_2O_3 or a mixture of them. Magnetic measurements performed using VSM-SQUID magnetometry show that the synthesised samples have superparamagnetic properties with a saturation magnetization of 35,6 emu/g and a blocking temperature of 50 K (Fig. c, d). Furthermore, the nanoballs are highly dispersible in different solvents (Ethanol, water and acetone) which makes them promising for different applications.

Cooperation: Department of Urology, TU Dresden
Funding: DFG

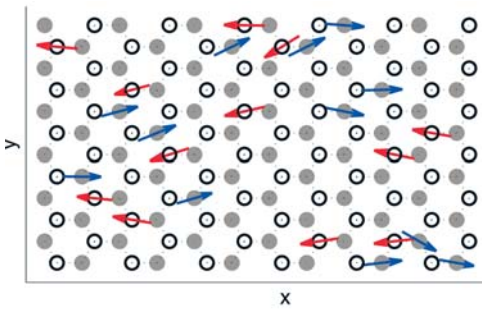

Fig.: Snapshot of the Monte-Carlo simulation. The arrows denote the spins of the magnetic impurities, one sees that they order antiferromagnetically.

Spin-polarized semiconductor induced by magnetic impurities in graphene

M. Daghofer, N. Zheng[1], A. Moreo[2,3]

This year's Nobel prize was awarded for groundbreaking experiments on graphene, the two-dimensional sheet of carbon atoms that is attractive for two different reasons: First, its electronic states are like massless Dirac Fermions, which leads to effects that are interesting from fundamental and theoretical points of view. Second, its high carrier mobility in combination with its thinness and flexibility makes it interesting for applications. In order to be applicable as a semi-conductor, a gap needs to be opened in the electronic states.

In Ref. [1], we studied theoretically how impurities adsorbed on graphene affect the electronic states, using analytical approximations as well as unbiased Monte-Carlo simulations. We found that for magnetic impurities, the mobile conduction electrons induce antiferromagnetic order, which in turn opens a gap. Such an effect is far more difficult to achieve with non-magnetic impurities. Furthermore, we found that if one could somehow make the impurities sit on only one sublattice, the conduction electrons would become spin polarized. When the gap is opened, the Dirac Fermions are no longer massless, but the impurities do not localize the electrons and their mobility is expected to remain very high.

[1] M. Daghofer et al. Phys. Rev. B **82**, 121405(R) (2010)

Cooperation: [1]College of William and Mary (VA, USA); [2]University of Tennessee at Knoxville (TN, USA); [3]Oak Ridge National Laboratory (TN, USA)
Funding: DFG, NSF, DOE

Electronic properties of molecular solids: the peculiar case of solid picene

F. Roth, M. Grobosch, B. Mahns, B. Büchner and M. Knupfer

Superconductivity is one of the most fascinating physical phenomena in solid state physics. The search for new superconducting materials is motivated by applications as well as fundamental science. Recently, a new organic superconductor, K-intercalated picene with high transition temperatures Tc (up to 18 K) has been discovered. This represents a major breakthrough as it has the second highest Tc of organic solids only below the one of alkali metal intercalated fullerenes. Designing new molecular solids with higher Tc or tailored electronic response requires a detailed microscopic understanding of the electronic states.

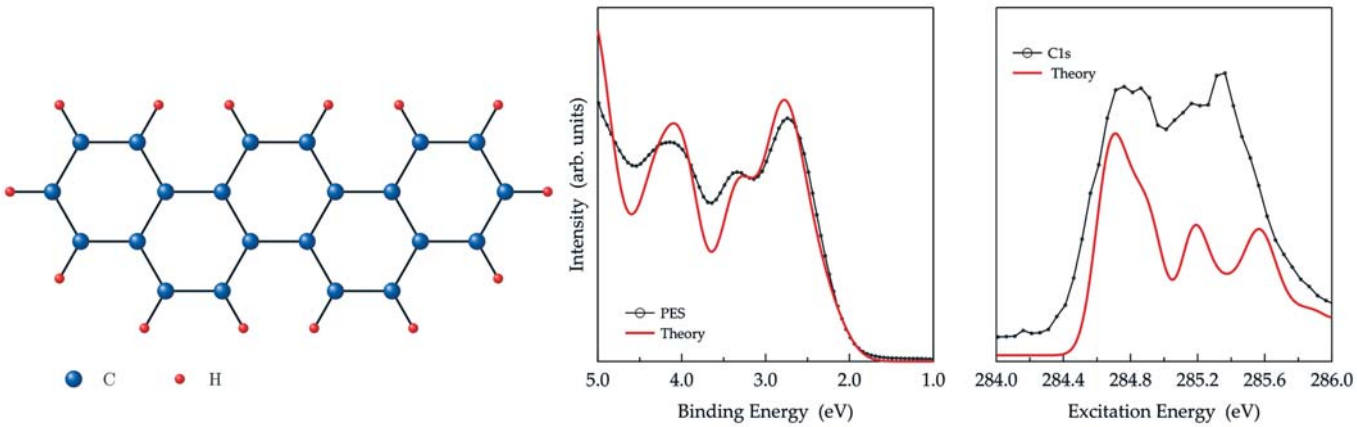

Fig.: Left: Schematic representation of the molecular structure of picene. **Middle:** Valence band photoemission data representing the occupied density of states. **Right:** C1s excitation data of solid picene representing the unoccupied density of states measured using EELS. In the case of the C1s comparison the theoretical data have been shifted such that the first peaks coincide.

We conducted a comprehensive investigation of the electronic properties of solid picene using state-of-the-art experimental tools and first-principles manybody calculations. Our results provide a detailed analysis of the occupied and empty states, highlighting the presence of four flat quasi-degenerate conduction bands that give rise to a high density of states around the Fermi level in the n-doped compound, help to reduce the impact of electronic correlations, and are hence responsible for the superconductivity. Moreover, the measured spectral properties can only be accounted for once the anisotropy of the structure, local-field corrections and electronic correlations are considered. For details see: F. Roth *et al.*, *New J. Phys.* **12,** 103036 (2010).

Cooperation: Nano-Bio Spectroscopy group and ETSF Scientific Development Centre, Universidad del Pais Vasco, San Sebastian, Spain
Funding: DFG

Magnetostructural correlations in polynuclear nickel(II) aminothiophenolate complexes

Y. Krupskaya, A. Alfonsov, A. Parameswaran, V. Kataev, R. Klingeler, G. Steinfeld[1], N. Beyer[1], M. Gressenbuch[1], B. Kersting[1], B. Büchner

The nickel(II) ion is a very promising building block for the realization of a single molecular magnet (SMM), because it has an integer spin ($3d^8$, $S_{Ni} = 1$) and often exhibits a significant single ion anisotropy. Therefore, Ni(II) is increasingly used for the synthesis of molecular magnetic complexes. However, the proper single ion properties are not enough to realize an SMM. Another important issue is the occurrence of a ferromagnetic coupling between the ions which is necessary to obtain a high spin ground state. Therefore the studies of the interplay of magnetic exchange interactions and the molecular structure of the complexes is of a particular interest. For that we have focussed on two novel polynuclear Ni(II)-based macrocyclic molecular complexes [1]. The first

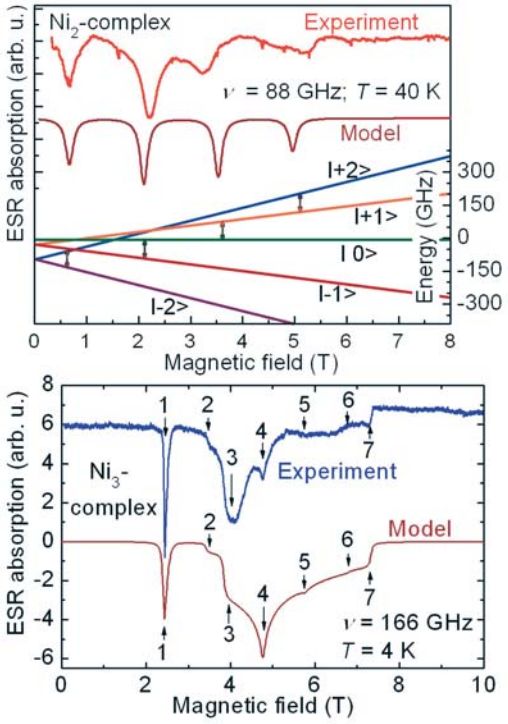

Fig.: Top: measured and simulated ESR spectra of an oriented powder sample of the Ni_2-complex. Four clearly separated absorption lines indicate the $S_{Ni2} = 2$ ground state with the zero field splitting of the spin levels. The energy level diagram was obtained from the modelling of the ESR spectra. This diagram corresponds to a negative sign of the single ion anisotropy. **Bottom:** measured and simulated ESR spectra of a powder sample of the Ni_3-complex. The modelling describes well the main features of the spectrum and reveals a positive sign of the single ion anisotropy.

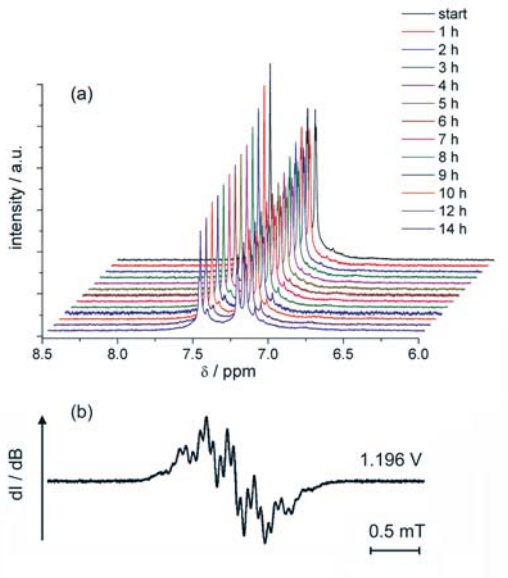

Fig.: *In situ* ^{1}H NMR spectroelectrochemistry **(a)** of the oxidation of DCNDBQT in CD_2Cl_2 with $TBAPF_6$ at an electrode potential of 1190mV (working electrode: carbon fibre) and **(b)** ESR spectrum of the DCNDBQT cation radical during the potentiostatic electrolysis at the potential of the first oxidation step in 0.1 M $TBAPF_6$ / CH_3CN (working electrode: platinum mesh).

complex contains two Ni ions coupled via two ~90° μ-S sulphur bridges. The second complex has three Ni ions coupled via two μ-S sulphur bridges with the Ni–S–Ni angles of 133°. One could expect that the different bond angles in the studied complexes should give rise to different exchange interactions between the Ni ions. Indeed our static magnetization measurements revealed a ferromagnetic coupling $J_{Ni2} = -42$ K and a total spin $S_{Ni2} = 2$ in the case of the Ni_2-complex and an antiferromagnetic coupling $J_{Ni3} = +140$ K for the Ni_3-complex yielding a total spin $S_{Ni3} = 1$. Our high-field frequency-dependent electron spin resonance (HF-ESR) measurements and simulations of the ESR spectra (see Fig.) enabled determination of all relevant parameters of the effective spin Hamiltonian describing the ground states of the complexes. For the Ni_2-complex we observe a bistable $S_z = \pm 2$ magnetic ground state with an "easy axis" and magnetic anisotropy parameter $D_{Ni2} = -1.1$ K. In contrast, for the Ni_3-complex our data reveal an "easy plane" situation in the ground state with $D_{Ni3} = +2.9$ K. Thus, we find that the variation of the angles of the sulphur bridging bonds and of the ligand structure has a very strong impact on the magnetic properties of the studied Ni(II)-based complexes. Such a control of exchange interactions and single ion anisotropy suggests a pathway for a targeted assembly of single molecular magnetic complexes with predetermined magnetic properties.

[1] Y. Krupskaya et al., ChemPhysChem 11, 1961-1970 (2010)

Cooperation: [1]Institute of Inorganic Chemistry, Univ. of Leipzig
Funding: DFG (FOR 1154)

Charged States of α,ω-Dicyano β,β′-Dibutylquaterthiophene

K. Haubner, S. Klod, J. Tarabek, F. Ziegs, E. Jähne, V. Lukes L. Dunsch

The influence of the molecular structure on the stabilisation of charged states was investigated by a combined application of spectroelectrochemical techniques using novel α,ω-dicyano substituted β,β′-dibutylquaterthiophene (DCNDBQT) with the short alkyl side chains and improved solubility. The redox processes of DCNDBQT were studied by voltammetry, *in situ* NMR (Fig. a) and ESR/Vis-NIR spectroelectrochemistry (Fig. b), *ex situ* mass spectrometry and *quantum chemical calculations* to follow both the paramagnetic and the diamagnetic species formed in redox reactions. The oxidation of DCNDBQT gives two separate redox steps with the first one being reversible. The UV-Vis NIR absorption bands at 646 and 1052 nm and the ESR signal recorded at the first anodic step prove the formation of a radical cation. In addition the optical data, NMR spectrolelectrochemistry and quantitative ESR analysis points to a reversible π-dimerization of the radical cation. The π-dimer and the radical cation are oxidized in the second anodic step to form a σ-dimer by a follow-up reaction of the dication.

As the substitution by cyano groups opens the route to cathodic reductions of the thiophene oligomer DCNDBQT undergoes a reduction in a single electron transfer which turned out to be quasi-reversible. By *in situ* ESR UV-Vis NIR spectroelectrochemistry the electrochemical generation of an anion radical was demonstrated. The anion radical of the quaterthiophene structure is not stable and undergoes further dimerisation and trimerisation to stabilize the charged structures as shown by ESR spectroscopy, NMR spectroelectrochemistry and mass spectrometry. The experimental data of the charged states both under oxidation and reduction were interpreted by quantum chemical calculations resulting in a good consistency of experiment and theory.

Cooperation: TU Dresden, CAS, Prague, STU Bratislava
Funding: DFG GACR project 203/07/J067

Intravital MR Contrast Agent based on an endohedral Gadolinium-Clusterfullerene-Conjugate: A new chance in cancer diagnostics

L. Dunsch, K. Braun[1], R. Pipkorn[1], M. Bock[1], T. Baeuerle[1], S. F. Yang[2], W. Waldeck[1] and M. Wiessler[1]

Requirements for successful intracellular imaging with MRT are a perspicuous signal and a sufficient accumulation of contrast agent (CA) within the target cells. There are numerous approaches but further developments of MR contrast agents with new properties are indispensable. All CAs used so far offer one feature in common: they are not able to penetrate the cellular membranes and their use is restricted to the blood stream and the interstitial space.

For a successful intracellular and intranuclear MRI we covalently linked $Gd_xSc_{3-x}N@C_{80}$ molecules with both the nuclear address (NLS) derived from SV40 T-antigen, which in turn is linked via a disulfide bridge to a peptide facilitating the passage across cell membranes (CPP). This is our BioShuttle-conjugate resulting in a Cell Nucleus (NLS)-$Gd_xSc_{3-x}N@C_{80}$. This Gd-cluster@-BioShuttle utilizing the cytoplasmically located importins, classified as substrates for the active RAN-GDP system, mediating an efficient transport of the $Gd_xSc_{3-x}N@C_{80}$ cargo into cell nuclei. To build such conjugates we improved methods for rapid and complete ligation of hydrophobic molecules like fullerenes (and especially their functionalized derivatives) to carrier molecules. The Diels-Alder-Reaction (DAR) turned out to be an applicable ligation method, but the reverse reaction proved to be restrictive and unsatisfactory. The use of the "DAR with an inverse electron demand (DARinv)" can circumvent these drawbacks. We exemplary demonstrate a successful intracellular MRI through a novel CA-delivery. The Fulleren-BioShuttle-conjugate features high proton relaxation and, in comparison to the commonly used contrast agents, high signal enhancement at very low Gd concentrations. This modularly designed contrast agent represents a new tool for improved monitoring and evaluation of interventions at the gene transcription level. Also, a widespread monitoring to track individual cells is possible, as well as sensing of microenvironments. BioShuttle can also deliver constructs for transfection or active pharmaceutical ingredients, and scaffolding for incorporation with the host's body. Using the Gd-cluster@-BioShuttle as MRI contrast agent allows an improved evaluation of radio- or chemotherapy treated tissues.

[1] K. Braun, et al. Int. J. Med. Sci. **2010** *7*(*3*) 136-146

Cooperation: [1]DKFZ Heidelberg,
Funding: DKFZ

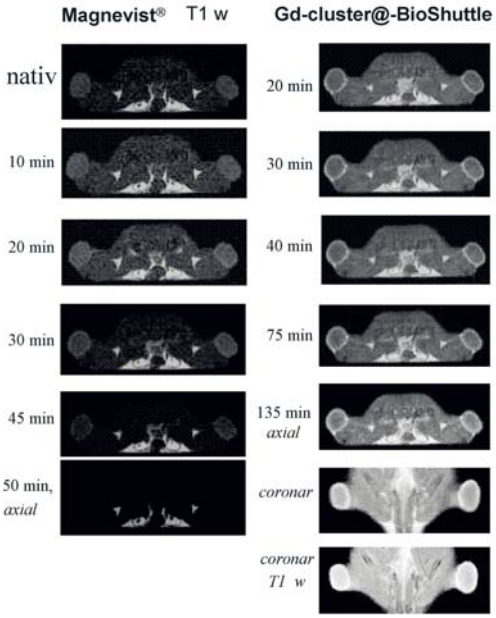

Fig.: Comparison of the time dependent accumulation of a conventional contrast agent (left) and the new Gd-cluster@Bio-Shuttle in the carcinoma of a rat

The role of the cluster on the relaxation of endohedral fullerene cage carbons – a NMR spin-lattice relaxation study of an internal relaxation reagent

S. Klod, L. Zhang and L. Dunsch

The endohedral nitride clusterfullerenes were investigated with respect to the strategy of an internal relaxation reagent by following the cluster size effects and the influence of f-electrons on the carbon relaxation. Due to the large relaxation times in major fullerenes it is difficult to measure ^{13}C-spectra within reasonable times. Therefore the use of relaxation agents was discussed to improve ^{13}C NMR measurements of these molecules. One of the drawbacks of this method is a loss in resolution due to a signal broadening. The role of an endohedral cluster in fullerene cages for the relaxation at the fullerene carbons is a matter of high interest for the NMR studies of fullerene structures opening the to endohedral relaxation reagents. For endohedral nitridecluster fullerenes

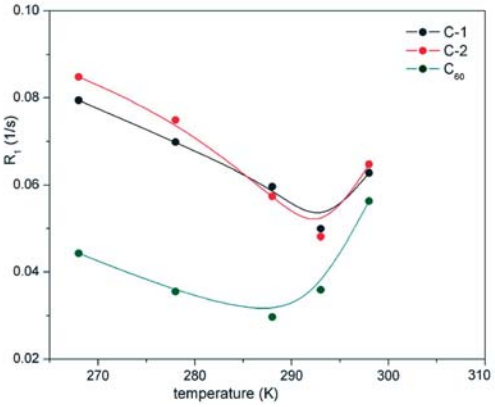

Fig.: Temperature dependence of the relaxation rate R_1 of I_h-$Lu_3N@C_{80}$ in comparison to I_h-C_{60}

I_h-$Sc_3N@C_{80}$, I_h-$Y_3N@C_{80}$ and I_h-$Lu_3N@C_{80}$ of I_h-C_{80} cage symmetry the relaxation rates were observed and an increase was found due to the presence of the cluster.[1] The results are compared to those on the relaxation of empty fullerenes.[2,3] In general the enlarged cage size increases the relaxation of the carbons. The encapsulated metal atoms have an additional dipole-dipole interaction to the relaxation rate of the carbon atoms depending on their magnetic character. For different metals the increased nitride cluster size is one reason for the observed stronger dipole-dipole interaction. In contrast, a higher shielding of a metal nucleus by its electron shell leads to a reduced magnetic effect. The negative charge on the cage increases the electron density thus decreasing T_1.
In temperature dependent studies, the diffusion is fast compared to the rotation of the molecule at higher temperatures what is typical for the spherical shape of the fullerene cage. Thus only a minor deformation of the cage by the endohedral voluminous cluster is found. The shape of the cage is preserved and less influenced by the type and size of the cluster.

[1] S. Klod et al. *J. Phys. Chem. C* **2010** *114*(*18*) 8264-8267
[2] S. Klod, L. Dunsch, *J. Phys. Chem. C* **2009** *113*(*34*) 15191-15195
[3] S. Klod, L. Dunsch, *ACS NANO* **2010** *4*(*6*) 3236-3240

Cooperation: University of Potsdam, Germany
Funding: Chinese Scholarship Council

An *in situ* Raman spectroelectrochemical study of an organic peapod: Sexithiophene encapsulated in single walled carbon nanotube

M. Kalbáč[1], L. Kavan[1], S. Gorantla, T. Gemming and L. Dunsch

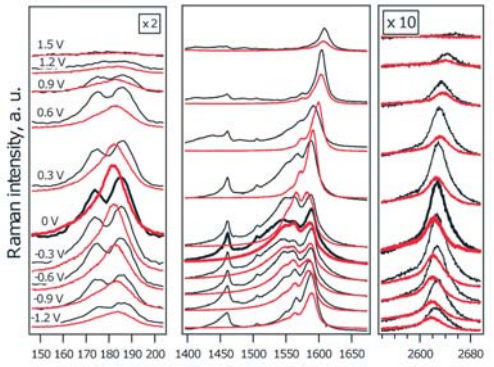

Fig.: Potential dependent Raman spectra (excited at 1.83 eV) of 6T@SWCNT (black) and pure SWCNT (red) on a Pt electrode in 0.2 M $LiClO_4$ + acetonitrile. The electrode potential was varied by steps of 0.3 V from 1.5 to –1.2 V vs. Ag pseudo-reference electrode for curves from top to bottom. Spectra are offset for clarity, but the intensity scale is identical for all spectra in the respective window.

It has been shown recently that the morphology of sexithiophene is dramatically influencing the performance of devices. However, it is very difficult to control the morphology in macroscopic crystals. The assembling of crystals inside SWCNT presents a challenge towards this control, since unusual crystal structures of many inorganic materials can be grown in this way. The diameter of single walled carbon nanotubes (SWCNT) is typically in the range of 1 to 2 nm. This dimension is comparable to the size of small organic molecules and therefore they can be confined in the interior of SWCNT.
The interaction of single wall carbon nanotubes (SWCNT) and the α-sexithiophene was studied by Raman spectroscopy and by in-situ Raman spectroelectrochemistry.[1] The encapsulation of α-sexithiophene in SWCNT and its interaction causes a bleaching of its photoluminescence and also small shifts of its Raman bands. The Raman features of the SWCNT with embedded α-sexithiophene (6T-peapods) change both in intensity and frequency as compared to those of pristine SWCNT, which is a consequence of a change of the resonant condition. The electrochemical doping demonstrates that the electrode potential applied on SWCNT wall causes changes of embedded α-sexithiophene. The effect of electrochemical charging on Raman features of pristine SWCNT and 6T@SWCNT has been compared. It is shown that the interaction of SWCNT with α-sexithiophene changes the electronic structure of SWCNT also in its charged state. This change of electronic structure is demonstrated both for semiconducting and metallic tubes.

[1] M. Kalbáč et al. *Chem. Eur. J.* **2010** *16*(*38*) 11753–11759

Cooperation: [1]Heyrovský Institute of Physical Chemistry, CAV, Prague
Funding: DFG GACR

A New Form of Endohedral Clusterfullerenes with Sulfur: Metal Sulfide in a C_{3v} C_{82} Fullerene Cage

L. Dunsch, S. F. Yang[1], L. Zhang, A. Svitova, S. Oswald, A. A. Popov

The row of endohedral clusterfullerenes, including so far nitrides ($M_3N@C_{80}$), oxides ($Sc_4O_{2,3}@C_{80}$), and carbides ($Sc_{3,4}C_2@C_{80}$, $M_2C_2@C_{82}$), has been extended by a new type of sulfur-containing clusterfullerenes: the metal sulfide (M_2S) has been stabilized within a fullerene cage for the first time.[1] While for trimetallic nitride clusters the fullerene cage is predominantly C_{80}-I_h, we found in the case of sulfur cluster the C_{82} cage as the dominating fullerene structure. Despite of the situation in nitride cluster with non-IPR C_{82} cages within $Gd_3N@C_{82}$, the new sulfide cluster $M_2S@C_{82}$ prefers an IPR cage (C_{82}-C_{3v}(8)). This is due to the fact the formal transfer of four electrons from the cluster to the cage results in the most stable C_{3v}(8) cage isomer for the charged state as the same to that in carbide clusterfullerenes, $M_2C_2@C_{82}$. The UV-Vis-NIR, electrochemical and FTIR spectroscopic characterization and extended DFT calculations further point to a close similarity of the $M_2S@C_{82}$ cage isomeric and electronic structure to that of the carbide clusterfullerenes $M_2C_2@C_{2n}$. The bonding in $M_2S@C_{82}$ was studied in detail by molecular orbital analysis as well as with the use of quantum theory of atom-in-molecules and electron localization function approaches. The analysis of the electronic structure shows that the bonding in sulfide and carbide clusterfullerenes is very similar. The sulfur atom is resembling the carbide unit. With the successful synthesis and isolation of several new representative sulfide clusterfullerenes like $Sc_2S@C_{82}$, $Y_2S@C_{82}$, $Dy_2S@C_{82}$, and $Lu_2S@C_{82}$, this study opens up a new route to the novel endohedral fullerenes.

[1] L. Dunsch et al. *J. Am. Chem. Soc.* **2010**, *132*, 5413-5421.

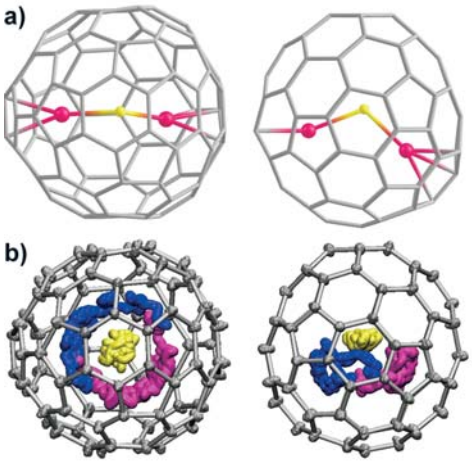

Fig.: (a) Molecular structure of the lowest energy isomer of $Sc_2S@C_{82}$ (two orientations are shown); **(b)** Born-Oppenheimer molecular dynamics trajectory for $Sc_2S@C_{82}$ (16 ps, 300 K) in the same orientations as shown in (a). Sulfur is shown in yellow, Sc – violet and blue, carbon – gray.

Cooperation: [1]Hefei National Laboratory for Physical Sciences at Microscale & Department of Materials Science and Engineering, Hefei
Funding: Alexander von Humboldt foundation

Charged states in polyaniline as studied by *in situ* ATR-FTIR spectroelectrochemistry

E. Dmitrieva, A. Kellenberger, Y. Harima and L. Dunsch

The role of phenazine-like units in the formation and stabilization of charged states in PANI was studied by *in situ* FTIR spectroelectrochemistry. The comparative FTIR studies of electrochemically prepared PANI and its copolymers with different ratios of phenosafranine (3,7-diamino-5-phenylphenazinium chloride) monomer give evidence ofn the existence of phenazine-like units in PANI. Several IR bands are attributed to the phenazine rings in PANI. During p-doping of PANI *in situ* FTIR spectra show a new peak at 1540 cm^{-1} attributed to the charge dependent changes in the phenazine-like units (Fig.). The anodic potential dependence of IR bands was compared to that of the ESR intensity and the absorption data [1] and points to the diamagnetic species like π-dimers formed at higher oxidation levels. By the potential dependence of the IR lines the π-dimers in the polymer was shown to be stabilized at the link of the phenazine unit to the linear PANI segment [2].

[1] E. Dmitrieva *et al.*, J. Phys. Chem. B. **113**, 16131 (2009)
[2] A. Kellenberger *et al.*, PCCP (2011) DOI: 10.1039/c0cp01264e.

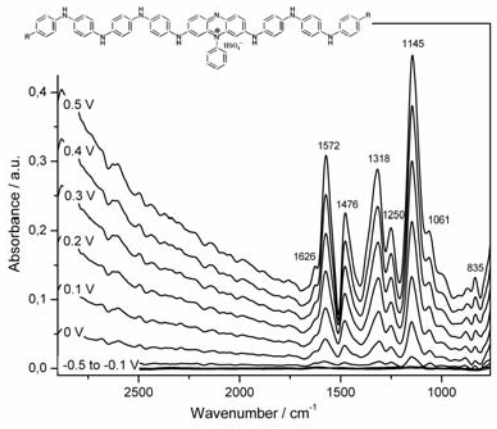

Fig.: *In situ* ATR-FTIR spectra during the anodic oxidation of PANI. The spectrum of the polymer in uncharged state is taken as reference spectrum. Insert: Proposed structure of PANI.

Cooperation: University of Hiroshima, Japan, and University Politehnica of Timisoara, Romania
Funding: BMBF and DFG-GACR

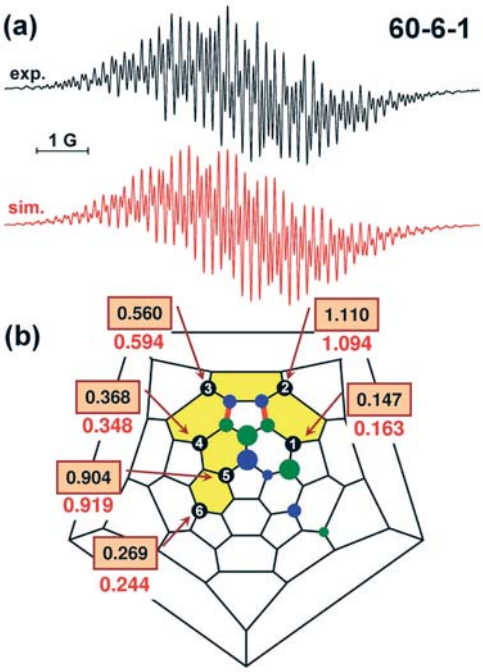

Fig.: (a) Experimental and simulated ESR spectra of $C_{60}(CF_3)_6^-$ radical-anion; **(b)** Schlegel diagram of $C_{60}(CF_3)_6$ with experimental (red) and DFT-computed (black) hyperfine coupling constants. CF_3 groups are shown as black dots with numbers, blue and green dots show distribution of single-occupied MO in the radical-anion.

ESR Vis-NIR Spectroelectrochemistry of Fullerene Derivatives: Unravelling the ESR Pattern of large non-symmetric Radicals with up to 30 Fluorine Atoms

A. A. Popov, I. E. Kareev[1], N. B. Shustova[2], S. H. Strauss[2], O. V. Boltalina[2], L. Dunsch.

By *in situ* ESR and Vis-NIR spectroelectrochemistry the charged states of recently synthesised $C_{60}(CF_3)_{2n}$ ($2n$ = 2–10) derivatives [1] and their complex pattern in spectroscopy have been studied in detail [2]. It was shown that the complex ESR spectra exhibited by the radical-monoanions of trifluoromethylated fullerene due to multiple CF_3 groups can be reliably unravelled by assuming a free rotation of CF_3 groups and applying DFT calculations with subsequent fitting procedure. By this method, assignment of the hfc values for individual CF_3 groups was possible for the non-symmetric anion-radicals as large as $C_{60}(CF_3)_{10}^-$ with 30 fluorine atoms. Strong variations of the hyperfine coupling constants of individual fluorine atoms within one CF_3 group was found and could be explained based on the analysis of the SOMO orbitals. In particular, it was found that small hfc constants are typical for the fluorine atoms located close to the nodal planes of SOMO. By comparing the results of U-B3LYP and RO-B3LYP calculations, it was shown that the direct term constitutes ca 80 % of the hfc constants; besides, in many cases the polarization term is positive, especially for the atoms with large hfc constants. Absorption spectra of the $C_{60}(CF_3)_{2n}$ anions exhibit NIR absorption bands, whose assignment is provided by time-dependent DFT calculations. DFT supported *in situ* spectroelectrochemistry appears to be the matter of choice to study the charged states of highly derivatized fullerenes.

[1] A.A. Popov, et al. *J. Am. Chem. Soc.* **2007**, *129* (37), 11551-11568.
[2] A.A. Popov, et al. *J.Am.Chem. Soc.* **2010**, *132* (33), 11709-11721.

Cooperation: [1]Institute of Problems of Chemical Physics, Russian Academy of Sciences, Chernogolovka (Russia); [2]Colorado State Uni. (Fort Collins, USA)
Funding: Alexander von Humboldt foundation, DAAD, Volkswagen Stiftung

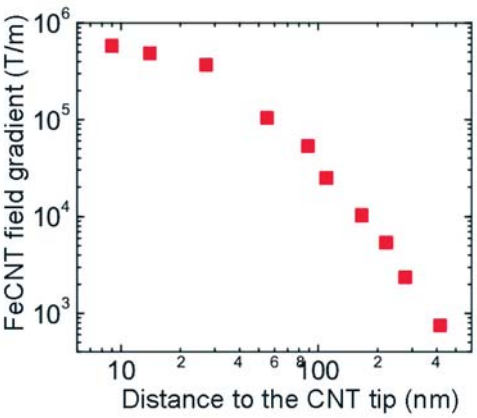

Fig.: The magnetic field gradient close to the tip of a FeCNT. The iron wire end is located ~30 nm further away. This additional distance causes an apparent gradient saturation at low distances.

Iron-filled carbon nanotubes – High magnetic field gradient probes

F. Wolny, T. Mühl, U. Weissker, S. Philippi, A. Leonhardt, B. Büchner

The defined magnetic properties of individual iron-filled carbon nanotubes (FeCNT) combined with their mechanical strength make them ideal candidates for an application as high resolution high stability magnetic force microscopy (MFM) probes [1,2]. The cylindrical shape of these iron nanowires allows for a straightforward calibration using a point monopole description. MFM imaging of permalloy dots has been used to determine the field gradient near the tip of FeCNT probes [3]. 6×10^5 T/m has been detected at a distance of ~10 nm to the nanotube tip which corresponds to a distance of ~ 40 nm to the Fe nanowire end. In case of FeCNT probes with reduced carbon shell thickness, a field gradient as high as 9×10^7 T/m can be expected.

[1] F. Wolny et al., Nanotechnology **21**, 435501 (2010).
[2] S. Vock et al., Applied Physics Letters **97**, 252505 (2010)
[3] F. Wolny et al., ArXiv cond-mat abstract 1011.0389

Cooperation: Ohio State Univ., USA
Funding: DFG

Research Area 4
Metastable alloys

Nucleation and microstructure formation in the eutectic TiFe

M. Stoica, A. Schlieter, U. Kühn, W. Löser, J. Eckert, S. Pauly, L. Giebeler

Typical commercial (α+β) Ti alloys have an ultimate tensile strength of about 1000 MPa and show a plastic elongation to failure of 10 – 15 % at room temperature. Compared with Fe– and Zr–based alloys, one of the most important property of Ti–based alloys is their low density (~ 4.5 g/cm^3), rendering these alloys as a potential candidate for automotive, aerospace and biomechanical applications. Das et al. [1] reported the possibility to obtain nanoscaled/ultrafine grained (NS/UFG) eutectic TiFe and TiFeSn alloys without any micrometer-size toughening dendritic phase exhibiting higher strength (around 1900 MPa) compared to commercial Ti–based alloys and much larger plastic strain (up to 13.5 %). In our present work, the eutectic $Ti_{70.5}Fe_{29.5}$ (at.%) alloy prepared by different processing techniques – in order to achieve different cooling conditions and, consequently, different morphologies – exhibits compressive strengths between 2200 to 2700 MPa and plastic strains between 7 to 19 %.

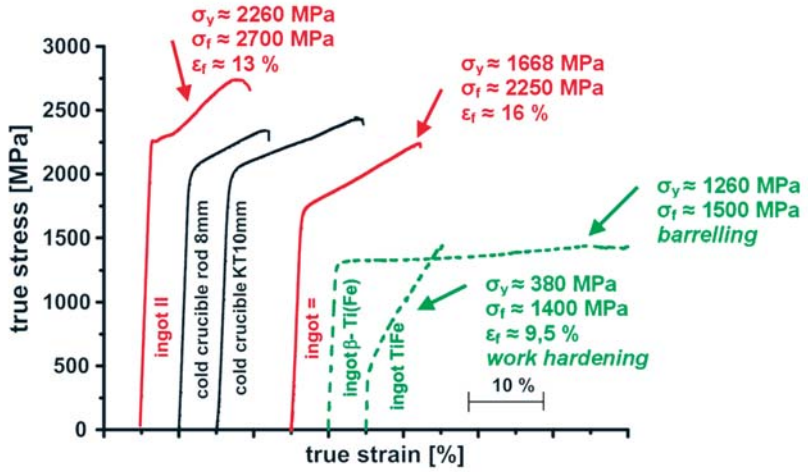

Fig.: Room-temperature compression stress-stain curves for the eutectic-phase material and the single-phase samples (dashed curves): (II) compressive load parallel to the lamellae, (=) compressive load perpendicular to the lamellae.

The eutectic $Ti_{70.5}Fe_{29.5}$ was prepared by rapid solidification (arc melting, cold crucible casting, and, respectively, tilt casting) and directional solidification (the Bridgman technique). The lamellar UFG microstructure is strongly determined by the cooling gradient and the lamellar spacing is typical 500 to 800 nm. Samples with such morphologies were tested in compression, upon two directions: parallel to the lamellae (||) and perpendicular to them (=). Fig. shows the measured stress-strain curves for the eutectic alloy. For comparison, the behavior of the single phase material, i.e. β-Ti(Fe) ingots, is plotted with dashed lines in the same picture. From there it is clear that the eutectic rapid cooled alloys show significantly better mechanical properties. Further studies will focus on mechanical properties, measured in tension, and the more detailed characterisation of the lamellar interface of the eutectic samples.

[1] Das J. et al. J. Mater Sci Eng A 2007;449:737-740.

Cooperation: MPI für Eisenforschung Düsseldorf, Uni Bayreuth, RWTH Aachen
Funding: DFG

New Hydrides

O. Gutfleisch, C. Rongeat, I. Lindemann, C. Bonatto-Minella, R. Domènech Ferrer, C. Geipel, B. Gebel, M. Herrich, L. Dunsch, L. Schultz

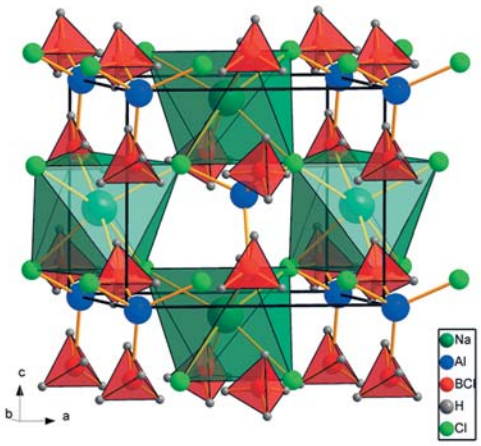

Fig.: The orthorhombic unit cell of $NaAl(BH_4)_xCl_{4-x}$ contains complex anions $[Al(BH_4)_xCl_{4-x}]^-$ and Na^+ cations. The stability range of the complex double-cation borohydride is rather narrow with 1<x<1,4.

Human development has caused a depletion of natural energy resources and climate changes with non-predictable consequences. New energy concepts are required for the future of our industrial society. The only known energy carrier with a high energy density and no emission of greenhouse gas is hydrogen.

Research of solid-state storage of hydrogen - for e.g. zero-emission vehicle propulsion and other mobile applications – is pursued by exploring functional complex hydrides such as alanates and borohydrides. These materials offer several advantages over conventional metal hydrides provided thermodynamics, kinetics decomposition pathways and the reabsorption of hydrogen in modest conditions can be controlled and mastered.

Our work includes the characterisation with high-pressure differential scanning calorimetry, gravimetric and pressure-composition-temperature analysis as well as the study of hydrogen dynamics using in-situ XPS, XRD and Raman in order to understand details of the complex sequence of transformations, to identify intermediate reaction products and rate determining steps in complex hydrides and reactive hydride composites. Novel processing techniques such as high hydrogen pressure reactive milling and high pressure annealing are used in order to identify new materials (see Fig.)with high reversible hydrogen contents.

One recent topic is the nanoconfinement of complex hydrides. In cooperation with the University of Utrecht, sodium alanat is melt-infiltrated into nanoporous carbon. It can be observed that not only the kinetics of hydrogen sorption had improved, but the thermodynamics had also changed. When hydrogenating at conditions at which Na_3AlH_6 would be expected to be the stable phase (e.g. 40 bar H_2 at 160 °C), instead nanoconfined $NaAlH_4$ was formed, indicating a shift of the $NaAlH_4 \leftrightarrow Na_3AlH_6$ thermodynamic equilibrium in these nanocomposites compared to bulk materials.

Cooperation: EMPA, Switzerland; GKSS Research Centre Geesthacht; FZ Karlsruhe; Univ. of Amsterdam, Netherlands; Univ. of Geneva, Switzerland; Swiss-Norwegian Beam Line at ESRF, France; Univ. of Utrecht, Netherlands; Univ. of Glasgow, UK
Funding: EU (NESSHY COSY), HGF (FuncHy), ECEMP (Sächsische Exzellenzinitiative)

Ductile $(Fe_{1-x}Ni_x)_{71}Nb_6B_{23}$ bulk metallic glasses

J.M. Park, D.H. Kim, N. Mattern, U. Kühn, J. Eckert

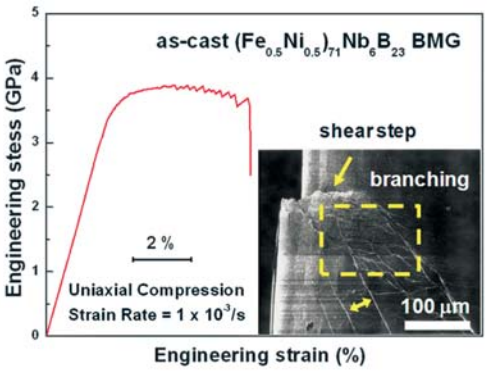

Fig.: Room temperature compressive engineering stress-strain curve obtained from the $(Fe_{0.5}Ni_{0.5})_{71}Nb_6B_{23}$ BMG sample, together with lateral surface morphology of failed sample.

The influence of partial replacement of Fe by Ni in $(Fe_{1-x}Ni_x)_{71}Nb_6B_{23}$ bulk metallic glasses (BMGs) has been investigated ($0 \le x \le 0.5$). Ni addition was chosen because its Poisson's ratio ($\nu = 0.31$) is larger than that of Fe ($\nu = 0.29$) and the enthalpy of mixing with Fe is only moderately negative ($\Delta H_{mix} = -2$ kJ/mol). Both properties enable to tune the elastic moduli of the BMGs and to induce nano-scale heterogeneities by the formation of chemically and topologically ordered clusters. Deformation curves of cast rods show an improved ductility with increased Ni content. Especially, the $(Fe_{0.5}Ni_{0.5})_{71}Nb_6B_{23}$ BMG exhibits a compressive plastic strain of $\varepsilon = 4.2\%$ and significant strain hardening-like behavior together with a still high ultimate compressive strength of $\sigma = 3.9$ GPa (Fig.). The improved ductility is in accordance with the enhancement of the Poisson's ratio of the $(Fe_{1-x}Ni_x)_{71}Nb_6B_{23}$ BMGs from $\nu = 0.323$ (x = 0) to $\nu = 0.356$ for (x = 0.5), and with the presence of local heterogeneities as detected by high resolution transmission electron microscopy [1]. The scanning electron microscope (SEM) observation of fractured $(Fe_{0.5}Ni_{0.5})_{71}Nb_6B_{23}$ BMG reveals an uniform plastic deformation by multiple shear banding (Fig.). The increase of ν is accompanied by the increase of ef-

fective volume of shear transformation zone (STZ) and the collective motion of STZs then initiates the nucleation of further shear bands. Therefore, BMGs with a higher ν-value can effectively improve the shear deformation ability, i.e., generate a larger number of shear bands during deformation, which is consistent with the present SEM observation. In general, our findings suggest that the atomic-scale modulation and the tuning of the elastic constants can effectively improve the mechanical properties of BMGs.

[1] J.M. Park et al. Appl. Phys. Lett. 96 (2010) 031905.

Cooperation: Yonsei University Seoul
Funding: Korea Ministry of Education, Science and Technology (Global Research Laboratory Program), Pakt für Forschung 2008

High-strength Al-based alloys by powder metallurgy of glassy precursors

S. Scudino, K.B. Surreddi, M. Sakaliyska, F. Ali, M. Samadi Khoshkhoo, T. Gemming, U. Kühn, M. Stoica, N. Mattern, H. Ehrenberg, J. Eckert

In this project, novel bulk Al-based alloys with high Al content have been produced by powder metallurgy methods from amorphous and partially amorphous materials. The results indicate that consolidation into highly-dense bulk samples cannot be achieved without extended crystallization of the material. Nevertheless, crystallization during consolidation is not detrimental and leads to bulk samples with a remarkably high strength of about 1250 – 1550 MPa (Fig.), which is 2 – 3 times larger than the conventional high-strength Al-based alloys. This is combined with a distinct plastic deformability of 3 – 6 %. The results obtained in the course of this project clearly indicate that the combined devitrification and consolidation of amorphous precursors is a particularly attractive method for the production of lightweight Al-based materials characterized by high strength combined with good plastic deformation. Through this method, the mechanical properties of the consolidated samples can be varied within a wide range of strength and ductility depending on the microstructure and the consolidation techniques used. This might open a new route for the development of novel and innovative high-performance Al-based materials for eco-friendly transport applications.

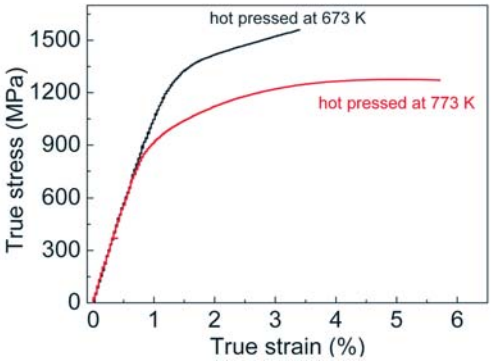

Fig.: Room temperature compression stress-strain curves for the $Al_{84}Gd_6Ni_7Co_3$ alloy produced by the combined devitrification and consolidation of amorphous precursors.

Cooperation: Univ. Bremen; Sejong Univ., Seoul/Korea; Univ. Torino, Italy; CNRS Grenoble, France; Slovak Univ. of Technology, Trnava, Slovak Republic.
Funding: DAAD, BMBF, Pieas

Interaction between mechanical defects and corrosion degradation of bulk metallic glasses (BMG)

A. Gebert, P. F. Gostin, J. Paillier, M. Uhlemann, U. Kühn, J. Eckert, L. Schultz

It is well established that the surface reactivity and corrosion behaviour of amorphous alloys is principally determined by various material-dependent factors, i.e. the metastability of the amorphous state, the alloy composition and ideally, the lack of microstructural defects and the chemically homogeneous amorphous nature. However, under real casting and rapid quenching conditions the preparation of absolutely defect-free bulk amorphous alloys is nearly impossible. Chemical defects (concentration fluctuations, high-melting inclusions, precipitated second phases etc.) or physical defects (pores, air pockets etc.) often exist. In particular in the case of Zr-based bulk glasses - though exhibiting excellent passivity in many environments - those defects cause a strong susceptibility to local corrosion. A so far mostly neglected aspect is that defects generated by mechanical deformation of glassy alloys may remarkably influence their surface reactivity. First systematic studies on the effect of different mechanically generated

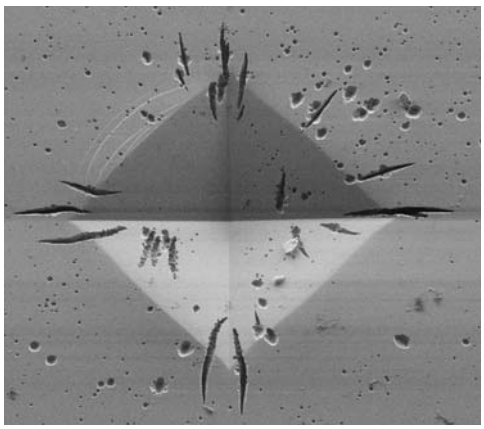

Fig.: Corrosion damage morphology developing at a mechanical defect on a BMG surface under the influence of the local mechanical stress field.

surface defect states on the corrosion behaviour of Zr-based bulk metallic glasses were conducted. It was revealed that the pitting initiation is dependent on the mechanical defect concentration. Pits are pinned to pre-formed shear bands at the sample surface. The stress field surrounding local mechanical defects governs the corrosion process and determines the corrosion damage morphology (Fig.). Consequently, enhanced pitting susceptibility of shot-peened glassy samples was detected.

[1] A. Gebert et al. Corrosion Science 52 (2010) 1711-1720
[2] J. Paillier et al. Materials Characterization 61 (2010) 1000-1008
[3] A. Gebert, Scripta Mater. 62 (2010), 635-638

Cooperation: Univ. of Cambridge, UK; Univ. of Torino, Italy; UAB Barcelona, Spain; TU Dresden
Funding: Pakt für Forschung 2008 "Cluster materials with competing properties"

Effective properties of nano-composite materials based on bulk metallic glasses

H. Hermann, V. Kokotin

Bulk metallic glasses with nanometre-scale inclusions can feature mechanical properties which are superior to the properties of the corresponding homogeneous glass. The understanding of this phenomenon is far from being complete. We have proposed an approach to the relation of local and effective properties of BMG-based nano-composites combining molecular dynamics simulations and continuum theoretical methods. The analytical treatment is based on effective medium theory and it takes into account the specific geometry of the BMG nano-composites. It is supposed that both the macroscopic system and the constituent phases are isotropic. Furthermore, it is assumed that the interfacial region between inclusion and matrix forms a separate phase the properties of which are different from those of the two basic components. This assumption is confirmed by computer simulations as illustrated by Fig. 1. The mean local packing density of the interphase is about 1% smaller than that of the matrix which gives rise to significant reduction of the elastic shear modulus of the interphase. We derived expressions describing the dependence of the effective property on volume fractions and local properties of inclusions, interphase, and matrix. Cross-property relations between elastic moduli and thermal conductivity are proved to exist and are considered to be interesting for the understanding of shear band initiation and related local heat production in BMG nano-composites under external strain.

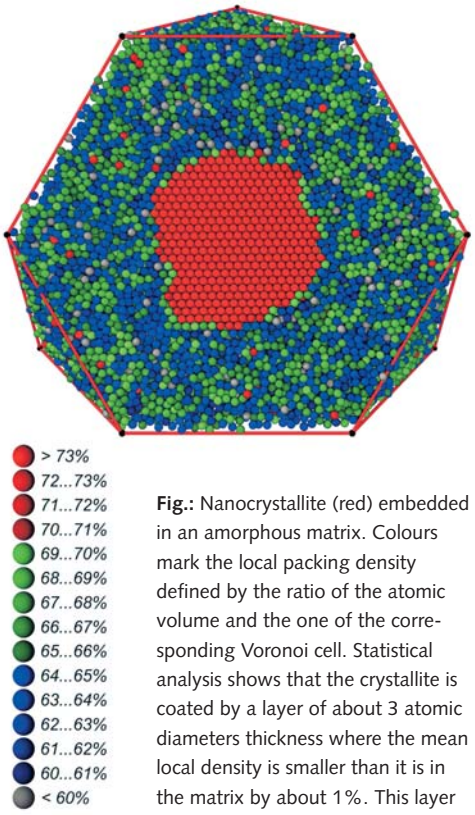

Fig.: Nanocrystallite (red) embedded in an amorphous matrix. Colours mark the local packing density defined by the ratio of the atomic volume and the one of the corresponding Voronoi cell. Statistical analysis shows that the crystallite is coated by a layer of about 3 atomic diameters thickness where the mean local density is smaller than it is in the matrix by about 1%. This layer is treated as a separate phase.

Cooperation: MPI für Eisenforschung Düsseldorf, Univ. of Appl. Sc. Darmstadt, Inst. for Combustion RAN Novosibirsk

New intermetallic anodes for Li-ion batteries

H. Ehrenberg, I. Chumak, S. Oswald, J. Eckert

Intermetallic anodes based on Al, Si and Sn are very attractive for applications in Li-ion batteries, because of their very high specific capacities. However, they suffer from a very poor cycling stability, caused by their brittleness in combination with huge volume changes between 100 and 300% during lithiation, which results in an ongoing breaking of particles and accompanied contact loss. A novel anode concept was recently suggested [1], which should overcome these limitations by a stabilizing effect of the competition between a homogeneous continuous solid solution in the lithiated state and a separation into immiscible phases in the delithiated state. The system Li(Al,Zn) was

shown to be a very promising example for this approach [1]. While LiAl and LiZn form a homogeneous continuous solid solution with a B32-type structure (NaTl type) in the charged lithiated state, Al and Zn are not miscible at room temperature and crystallize in the fcc Al and hexagonal Zn structures. The interplay between atomic mixing and precipitation has a positive effect on the microstructure and results in a better cycling stability than for Al alone. However, further stabilization of the solid-electrolyte "interphase"(SEI) is necessary, because after 20 cycles about 40 % of the lithium is not mobile anymore, but fixed in an inorganic oxidic environment as revealed by ^{7}Li MAS-NMR spectroscopy.

The interplay between phase formation and microstructure is one of the main challenges for the development of novel anodes in Li-ion batteries, based on Li-rich intermetallic compounds in the charged state and Li-poor in the discharged one. The phase sequences are studied by *in situ* synchrotron diffraction and reveal that even in some binary systems, for example Li-Zn, still unknown phases exist. Sufficient cycling stability can only be obtained in a composite anode, which is flexible enough to compensate the charge-dependent volume changes without significant losses of electronic contact or lithium mobility.

[1] Chumak et al. J. Mater. Res. 25 (2010) 1492-1499.

Cooperation: TU Darmstadt, Ivan Franko Lviv National University (Ukraine), Westfälische Wilhelms-Univ. Münster

Funding: DFG, PAK 177 "Functional materials and materials analytics for high-power batteries"; Sächsische Landesexzellenzinitiative, Spitzencluster „Atomares Design und Defekt-Engineering (ADDE)"

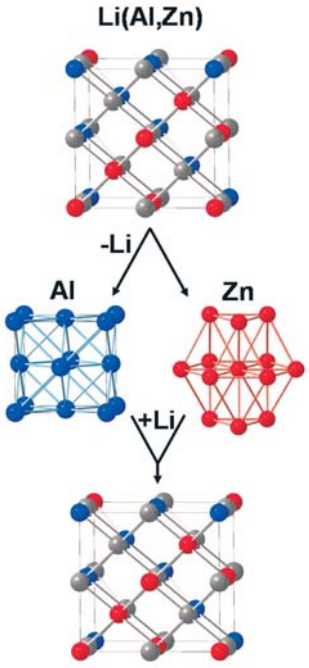

Fig.: Crystal structures of the involved end members during the reversible electrochemical delithiation of $Li(Al_{0.8}Zn_{0.2})$.

Deformation mechanisms of a wire drawn antiferromagnetic FeMnNiCr alloy

D. Geißler, J. Freudenberger, A. Kauffmann, M. Krautz, T. Marr, H. Klauß, D. Seifert, T. Wolf, C. Rodig, H.-P. Trinks, M. Frey, A. Voss, M. Gründlich, S. Yin, J. Eickemeyer and L. Schultz

A variety of antiferromagnetic FeMn-based austenitic alloys show pronounced magneto-volume effects at the Néel temperature as a prerequisite for Élinvar applications. These alloys reveal the typical deformation behaviour of low stacking fault energy (SFE) materials. The mechanisms of plastic deformation interrelate to their high strength and ductility. By combining microstructural features, texture evolution and tensile stress-strain response of a Fe-24Mn-7Ni-8Cr (mass percent) alloy the deformation mechanisms were identified. A slip-dominated deformation process and, at a later stage of deformation, twinning induced plasticity (TWIP) is observed. The annealed starting material exhibits a bimodal fibre texture and the occurrence of TWIP is texture sensitive, i.e. deformation twinning is only observable in grains of a single texture component, as shown in the Figure. Based on these results, a model is derived, which reflects an orientational and configurational peculiarity of fcc stacking faults bound by two Shockley partial dislocations. With this model the onset point of twinning is reflected by the starting point of stacking fault growth, i.e. movement of the leading partial and stopping of the trailing partial. Calculations based on this model allow to compatibly describe the mechanical behaviour apparent from tensile testing with respect to the microstructural evolution. Finally, a reasonable SFE of about 8 ... 9 mJ/m^2 can be extracted from tensile test data.

Cooperation: TU Bergakademie Freiberg; Stahlzentrum Freiberg e.V.; Gurofa GmbH, Glashütte; ¯evico GmbH, Dresden

Funding: DFG and BMBF

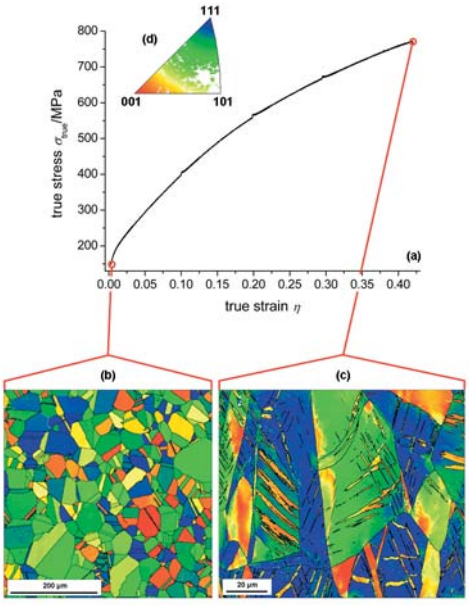

Fig.: Microstructural changes due to deformation in a Fe-24Mn-7Ni-8Cr alloy: **(a)** true stress vs. true strain curve (tensile test), EBSD maps of the microstructure **(b)** in the annealed condition and **(c)** in the deformed state (η = 0.42), (d) inverse pole figure defining the color code for the grain orientation. Deformation twins (thin bands intersecting the grain interiors) only occur in grains of the <111>-fibre texture component oriented in the direction of the tensile axis.

Research Area 5
Stress-driven architectures and phenomena

Ordered SiGe islands on patterned Si(001) substrates: fundamental and applications

J. J. Zhang, A. Rastelli, O. G. Schmidt

The performance of Si-based metal–oxide–semiconductor field-effect transistors (MOSFETs) can be significantly enhanced by strain. In n-channel MOSFETs, the electron mobility in the Si channel can be enhanced through tensile strain induced by a buried $Si_{1-x}Ge_x$ layer. An alternative route is represented by Si channels above coherently strained SiGe islands, which was proposed by Schmidt and Eberl ten years ago [1] and recently became reality [2]. The advantage of SiGe islands over planar SiGe layers is that islands only induce strain locally in the Si channel and they can therefore have a larger Ge content. Although the Ge fraction in the SiGe islands increases approximately linearly with decreasing temperature, the island width decreases quadratically. Therefore, strain maximization requires a careful choice of growth parameters yielding large and relatively Ge-rich islands.

In this work, we address this issue by fabricating site-controlled arrays of two closely-stacked SiGe/Si island layers on pit-patterned Si(001) substrates. Finite element method calculations of the strain distribution with the realistic structure reveal that (i) the Si spacer between a pair of islands can act as a lateral quantum dot molecule made of four nearby dots for electrons and (ii) the tensile strain in a Si cap deposited on top of the stack is significantly enhanced with respect to a single layer (Fig.) [3]. In addition, by guiding the formation of QDs on periodically patterned substrates, we find that the QDs are able to cope with the increasing stress by cyclically incorporating large amounts of material from the substrate and corresponding changes of their shape. This allows them to keep growing in size while delaying relaxation mediated by defects [4].

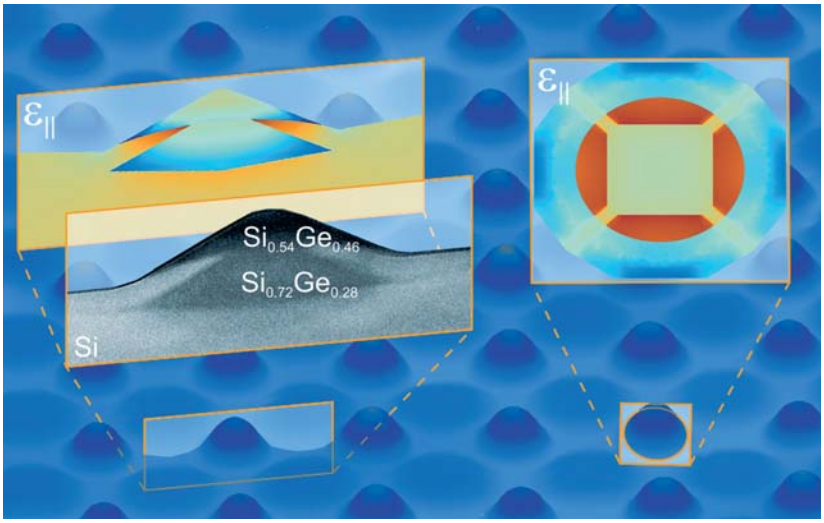

[1] O. G. Schmidt and K. Eberl, IEEE Trans. Electron Devices **48**, 1175 (2001).
[2] V. Jovanovi *et al.*, IEEE Electron Device Lett. **31**, 1083 (2010).
[3] J. J. Zhang *et al.*, Appl. Phys. Lett. **96**, 193101 (2010).
[4] J. J. Zhang *et al.*, Phys. Rev. Lett. **105**, 166102 (2010).

Cooperation: Univ. of Linz, Univ. of Milano-Bicocca
Funding: EC (d-DOTFET), DFG

Wrinkling and rolling of strained nanomembranes

P. Cendula, S. Kiravittaya, Y. F. Mei, Ch. Deneke, and O. G. Schmidt

A thin bilayer film with initial compressive strain can either bend or wrinkle if it is fixed at one end and free on the other, Figs. (a-c). Interestingly, the competing mechanisms of wrinkling and bending, as the strain gradient inside the film changes, have not been quantified so far. The roll up of a strained film into a cylindrical geometry seems particularly appealing since size, orientation, and number of rotations become well controlled entities.

Whether the film bends or wrinkles sensitively depends on the built-in strain gradient $\Delta\varepsilon = \varepsilon_2 - \varepsilon_1$ across the film thickness. By an energetic comparison between bent/rolled and wrinkled films, we have calculated a quantitative phase diagram for the formation of bent and wrinkled structures, Fig. (d). If the strain gradient is large and the average strain $\bar{\varepsilon} = (\varepsilon_2 + \varepsilon_1)/2$ is small, the film bends into a curved structure with radius R_0, whereas for a small strain gradient and large average strain the film wrinkles.

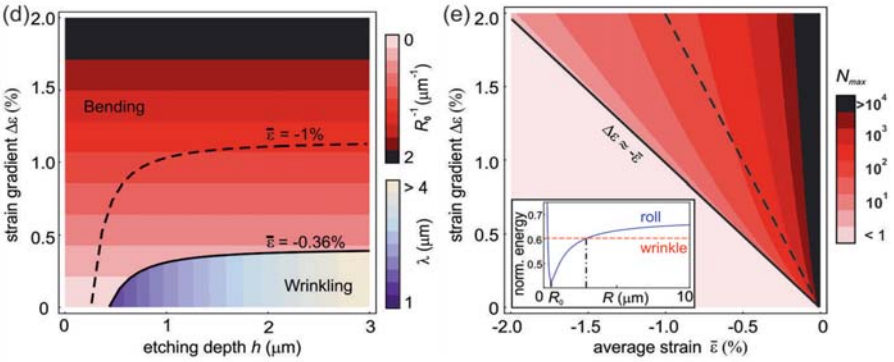

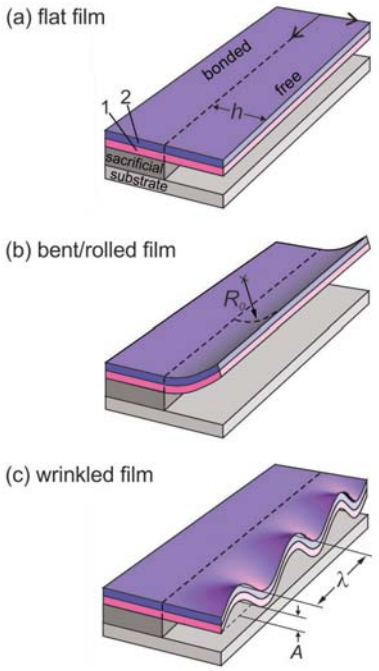

We further consider the tube, which has already rolled up some rotations, and an additional portion of the released layer is going to be relaxed. This portion can continue to roll up with radius $R > R_0$ and larger elastic energy or alternatively form wrinkles with different elastic energy, inset of Fig. (e). When the wrinkle elastic energy is lower than the roll elastic energy, rolling will stop as it is no longer energetically favorable. The maximum number of rotations given by our model is shown in Fig. (e) and hundreds of rotations are predicted for typical bilayer films (dashed line).

Our considerations provide the theoretical framework to fundamentally understand bending and wrinkling of free-hanging films. Our work is of practical interest for many applications, material combinations, geometries and length scales.

Fig.: Schematics of **(a)** flat film released over length h, which can relax into **(b)** bent film with inner radius R_0, or into **(c)** wrinkled film with amplitude A and wavelength λ. **(d)** Diagram of favorable film shapes for typical 10/10 nm $In_{0.1}Ga_{0.9}As/GaAs$ bilayer. Solid curve shows the boundary between bent and wrinkled shapes. Tube radius R_0 is shown for the bent structure and wavelength λ for the wrinkled structure. **(e)** Contour of the maximum number of tube rotations N_{max} as a function of average strain and strain gradient. The inset shows a comparison between the strain energies of roll up and wrinkling for $\bar{\varepsilon} = -1.0\,\%$ and $\Delta\varepsilon = -2.0\,\%$.

Funding: BMBF (Grant No. 03N8711)

Electronic properties of rolled-up materials

C. Ortix, J. van den Brink

The experimental progress in synthesizing low-dimensional nanostructures with novel geometries has triggered the interest in the quantum physics on curved two-dimensional manifolds. As opposed to classical particles, a quantum particle retains some knowledge of the surrounding three-dimensional space. In spite of the absence of interactions, it indeed experiences a purely quantum attractive potential of geometrical nature [1]. Such a curvature-induced potential has been shown to cause many intriguing phenomena as for instance topological bandgaps in periodic curved surfaces. We investigated the electronic properties of rolled-up nanostructures, in particular, in the form of Archimedean spirals [2].

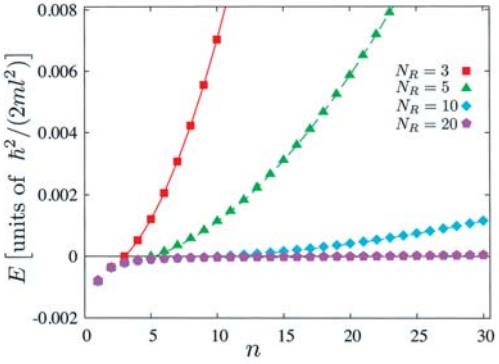

Fig.: Electronic spectrum of an Archimedean spiral with different number of rotations as obtained from exact diagonalization of the Hamiltonian.

They are unique structures that mimic the cylindrical symmetry of a radial crystal. It turns out that the characteristic Coulomb-like behavior of the curvature-induced geometric potential leads to the appearance of atomic-like electronic states localized at the points of largest curvature. Interestingly, the number of these bound states corresponds precisely to the rotation number of the rolled-up nanotube (Fig.) therefore proofing the close relation among the geometrical and the electronic properties of these novel nanodevices. An external magnetic field adds a new degree of freedom to manipulate the quantum states of the carriers. The competition among the typical magnetic length and the radial superlattice constant results in the formation of quasi-1D conducting channels. It is conceivable that these features are at the heart of the topology dependent electron transport of these materials.

[1] R.C.T. Da Costa, PRA 23, 1982 (1981)
[2] C. Ortix and J. van den Brink, PRB 81, 165419 (2010)

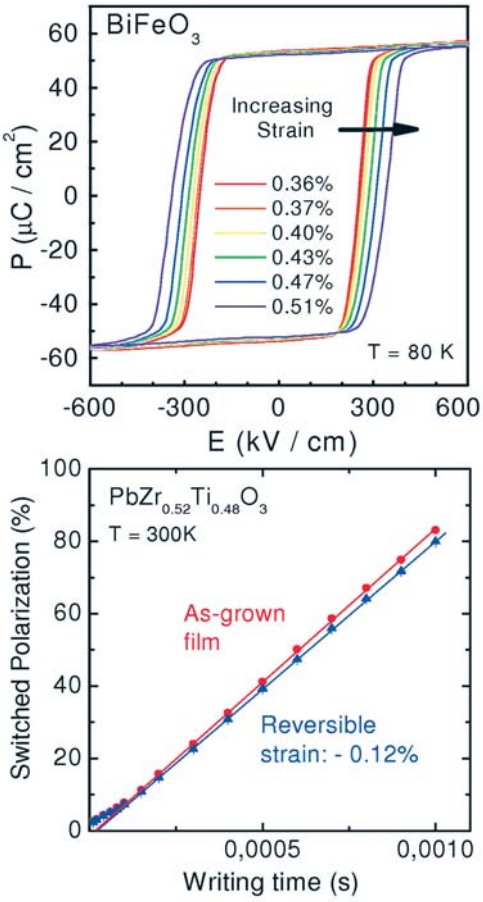

Fig.: Polarization loop of a 200 nm thick $BiFeO_3$ film in defined reversible strain states (upper panel), and switched fraction of polarization in a PZT capacitor structure in two strain states controlled by the piezoelectric substrate (lower panel).

Strain-dependent ferroic switching in oxide heterostructures

A. Herklotz, O. Bilani, M. C. Dekker, C. Deneke, A. Efimenko, K. Nenkov, J. Plumhof, A. Rastelli, A. D. Rata, O. G. Schmidt, L. Schultz, K. Dörr

Magnetic and ferroelectric materials form a foundation for numerous modern technologies. Many applications require thin films or nanostructures of these materials which contain heterogeneous interfaces exerting mechanical constraints. Therefore, most of the applied ferroic materials are subject to lattice strains.

We investigate the role of lattice strains in epitaxial films of oxide ferroelectrics ($BiFeO_3$, $PbZr_{1-x}Ti_xO_3$, $BaTiO_3$) and magnets (doped $LaMnO_3$ and $LaCoO_3$, $SrRuO_3$) grown by Pulsed Laser Deposition. In particular, films on piezoelectric substrate crystals of $Pb(Mg_{1/3}Nb_{2/3})_{0.72}Ti_{0.28}O_3(001)$ (PMN-PT) allow for the reversible uniform strain control during experiments. This approach is utilized to measure the strain dependences of coercive fields and switching times as characteristics of the dynamic response which are only accessible in a reversible-strain experiment. *Ab initio* and thermodynamic theories have succeeded to derive the strain-dependent polarization for a number of (mostly ferroelectric) materials in good agreement with experiments. Our measurements reveal that the switching dynamics of ferroelectrics show strong strain dependence, too. The underlying mechanisms of domain nucleation and wall motion are influenced by defects and intrinsic properties of the crystallographic lattice in a not yet well-understood way. We believe that reversible-strain experiments are promising to provide a foundation of reliable data for the development of theoretical models.

Cooperation: Oak Ridge National Laboratory, University of Bonn, MLU Halle-Wittenberg, TU Dresden
Funding: DFG, A. v. Humboldt Foundation

Strain-tuning of the excitonic fine structure splitting in single self-assembled semiconductor quantum dots

J. D. Plumhof, F. Ding, A. Herklotz, K. Dörr, A. Rastelli, O. G. Schmidt

Optically active self-assembled semiconductor quantum dots (QDs) are attractive for the generation of single and entangled photons on demand.

For the creation of polarization entangled photon pairs it is important to decrease the fine structure splitting (FSS) of the neutral exciton, related to the QD anisotropy, to energies smaller than the emission linewidth (a few μeV). We employ a piezoelectric

actuator (PMN-PT) to manipulate the excitonic emission of GaAs/AlGaAs as well as InGaAs/GaAs QDs embedded in ~200 nm thick (Al)GaAs membranes.
By attaching the membranes on the PMN-PT we can apply highly anisotropic stress to the nanostructures. Polarization resolved micro-photoluminescence is used to determine the excitonic FSS as well as the orientation of the linear polarization of the emitted light. The strain makes it possible to manipulate the FSS in a range of 70 μeV. Fig. (a) shows the behaviour of the FSS vs. the mean excitonic emission energy as the strain is varied. We see that the magnitude of FSS reaches a minimum before increasing again. Fig. (b) shows that the polarization angle of the emitted light relative to the main strain-axis rotates by up to 70 degrees. These effects can be explained as an anticrossing of the bright excitonic states. Most importantly the approach can be used to tune the FSS down to values suitable for the generation of entangled photon pairs.

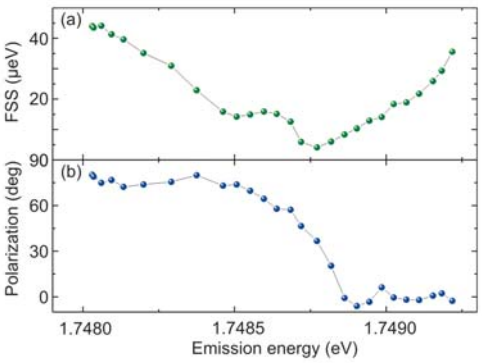

Fig.: (a) FSS of the emission of a GaAs/AlGaAs QD vs. the mean emission energy. **(b)** Polarization angle of the emitted light vs. mean emission energy.

Cooperation: Masaryk Univ. Brno, Czech Republic, Univ. of Stuttgart

Direct Laser Writing of Nanoscale Light-Emitting Diodes

S. Kumar, A. Rastelli , and O. G. Schmidt

The most common approach to create narrow current channels in optoelectronic devices relies on deep etching of semiconductor multilayers. We have developed a new technique to define a narrow current channel in a mesoscopic device by means of a focused laser beam.
Using this technique we have fabricated sub-micrometer light emitting diodes (LEDs) in a mesoscopic semiconductor structure. Our devices are p-i-n resonant tunnelling LEDs with a two dimensional AlAs/GaAs/AlAs quantum well embedded in the intrinsic (i) layer, see Fig. a. This is sandwiched between a bottom n-type GaAs contact layer and a top p-type layer of $Ga_{1-x}Mn_xAs$ with $x > 5\%$.

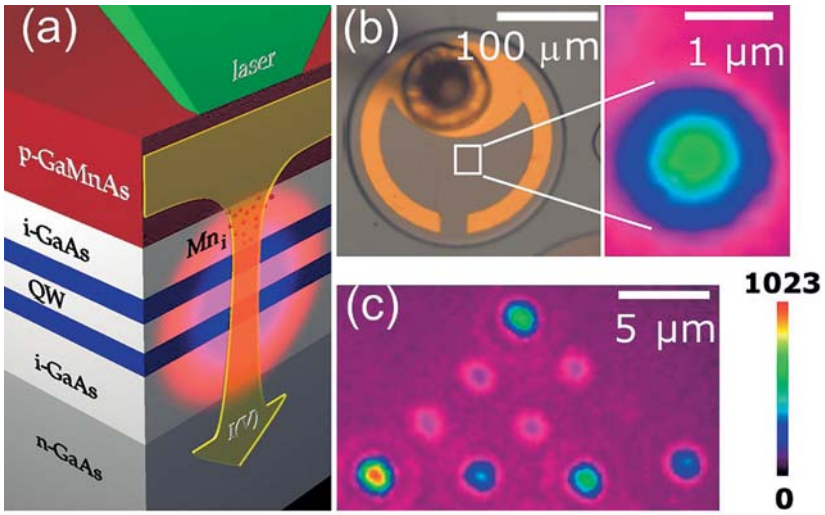

Fig.: (a) Schematic showing the p-i-n diode and the thermally-induced diffusion of Mn_i ions from the p-type GaMnAs layer towards the AlAs/GaAs/AlAs QW. **(b)** Optical microscopy image of the diode and colour-coded image of the electroluminescence (EL) intensity emitted by an LED fabricated by local laser annealing at the energy of the GaAs EL peak (T = 293 K and V = 2 V). The white square indicates the location of the annealed spot on the diode. **(c)** An array of LEDs as a colour-coded image of the EL intensity (V = 2 V, T = 6 K)

The local heating produced by the laser beam allows spatially controlled diffusion of mobile interstitial manganese (Mn_i) ions out of the GaMnAs layer towards the underlying QW heterostructure. This activates nanoscale regions of the LED to emit light at a bias well below the threshold voltage for emission from the non-annealed regions, see Figs. (b,c). The technique, which also provides real-time in-situ control of the nanostructures during their formation, may be advantageous with respect to deep etching for thermal management at high injection currents.

Cooperation: Univ. of Nottingham
Funding: DFG, Royal Society, EPSRC

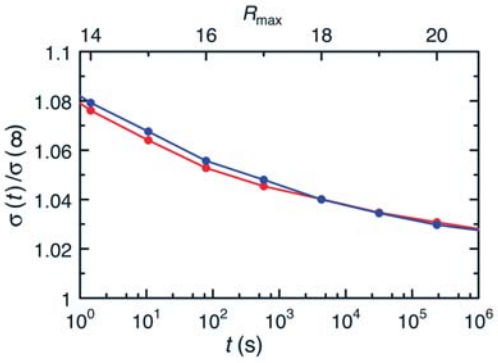

Fig.: Long-time relaxation of the conductivity for two samples of 640^3 sites with random on-site potential. Here, the spatial factor of the nearest-neighbour hopping rate is estimated to be $10^{12}\,s^{-1}$, and the decay length of the wave function of the localised states is assumed to be equal to the nearest-neighbour distance.

Possible mechanism of long-time relaxation in the electron glass

A. Möbius

Long-time relaxation of electronic transport in high-resistivity materials such as amorphous InO [1] has been puzzling for nearly two decades. Various models based on complex changes of the occupation of the localized states have been proposed, see e.g. [2, 3].

The exponentially low rate of long-range single-particle hops, however, seems to provide a simpler explanation: In the formation of the Coulomb gap, such long-range hops are responsible for the low-energy part of the single-particle density of states. Roughly speaking, only after complete relaxation concerning all hops up to a certain length, the single-particle density can be expected to be correct for energy values down to the Coulomb interaction energy corresponding to this length. Thus the related energy-bound is inversely proportional only to the logarithm of the relaxation time.

Using own software which had been developed for the study of the Coulomb gap in very large samples [4], low-energy system states were constructed by means of relaxation versus single-particle hops. In this, restrictions concerning maximum hopping length R_{max} and minimum energy reduction for the individual hops emulated the influence of finite time t and finite temperature T, respectively. Percolation analyses concerning the fastest single-particle hops, which are possible for the obtained system states, yielded estimates of the characteristic hopping time and thus of the conductivity. The figure demonstrates for k_BT being equal to 1/50 of the Coulomb interaction of nearest neighbours that this mechanism may indeed explain aging of the conductivity σ on experimentally relevant time scales.

[1] M. Ben-Chorin et al. Phys. Rev. B 48 (1993) 15025.
[2] A.L. Efros et al. phys. stat. (b) 241 (2004) 20.
[3] A. Amir et al.Phys. Rev. Lett. 105 (2010) 070601.
[4] A. Möbius et al. Journal of Physics: Conf. Series 150 (2009) 022057.

Funding: KITP Santa Barbara, workshop "Electron Glasses"

The Institute by numbers

Personnel

In 2010 the Leibniz Institute for Solid State and Material Research Dresden employed 535 staff members, including 113 doctorate students, 44 post docs, and 23 apprentices. The quote of female staff is 35 %. Furthermore, in 2010, the IFW hosted 54 fellows, that came with their own money to work at the institute. 35 diploma students worked at the IFW and 39 trainees did a practical course at the institute in 2010. The total number of guest scientists, above all was 173.

77 % of the staff belongs to the five scientific IFW institutes, 9 % to the Research Technology Department, 7 % to Administration, 3 % to the Executive Board and support staff. The percentage of apprentices amounts to 4 %.

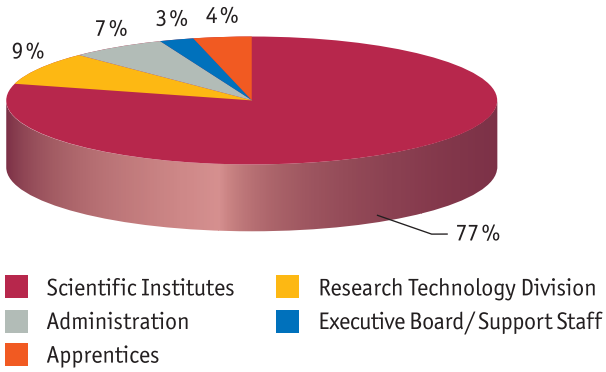

Financing

Total budget	41,258 k€
Thereof	
Federal States of Germany	13,804 k€
Free State of Saxony	13,804 k€
Third party funding spent	13,394 k€
Return on infrastructure, interest, royalties	256 k€
Third party funding	
by the DFG	3,131 k€
by the EC	3,599 k€
by the Federal States of Germany	1,545 k€
by Free State of Saxony	2,720 k€
by industry	1,802 k€
by foundations / others	598 k€
Total	13,394 k€

Expenditures

Remuneration costs	20,479 k€
Equipment, infrastructure and consumables	9,731 k€
Investment	11,048 k€
Total	41,258 k€

Patents

By December 31, 2010 the institute can boast of a total of 129 German and 203 patents registered abroad. In 2010 a total of 14 inventions of the IFW were filed as a patent applications in Germany.

Publications 2010

Monographs and Editorships

1) J.P. Liu; O. Gutfleisch; E. Fullerton; D. Sellmyer (eds.) *Nanoscale magnetic materials and applications*, Springer, New York, 2009, 732 S.
2) K. Postava; K. Lafdi; M.H. Ruemmeli (eds.) *Journal of Scientific Conference Proceedings: A Special Issue on 1st Nanomaterials and Nanotechnology Meeting (NanoOstrava 2008)*, American Scientific Publishers, 2010,

Journal papers

1) P. Adelhelm, J. Gao, M.H.W. Verkuijlen, C. Rongeat, M. Herrich, P.J.M. van Bentum, O. Gutfleisch, A.P.M. Kentgens, K.P. de Jong, P.E. de Jongh, *Comprehensive study of melt infiltration for the synthesis of NaAlH4/C nanocomposites*, Chemistry of Materials 22 (2010), S. 2233-2238.
2) U. Adem, L. Wang, D. Fausti, W. Schottenhamel, P.H.M. van Loosdrecht, A. Vasiliev, L.N. Bezmaternykh, B. Buechner, C. Hess, R. Klingeler, *Magnetodielectric and magnetoelastic coupling in TbFe3(BO3)4*, Physical Review B 82 (2010) Nr. 6, S. 64406/1-5.
3) N. Akopian, U. Perinetti, L. Wang, A. Rastelli, O.G. Schmidt, V. Zwiller, *Tuning single GaAs quantum dots in resonance with a rubidium vapor*, Applied Physics Letters 97 (2010), S. 82103/1-3.
4) A. Alfonsov, F. Muranyi, V. Kataev, N. Leps, R. Klingeler, A. Kondrat, C. Hess, J. Werner, G. Behr, B. Buechner, *High field ESR spectroscopy on Gd01-xFxFeAs*, Journal of Low Temperature Physics 159 (2010) Nr. 1-2, S. 172-175.
5) V.A. Alyoshin, I.P. Romanova, D. Mikhailova, S. Oswald, A. Senyshyn, H. Ehrenberg, *Oxygen nonstoichiometry of tetragonal La2-xSrxCu04-delta (x) 0.15-1.2) and in situ XPS studies at elevated temperatures*, Journal of Physical Chemistry A 114 (2010), S. 13362-13369.
6) A.V. Andreev, M.D. Kuzmin, Y. Narumi, Y. Skourski, N.V. Kudrevatykh, K. Kindo, F.R. de Boer, J. Wosnitza, *High-field magnetization study of a Tm2Co17 single crystal*, Physical Review B 81 (2010) Nr. 13, S. 134429/1-5.
7) A.V. Andreev, S. Yoshii, M.D. Kuzmin, F.R. de Boer, K. Kindo, M. Hagiwara, *A high-field magnetization study of a Nd2Fe14Si3 single crystal*, Journal of Physics / Condensed Matter 21 (2009) Nr. 14, S. 14005/1-8.
8) R.K. Annabattula, J.M. Veenstra, Y.F. Mei, O.G. Schmidt, P.R. Onck, *Self-organization of linear nanochannel networks*, Physical Review B 81 (2010) Nr. 22, S. 224114/1-7.
9) V.Y. Aristov, O.V. Molodtsova, C. Laubschat, V.M. Zhilin, I.M. Aristova, V.V. Kveder, M. Knupfer, *Properties of hybrid organic-inorganic systems: Au nanoparticles embedded into an organic CuPc matrix*, Applied Physics Letters 97 (2010) Nr. 11, S. 113103/1-3.
10) V.Y. Aristov, O.V. Molodtsova, V.V. Maslyuk, V.V. Vyalikh, T. Bredow, I. Mertig, A.B. Preobrajenski, M. Knupfer, *Electronic properties of potassium-doped FePc*, Organic Electronics 11 (2010) Nr. 8, S. 1461-1468.
11) V.Y. Aristov, O.V. Molodtsova, D.V. Vyalikh, M. Knupfer, P. De Padova, G. Le Laye, *Core-level photoelectron study of indium chains on Si(1 1 1) at 10K*, Journal of Electron Spectroscopy and Related Phenomena 177 (2010) Nr. 1, S. 1-4.
12) V.Y. Aristov, G. Urbanik, K. Kummer, D.V. Vyalikh, O.V. Molodtsova, A.B. Preobrajenski, A.A. Zakharov, C. Hess, T. Haenke, B. Buechner, I. Vobornik, J. Fujii, G. Panaccione, Y.A. Ossipyan, M. Knupfer, *Graphene synthesis on cubic SiC/Si Wafers. Perspectives for mass production of graphene-based electronic devices*, Nano Letters 10 (2010), S. 992-995.
13) M.E. Arroyo y de Dompablo, N. Biskup, J.M. Gallardo-Amores, E. Moran, H. Ehrenberg, U. Amador, *Gaining insights into the energetics of FePO4 polymorphs*, Chemistry of Materials 22 (2010), S. 994-1001.
14) P. Ayala, R. Arenal, M. Ruemmeli, A. Rubio, T. Pichler, *The doping of carbon nanotubes with nitrogen and their potential applications*, Carbon 48 (2010), S. 575-586.
15) P. Ayala, J. Reppert, M. Grobosch, M. Knupfer, T. Pichler, A.M. Rao, *Evidence for substitutional boron in doped single-walled carbon nanotubes*, Applied Physics Letters 96 (2010) Nr. 18, S. 183110/1-3.
16) A. Bachmatiuk, F. Boerrnert, F. Schaeffel, M. Zaka, G. Simha Martynkowa, D. Placha, R. Schoenfelder, P.M.F.J. Costa, N. Ioannides, J.H. Warner, R. Klingeler, B. Buechner, M.H. Ruemmeli, *The formation of stacked-cup carbon nanotubes using chemical vapor deposition from ethanol over silica*, Carbon 48 (2010), S. 3175-3181.
17) A. Bachmatiuk, M.H. Ruemmeli, *Synthesis and formation of carbon nanotubes (original in polish)*, Przemysl Chemiczny w Polsce (Chemical Industry in Poland) 89 (2010) Nr. 9, S. 1037-1042.
18) A. Bachmatiuk, F. Schaeffel, D. Placha, G.S. Martynkova, N. Ioannides, T. Gemming, T. Pichler, R.J. Kalenczuk, E. Borowiak-Palen, M.H. Ruemmeli, *Tuning carbon nanotubes through poor metal addition to iron catalysts in CVD* , Fullerenes, Nanotubes and Carbon Nanostructures 18 (2010), S. 37-44.
19) A. Backen, S.R. Yeduru, M. Kohl, S. Baunack, A. Diestel, B. Holzapfel, L. Schultz, S. Faehler, *Comparing properties of substrate-constrained and freestanding epitaxial Ni–Mn–Ga films*, Acta Materialia 58 (2010), S. 3415-3421.
20) A. Bajpai, P. Borisov, S. Gorantla, R. Klingeler, J. Thomas, T. Gemming, W. Kleemann, B. Buechner, *Interface-driven magnetoelectric effects in granular CrO2*, epl 91 (2010) Nr. 1, S. 17006/1-6.

21) A. Bajpai, R. Klingeler, N. Wizent, A.K. Nigam, S.-W. Cheong, B. Buechner, *Unusual field dependence of remanent magnetization in granular CrO2: the possible relevance of piezomagnetism*, Journal of Physics: Condensed Matter 22 (2010), S. 96005/1-6.

22) M. Bakr Mohamed, A. Senyshyn, H. Ehrenberg, H. Fuess, *Structural, magnetic, dielectric properties of multiferroic GaFeO3 prepared by solid state reaction and sol–gel methods*, Journal of Alloys and Compounds 492 (2010), S. L20-L27.

23) N. Balchev, K. Nenkov, V. Antonov, J. Pirov, B. Kunev, *Superconductivity and critical fields in undoped and Sn-doped MoSr2YCu2O8-delta*, Physica C 470 (2010), S. 2040-2046.

24) N. Balchev, K. Nenkov, G. Mihova, J. Pirov, B. Kunev, *Superconducting properties of Ca-doped MoSr2YCu2O8-delta*, Physica C 470 (2010), S. 178-182.

25) P. Banerjee, F. Wolny, D.V. Pelekhov, M.R. Herman, K.C. Fong, U. Weissker, T. Muehl, Y. Obukhov, A. Leonhardt, B. Buechner, P.C. Hammel, *Magnetization reversal in an individual 25 nm iron-filled carbon nanotube*, Applied Physics Letters 96 (2010) Nr. 25, S. 252505/1-3.

26) S. Baran, M. Balanda, L. Gondek, A. Hoser, K. Nenkov, B. Penc, A. Szytula, *Nature of magnetic phase transitions in TbCu2X2 (X = Si, Ge) and HoCu2Si2 compounds*, Journal of Alloys and Compounds 507 (2010) Nr. 1, S. 16-20.

27) S. Baran, L. Gondek, K. Nenkov, B. Penc, A. Szytula, A. Zarzycki, I. Puente Orench, J.A. Rodriguez-Velamazan, *Magnetic phase transitions in RIrGe2 (R=Tb,Ho) compounds*, Journal of Magnetism and Magnetic Materials 322 (2010) Nr. 4, S. 405-412.

28) N.S. Barekar, S. Pauly, R.B. Kumar, U. Kuehn, B.K. Dhindaw, J. Eckert, *Structure–property relations in bulk metallic Cu–Zr–Al alloys*, Materials Science and Engineering A 527 (2010) Nr. 21-22, S. 5867-5872.

29) C. Bechtold, J. Buschbeck, A. Lotnyk, B. Erkartal, S. Hamann, C. Zamponi, L. Schultz, A. Ludwig, L. Kienle, S. Faehler, E. Quandt, *Artificial single variant martensite in freestanding Fe70Pd30 films obtained by coherent epitaxial growth*, Advanced Materials 22 (2010), S. 2668-2671.

30) G. Behr, W. Loeser, N. Wizent, P. Ribeiro, M.-O. Apostu, D. Souptel, *Influence of heat distribution and zone shape in the floating zone growth of selected oxide compounds*, Journal of Materials Science 45 (2010) Nr. 8, S. 2223-2227.

31) E. Beyreuther, A. Thiessen, S. Grafstroem, L.M. Eng, M.C. Dekker, K. Doerr, *Large photoconductivity and light-induced recovery of the insulator-metal transition in ultrathin La0.7Ce0.3MnO3-delta films*, Physical Review B 80 (2009) Nr. 7, S. 75106/1-6.

32) E. Beyreuther, A. Thiessen, S. Grafstroem, K. Doerr, L.M. Eng, *Large photoconductivity of oxygen-deficient La0.7Ca0.3MnO3/SrTiO3 heterostructures*, Journal of Physics: Condensed Matter 22 (2010) Nr. 17, S. 175506/1-7.

33) A. Bhaskar, N.N. Bramnik, A. Senyshyn, H. Fuess, H. Ehrenberg, *Synthesis, characterization, and comparison of electrochemical properties of LiM0.5Mn1.5O4 (M = Fe, Co, Ni) at different temperatures*, Journal of the Electrochemical Society 157 (2010) Nr. 6, S. A689-A695.

34) X. Bie, C. Wang, H. Ehrenberg, Y. Wei, G. Chen, X. Meng, G. Zou, F. Du, *Room-temperature ferromagnetism in pure ZnO nanoflowers*, Solid State Sciences 12 (2010) Nr. 8, S. 1364-1367.

35) M.D. Biegalski, K. Doerr, D.H. Kim, H.M. Christen, *Applying uniform reversible strain to epitaxial oxide films*, Applied Physics Letters 96 (2010) Nr. 15, S. 151905/1-3.

36) J. Bielecki, R. Rauer, E. Zanghellini, R. Gunnarsson, K. Doerr, L. Boerjesson, *Two-component heat diffusion observed in LaMnO3 and La0.7Ca0.3MnO3*, Physical Review B 81 (2010) Nr. 6, S. 64434/1-6.

37) C.G.F. Blum, C.A. Jenkins, J. Barth, C. Felser, S. Wurmehl, G. Friemel, C. Hess, G. Behr, B. Buechner, A. Reller, S. Riegg, S.G. Ebbinghaus, T. Ellis, P.J. Jacobs, J.T. Kohlhepp, H.J.M. Swagten, *Highly ordered, half-metallic Co2FeSi single crystals*, Applied Physics Letters 95 (2009) Nr. 16, S. 161903/1-3.

38) M. Boehme, B. Kuila, H. Schloerb, B. Nandan, M. Stamm, *Thin films of block copolymer supramolecular assemblies:Microphase separation and nanofabrication*, Physica Status Solidi / B 247 (2010) Nr. 10, S. 2458-2469.

39) F. Boerrnert, C. Boerrnert, S. Gorantla, X. Liu, A. Bachmatiuk, J.-O. Joswig, F.R. Wagner, F. Schaeffel, J.H. Warner, R. Schoenfelder, B. Rellinghaus, T. Gemming, J. Thomas, M. Knupfer, B. Buechner, M.H. Ruemmeli, *Single-wall-carbon-nanotube/single-carbon-chain molecular junctions*, Physical Review B 81 (2010) Nr. 8, S. 85439/1-5.

40) F. Boerrnert, S. Gorantla, A. Bachmatiuk, J.H. Warner, I. Ibrahim, J. Thomas, T. Gemming, J. Eckert, G. Cuniberti, B. Buechner, M.H. Ruemmeli, *In situ observations of self-repairing single-walled carbon nanotubes*, Physical Review B 81 (2010) Nr. 20, S. 201401(R)/1-4.

41) C.C. Bof Bufon, J.D.C. Gonzalez, D.J. Thurmer, D. Grimm, M. Bauer, O.G. Schmidt, *Self-assembled ultra-compact energy storage elements based on hybrid nanomembranes*, Nano Letters 10 (2010) Nr. 7, S. 2506-2510.

42) S.V. Borisenko, V.B. Zabolotnyy, D.V. Evtushinsky, T.K. Kim, I.V. Morozov, A.N. Yaresko, A.A. Kordyuk, G. Behr, A. Vasiliev, R. Follath, B. Buechner, *Superconductivity without Nesting in LiFeAs*, Physical Review Letters 105 (2010) Nr. 6, S. 67002/1-4.

43) E. Borowiak-Palen, A. Steplewska, A. Bachmatiuk, M.H. Ruemmeli, R.K. Kalenczuk, *Carbon nanotubes grown with non-ferromagnetic catalysts in alcohol CVD*, Materials Science Forum 636-637 (2010), S. 703-708.

44) L. Braicovich, M. Moretti Sala, L.J.P. Ament, V. Bisogni, M. Minola, G. Balestrino, D. Di Castro, G.M. De Luca, M. Salluzzo, G. Ghiringhelli, J. van den Brink, *Momentum and polarization dependence of single-magnon spectral weight for Cu L3-edge resonant inelastic x-ray scattering from layered cuprates*, Physical Review B 81 (2010) Nr. 17, S. 174533/1-5.

45) L. Braicovich, J. van den Brink, V. Bisogni, M. Moretti Sala, L.J.P. Ament, N.B. Brookes, G.M. De Luca, M. Salluzzo, T. Schmitt, V.N. Strocov, G. Ghiringhelli, *Magnetic excitations and phase separation in the underdoped La2xSrxCuO4 superconductor measured by resonant inelastic X-Ray scattering*, Physical Review Letters 104 (2010) Nr. 7, S. 77002/1-4.

46) K. Braun, L. Dunsch, R. Pipkorn, M. Bock, T. Baeuerle, S. Yang, W. Waldeck, M. Wiessler, *Gain of a 500-fold sensitivity on an intravital MR contrast agent based on an endohedral Gadolinium-Cluster-Fullerene-Conjugate: A new chance in cancer diagnostics*, International Journal of Medical Sciences 7 (2010), S. 136-146.

47) J. Buschbeck, S. Hamann, A. Ludwig, B. Holzapfel, L. Schultz, S. Faehler, *Correlation of phase transformations and magnetic properties in annealed epitaxial Fe-Pd magnetic shape memory alloy films*, Journal of Applied Physics 107 (2010) Nr. 11, S. 113919/1-3.

48) A.B. Butenko, A.A. Leonov, A.N. Bogdanov, U.K. Roessler, *Influence of the Dzyaloshinskii-Moriya interaction on vortex states in magnetic nanodisks*, Journal of Physics: Conference Series 200 (2010) Nr. 4, S. 42012/1-4.

49) A.B. Butenko, A.A. Leonov, A.N. Bogdanov, U.K. Roessler, *Theory of vortex states in magnetic nanodisks with induced Dzyaloshinskii-Moriya interactions*, Physical Review B 80 (2010) Nr. 13, S. 134410/1-8.

50) A.B. Butenko, A.A. Leonov, U.K. Roessler, A.N. Bogdanov, *Stabilization of skyrmion textures by uniaxial distortions in noncentrosymmetric cubic helimagnets*, Physical Review B 82 (2010) Nr. 5, S. 52403/1-4.

51) M. Bystrzejewski, A. Huczko, P. Kowalczyk, M. Rogala, M. Szybowicz, M.H. Ruemmeli, T. Gemming, H. Lange, *Ultra highly selective synthesis of double-walled carbon nanotubes*, Fullerenes, Nanotubes, and Carbon Nanostructures 18 (2010), S. 137-147.

52) M. Bystrzejewski, A. Huczko, H. Lange, T. Gemming, B. Buechner, M.H. Ruemmeli, *Dispersion and diameter separation of multi-wall carbon nanotubes in aqueous solutions*, Journal of Colloid and Interface Science 345 (2010) Nr. 2, S. 138-142.

53) M. Bystrzejewski, M.H. Ruemmeli, T. Gemming, H. Lange, A. Huczko, *Catalyst-free synthesis of onion-like carbon nanoparticles*, New Carbon Materials 25 (2010) Nr. 1, S. 1-8.

54) M. Bystrzejewski, M. Szala, W. Kicinski, W. Kaszuwara, M.H. Ruemmeli, T. Gemming, A. Huczko, *Self-sustaining high-temperature synthesis of car-bon-encapsulated magnetic nanoparticles from organic and inorganic metal precursors*, New Carbon Materials 25 (2010) Nr. 2, S. 81-88.

55) M. Calin, J. Das, K.B. Kim, S. Pauly, N. Mattern, J. Eckert, *Enhanced work hardening of Cu-based bulk metallic glass composites by in-situ formed nano-scale heterogeneities*, Materials Science Forum 633-634 (2010), S. 665-673.

56) C.D. Cao, R. Klingeler, H. Vinzelberg, N. Leps, W. Loeser, G. Behr, F. Muranyi, V. Kataev, B. Buechner, *Magnetic anisotropy and ferromagnetic correlations above the Curie temperature in Eu2CuSi3 single crystals*, Physical Review B 82 (2010) Nr. 13, S. 134446/1-7.

57) N. Chen, S. Klod, P. Rapta, A.A. Popov, L. Dunsch, *Direct arc-discharge assisted synthesis of C60H2(C3H5N): A cis-1-pyrrolino C60 fullerene hydride with unusual redox properties*, Chemistry of Materials 22 (2010), S. 2608-2615.

58) X. Chen, P. Lukaszczuk, C. Tripisciano, M.H. Ruemmeli, J. Srenscek-Nazzal, I. Pelech, R.J. Kalenczuk, E. Borowiak-Palen, *Enhancement of the structure stability of MOF-5 confined to multiwalled carbon nanotubes*, Physica Status Solidi B 247 (2010) Nr. 11-12, S. 2664-2668.

59) R. Chulist, W. Skrotzki, C.-G. Oertel, A. Boehm, M. Poetschke, *Change in microstructure during training of a Ni50Mn29Ga21 bicrystal*, Scripta Materialia 63 (2010) Nr. 5, S. 548-551.

60) I. Chumak, G. Dmytriv, V. Pavlyuk, S. Oswald, J. Eckert, H. Trill, H. Eckert, H. Pauly, H. Ehrenberg, *Li(Al1-zZnz) alloys as anode materials for rechargeable Li-ion batteries*, Journal of Materials Research 25 (2010) Nr. 8, S. 1492-1499.

61) I. Chumak, K.W. Richter, H. Ehrenberg, *Redetermination of iron dialuminide, FeAl2*, Acta Crystallographica C 66 (2010), S. i87-i88.

62) D. Chylarecka, C. Waeckerlin, T.K. Kim, K. Mueller, F. Nolting, A. Kleibert, N. Ballav, T.A. Jung, *Self-assembly and superexchange coupling of magnetic molecules on oxygen-reconstructed ferromagnetic thin film*, The Journal of Physical Chemistry Letters 1 (2010), S. 1408-1413.

63) V. Cloet, T. Thersleff, O. Stadel, S. Hoste, B. Holzapfel, I. Van Driessche, *Transmission electron microscopy analysis of a coated conductor produced by chemical deposition methods*, Acta Materialia 58 (2010), S. 1489-1494.

64) D.Y. Cong, S. Roth, J. Liu, Q. Luo, M. Poetschke, C. Huerrich, L. Schultz, *Superparamagnetic and superspin glass behaviors in the martensitic state of Ni43.5Co6.5Mn39Sn11 magnetic shape memory alloy*, Applied Physics Letters 96 (2010) Nr. 11, S. 112504/1-3.

65) D.Y. Cong, S. Roth, M. Poetschke, C. Huerrich, L. Schultz, *Phase diagram and composition optimization for magnetic shape memory effect in Ni–Co–Mn–Sn alloys*, Applied Physics Letters 97 (2010) Nr. 2, S. 21908/1-3.

66) J.W. Cui, R.T. Qua, F.F. Wu, Z.F. Zhang, B.L. Shen, M. Stoica, J. Eckert, *Shear band evolution during large plastic deformation of brittle and ductile metallic glasses*, Philosophical Magazine Letters 90 (2010), S. 573-579.

67) J. Cwik, T. Palewski, K. Nenkov, J. Lyubina, O. Gutfleisch, J. Klamut, *Magnetic properties and magnetocaloric effect in Dy1-xScxNi2 solid solutions*, Journal of Alloys and Compounds 506 (2010) Nr. 2, S. 626-630.

68) J. Cwik, T. Palewski, K. Nenkov, J. Lyubina, J. Klamut, *Magnetic and magnetocaloric properties of laves phase Dy1-xGdx(Co1-xNix)2 solid solutions*, Journal of Low Temperature Physics 159 (2010) Nr. 1-2, S. 37-41.

69) J. Cwik, T. Palewski, K. Nenkov, J. Lyubina, J. Warchulska, O. Gutfleisch, J. Klamut, *Magnetic properties and specific heat of laves phase Tb1¡xScxNi2 (x = 0:1, 0.2) solid solutions*, Acta Physica Polonica 118 (2010) Nr. 5, S. 877-878.

70) M. Daghofer, Q.-L. Luo, R. Yu, D.X. Yao, A. Moreo, E. Dagotto, *Orbital-weight redistribution triggered by spin order in the pnictides*, Physical Review B 81 (2010) Nr. 18, S. 180514/1-4.

71) M. Daghofer, A. Moreo, *Comment on "Nonmagnetic impurity resonances as a signature of sign-reversal pairing in FeAs-based superconductors*, Physical Review Letters 104 (2010) Nr. 8, S. 89701/1-1.

72) M. Daghofer, N. Zheng, A. Moreo, *Spin-polarized semiconductor induced by magnetic impurities in graphene*, Physical Review B 82 (2010) Nr. 12, S. 121405/1-4.

73) A.N. Darinskii, M. Weihnacht, H. Schmidt, *Surface acoustic wave scattering from steps, grooves, and strips on piezoelectric substrates*, IEEE Transactions on Ultrasonics, Ferroelectrics, and Frequency Control 57 (2010) Nr. 9, S. 2042-2050.

74) A.N. Darinskii, M. Weihnacht, H. Schmidt, *Usage of symmetry in the simulation of interdigital transducers*, IEEE Transactions on Ultrasonics, Ferroelectrics, and Frequency Control 57 (2010) Nr. 10, S. 2356-2359.

75) J. Das, R. Theissmann, W. Loeser, J. Eckert, *Effect of Sn on microstructure and mechanical properties of Ti-Fe-(Sn) ultrafine eutectic composites*, Journal of Materials Research 25 (2010) Nr. 5, S. 943-956.

76) L. de Abreu Vieira, M. Doebeli, A. Dommann, E. Kalchbrenner, A. Neels, J. Ramm, H. Rudigier, J. Thomas, B. Widrig, *Approaches to influence the microstructure and the properties of Al–Cr–0 layers synthesized by cathodic arc evaporation*, Surface and Coatings Technology 204 (2010), S. 1722-1728.

77) Y.S. Dedkov, E.N. Voloshina, M. Richter, *Preparation and photoemission investigation of bulklike alpha-Mn films on W(110)* , Physical Review B 81 (2010) Nr. 8, S. 85404/1-5.

78) S. de Jong, E. van Heumen, S. Thirupathaiah, R. Huisman, F. Massee, J.B. Goedkoop, R. Ovsyannikov, J. Fink, H.A. Duerr, A. Gloskovskii, H.S. Jeevan, P. Gegenwart, A. Erb, L. Patthey, M. Shi, R. Follath, A. Varykhalov, M.S. Golden, *Droplet-like Fermi surfaces in the anti-ferromagnetic phase of EuFe2As2, an Fe-pnictide superconductor parent compound*, epl 89 (2010), S. 27007/1-6.

79) C. Deneke, A. Malachias, S. Kiravittaya, M. Benyoucef, T.H. Metzger, O.G. Schmidt, *Strain states in a quantum well embedded into a rolled-up microtube: X-ray and photoluminescence studies*, Applied Physics Letters 96 (2010) Nr. 14, S. 143101/1-3.

80) J.T. Devreese, V.M. Fomin, V.N. Gladilin, J. Tempere, *Oscillatory persistent currents in quantum rings: Semiconductors versus superconductors*, Physica / C 470 (2010) Nr. 19, S. 848-852.

81) M. Dimitrakopoulou, B. Buechner, M.H. Ruemmeli, *Silicon nanowires: Growth mechanisms and synthesis routes*, Global Journal of Physical Chemistry 1 (2010) Nr. 1, S. 36-58.

82) F. Ding, N. Akopian, B. Li, U. Perinetti, A. Govorov, F.M. Peeters, C.C. Bof Bufon, C. Deneke, Y.H. Chen, A. Rastelli, O.G. Schmidt, V. Zwiller, *Gate controlled Aharonov-Bohm-type oscillations from single neutral excitons in quantum rings*, Physical Review B 82 (2010) Nr. 7, S. 75309/1-8.

83) F. Ding, H. Ji, Y. Chen, A. Herklotz, K. Doerr, Y. Mei, A. Rastelli, O.G. Schmidt, *Stretchable graphene: A close look at fundamental parameters through biaxial straining*, Nano Letters 10 (2010) Nr. 9, S. 3453-3458.

84) F. Ding, R. Singh, J.D. Plumhof, T. Zander, V. Krapek, Y.H. Chen, M. Benyoucef, V. Zwiller, K. Doerr, G. Bester, A. Rastelli, O.G. Schmidt, *Tuning the exciton binding energies in single self-assembled in GaAs/GaAs quantum dots by piezoelectric-induced biaxial stress*, Physical Review Letters 104 (2010) Nr. 6, S. 67405/1-4.

85) M. Doerr, S. Schoenecker, A. Haase, E. Kampert, J.A.A.J. Perenboom, M. Richter, M. Rotter, M.S. Kim, M. Loewenhaupt, *High field magnetoelastic quantum oscillations of palladium*, Journal of Low Temperature Physics 159 (2010) Nr. 1-2, S. 20-23.

86) S.-L. Drechsler, J. Malek, R.O. Kuzian, S. Nishimoto, U. Nitzsche, W.E.A. Lorenz, R. Klingeler, B. Buechner, M. Knupfer, *Intersite coulomb interactions in edge-shared Cu02 chains: Optics and EELS*, Physica C 470 (2010) Nr. Supplement 1, S. S84-S85.

87) S.-L. Drechsler, J. Malek, W.E.A. Lorenz, R.O. Kuzian, R. Klingeler, S. Nishimoto, U. Nitzsche, M. Knupfer, N. Wizent, G. Behr, H. Rosner, H. Eschrig, B. Buechner, *Progress in the theoretical description of a strongly frustrated edge-shared model chain cuprate: Li2Cu02*, Journal of Physics: Conference Series 200 (2010), S. 12028/1-4.

88) S.-L. Drechsler, F. Roth, M. Grobosch, R. Schuster, K. Koepernik, H. Rosner, G. Behr, M. Rotter, D. Johrendt, B. Buechner, M. Knupfer, *Insight into the physics of Fe-pnictides from optical and T = 0 penetration depth data*, Physica C 470 (2010) Nr. Supplement 1, S. S332-S333.

89) L. Dunsch, S. Yang, L. Zhang, A. Svitova, S. Oswald, A.A. Popov, *Metal sulfide in a C82 fullerene cage: A new form of endohedral clusterfullerenes*, Journal of the American Chemical Society 132 (2010), S. 5413-5421.

90) V. Efimova, A. Derzsi, A. Zlotorowicz, V. Hoffmann, Z. Donko, J. Eckert, *Influence of the anode material on the characteristics of an analytical glow discharge cell*, Spectrochimica Acta, Part B 65 (2010) Nr. 4, S. 311-315.

91) J. Eickemeyer, R. Huehne, A. Gueth, C. Rodig, U. Gaitzsch, J. Freudenberger, L. Schultz, B. Holzapfel, *Textured Ni–9.0 at.% Wsubstrate tapes for YBCO-coated conductors*, Superconductor Science and Technology 23 (2010) Nr. 8, S. 85012/1-6.

92) A.A. El-Gendy, O. Vyacheslav Khavrus, S. Hampel, A. Leonhardt, B. Buechner, R. Klingeler, *Morphology, structural control, and magnetic properties of carbon-coated nanoscaled NiRu alloys*, The Journal of Physical Chemistry C 114 (2010), S. 10745-10749.

93) J. Engelmann, T. Shapoval, S. Haindl, L. Schultz, B. Holzapfel, *Growth and characterization of NbN/SmCo5 bilayers: The influence of magnetic stray field on the upper critical field of the superconductor* , Journal of Physics: Conference Series 234 (2010) Nr. 1, S. 12012/1-5.

94) H. Eschrig, *T>0 ensemble-state density functional theory via Legendre transform*, Physical Review B 82 (2010) Nr. 20, S. 205120/1-9.

95) H. Eschrig, *A Viewpoint on: T>0 ensemble-state density functional theory via Legendre transform, Prodan, Emil: Viewpoint: Raising the temperature on density-functional theory*, Physics 3 (2010), S. 99/1-3.

96) H. Eschrig, A. Lankau, K. Koepernik, *Calculated cleavage behavior and surface states of LaOFeAs*, Physical Review B 81 (2010) Nr. 15, S. 155447/1-9.

97) D.V. Evtushinsky, D.S. Inosov, G. Urbanik, V.B. Zabolotnyy, R. Schuster, P. Sass, T. Haenke, C. Hess, B. Buechner, R. Follath, P. Reutler, A. Revcolevschi, A.A. Kordyuk, S.V. Borisenko, *Bridging charge-orbital ordering and fermi surface instabilities in half-doped single-layered manganite La0:5Sr1:5Mn04*, Physical Review Letters 105 (2010) Nr. 14, S. 147201/1-4.

98) P. Feng, I. Moench, G. Huang, S. Harazim, J.S. Smith, Y. Mei, O.G. Schmidt, *Local-illuminated ultrathin silicon nanomembranes with photovoltaic effect and negative transconductance*, Advanced Materials 22 (2010), S. 3667-3671.

99) V.M. Fomin, P. Kratzer, *Thermoelectric transport in periodic one-dimensional stacks of InAs/GaAs quantum dots*, Physical Review B 82 (2010) Nr. 4, S. 45318/1-10.

100) V. Franco, A. Conde, M.D. Kuzmin, J.M. Romero-Enrique, *The magnetocaloric effect in materials with a second order phase transition: Are TC and Tpeak necessarily coincident?*, Journal of Applied Physics 105 (2009) Nr. 7, S. 7A917/1-3.

101) J. Freudenberger, A. Kauffmann, H. Klauss, T. Marr, K. Nenkov, V. Subramanya Sarma, L. Schultz, *Studies on recrystallization of single-phase copper alloys by resistance measurements*, Acta Materialia 58 (2010), S. 2324-2329.

102) J. Freudenberger, J. Lyubimova, A. Gaganov, H. Witte, A.L. Hickman, H. Jones, M. Nganbe, *Non-destructive pulsed field CuAg-solenoids*, Materials Science and Engineering A 527 (2010) Nr. 7-8, S. 2004-2013.

103) G. Fuchs, S.-L. Drechsler, N. Kozlova, M. Bartkowiak, G. Behr, K. Nenkov, H.-H. Klauss, J. Freudenberger, M. Knupfer, F. Hammerath, G. Lang, H.-J. Grafe, B. Buechner, L. Schultz, *Evidence for Pauli-limiting behaviour at high fields and enhanced upper critical fields near T_c in several disordered FeAs based superconductors*, Physica C 470 (2010) Nr. Supplement 1, S. S288-S290.

104) G. Fuchs, S.-L. Drechsler, N. Kozlova, J. Freudenberger, M. Bartkowiak, J. Wosnitza, G. Behr, K. Nenkov, B. Buechner, L. Schultz, *Upper critical field measurements up to 60 T in Arsenic-deficient La00.9F0.1FeAs1-delta- Pauli limiting behavior at high fields vs. improved superconductivity at low fields*, Journal of Low Temperature Physics 159 (2010) Nr. 1-2, S. 164-167.

105) J. Fuzer, P. Kollar, J. Fuzerova, S. Roth, *Soft magnetic properties of nanostructured vitroperm alloy powder cores*, IEEE Transactions on Magnetics 46 (2010) Nr. 2, S. 471-474.

106) U. Gaitzsch, J. Eickemeyer, C. Rodig, J. Freudenberger, B. Holzapfel, L. Schultz, *Paramagnetic substrates for thin film superconductors: Ni–W and Ni–W–Cr*, Scripta Materialia 62 (2010) Nr. 7, S. 512-515.

107) J. Gao, P. Adelhelm, M.H.W. Verkuijlen, C. Rongeat, M. Herrich, P.J.M. van Bentum, O. Gutfleisch, A.P.M. Kentgens, K.P. de Jong, P.E. de Jongh, *Confinement of NaAlH4 in nanoporous carbon: Impact on H2 release, reversibility, and thermodynamics*, Journal of Physical Chemistry C 114 (2010), S. 4675-4682.

108) Y. Ge, O. Heczko, S.-P. Hannula, S. Faehler, *Probing structure and microstructure of epitaxial Ni–Mn–Ga films by reciprocal space mapping and pole figure measurements*, Acta Materialia 58 (2010) Nr. 20, S. 6665-6671.

109) A. Gebert, A. Concustell, A.L. Greer, L. Schultz, J. Eckert, *Effect of shot-peening on the corrosion resistance of a Zr-based bulk metallic glass*, Scripta Materialia 62 (2010) Nr. 9, S. 635-638.

110) A. Gebert, P.F. Gostin, L. Schultz, *Effect of surface finishing of a Zr-based bulk metallic glass on its corrosion behaviour*, Corrosion Science 52 (2010), S. 1711-1720.

111) A.V. Germanenko, N. Kozlova, G.M. Minkov, O.E. Rut, A.A. Sherstobitov, J. Freudenberger, *g-Factor of low mobility 2D GaAs electron gas as determined from high magnetic field experiments*, Physica E 42 (2010), S. 960-963.

112) G. Giovannetti, S. Kumar, A. Stroppa, J. van den Brink, S. Picozzi, *Multiferroicity in TTF-CA organic molecular crystals predicted through ab initio calculations*, Physical Review Letters 103 (2009) Nr. 16, S. 266401/1-4.

113) J. Gluch, T. Roessler, D. Schmidt, S.B. Menzel, M. Albert, J. Eckert, *TEM characterization of ALD layers in deep trenches using a dedicated FIB lamellae preparation method*, Thin Solid Films 518 (2010), S. 4553-4555.

114) G. Goerigk, N. Mattern, *Spinodal decomposition in Ni-Nb-Y metallic glasses analyzed by quantitative anomalous small-angle X-ray scattering*, Journal of Physics: Conference Series 247 (2010) Nr. 1, S. 12022/1-13.

115) S. Gorantla, S. Avdoshenko, F. Boerrnert, A. Bachmatiuk, M. Dimitrakopoulou, F. Schaeffel, R. Schoenfelder, J. Thomas, T. Gemming, J.H. Warner, G. Cuniberti, J. Eckert, B. Buechner, M.H. Ruemmeli, *Enhanced pi-pi interactions between a C60 fullerene and a buckle bend on a double-walled carbon nanotube*, Nano Research 3 (2010) Nr. 2, S. 92-97.

116) S. Gorantla, F. Boerrnert, A. Bachmatiuk, M. Dimitrakopoulou, R. Schoenfelder, F. Schaeffel, J. Thomas, T. Gemming, E. Borowiak-Palen, J.H. Warner, B.I. Yakobson, J. Eckert, B. Buechner, M.H. Ruemmeli, *In situ observations of fullerene fusion and ejection in carbon nanotubes*, Nanoscale 2 (2010) Nr. 10, S. 2077-2079.

117) P.F. Gostin, A. Gebert, L. Schultz, *Comparison of the corrosion of bulk amorphous steel with conventional steel*, Corrosion Science 52 (2010), S. 273-281.

118) E.B. Gowd, B. Nandan, M.K. Vyas, N.C. Bigall, A. Eychmueller, H. Schloerb, M. Stamm, *Highly ordered palladium nanodots and nanowires from switchable block copolymer thin films*, Nanotechnology 20 (2010) Nr. 41, S. 415302/1-10.

119) H.-J. Grafe, N.J. Curro, B.L. Young, A. Vyalikh, J. Vavilova, G.D. Gu, M. Huecker, B. Buechner, *Charge order and low frequency spin dynamics in lanthanum cuprates revealed by nuclear magnetic resonance*, The European Physical Journal Special Topics 188 (2010) Nr. 1, S. 89-101.

120) M. Grobosch, C. Schmidt, R. Kraus, M. Knupfer, *Electronic properties of transition metal phthalocyanines: The impact of the central metal atom (d5–d10)*, Organic Electronics 11 (2010) Nr. 9, S. 1483-1488.
121) M. Grobosch, C. Schmidt, W.J.M. Naber, W.G. van der Wiel, M. Knupfer, *A photoemission study of interfaces between organic semiconductors and Co as well as Al2O3/Co contacts*, Synthetic Metals 160 (2010), S. 238-243.
122) D. Haberer, D.V. Vyalikh, S. Taioli, B. Dora, M. Farjam, J. Fink, D. Marchenko, T. Pichler, K. Ziegler, S. Simonucci, M.S. Dresselhaus, M. Knupfer, B. Buechner, A. Grueneis, *Tunable band gap in hydrogenated quasi-free-standing graphene*, Nano Letters 10 (2010) Nr. 9, S. 3360-3366.
123) V. Haehnel, S. Faehler, P. Schaaf, M. Miglierini, C. Mickel, L. Schultz, H. Schloerb, *Towards smooth and pure iron nanowires grown by electrodeposition in self-organized alumina membranes*, Acta Materialia 58 (2010) Nr. 7, S. 2330-2337.
124) V. Haehnel, S. Faehler, L. Schultz, H. Schloerb, *Electrodeposition of Fe70Pd30 nanowires from a complexed ammonium–sulfosalicylic electrolyte with high stability*, Electrochemistry Communications 12 (2010) Nr. 8, S. 1116-1119.
125) V. Haehnel, C. Mickel, S. Faehler, L. Schultz, H. Schloerb, *Structure, microstructure, and magnetism of electrodeposited Fe70Pd30 nanowires*, Journal of Physical Chemistry C 114 (2010), S. 19278-19283.
126) M. Haertel, J. Richter, D. Ihle, S.-L. Drechsler, *Thermodynamics of a two-dimensional frustrated spin1-2 Heisenberg ferromagnet*, Physical Review B 81 (2010) Nr. 17, S. 174421/1-5.
127) W. Haessler, P. Kovac, M. Eisterer, A.B. Abrahamsen, M. Herrmann, C. Rodig, K. Nenkov, B. Holzapfel, T. Melisek, M. Kulich, M. von Zimmermann, J. Bednarcik, J.C. Grivel, *Anisotropy of the critical current in MgB2 tapes made of high energy milled precursor powder*, Superconductor Science and Technology 23 (2010) Nr. 6, S. 65011/1-6.
128) S. Haindl, M. Kidszun, A. Kauffmann, K. Nenkov, N. Kozlova, J. Freudenberger, T. Thersleff, J. Haenisch, J. Werner, E. Reich, L. Schultz, B. Holzapfel, *High upper critical fields and evidence of weak-link behavior in superconducting LaFeAsO1-xFx thin films*, Physical Review Letters 104 (2010) Nr. 7, S. 77001/1-4.
129) C. Hamann, J. McCord, L. Schultz, B.P. Toperverg, K. Theis-Broehl, M. Wolff, R. Kaltofen, I. Moench, *Competing magnetic interactions in exchange-bias-modulated films*, Physical Review B 81 (2010) Nr. 2, S. 24420/1-9.
130) S. Hamann, M.E. Gruner, S. Irsen, J. Buschbeck, C. Bechtold, I. Kock, S.G. Mayr, A. Savan, S. Thienhaus, E. Quandt, S. Faehler, P. Entel, A. Ludwig, *The ferromagnetic shape memory system Fe–Pd–Cu*, Acta Materialia 58 (2010) Nr. 18, S. 5949-5961.
131) F. Hammerath, S.-L. Drechsler, H.-J. Grafe, G. Lang, G. Fuchs, G. Behr, I. Eremin, M.M. Korshunov, B. Buechner, *Unusual disorder effects in superconducting LaFeAs1-00.9F0.1 as revealed by 75As NMR spectroscopy*, Physical Review B 81 (2010) Nr. 14, S. 140504(R)/1-4.
132) A.H. Hashem, A.E. Abdel Ghany, K. Nikolowski, H. Ehrenberg, *Effect of carbon coating process on the structure and electrochemical performance of LiNi0.5Mn0.5O2 used as cathode in Li-ion batteries*, Ionics 16 (2010) Nr. 4, S. 305-310.
133) A.M. Hashem, H.M. Abuzeid, K. Nikolowski, H. Ehrenberg, *Table sugar as preparation and carbon coating reagent for facile synthesis and coating of rod-shaped MnO2*, Journal of Alloys and Compounds 497 (2010) Nr. 1-2, S. 300-303.
134) M. Havlicek, W. Jantsch, M.H. Ruemmeli, R. Schoenfelder, K. Yanagi, Y. Miyata, H. Kataura, F. Simon, H. Peterlik, H. Kuzmany, *Electron spin resonance from semiconductor-metal separated SWCNTs*, Physica Status Solidi B 247 (2010) Nr. 11-12, S. 2851-2854.
135) O. Heczko, L. Straka, V. Novak, S. Faehler, *Magnetic anisotropy of nonmodulated Ni–Mn–Ga martensite revisited*, Journal of Applied Physics 107 (2010) Nr. 9, S. 9A914/1-3.
136) I. Hellmann, G.S. Zakharova, V.L. Volkov, C. Taeschner, A. Leonhardt, B. Buechner, R. Klingeler, *Static susceptibility and heat capacity studies on V3O7 H2O7 nanobelts*, Journal of Magnetism and Magnetic Materials 322 (2010) Nr. 7, S. 878-881.
137) A. Herklotz, A.D. Rata, L. Schultz, K. Doerr, *Reversible strain effect on the magnetization of LaCoO3 films*, Physical Review B 79 (2009) Nr. 9, S. 92409/1-4.
138) A. Herklotz, M.D. Biegalski, H.-S. Kim, L. Schultz, K. Doerr, H.M. Christen, *Wide-range strain tunability provided by epitaxial LaAl1-xScxO3 template films*, New Journal of Physics 12 (2010) Nr. 11, S. 113053/1-6.
139) A. Herklotz, J.D. Plumhof, A. Rastelli, O.G. Schmidt, L. Schultz, K. Doerr, *Electrical characterization of PMN–28%PT (001) crystals used as thin-film substrates*, Journal of Applied Physics 108 (2010) Nr. 9, S. 94101/1-7.
140) H. Hermann, *Optimization of dielectric and elastic properties of nanoporous ultralow-k dielectric materials*, in: AIP Conference Proceedings, 1300, 153-158 (2010).
141) H. Hermann, *Effective dielectric and elastic properties of nanoporous low-k media*, Modelling and Simulation in Materials Science and Engineering 18 (2010) Nr. 5, S. 55007/1-19.
142) R. Hermann, G. Gerbeth, J. Priede, A. Krauze, G. Behr, B. Buechner, *Convectional controlled crystal–melt interface using two-phase radio-frequency electromagnetic heating*, Journal of Materials Science 45 (2010) Nr. 8, S. 2228-2232.
143) C. Hermannstaedter, G.J. Beirne, M. Witzany, M. Heldmaier, J. Peng, G. Bester, L. Wang, A. Rastelli, O.G. Schmidt, P. Michler, *Influence of the charge carrier tunneling processes on the recombination dynamics in single lateral quantum dot molecules*, Physical Review B 82 (2010) Nr. 8, S. 85309/1-7.
144) N. Hlubek, P. Ribeiro, R. Saint-Martin, A. Revcolevschi, G. Roth, G. Behr, B. Buechner, C. Hess, *Ballistic heat transport of quantum spin excitations as seen in SrCuO2*, Physical Review B 81 (2010) Nr. 2, S. 20405R/1-4.

145) N. Hlubek, M. Sing, S. Glawion, R. Claessen, S. van Smaalen, P.H.M. van Loosdrecht, B. Buechner, C. Hess, *Heat conductivity of the spin-Peierls compounds TiOCl and TiOBr*, Physical Review B 81 (2010) Nr. 14, S. 144428/1-5.

146) M.G. Holder, A. Jesche, P. Lombardo, R. Hayn, D.V. Vyalikh, S. Danzenbacher, K. Kummer, C. Krellner, C. Geibel, Y. Kucherenko, T.K. Kim, R. Follath, S.L. Molodtsov, C. Laubschat, *CeFePO: f-d hybridization and quenching of superconductivity*, Physical Review Letters 104 (2010) Nr. 9, S. 96402/1-4.

147) G. Hrkac, T.G. Woodcock, C. Freeman, A. Goncharov, J. Dean, T. Schrefl, O. Gutfleisch, *The role of local anisotropy profiles at grain boundaries on the coercivity of Nd2Fe14B magnets*, Applied Physics Letters 97 (2010) Nr. 23, S. 232511/1-3.

148) G. Huang, V.A. Bolanos, F. Ding, S. Kiravittaya, Y. Mei, O.G. Schmidt, *Rolled-Up optical microcavities with subwavelength wall thicknesses for enhanced liquid sensing applications*, ACS nano 4 (2010) Nr. 6, S. 3123-3130.

149) R. Huehne, J. Eickemeyer, V.S. Sarma, A. Gueth, T. Thersleff, J. Freudenberger, O. de Haas, M. Weigand, J.H. Durrell, L. Schultz, B. Holzapfel, *Application of textured highly alloyed Ni–W tapes for preparing coated conductor architectures*, Superconductor Science and Technology 23 (2010) Nr. 3, S. 34015/1-7.

150) R. Huehne, K. Gueth, R. Gaertner, M. Kidszun, F. Thoss, B. Rellinghaus, L. Schultz, B. Holzapfel, *Application of textured IBAD-TiN buffer layers in coated conductor architectures*, Superconductor Science and Technology 23 (2010) Nr. 1, S. 14010/1-6.

151) C. Huerrich, S. Roth, M. Poetschke, B. Rellinghaus, L. Schultz, *Isothermal martensitic transformation in polycrystalline Ni50Mn29Ga21*, Journal of Alloys and Compounds 494 (2010), S. 40-43.

152) E.M.M. Ibrahim, V.O. Khavrus, A. Leonhardt, S. Hampel, S. Oswald, M.H. Ruemmeli, B. Buechner, *Synthesis, characterization, and electrical properties of nitrogen-doped single-walled carbon nanotubes with different nitrogen content*, Diamond and Related Materials 19 (2010), S. 1199-1206.

153) K.R. Idzika, P. Rapta, P.J. Cywinskie, R. Beckerta, L. Dunsch, *Synthesis and electrochemical characterization of new optoelectronic materials based on conjugated donor–acceptor system containing oligo-tri(heteroaryl)-1,3,5-triazines*, Electrochimica Acta 55 (2010) Nr. 17, S. 4858-4864.

154) Y. Ihara, P. Wzietek, H. Alloul, M.H. Ruemmeli, T. Pichler, F. Simon, *Incidence of the Tomonaga-Luttinger liquid state on the NMR spin-lattice relaxation in carbon nanotubes*, epl 90 (2010), S. 17004/1-5.

155) K. Iida, J. Haenisch, T. Thersleff, F. Kurth, M. Kidszun, S. Haindl, R. Huehne, L. Schultz, B. Holzapfel, *Scaling behavior of the critical current in clean epitaxial Ba(Fe1-xCox)2As2 thin films*, Physical Review B 81 (2010) Nr. 10, S. 100507(R)/1-4.

156) K. Iida, S. Haindl, T. Thersleff, J. Haenisch, F. Kurth, M. Kidszun, R. Huehne, I. Moench, L. Schultz, B. Holzapfel, R. Heller, *Influence of Fe buffer thickness on the crystalline quality and the transport properties of Fe/Ba(Fe1-xCox)2As2 bilayers*, Applied Physics Letters 97 (2010) Nr. 17, S. 172507/1-3.

157) K. Iida, K. Nenkov, G. Fuchs, G. Krabbes, B. Holzapfel, B. Buechner, L. Schultz, *Effect of addition of planetary milled Gd-211 on the microstructures and superconducting properties of air-processed single grain Gd–Ba–Cu–O/Ag bulk superconductors*, Physica C 470 (2010), S. 1153-1157.

158) D.S. Inosov, T. Shapoval, V. Neu, U. Wolff, J.S. White, S. Haindl, J.T. Park, D.L. Sun, C.T. Lin, E.M. Forgan, M.S. Viazovska, J.H. Kim, M. Laver, K. Nenkov, O. Khvostikova, S. Kuehnemann, V. Hinkov, *Symmetry and disorder of the vitreous vortex lattice in overdoped BaFe2-xCoxAs2: Indication for strong single-vortex pinning*, Physical Review B 81 (2010) Nr. 1, S. 14513/1-12.

159) D.S. Inosov, J.S. White, D.V. Evtushinsky, I.V. Morozov, A. Cameron, U. Stockert, V.B. Zabolotnyy, T.K. Kim, A.A. Kordyuk, S.V. Borisenko, E.M. Forgan, R. Klingeler, J.T. Park, S. Wurmehl, A.N. Vasiliev, G. Behr, C.D. Dewhurst, V. Hinkov, *Weak superconducting pairing and a single isotropic energy gap in stoichiometric LiFeAs*, Physical Review Letters 104 (2010) Nr. 18, S. 187001/1-4.

160) N. Jenkins, Y. Fasano, C. Berthod, I. Maggio-Aprile, A. Piriou, E. Giannini, B.W. Hoogenboom, C. Hess, T. Cren, O. Fischer, *Imaging the essential role of spin fluctuations in high-Tc superconductivity*, Physical Review Letters 103 (2009) Nr. 22, S. 227001/1-4.

161) H.O. Jeschke, H.C. Kandpal, I. Opahle, Y.-Z. Zhang, R. Valenty, *First principles determination of the model parameters in kappa-(ET)2Cu2(CN)3*, Physica B 405 (2010), S. S224-S228.

162) H. Ji, Y. Mei, O.G. Schmidt, *Swiss roll nanomembranes with controlled proton diffusion as redox micro-supercapacitors*, Chemical Communications 46 (2010), S. 3881-3883.

163) H.X. Ji, X.L. Wu, L.Z. Fan, C. Krien, I. Fiering, Y.G. Guo, Y.F. Mei, O.G. Schmidt, *Self-wound composite nanomembranes as electrode materials for lithium ion batteries*, Advanced Materials 22 (2010) Nr. 41, S. 4591-4595.

164) V. Jovanovic, C. Biasotto, L.K. Nanver, J. Moers, D. Gruetzmacher, J. Gerharz, G. Mussler, J. van der Cingel, J.J. Zhang, G. Bauer, O.G. Schmidt, L. Miglio, *n-Channel MOSFETs fabricated on SiGe dots for strain-enhanced mobility*, IEEE Electron Device Letters 31 (2010) Nr. 10, S. 1083-1085.

165) P. Jovari, I. Kaban, B. Bureau, A. Wilhelm, P. Lucas, B. Beuneu, D.A. Zajac, *Structure of Te-rich Te–Ge–X (X = I, Se, Ga) glasses*, Journal of Physics: Condensed Matter 22 (2010) Nr. 40, S. 404207/1-9.

166) I. Kaban, S. Curiotto, D. Chatain, W. Hoyer, *Surfaces, interfaces and phase transitions in Al–In monotectic alloys*, Acta Materialia 58 (2010), S. 3406-3414.

167) I. Kaban, P. Jovari, T. Petkova, P. Petkov, A. Stoilova, W. Hoyer, B. Beuneu, *Structure of GeSe4–In and GeSe5–In glasses*, Journal of Physics: Condensed Matter 22 (2010) Nr. 40, S. 404205/1-8.

168) I. Kaban, P. Jovari, M. Stoica, N. Mattern, J. Eckert, W. Hoyer, B. Beuneu, *On the atomic structure of Zr60Cu20Fe20 metallic glass*, Journal of Physics: Condensed Matter 22 (2010) Nr. 40, S. 404208/1-5.

169) M. Kalbac, L. Kavan, S. Gorantla, T. Gemming, L. Dunsch, *Sexithiophene encapsulated in a single-walled carbon nanotube: An In Situ raman spectroelectrochemical study of a peapod structure*, Chemistry - A European Journal 16 (2010) Nr. 38, S. 11753-11759.

170) A. Kario, W. Haessler, M. Herrmann, C. Rodig, J. Scheiter, B. Holzapfel, L. Schultz, S. Schlachter, B. Ringsdorf, W. Goldacker, A. Morawski, *Properties of MgB2 tapes prepared by using MA in-ex situ powder*, IEEE Transactions on Applied Superconductivity 20 (2010), S. 1521-1523.

171) A. Kario, A. Morawski, W. Haessler, M. Herrmann, C. Rodig, M. Schubert, K. Nenkov, B. Holzapfel, L. Schultz, B.A. Glowacki, S.C. Hopkins, *Novel ex situ MgB2 barrier for in situ monofilamentary MgB2 conductors with Fe and Cu sheath material*, Superconductor Science and Technology 23 (2010) Nr. 2, S. 25018/1-6.

172) A. Kario, A. Morawski, W. Haessler, K. Nenkov, M. Schubert, M. Herrmann, B. Ringsdorf, S.I. Schlachter, W. Goldacker, B. Holzapfel, L. Schultz, *Ex situ MgB2 barrier behavior of monofilament in situ MgB2 wires with Glidcop® sheath material*, Superconductor Science and Technology 23 (2010) Nr. 11, S. 115007/1-9.

173) V. Kataev, A. Alfonsov, E. Vavilova, A. Podlesnyak, D.I. Khomskii, B. Buechner, *Formation of magnetic polarons in lightly Ca doped LaCoO3*, Journal of Physics: Conference Series 200 (2010), S. 12080/1-4.

174) G. Katsaros, P. Spathis, M. Stoffel, F. Fournel, M. Mongillo, V. Bouchiat, F. Lefloch, A. Rastelli, O.G. Schmidt, S. De Franceschi, *Hybrid superconductor-semiconductor devices made from self-assembled SiGe nanocrystals on silicon*, nature nanotechnology 5 (2010), S. 458-464.

175) S. Kaufmann, U.K. Roessler, O. Heczko, M. Wuttig, J. Buschbeck, L. Schultz, S. Faehler, *Adaptive modulations of martensites*, Physical Review Letters 104 (2010) Nr. 14, S. 145702/1-3.

176) V. Khavrus, I. Shelevytsky, *Introduction to solar motion geometry on the basis of a simple model*, Physics Education 45 (2010) Nr. 6, S. 641-653.

177) V.O. Khavrus, E.M.M. Ibrahim, A. Leonhardt, S. Hampel, S. Oswald, C. Taeschner, B. Buechner, *Conditions of simultaneous growth and separation of single- and multiwalled carbon nanotubes*, Journal of Physical Chemistry C 114 (2010), S. 843-848.

178) O. Khvostikova, B. Assfour, G. Seifert, H. Hermann, A. Horst, H. Ehrenberg, *Novel experimental methods for assessment of hydrogen storage capacity and modelling of sorption in Cu-BTC*, International Journal of Hydrogen Energy 35 (2010) Nr. 20, S. 11042-11051.

179) M. Kidszun, R. Huehne, B. Holzapfel, L. Schultz, *Ion-beam-assisted deposition of textured NbN thin films*, Superconductor Science and Technology 23 (2010) Nr. 2, S. 25010/1-6.

180) J.-W. Kim, K. Nenkov, L. Schultz, K. Doerr, *Magnetic properties of thick multiferroic hexagonal HoMnO3 films*, Journal of Magnetism and Magnetic Materials 321 (2009) Nr. 11, S. 1727-1730.

181) T.E. Kim, J.M. Park, S.W. Sohn, D.H. Kim, W.T. Kim, M. Stoica, U. Kuehn, J. Eckert, *Effect of carbon addition on the microstructural evolution and mechanical properties in hypo-eutectic Fe-Zr(-Nb) alloys*, Materials Transactions 51 (2010) Nr. 4, S. 799-802.

182) N.S. Kiselev, C. Bran, U. Wolff, L. Schultz, A.N. Bogdanov, O. Hellwig, V. Neu, U.K. Roessler, *Metamagnetic domains in antiferromagnetically coupled multilayers with perpendicular anisotropy*, Physical Review B 81 (2010) Nr. 5, S. 54409/1-4.

183) R. Klingeler, N. Leps, I. Hellmann, A. Popa, U. Stockert, C. Hess, V. Kataev, H.-J. Grafe, F. Hammerath, G. Lang, S. Wurmehl, G. Behr, L. Harnagea, S. Singh, B. Buechner, *Local antiferromagnetic correlations in the iron pnictide superconductors LaFeAsO1-xFx and Ca(Fe1-xCox)2As2 as seen via normal-state susceptibility*, Physical Review B 81 (2010) Nr. 2, S. 24506/1-5.

184) R. Klingeler, L. Wang, U. Koehler, G. Behr, C. Hess, B. Buechner, *Thermal expansion of RFeAsO (R=La,Ce,Pr,Sm,Gd)*, Journal of Physics: Conference Series 200 (2010), S. 12088/1-4.

185) S. Klod, L. Zhang, L. Dunsch, *The role of the cluster on the relaxation of endohedral fullerene cage carbons: A NMR spin-lattice relaxation study of an internal relaxation reagent*, Journal of Physical Chemistry C 114 (2010), S. 8264-8267.

186) K. Koch, K. Koepernik, D. Van Neck, H. Rosner, S. Cottenier, *Electron penetration into the nucleus and its effect on the quadrupole interaction*, Physical Review A 81 (2010) Nr. 3, S. 32507/1-16.

187) M. Kohl, S. Reddy, Y.F. Khelfaoui, B. Krevet, A. Backen, S. Faehler, T. Eichhorn, G. Jakob, A. Mecklenburg, *Recent progress in FSMA microactuator developments*, Materials Science Forum 635 (2010), S. 145-154.

188) A. Koitzsch, D.S. Inosov, H. Shiozawa, V.B. Zabolotnyy, S.V. Borisenko, A. Varykhalov, C. Hess, M. Knupfer, U. Ammerahl, A. Revcolevschi, B. Buechner, *Observation of the Fermi surface, the band structure, and their diffraction replicas of Sr14-xCaxCu24O41 by angle-resolved photoemission spectroscopy*, Physical Review B 81 (2010) Nr. 11, S. 113110/1-4.

189) A. Koitzsch, R. Kraus, T. Kroll, M. Knupfer, B. Buechner, H. Eschrig, D.R. Batchelor, G.L. Sun, D.L. Sun, C.T. Lin, *Observation of two-hole satellite in the resonant x-ray photoemission spectra of Ba1-xKxFe2As2 single crystals*, Physical Review B 81 (2010) Nr. 17, S. 174519/1-6.

190) X.H. Kong, C. Deneke, H. Schmidt, D.J. Thurmer, H.X. Ji, M. Bauer, O.G. Schmidt, *Surface acoustic wave mediated dielectrophoretic alignment of rolled-up microtubes in microfluidic systems*, Applied Physics Letters 96 (2010) Nr. 13, S. 134105/1-3.

191) T. Kordel, C. Wehrenfennig, D. Meier, T. Lottermoser, M. Fiebig, I. Gelard, C. Dubourdieu, J.-W. Kim, L. Schultz, K. Doerr, *Nanodomains in multiferroic hexagonal RMnO3 films (R=Y,Dy,Ho,Er)*, Physical Review B 80 (2009) Nr. 4, S. 45409/1-8.

192) R. Koseva, I. Moench, J. Schumann, K.-F. Arndt, O.G. Schmidt, *Bismuth Hall probes: Preparation, properties and application*, Thin Solid Films 518 (2010), S. 4847-4851.

193) J.A. Koza, F. Karnbach, M. Uhlemann, J. McCord, C. Mickel, A. Gebert, S. Baunack, L. Schultz, *Electrocrystallisation of CoFe alloys under the influence of external homogeneous magnetic fields - properties of deposited thin films*, Electrochimica Acta 55 (2010) Nr. 3, S. 819-831.

194) J.A. Koza, I. Mogi, K. Tschulik, M. Uhlemann, C. Mickel, A. Gebert, L. Schultz, *Electrocrystallisation of metallic films under the influence of an external homogeneous magnetic field - Early stages of the layer growth*, Electrochimica Acta 55 (2010) Nr. 22, S. 6533-6541.

195) C. Kramberger, E. Einarsson, S. Huotari, T. Thurakitseree, S. Maruyama, M. Knupfer, T. Pichler, *Interband and plasma excitations in single-walled carbon nanotubes and graphite in inelastic x-ray and electron scattering*, Physical Review B 81 (2010) Nr. 20, S. 205410/1-5.

196) R. Kraus, B. Buechner, M. Knupfer, S. Glawion, M. Sing, R. Claessen, *Anisotropic crystal field, Mott gap, and interband excitations in TiOCl: An electron energy-loss study*, Physical Review B 81 (2010) Nr. 12, S. 125133/1-4.

197) Y. Krupskaya, A. Alfonsov, A. Parameswaran, V. Kataev, R. Klingeler, G. Steinfeld, N. Beyer, M. Gressenbuch, B. Kersting, B. Buechner, *Interplay of magnetic exchange interactions and NiSNi bond angles in polynuclear Nickel(II) complexes*, ChemPhysChem 11 (2010), S. 1961-1970.

198) Y. Krupskaya, A. Parameswaran, A. Alfonsov, R. Klingeler, V. Kataev, N. Beyer, J. Lach, M. Gressenbuch, B. Kersting, B. Buechner, *High-field ESR and magnetization study of a novel macrocyclic chelate trinuclear Ni(II) complex*, Journal of Low Temperature Physics 159 (2010) Nr. 1-2, S. 84-87.

199) V. Ksenofontov, M. Wojcik, S. Wurmehl, H. Schneider, B. Balke, G. Jakob, C. Felser, *Hyperfine magnetic field on iron atoms and Co–Fe disordering in Co2FeSi*, Journal of Applied Physics 107 (2010) Nr. 9, S. 9B106/1-3.

200) U. Kuehn, J. Romberg, N. Mattern, H. Wendrock, J. Eckert, *Transformation-induced plasticity in Fe-Cr-V-C*, Journal of Materials Research 25 (2010) Nr. 2, S. 368-374.

201) S. Kumar, G. Giovannetti, J. van den Brink, S. Picozzi, *Theoretical prediction of multiferroicity in double perovskite Y2NiMnO6*, Physical Review B 82 (2010) Nr. 13, S. 134429/1-6.

202) S. Kumar, J. van den Brink, *Frustration-induced insulating chiral spin state in itinerant triangular-lattice magnets*, Physical Review Letters 105 (2010) Nr. 21, S. 216405/1-4.

203) S. Kumar, J. van den Brink, A.P. Kampf, *Spin-spiral states in undoped manganites: Role of finite hund`s rule coupling*, Physical Review Letters 104 (2010) Nr. 1, S. 17201/1-4.

204) F. Kurth, M. Weisheit, K. Leistner, T. Gemming, B. Holzapfel, L. Schultz, S. Faehler, *Finite-size effects in highly ordered ultrathin FePt films*, Physical Review B 82 (2010) Nr. 18, S. 184404/1-8.

205) I.V. Kuvychko, A.A. Popov, A.V. Streletskii, L.C. Nye, T. Drewello, S.H. Strauss, O.V. Boltalina, *Dynamic HPLC study of C70 chlorination reveals a surprisingly selective synthesis of C70Cl8*, Chemical Communication 46 (2010), S. 8204-8206.

206) I.V. Kuvychko, A.V. Streletskii, N.B. Shustova, K. Seppelt, T. Drewello, A.A. Popov, S.H. Strauss, O.V. Boltalina, *Soluble chlorofullerenes C60Cl2,4,6,8,10. Synthesis, purification, compositional analysis, stability, and experimental/theoretical structure elucidation, including the X-ray structure of C1-C60Cl10*, Journal of the American Chemical Society 132 (2010) Nr. 18, S. 6443-6462.

207) M.D. Kuzmin, D. Givord, V. Skumryev, *Why the iron magnetization in Gd2Fe14B and the spontaneous magnetization of Y2Fe14B depend on temperature differently*, Journal of Applied Physics 107 (2010) Nr. 11, S. 113924/1-4.

208) M.D. Kuzmin, *Deducing model parameters of ferrimagnets from high-field magnetization curves*, Physical Review B 79 (2009) Nr. 21, S. 212405/1-4.

209) M. Kuzmin, R. Hayn, V. Oison, *Ab initio calculated XANES and XMCD spectra of Fe(II) phthalocyanine*, Physical Review B 79 (2009) Nr. 2, S. 24413/1-5.

210) O.E. Kvitnitskaya, Y.G. Naidyuk, I.K. Yanson, T. Niemeier, G. Fuchs, B. Holzapfel, L. Schultz, *Point-contact study of a LuNi2B2C borocarbide superconducting film*, Superconductor Science and Technology 23 (2010), S. 115001/1-5.

211) Y.-W. Lai, R. Schaefer, L. Schultz, J. McCord, *Volume magnetic domain mirroring in magnetic shape memory crystals*, Applied Physics Letters 96 (2010) Nr. 2, S. 22507/1-3.

212) B. Lake, A.M. Tsvelik, S. Notbohm, D.A. Tennant, T.G. Perring, M. Reehuis, C. Sekar, G. Krabbes, B. Buechner, *Confinement of fractional quantum number particles in a condensed-matter system*, nature physics 6 (2010) Nr. 1, S. 50-55.

213) G. Lang, H.-J. Grafe, F. Hammerath, K. Manthey, D. Paar, G. Behr, J. Werner, J. Hamann-Borrero, B. Buechner, *Probing of the charge distribution in iron pnictides*, Physica C 470 (2010), S. S454-S455.

214) G. Lang, H.-J. Grafe, D. Paar, F. Hammerath, K. Manthey, G. Behr, J. Werner, B. Buechner, *Nanoscale electronic order in iron pnictides*, Physical Review Letters 104 (2010) Nr. 9, S. 97001/1-4.

215) A. Lankau, K. Koepernik, S. Borisenko, V. Zabolotnyy, B. Buechner, J. van den Brink, H. Eschrig, *Absence of surface states for LiFeAs investigated using density functional calculations*, Physical Review B 82 (2010) Nr. 18, S. 184518/1-5.

216) M.H. Lee, J. Das, K.S. Lee, U. Kuehn, J. Eckert, *Effect of prestraining on the deformation and fracture behavior of Zr44Ti11Cu9.8Ni10.2Be25*, Intermetallics 18 (2010) Nr. 10, S. 1902-1907.

217) M.H. Lee, K.T. Kim, T. Gemming, D.J. Sordelet, J. Eckert, *Enhanced gas adsorption property of hybrid nanopore-structured copper oxide synthesized from the carbon nanotube/copper composites*, Journal of Applied Physics 108 (2010) Nr. 6, S. 64303/1-6.

218) M.H. Lee, J.K. Lee, K.B. Kim, D.J. Sordelet, J. Eckert, J.C. Bae, *Mechanical behavior of metallic glass reinforced nanostructured tungsten composites synthesized by spark plasma sintering*, Intermetallics 18 (2010) Nr. 10, S. 2009-2013.

219) M.H. Lee, K.S. Lee, J. Das, J. Thomas, U. Kuehn, J. Eckert, *Improved plasticity of bulk metallic glasses upon cold rolling*, Scripta Materialia 62 (2010) Nr. 9, S. 678-681.

220) P.V. Leksin, N.N. Garifyanov, I.A. Garifullin, J. Schumann, H. Vinzelberg, V. Kataev, R. Klingeler, O.G. Schmidt, B. Buechner, *Full spin switch effect for the superconducting current in a superconductor/ferromagnet thin film heterostructure*, Applied Physics Letters 97 (2010) Nr. 10, S. 102505/1-3.

221) R. Li, G. Liu, M. Stoica, J. Eckert, *FeCo-based multiphase composites with high strength and large plastic deformation*, Intermetallics 18 (2010) Nr. 1, S. 134-139.

222) R. Li, S. Pang, M. Stoica, J.M. Park, U. Kuehn, T. Zhang, J. Eckert, *Mechanical properties of rapidly solidified Fe–Al–B ternary alloys*, Journal of Alloys and Compounds 504 (2010) Nr. Suppl. 1, S. S472-S475.

223) R. Li, M. Stoica, G. Liu, J. Eckert, *Evolution of constitution, structure and morphology in FeCo-based multicomponent alloys*, Metallurgical and Materials Transactions A 41 (2010) Nr. 7, S. 1640-1645.

224) R. Li, M. Stoica, G. Wang, J.M. Park, Y. Li, T. Zhang, J. Eckert, *Glass formation, thermal properties, and elastic constants of La-Al-Co alloys*, Journal of Materials Research 25 (2010) Nr. 7, S. 1398-1404.

225) K.R. Lim, J.H. Na, J.M. Park, W.T. Kim, D.H. Kim, *Enhancement of plasticity in Ti-based metallic glass matrix composites by controlling characteristic and volume fraction of primary phase*, Journal of Materials Research 25 (2010) Nr. 11, S. 2183-2191.

226) J.-H. Lin, C.-S. Chen, M.H. Ruemmeli, Z.-Y. Zeng, *Self-assembly formation of multi-walled carbon nanotubes on gold surfaces*, Nanoscale 2 (2010), S. 2835-2840.

227) I. Lindemann, R.D. Ferrer, L. Dunsch, Y. Filinchuk, R. Cerny, H. Hagemann, V. DAnna, L.M.L. Daku, L. Schultz, O. Gutfleisch, *Al3Li4 (BH4)13: A complex double-cation borohydride with a new structure*, Chemistry - A European Journal 16 (2010) Nr. 29, S. 8707-8712.

228) K. Lipert, S. Bahr, F. Wolny, P. Atkinson, U. Weissker, T. Muehl, O.G. Schmidt, B. Buechner, R. Klingeler, *An individual iron nanowire-filled carbon nanotube probed by micro-Hall magnetometry*, Applied Physics Letters 97 (2010) Nr. 21, S. 212503/1-3.

229) K. Lipert, M. Ritschel, A. Leonhardt, Y. Krupskaya, B. Buechner, R. Klingeler, *Magnetic properties of carbon nanotubes with and without catalyst*, Journal of Physics: Conference Series 200 (2010), S. 72061/1-4.

230) F Lipps, F. Pezzoli, M. Stoffel, A. Rastelli, V. Kataev, O.G. Schmidt, B. Buechner, *Spin resonance of electrons confined by SiGe nanostructures*, Journal of Physics: Conference Series 200 (2010) Nr. 6, S. 62010/1-4.

231) F. Lipps, F. Pezzoli, M. Stoffel, C. Deneke, J. Thomas, A. Rastelli, V. Kataev, O.G. Schmidt, B. Buechner, *Electron spin resonance study of Si/SiGe quantum dots*, Physical Review B 81 (2010) Nr. 12, S. 125312/1-9.

232) P. Lukaszczuk, E. Borowiak-Palen, M.H. Ruemmeli, R.J. Kalenczuk, *On the efficiency of bile salt for stable suspension and isolation of single-walled carbon nanotubes - spectroscopic and microscopic investigations*, Applied Physics /A 100 (2010) Nr. 2, S. 505-510.

233) Q. Luo, G. Martins, D.-X. Yao, M. Daghofer, R. Yu, A. Moreo, E. Dagotto, *Neutron and ARPES constraints on the couplings of the multiorbital Hubbard model for the iron pnictides*, Physical Review B 82 (2010) Nr. 10, S. 104508/1-16.

234) Q. Luo, B. Schwarz, N. Mattern, J. Eckert, *Giant irreversible positive to large reversible negative magnetic entropy change evolution in Tb-based bulk metallic glass*, Physical Review B 82 (2010) Nr. 2, S. 24204/1-6.

235) M.U. Lutz, U. Weissker, F. Wolny, C. Mueller, M. Loeffler, T. Muehl, A. Leonhardt, B. Buechner, R. Klingeler, *Magnetic properties of a-Fe and Fe3C nanowires*, Journal of Physics: Conference Series 200 (2010), S. 72062/1-4.

236) T. Lutz, T. Suzuki, G. Costantini, L. Wang, S. Kiravittaya, A. Rastelli, O.G. Schmidt, K. Kern, *Reversing the shape transition of InAs/GaAs (001) quantum dots by etching-induced lateral In segregation*, Physical Review B 81 (2010) Nr. 20, S. 205414/1-4.

237) J. Lyubimova, J. Freudenberger, A. Gaganov, H. Klauss, L. Schultz, *Strain enhanced high strength Cu-Ag-Zr conductors*, Materials Science Forum 633-634 (2010), S. 707-715.

238) J. Lyubimova, J. Freudenberger, C. Mickel, T. Thersleff, A. Kauffmann, L. Schultz, *Microstructural inhomogeneities in Cu–Ag–Zr alloys due to heavy plastic deformation*, Materials Science and Engineering A 527 (2010) Nr. 3, S. 606-613.

239) J. Lyubina, K.-H. Mueller, M. Wolf, U. Hannemann, *A two-particle exchange interaction model*, Journal of Magnetism and Magnetic Materials 322 (2010) Nr. 19, S. 2948-2955.

240) J. Lyubina, R. Schaefer, N. Martin, L. Schultz, O. Gutfleisch, *Novel design of La(Fe,Si)13 alloys towards high magnetic refrigeration performance*, Advanced Materials 22 (2010) S. 3735–3739.

241) O. Makarovsky, S. Kumar, A. Rastelli, A. Patane, L. Eaves, A.G. Balanov, O.G. Schmidt, R. Campion, C.T. Foxon, *Direct laser writing of nanoscale light-emitting diodes*, Advanced Materials 22 (2010) Nr. 29, S. 3176-3180.

242) A. Malachias, M. Stoffel, M. Schmidbauer, T.U. Schulli, G. Medeiros-Ribeiro, O.G. Schmidt, R. Magalhaes-Paniago, T.H. Metzger, *Atomic ordering dependence on growth method in Ge:Si(001) islands: Influence of surface kinetic and thermodynamic interdiffusion mechanisms*, Physical Review B 82 (2010) Nr. 3, S. 35307/1-9.

243) T. Marr, J. Freudenberger, A. Kauffmann, J. Scharnweber, C.-G. Oertel, W. Skrotzki, U. Siegel, U. Kuehn, J. Eckert, U. Martin, L. Schultz, *Damascene light-weight metals*, Advanced Engineering Materials 12 (2010) Nr. 12, S. 1191-1197.

244) T. Marr, J. Freudenberger, L. Schultz, J. Scharnweber, C.-G. Oertel, W. Skrotzki, U. Siegel, U. Kuehn, J. Eckert, *Damaszen Leichtmetall*, Metall 64 (2010) Nr. 4, S. 168-170.

245) N. Mattern, T. Gemming, J. Thomas, G. Goerigk, H. Franz, J. Eckert, *Phase separation in Ni–Nb–Y metallic glasses*, Journal of Alloys and Compounds 495 (2010) Nr. 2, S. 299-304.

246) N. Mattern, U. Vainio, B. Schwarz, J.M. Park, D.H. Kim, J. Eckert, *Phase separation in Ni70Nb30-xYx glasses*, Intermetallics 18 (2010), S. 1842-1845.

247) Y. Mei, S. Kiravittaya, S. Harazim, O.G. Schmidt, *Principles and applications of micro and nanoscale wrinkles*, Materials Science and Engineering R 70 (2010) Nr. 3-6, S. 209-224.

248) T. Meissner, D. Kuehnel, W. Busch, S. Oswald, V. Richter, A. Michaelis, K. Schirmer, A. Potthoff, *Physical-chemical characterization of tungsten carbide nanoparticles as a basis for toxicological investigations*, Nanotoxicology 4 (2010) Nr. 2, S. 196-206.

249) A. Melcher, A. Unser, M. Reichardt, B. Nestler, M. Poetschke, M. Selzer, *Conversion of EBSD data by a quaternion based algorithm to be used for grain structure simulations*, Technische Mechanik 30 (2010) Nr. 4, S. 401-413.

250) S. Miao, S.G. Hickey, B. Rellinghaus, C. Waurisch, A. Eychmueller, *Synthesis and characterization of cadmium phosphide quantum dots emitting in the visible red to near-infrared*, Journal of the American Chemical Society 132 (2010), S. 5613-5615.

251) O. Mieth, H. Klumbies, V.S. Vidyarthi, G. Gerlach, K. Doerr, L.M. Eng, *Low-voltage electron emission from thin [Pb(Mg1/3Nb2/3)O3]0.72 [PbTiO3]0.28 single crystals induced by ferroelectric polarization switching*, New Journal of Physics 11 (2009) Nr. 2, S. 23004/1-9.

252) M. Mihalik, M. Divis, V. Sechovsky, N. Kozlova, J. Freudenberger, N. Stuesser, A. Hoser, *Magnetism in polymorphic phases: Case of PrIr2Si2*, Physical Review B 81 (2010) Nr. 17, S. 174431/1-11.

253) D. Mikhailova, N. Narayanan, W. Gruner, A. Voss, A. Senyshyn, D.M. Trots, H. Fuess, H. Ehrenberg, *The role of oxygen stoichiometry on phase stability, structure, and magnetic properties of Sr2CoIrO6-delta*, Inorganic Chemistry 49 (2010), S. 10348-10356.

254) D. Mikhailova, N. Narayanan, A. Voss, H. Ehrenberg, D.M. Trots, C. Ritter, J. Eckert, H. Fuess, *Solid solution Sr2Sc1+xRe1–xO6 with a perovskite-like structure: Phase transitions and magnetic properties*, European Journal of Inorganic Chemistry 8 (2010), S. 1196-1206.

255) D. Mikhailova, A. Sarapulova, A. Voss, A. Thomas, S. Oswald, W. Gruner, D.M. Trots, N.N. Bramnik, H. Ehrenberg, *Li3V(MoO4)3: A new material for both Li extraction and insertion*, Chemistry of Materials 22 (2010), S. 3165-3173.

256) V. Miluykov, I. Bezkishko, D. Krivolapov, O. Kataeva, O. Sinyashin, E. Hey-Hawkins, A. Parameswaran, Y. Krupskaya, V. Kataev, R. Klingeler, B. Buechner, *Binuclear 1,2-diphosphacyclopentadienyl manganese(I) complexes: Synthesis, structure and magnetic properties*, Organometallics 29 (2010), S. 1339-1342.

257) N. Miura, N.V. Kozlova, K. Doerr, J. Freudenberger, L. Schultz, O. Drachenko, K. Sawano, Y. Shiraki, *Quantum transport and cyclotron resonance study of Ge/SiGe quantum wells in high magnetic fields*, Journal of Low Temperature Physics 159 (2010) Nr. 1-2, S. 222-225.

258) A. Moebius, *Indications for a line of continuous phase transitions at finite temperatures connected with the apparent metal–insulator transition in 2d disordered systems*, Physica E 42 (2010), S. 1243-1246.

259) A. Moebius, M. Richter, *Comment on ''Density of states and critical behavior of the coulomb glass''*, Physical Review Letters 105 (2010) Nr. 3, S. 39701-1.

260) I. Morozov, A. Boltalin, O. Volkova, A. Vasiliev, O. Kataeva, U. Stockert, M. Abdel-Hafiez, D. Bombor, A. Bachmann, Harnage L., M. Fuchs, H.-J. Grafe, G. Behr, R. Klingeler, S. Borisenko, C. Hess, S. Wurmehl, B. Buechner, *Single crystal growth and characterization of superconducting LiFeAs*, Crystal Growth and Design 10 (2010) Nr. 10, S. 4429-4432.

261) K. Morrison, J. Lyubina, J.D. Moore, A.D. Caplin, K.G. Sandeman, O. Gutfleisch, L.F. Cohen, *Contributions to the entropy change in melt-spun LaFe11.6Si1.4*, Journal of Physics D 43 (2010) Nr. 13, S. 132001/1-5.

262) G. Mutschke, K. Tschulik, T. Weier, M. Uhlemann, A. Bund, J. Froehlich, *On the action of magnetic gradient forces in micro-structured copper deposition*, Electrochimica Acta 55 (2010) Nr. 28, S. 9060-9066.

263) N. Narayanan, D. Mikhailova, A. Senyshyn, D.M. Trots, R. Laskowski, P. Blaha, K. Schwarz, H. Fuess, H. Ehrenberg, *Temperature and composition dependence of crystal structures and magnetic and electronic properties of the double perovskites*, Physical Review B 82 (2010) Nr. 2, S. 24403/1-12.

264) V. Neu, R. Biele, A. Singh, L. Schultz, *Modeling of intergrain exchange coupling for quantitative predictions of dm plots*, IEEE Transactions on Magnetics 46 (2010), S. 2331-2333.

265) V. Neu, K. Haefner, L. Schultz, *Dynamic coercivity and thermal stability of epitaxial exchange spring trilayers*, Journal of Magnetism and Magnetic Materials 322 (2010) Nr. 9-12, S. 1613-1616.

266) R. Niemann, O. Heczko, L. Schultz, S. Faehler, *Metamagnetic transitions and magnetocaloric effect in epitaxial Ni-Co-Mn-In films*, Applied Physics Letters 97 (2010) Nr. 22, S. 222507/1-3.

267) T. Niemeier, R. Huehne, A. Koehler, G. Behr, L. Schultz, B. Holzapfel, *Biaxially textured LuNi2B2C thin films on MgO single crystals*, Journal of Alloys and Compounds 507 (2010) Nr. 2, S. 345-349.

268) S. Nishimoto, M. Arikawa, *Dimerization transition of three-leg Heisenberg tube*, Journal of Physics: Conference Series 200 (2010) Nr. 2, S. 22039/1-4.

269) S. Nishimoto, E. Jeckelmann, D.J. Scalapino, *Circulating-current phase in the three-band model for two-leg CuO ladders*, Physica C 470 (2010) Nr. Suppl. 1, S. 553-554.

270) S. Nishimoto, M. Nakamura, A. O'Brien, P. Fulde, *Metal-insulator transition of fermions on a kagome lattice at 1/3 filling*, Physical Review Letters 104 (2010) Nr. 19, S. 196401/1-4.

271) S. Nishimoto, T. Shirakawa, *Finite-size scaling of correlation functions in the one-dimensional Anderson-Hubbard model*, Physical Review B 81 (2010) Nr. 11, S. 113105/1-4.

272) S. Nishimoto, M. Tsuchiizu, *Correlation function for the one-dimensional extended Hubbard model at quarter filling*, Physical Review B 81 (2010) Nr. 8, S. 85116/1-6.

273) R.M. Oliveira, J.A.N. Goncalves, M. Ueda, S. Oswald, S.C. Baldissera, *Improved corrosion resistance of tool steel H13 by means of cadmium ion implantation and deposition*, Surface and Coatings Technology 204 (2010), S. 2981-2985.

274) C. Ortix, J. van den Brink, *Effect of curvature on the electronic structure and bound-state formation in rolled-up nanotubes*, Physical Review B 81 (2010) Nr. 16, S. 165419/1-5.

275) S. Oswald, *Growth studies of Ti-based films deposited on Si and SiO2 using angle-resolved XPS*, Surface and Interface Analysis 42 (2010), S. 1289-1294.

276) S. Oswald, K. Nikolowski, H. Ehrenberg, *XPS investigations of valence changes during cycling of LiCrMnO4-based cathodes in Li-ion batteries*, Surface and Interface Analysis 42 (2010), S. 916-921.

277) S. Oswald, F. Oswald, *Application of angle-resolved X-ray photon electron spectroscopy for interface and layer growth studies demonstrated on Ti/Ta-based films deposited on SiO2*, Analytical and Bioanalytical Chemistry 396 (2010) Nr. 8, S. 2805-2812.

278) D. Paar, H.-J. Grafe, G. Lang, F. Hammerath, K. Manthey, G. Behr, J. Werner, B. Buechner, *NMR study of the electronic properties of superconducting La00.9F0.1FeAs*, Physica C 470 (2010), S. S468-S469.

279) G. Paasch, S. Scheinert, *Charge carrier density of organics with Gaussian density of states: Analytical approximation for the Gauss–Fermi integral* , Journal of Applied Physics 107 (2010) Nr. 10, S. 104501/1-4.

280) J. Paillier, A. Gebert, *Effect of hydrofluoric acid treatment on the crystallisation behaviour of Zr–Ti–Cu–Al–Ni metallic glass*, Thermochimica Acta 497 (2010) Nr. 1-2, S. 85-95.

281) J. Paillier, C. Mickel, P.F. Gostin, A. Gebert, *Characterization of corrosion phenomena of Zr–Ti–Cu–Al–Ni metallic glass by SEM and TEM*, Materials Characterization 61 (2010) Nr. 10, S. 1000-1008.

282) D. Pal, K. Mandal, O. Gutfleisch, *Large negative magnetoresistance in nickel-rich Ni–Mn–Ga Heusler alloys*, Journal of Applied Physics 107 (2010) Nr. 9, S. 9B103/1-3.

283) N.Y. Panarina, Y.I. Talanov, T.S. Shaposhnikova, N.R. Beysengulov, E. Vavilova, G. Behr, A. Kondrat, C. Hess, N. Leps, S. Wurmehl, R. Klingeler, V. Kataev, B. Buechner, *Pinning effects in ceramic Sm01-xFxFeAs as revealed by microwave absorption*, Physical Review B 81 (2010) Nr. 22, S. 224509/1-9.

284) N.Y. Panarina, Y.I. Talanov, T.S. Shaposhnikova, N.R. Beysengulov, E.L. Vavilova, V.E. Kataev, G. Behr, A. Kondrat, C. Hess, N. Leps, R. Klingeler, B. Buechner, *Microwave absorption study of polycrystalline Sm01-xFxFeAs*, Journal of Physics: Conference Series 200 (2010), S. 12154/1-4.

285) J.M. Park, J. Jayaraj, D.H. Kim, N. Mattern, G. Wang, J. Eckert, *Tailoring of in situ Ti-based bulk glassy matrix composites with high mechanical performance*, Intermetallics 18 (2010) Nr. 10, S. 1908-1911.

286) J.M. Park, D.H. Kim, K.B. Kim, J. Eckert, *Improving the plasticity of a high strength Fe–Si–Ti ultrafine composite by introduction of an immiscible element*, Applied Physics Letters 97 (2010) Nr. 25, S. 251915/1-3.

287) J.M. Park, K.B. Kim, D.H. Kim, N. Mattern, R. Li, G. Liu, J. Eckert, *Multi-phase Al-based ultrafine composite with multi-scale microstructure*, Intermetallics 18 (2010) Nr. 10, S. 1829-1833.

288) J.M. Park, J.H. Na, D.H. Kim, K.B. Kim, N. Mattern, U. Kuehn, J. Eckert, *Medium range ordering and its effect on plasticity of Fe–Mn–B–Y–Nb bulk metallic glass*, Philosophical Magazine 90 (2010) Nr. 19, S. 2619-2633.

289) J.M. Park, S. Pauly, N. Mattern, D.H. Kim, K.B. Kim, J. Eckert, *Microstructural modulations enhance the mechanical properties in Al-Cu-(Si, Ga) ultrafine composites*, Advanced Engineering Materials 12 (2010) Nr. 11, S. 1137-1141.

290) J.M. Park, G. Wang, R. Li, N. Mattern, J. Eckert, D.H. Kim, *Enhancement of plastic deformability in Fe–Ni–Nb–B bulk glassy alloys by controlling the Ni-to-Fe concentration ratio*, Applied Physics Letters 96 (2010) Nr. 3, S. 31905/1-3.

291) A.K. Patra, M. Eisterer, R. Biele, S. Faehler, L. Schultz, V. Neu, *The temperature dependent anisotropy constants of epitaxially grown PrCo5+x*, Journal of Applied Physics 108 (2010) Nr. 7, S. 73912/1-5.

292) S. Pauly, J. Bednarcik, U. Kuehn, J. Eckert, *Plastically deformable Cu-Zr intermetallics*, Scripta Materialia 63 (2010), S. 336-338.

293) S. Pauly, S. Gorantla, G. Wang, U. Kuehn, J. Eckert, *Transformation-mediated ductility in CuZr-based bulk metallic glasses*, nature materials 9 (2010), S. 473-477.

294) S. Pauly, G. Liu, S. Gorantla, G. Wang, U. Kuehn, D.H. Kim, J. Eckert, *Criteria for tensile plasticity in Cu-Zr-Al bulk metallic glasses*, Acta Materialia 58 (2010) Nr. 14, S. 4883-4890.

295) R. Pellicelli, M. Solzi, V. Neu, K. Haefner, C. Pernechele, M. Ghidini, *Characterization and modeling of the demagnetization processes in exchange-coupled SmCo5 /Fe/SmCo5 trilayers*, Physical Review B 81 (2010) Nr. 18, S. 184430/1-11.

296) J. Peng, C. Hermannstaedter, M. Witzany, M. Heldmaier, L. Wang, S. Kiravittaya, A. Rastelli, O.G. Schmidt, P. Michler, G. Bester, *Heterogeneous confinement in laterally coupled InGaAs/GaAs quantum dot molecules under lateral electric fields*, Physical Review B 81 (2010) Nr. 20, S. 205315/1-3.

297) G. Pernot, M. Stoffel, I. Savic, F. Pezzoli, P. Chen, G. Savelli, G. Jacquot, J. Schumann, U. Denker, I. Moench, C. Deneke, O.G. Schmidt, J.M. Rampnoux, S. Wang, M. Plissonnier, A. Rastelli, S. Dilhaire, N. Mingo, *Precise control of thermal conductivity at the nanoscale through individual phonon-scattering barriers*, nature materials 9 (2010), S. 491-495.

298) D.V. Peryshkov, A.A. Popov, S.H. Strauss, *Latent porosity in potassium dodecafluoro-closo-dodecaborate(2-). Structures and rapid room temperature interconversions of crystalline K2B12F12,K2(H2O)2B12F12, and K2(H2O)4B12F12 in the presence of water vapor*, Journal of the American Chemical Society 132 (2010) Nr. 39, S. 13902-13913.

299) M. Pfeiffer, K. Lindfors, C. Wolpert, P. Atkinson, M. Benyoucef, A. Rastelli, O.G. Schmidt, H. Giessen, M. Lippitz, *Enhancing the optical excitation efficiency of a single self-assembled quantum dot with a plasmonic nanoantenna*, Nano Letters 10 (2010) Nr. 11, S. 4555-4558.

300) D.H. Pi, J.M. Park, G.A. Song, J.H. Han, K.R. Lim, S. Yi, S.H. Yi, D.H. Kim, N.S. Lee, Y. Seo, K.B. Kim, *Effect of Si on microstructure and mechanical properties of Fe-based ultrafine eutectic composites*, Intermetallics 18 (2010) Nr. 10, S. 1856-1859.

301) D.H. Pi, G.A. Song, J.H. Han, J.M. Park, G.R. Lim, D.H. Kim, S. Yi, S.H. Yie, N.S. Lee, Y. Seo, K.B. Kim, *Effect of Nb on microstructure and mechanical properties of ultrafine eutectic Fe-Ni-B-Si composites*, Journal of Alloys and Compounds 504 S (2010), S. S487-S490.

302) P. Pieta, G.Z. Zukowska, S.K. Das, F. D`Souza, A. Petr, L. Dunsch, W. Kutner, *Mechanism of reductive C60 electropolymerization in the presence of dioxygen and application of the resulting fullerene polymer for preparation of a conducting composite with single-wall carbon nanotubes*, Journal of Physical Chemistry C 114 (2010), S. 8150-8160.

303) D. Placha, G.S. Martynkova, M.H. Ruemmeli, *Variations in the sorptive properties of organovermiculites modified with hexadecyltrimethylammonium and hexadecylpyridinium cations*, Journal of Scientific Conference Proceedings 2 (2010), S. 36-41.

304) J.D. Plumhof, V. Krapek, L. Wang, A. Schliwa, D. Bimberg, A. Rastelli, O.G. Schmidt, *Experimental investigation and modeling of the fine structure splitting of neutral excitons in strain-free GaAs/ AlxGa1-xAs quantum dots*, Physical Review B 81 (2010), S. 121309/1-4.

305) M. Poetschke, S. Weiss, U. Gaitzsch, D. Cong, C. Huerrich, S. Roth, L. Schultz, *Magnetically resettable 0.16% free strain in polycrystalline Ni–Mn–Ga plates*, Scripta Materialia 63 (2010) Nr. 4, S. 383-386.

306) A.A. Popov, C. Chen, S. Yang, F. Lipps, L. Dunsch, *Spin-flow vibrational spectroscopy of molecules with flexible spin density: Electrochemistry, ESR, cluster and spin dynamics, and bonding in TiSc2N@C80*, ACS nano 4 (2010) Nr. 8, S. 4857-4871.

307) A.A. Popov, I.E. Kareev, N.B. Shustova, S.H. Strauss, O.V. Boltalina, L. Dunsch, *Unraveling the electron spin resonance pattern of nonsymmetric radicals with 30 fluorine atoms: Electron spin resonance and vis-near-infrared spectroelectrochemistry of the anion radicals and dianions of C60(CF3)2n (2n) 2-10) derivatives and density functional theory-assisted assignment*, Journal of the American Chemical Society 132 (2010), S. 11709-11721.

308) A.A. Popov, N.B. Shustova, A.L. Svitova, M.A. Mackey, C.E. Coumbe, J.P. Phillips, S. Stevenson, S.H. Strauss, O. Boltalina, L. Dunsch, *Redox-tuning endohedral fullerene spin states: From the dication to the trianion radical of Sc3N@C-80(CF3)(2) in five reversible single-electron steps*, Chemistry- A European Journal 16 (2010) Nr. 16, S. 4721-4724.

309) A.A. Popov, L. Zhang, L. Dunsch, *A pseudoatom in a cage: Trimetallofullerene Y3@C80 mimics Y3N@C80 with nitrogen substituted by a pseudoatom*, ACS nano 4 (2010) Nr. 2, S. 795-802.

310) E.A. Popova, A.N. Vasiliev, V.L. Temerov, L.N. Bezmaternykh, N. Tristan, R. Klingeler, B. Buechner, *Magnetic and specific heat properties of YFe3(BO3)4 and ErFe3(BO3)4*, Journal of Physics: Condensed Matter 22 (2010) Nr. 11, S. 116006/1-8.

311) J. Potfajova, B. Schmidt, M. Helm, T. Gemming, M. Benyoucef, A. Rastelli, O.G. Schmidt, *Microcavity enhanced silicon light emitting pn-diode*, Applied Physics Letters 96 (2010) Nr. 15, S. 151113/1-3.

312) A.K. Pramanik, L. Harnagea, S. Singh, S. Aswartham, G. Behr, S. Wurmehl, C. Hess, R. Klingeler, B. Buechner, *Critical current and vortex dynamics in single crystals of Ca(Fe1-xCox)2As2*, Physical Review B 82 (2010) Nr. 1, S. 14503/1-7.

313) R.T. Qu, M. Stoica, J. Eckert, Z.F. Zhang, *Tensile fracture morphologies of bulk metallic glass*, Journal of Applied Physics 108 (2010) Nr. 6, S. 63509/1-9.

314) P. Rapta, K.R. Idzik, V. Lukes, R. Beckert, L. Dunsch, *Alternative charge stabilisation and a changing reactivity of 1,3,5-triazine based starburst compounds as studied by in situ ESR/UV–vis–NIR spectroelectrochemistry*, Electrochemistry Communications 12 (2010) Nr. 4, S. 513-516.

315) H. Reuther, C. Mueller, A. Leonhardt, M.C. Kutz, *Investigation of the formation of Fe-filled carbon nanotubes*, Journal of Physics: Conference Series 217 (2010) Nr. 1, S. 12098/1-4.

316) R.O. Rezaev, S. Kiravittaya, V.M. Fomin, A. Rastelli, O.G. Schmidt, *Engineering self-assembled SiGe islands for robust electron confinement in Si*, Physical Review B 82 (2010) Nr. 15, S. 153306/1-4.

317) T. Roessler, J. Gluch, M. Albert, J.W. Bartha, *Electrical characterisation of HfYO MIM-structures deposited by ALD*, Thin Solid Films 518 (2010), S. 4680-4683.

318) C. Rongeat, V. D'Anna, H. Hagemann, A. Borgschulte, A. Zuettel, L. Schultz, O. Gutfleisch, *Effect of additives on the synthesis and reversibility of Ca(BH4)2*, Journal of Alloys and Compounds 493 (2010), S. 281-287.

319) S. Rosenzweig, *Lehrer in die Forschnung*, Physik in unserer Zeit 41 (2010) Nr. 2, S. 99.

320) S. Rosenzweig, J. Haenisch, R. Huehne, B. Holzapfel, L. Schultz, *Tc optimisation of GdBa2Cu3O7 thin films grown by pulsed laser deposition*, Journal of Physics / Conference Series 234 (2010) Nr. 1, S. 12035/1-5.

321) S. Rosenzweig, J. Haenisch, K. Iida, A. Kauffmann, C. Mickel, T. Thersleff, J. Freudenberger, R. Huehne, B. Holzapfel, L. Schultz, *Irreversibility field up to 42 T of GdBa2Cu3O7-delta thin films grown by PLD and its dependence on deposition parameters*, Superconductor Science and Technology 23 (2010) Nr. 10, S. 105017/1-6.

322) F. Roth, M. Gatti, P. Cudazzo, M. Grobosch, B. Mahns, B. Buechner, A. Rubio, M. Knupfer, *Electronic properties of molecular solids: the peculiar case of solid picene*, New Journal of Physics 12 (2010) Nr. 10, S. 103036/1-8.

323) F. Roth, C. Hess, B. Buechner, U. Ammerahl, A. Revcolevschi, M. Knupfer, *Plasmons and interband transitions of Ca11Sr3Cu24O41 investigated by electron energy-loss spectroscopy*, Physical Review B 82 (2010) Nr. 24, S. 245110/1-7.

324) F. Roth, A. Koenig, R. Kraus, M. Grobosch, T. Kroll, M. Knupfer, *Probing the molecular orbitals of FePc near the chemical potential using electron energy-loss spectroscopy*, European Physical Journal B 74 (2010) Nr. 3, S. 339-344.

325) M.H. Ruemmeli, A. Bachmatiuk, A. Scott, F. Boerrnert, J.H. Warner, V. Hoffman, J.-H. Lin, G. Cuniberti, B. Buechner, *Direct low-temperature nanographene CVD synthesis over a dielectric insulator*, ACS nano 4 (2010) Nr. 7, S. 4206-4210.

326) M.H. Ruemmeli, F. Schaeffel, A. Bachmatiuk, D. Adebimpe, G. Trotter, F. Boerrnert, A. Scott, E. Coric, M. Sparing, B. Rellinghaus, P.G. McCormick, G. Cuniberti, M. Knupfer, L. Schultz, B. Buechner, *Investigating the outskirts of Fe and Co catalyst particles in alumina-supported catalytic CVD carbon nanotube growth*, ACS nano 4 (2010) Nr. 2, S. 1146-1152.

327) D. Rutzinger, C. Bartsch, M. Doerr, H. Rosner, V. Neu, T. Doert, M. Ruck, *Lattice distortions in layered type arsenides LnTAs2 (Ln=La–Nd, Sm, Gd, Tb; T=Ag, Au): Crystal structures, electronic and magnetic properties*, Journal of Solid State Chemistry 183 (2010), S. 510-520.

328) H. Ryu, D. Kaelblein, R.T. Weitz, F. Ante, U. Zschieschang, K. Kern, O.G. Schmidt, H. Klauk, *Logic circuits based on individual semiconducting and metallic carbon-nanotube devices*, Nanotechnology 21 (2010) Nr. 47, S. 475207/1-5.

329) S. Sahoo, A. Hucht, M.E. Gruner, G. Rollmann, P. Entel, A. Postnikov, J. Ferrer, L. Fernandez-Seivane, M. Richter, D. Fritsch, S. Sil, *Magnetic properties of small Pt-capped Fe, Co, and Ni clusters: A density functional theory study*, Physical Review / B 82 (2010) Nr. 5, S. 54418/1-14.

330) M. Samsel-Czekala, *Electronic structure and Fermi surface of UNZ (Z=Se and Te) by ab initio calculations*, Physical Review B 81 (2010) Nr. 19, S. 195115/1-7.

331) M. Samsel-Czekala, S. Elgazzar, P.M. Oppeneer, E. Talik, W. Walerczyk, R. Troc, *The electronic structure of UCoGe by ab initio calculations and XPS experiment*, Journal of Physics Condensed Matter 22 (2010) Nr. 1, S. 15503/1-11.

332) S. Sanchez, A.A. Solovev, Y. Mei, O.G. Schmidt, *Dynamics of biocatalytic microengines mediated by variable friction control*, Journal of the American Chemical Society 132 (2010) Nr. 38, S. 13144-13145.

333) J. Sanchez-Barriga, J. Minar, J. Braun, A. Varykhalov, V. Boni, I. Di Marco, O. Rader, V. Bellini, F. Manghi, H. Ebert, M.I. Katsnelson, A.I. Lichtenstein, O. Eriksson, W. Eberhardt, H.A. Duerr, J. Fink, *Quantitative determination of spin-dependent quasiparticle lifetimes and electronic correlations in hcp cobalt*, Physical Review B 82 (2010) Nr. 10, S. 104414/1-12.

334) F. Scaglione, A. Gebert, L. Battezzati, *Dealloying of an Au-based amorphous alloy*, Intermetallics 18 (2010) Nr. 12, S. 2338-2342.

335) R. Schaarschuch, M. Reibold, S. Haindl, V. Neu, J. Thomas, T. Gemming, C.-G. Oertel, B. Holzapfel, L. Schultz, W. Skrotzki, *Textured growth and microstructure of pulsed laser deposited Nb/Cr/SmCo5 hybrid structures*, Physica Status Solidi A 207 (2010) Nr. 8, S. 1785-1791.

336) R. Schaefer, C. Hamann, J. McCord, L. Schultz, V. Kambersky, *The magneto-optical gradient effect in an exchange-biased thin film: experimental evidence for classical diffraction theory*, New Journal of Physics 12 (2010) Nr. 5, S. 53006/1-10.

337) F. Schaeffel, J.H. Warner, A. Bachmatiuk, U. Queitsch, B. Rellinghaus, B. Buechner, L. Schultz, M.H. Ruemmeli, *Tracking down the catalytic hydrogenation of multilayer graphene*, Physica Status Solidi C 7 (2010) Nr. 11-12, S. 2731-2734.

338) D. Scharnweber, F. Schlottig, S. Oswald, K. Becker, H. Worch, *How is wettability of titanium surfaces influenced by their preparation and storage conditions?*, Journal of Materials Science/ Materials in Medicine 21 (2010) Nr. 2, S. 525-532.

339) N. Scheerbaum, Y.W. Lai, T. Leisegang, M. Thomas, J. Liu, K. Khlopkov, J. McCord, S. Faehler, R. Traeger, D.C. Meyer, L. Schultz, O. Gutfleisch, *Constraint-dependent twin variant distribution in Ni2MnGa single crystal, polycrystals and thin film: An EBSD study*, Acta Materialia 58 (2010) Nr. 14, S. 4629-4638.

340) T. Schied, A. Lotnyk, C. Zamponi, L. Kienle, J. Buschbeck, M. Weisheit, B. Holzapfel, L. Schultz, S. Faehler, *Fe-Pd thin films as a model system for self-organized exchange coupled nanomagnets*, Journal of Applied Physics 108 (2010) Nr. 3, S. 33902/1-6.

341) A. Schlieter, U. Kuehn, J. Eckert, H.-J. Seifert, *Microstructure, thermal, and mechanical characterization of rapidly solidified high strength Fe84.3Cr4.3Mo4.6V2.2C4.6*, Journal of Materials Research 25 (2010) Nr. 6, S. 1164-1171.

342) H. Schloerb, V. Haehnel, M. Singh Khatri, A. Srivastav, A. Kumar, L. Schultz, S. Faehler, *Magnetic nanowires by electrodeposition within templates*, Physica Status Solidi / B 247 (2010) Nr. 10, S. 2364-2379.

343) S. Schmitz, H.-G. Lindenkreuz, N. Mattern, W. Loeser, B. Buechner, *Liquid phase separation in GdeTi and GdeZr melts*, Intermetallics 18 (2010) Nr. 10, S. 1941-1945.

344) M. Schubert, W. Haessler, C. Rodig, M. Herrmann, A. Kario, J. Scheiter, B. Holzapfel, L. Schultz, *Untersuchung an MgB2-Hochtemperatursupraleiter -Draehten und -Baendern mit neuem Huellwerkstoff und deren Gefuege- Eigenschafts Korrelation*, Praktische Metallographie, Sonderband 42 (2010), S. 147-152.

345) C. Schulze, M. Faustini, J. Lee, H. Schletter, M.U. Lutz, P. Krone, M. Gass, K. Sader, A.L. Bleloch, M. Hietschold, M. Fuger, D. Suess, J. Fidler, U. Wolff, V. Neu, D. Grosso, D. Makarov, M. Albrecht, *Magnetic films on nanoperforated templates: a route towards percolated perpendicular media*, Nanotechnology 21 (2010) Nr. 49, S. 495701/1-9.

346) S. Schulze, G. Huang, M. Krause, D. Aubyn, V.A. Bolanos Quinones, C.K. Schmidt, Y. Mei, O.G. Schmidt, *Morphological differentiation of neurons on microtopographic substrates fabricated by rolled-up nanotechnology*, Advanced Engineering Materials 12 (2010) Nr. 9, S. B558-B564.

347) B. Schwarz, D. Kraft, R. Theissmann, H. Ehrenberg, *Magnetic properties of the (CoxMn1-x)4Nb2O9 solid solution series*, Journal of Magnetism and Magnetic Materials 322 (2010) Nr. 5, S. L1-L3.

348) B. Schwarz, N. Mattern, S. Oswald, J. Eckert, *Surface oxidation and magnetic properties of (Cu60Co40)68Zr32 glassy ribbons*, Journal of Alloys and Compounds 506 (2010) Nr. 2, S. 520-525.

349) B. Schwarz, B. Podmilsak, N. Mattern, J. Eckert, *Magnetocaloric effect in Gd-based Gd60FexCo30-xAl10 metallic glasses*, Journal of Magnetism and Magnetic Materials 322 (2010) Nr. 16, S. 2298-2303.

350) S. Scudino, F. Ali, K.B. Surreddi, K.G. Prashanth, M. Sakaliyska, J. Eckert, *Al-based metal matrix composites reinforced with nanocrystalline Al-Ti-Ni particles*, Journal of Physics: Conference Series 240 (2010) Nr. 1, S. 12154/1-4.

351) S. Scudino, M. Sakaliyska, K.B. Surreddi, F. Alia, J. Eckert, *Structure and mechanical properties of Al–Mg alloys produced by copper mold casting*, Journal of Alloys and Compounds 504 (2010) Nr. Supplement 1, S. S483-S486.

352) S. Scudino, K.B. Surreddi, J. Eckert, *Mechanical properties of cold-rolled Zr60Ti5Ag5Cu12.5Ni10Al7.5 metallic glass*, Physica Status Solidi A 207 (2010), S. 1118-1121.

353) S. Scudino, K.B. Surreddi, M.S. Khoshkhoo, M. Sakaliyska, G. Wang, J. Eckert, *Improved room temperature plasticity of Zr41.2Ti13.8Cu12.5Ni10Be22.5 bulk metallic glass by channel-die compression*, Advanced Engineering Materials 12 (2010) Nr. 11, S. 1123-1126.

354) S. Scudino, K.B. Surreddi, G. Wang, J. Eckert, *Enhanced plastic deformation of Zr41.2Ti13.8Cu12.5Ni10Be22.5 bulk metallic glass by the optimization of frictional boundary restraints*, Scripta Materialia 62 (2010) Nr. 10, S. 750-753.

355) A. Sebetci, M. Richter, *Gd@C82: Origin of the antiferromagnetic coupling between endohedral Gd and the free spin on the carbon cage*, Journal of Physical Chemistry C 114 (2010), S. 15-19.

356) M. Seifert, L. Schultz, V. Neu, *Investigation of the c-axis and basal plane anisotropy in epitaxial NdCo5 thin films*, Journal of Applied Physics 107 (2010) Nr. 9, S. 9A711/1-3.

357) A. Senyshyn, B. Schwarz, T. Lorenz, V.T. Adamiv, Y.V. Burak, J. Banys, R. Grigalaitis, L. Vasylechko, H. Ehrenberg, H. Fuess, *Low-temperature crystal structure, specific heat, and dielectric properties of lithium tetraborate Li2B4O7*, Journal of Applied Physics 108 (2010) Nr. 9, S. 93524/1-9.

358) T. Shapoval, V. Metlushko, M. Wolf, B. Holzapfel, V. Neu, L.Schultz, *Direct observation of superconducting vortex clusters pinned by a periodic array of magnetic dots in ferromagnetic/superconducting hybrid structures*, Physical Review B 81 (2010) Nr. 9, S. 92505/1-4.

359) T. Shapoval, V. Metlushko, M. Wolf, V. Neu, B. Holzapfel, L. Schultz, *Enhanced pinning of superconducting vortices at circular magnetic dots in the magnetic-vortex state*, Physica C 470 (2010) Nr. 19, S. 867-870.

360) S. Shin, R. Schaefer, B.C. De Cooman, *Grain boundary penetration by lancet domains in Fe-3%Si grain-oriented steel*, IEEE Transactions on Magnetics 46 (2010) Nr. 9, S. 3574-3581.

361) O. Shuleshova, D. Holland-Moritz, W. Loeser, A. Voss, H. Hartmann, U. Hecht, V.T. Witusiewicz, D.M. Herlach, B. Buechner, *In situ observations of solidification processes in gamma—TiAl alloys by synchrotron radiation*, Acta Materialia 58 (2010) Nr. 7, S. 2408-2418.

362) N.B. Shustova, I.E. Kareev, I.V. Kuvychko, J.B. Whitaker, S.F. Lebedkin, A.A. Popov, L. Dunsch, Y.-S. Chen, K. Seppelt, S.H. Strauss, O.V. Boltalina, *High-temperature and photochemical syntheses of C60 and C70 fullerene derivatives with linear perfluoroalkyl chains*, Journal of Fluorine Chemistry 131 (2010), S. 1198-1212.

363) N.B. Shustova, Z. Mazej, Y.-S. Chen, A.A. Popov, S.H. Strauss, O.V. Boltalina, *Saturnene revealed: X-ray crystal structure of D5d-C60F20 formed in reactions of C60 with AxMFy fluorinating agents (A=Alkali Metal; M=3d Metal)*, Angewandte Chemie - International Edition 49 (2010) Nr. 4, S. 812-815.

364) A. Singh, J. Haenisch, V. Matias, F. Ronning, N. Mara, D. Pohl, B. Rellinghaus, D. Reagor, *Transforming insulating rutile single crystal into a fully ordered nanometer-thick transparent semiconductor*, Nanotechnology 21 (2010) Nr. 41, S. 415303/1-5.

365) Y. Skourski, M.D. Kuzmin, K.P. Skokov, K.-H. Mueller, J. Wosnitza, *Probing 3d-4f exchange interactions by high-field magnetization measurements*, Acta Physica Polonica 115 (2009) Nr. 1, S. 178-180.

366) V. Skumryev, M.D. Kuzmin, M. Gospodinov, J. Fontcuberta, *Anisotropic paramagnetic response of hexagonal RMn03*, Physical Review B 79 (2009) Nr. 21, S. 212414/1-4.
367) E. Smirnova, A. Sotnikov, N. Zaitseva, H. Schmidt, M. Weihnacht, *Acoustic properties of multiferroic PbFe1/2Ta1/203*, Physics Letters A 374 (2010) Nr. 41, S. 4256-4259.
368) E.J. Smith, Z. Liu, Y. Mei, O.G. Schmidt, *Combined surface plasmon and classical waveguiding through metamaterial fiber design*, Nano Letters 10 (2010) Nr. 1, S. 1-5.
369) E.J. Smith, Z. Liu, Y.F. Mei, O.G. Schmidt, *Erratum: „System investigation of a rolled-up metamaterial optical hyperlens structure" [Appl. Phys. Lett. 95, 083104 (2009)]*, Applied Physics Letters 96 (2010) Nr. 1, S. 19902/1-2.
370) A.A. Solovev, Y. Mei, O.G. Schmidt, *Catalytic microstrider at the air-liquid interface*, Advanced Materials 22 (2010) Nr. 39, S. 4340-4344.
371) A.A. Solovev, S. Sanchez, M. Pumera, Y.F. Mei, O.G. Schmidt, *Magnetic control of tubular catalytic microbots for the transport, assembly, and delivery of micro-objects*, Advanced Functional Materials 20 (2010), S. 2430-2435.
372) G.A. Song, D.H. Kim, D.H. Kim, M.H. Lee, J.K. Lee, J.M. Park, J. Eckert, Y. Seo, K.B. Kim, *Deformation mechanisms of a bimodal eutectic Mg72Cu5Zn23 ultrafine composite*, Materials Letters 64 (2010), S. 534-536.
373) A.V. Sotnikov, H. Schmidt, M. Weihnacht, E.P. Smirnova, T.Y. Chemekova, Y.N. Makarov, *Elastic and piezoelectric properties of AlN and LiAlO2 single crystals*, IEEE Transactions on Ultrasonics, Ferroelectrics, and Frequency Control 57 (2010) Nr. 4, S. 808-811.
374) A.V. Sotnikov, E.P. Smirnova, H. Schmidt, M. Weihnacht, V.V. Lemanov, *Polar state in Li-doped SrTiO3*, Ferroelectrics 405 (2010) Nr. 1, S. 13-19.
375) M. Spindler, S.B. Menzel, J. Eckert, C. Eggs, *Influence of Al on resistance and power durability of Cu- based SAW metallizations*, IOP Conference Series: Materials Science and Engineering 8 (2010) Nr. 1, S. 12013/1-5.
376) V.C. Srivastava, K.B. Surreddi, S. Scudino, M. Schowalter, V. Uhlenwinkel, A. Schulz, J. Eckert, A. Rosenauer, H.-W. Zoch, *Microstructure and mechanical properties of partially amorphous Al85Y8Ni5Co2 plate produced by spray forming*, Materials Science and Engineering A 527 (2010) Nr. 10-11, S. 2747-2758.
377) M. Stoica, J. Das, J. Bednarcik, G. Wang, G. Vaughan, W.H. Wang, J. Eckert, *Mechanical response of metallic glasses: Insights from in-situ high energy X-ray diffraction*, JOM: the Journal of the Minerals, Metals and Materials Society 62 (2010) Nr. 2, S. 76-82.
378) M. Stoica, R. Li, A.R. Yavari, G. Vaughan, J. Eckert, N. Van Steenberge, D.R. Romera, *Thermal stability and magnetic properties of FeCoBSiNb bulk metallic glasses*, Journal of Alloys and Compounds 504S (2010), S. S123-128.
379) M. Stoica, S. Roth, J. Eckert, T. Karan, S. Ram, G. Vaughan, A.R. Yavari, *FeCoBSiNb bulk metallic glasses with Cu additions*, Physica Status Solidi C 7 (2010) Nr. 5, S. 1331-1335.
380) M. Stoica, N. Van Steenberge, J. Bednarcik, N. Mattern, H. Franz, J. Eckert, *Changes in short-range order of Zr55Cu30Al10Ni5 and Zr55Cu20Al10Ni10Ti5 BMGs upon annealing*, Journal of Alloys and Compounds 506 (2010) Nr. 1, S. 85-87.
381) S. Strehle, S. Menzel, J.W. Bartha, K. Wetzig, *Electroplating of Cu(Ag) thin films for interconnect applications*, Microelectronic Engineering 87 (2010) Nr. 2, S. 180-186.
382) V. Subramanya Sarmaa, J. Wang, W.W. Jian, A. Kauffmann, H. Conrad, J. Freudenberger, Y.T. Zhu, *Role of stacking fault energy in strengthening due to cryo-deformation of FCC metals*, Materials Science and Engineering A 527 (2010) Nr. 29/30, S. 7624-7630.
383) R. Sueptitz, J. Das, S. Baunack, A. Gebert, L. Schultz, J. Eckert, *Corrosion and pitting behaviour of ultrafine eutectic Ti–Fe–Sn alloys*, Journal of Alloys and Compounds 503 (2010) Nr. 1, S. 19-24.
384) R. Sueptitz, K. Tschulik, M. Uhlemann, A. Gebert, L. Schultz, *Impact of magnetic field gradients on the free corrosion of iron*, Electrochimica Acta 55 (2010) Nr. 18, S. 5200-5203.
385) R. Sueptitz, M. Uhlemann, A. Gebert, L. Schultz, *Corrosion, passivation and breakdown of passivity of neodymium*, Corrosion Science 52 (2010) Nr. 3, S. 886-891.
386) K.B. Surreddi, S. Scudino, M. Sakaliyska, K.G. Prashanth, D.J. Sordelet, J. Eckert, *Crystallization behavior and consolidation of gas-atomized Al84Gd6Ni7Co3 glassy powder*, Journal of Alloys and Compounds 491 (2010), S. 137-142.
387) K.B. Surreddi, V.C. Srivastava, S. Scudino, M. Sakaliyska, V. Uhlenwinkel, J.S. Kim, J. Eckert, *Production of high-strength Al85Y8Ni5Co2 bulk alloy by spark plasma sintering*, Journal of Physics: Conference Series 240 (2010), S. 12155/1-4.
388) R. Tamm, K.S. Rao, S. Faehler, V. Neu, A. Singh, C.-G. Oertel, L. Schultz, B. Holzapfel, W. Skrotzki, *Texture formation in epitaxial hard magnetic Sm2Co7 thin films*, Physica Status Solidi A 207 (2010) Nr. 1, S. 106-116.
389) H.B. Tanh Jeazet, K. Gloe, T. Doert, O.N. Kataeva, A. Jaeger, G. Geipel, G. Bernhard, B. Buechner, K. Gloe, *Self-assembly of neutral hexanuclear circular copper(II) meso-helicates: topological control by sulfate ions*, Chemical Communications 46 (2010) Nr. 14, S. 2373-2375.
390) M. Taut, H. Eschrig, *Exact solutions for a two-electron quantum dot model in a magnetic field and application to more complex sytems*, Zeitschrift fuer physikalische Chemie 224 (2010) Nr. 3-4, S. 631-649.
391) A. Taylor, Y. Krupskaya, S. Costa, S. Oswald, K. Kraemer, S. Fuessel, R. Klingeler, B. Buechner, E. Borowiak-Palen, M.P. Wirth, *Functionalization of carbon encapsulated iron nanoparticles*, Journal of Nanoparticle Research 12 (2010), S. 513-519.
392) A. Taylor, Y. Krupskaya, K. Kraemer, S. Fuessel, R. Klingeler, B. Buechner, M.P. Wirth, *Cisplatin-loaded carbon-encapsulated iron nanoparticles and their in vitro effects in magnetic fluid hyperthermia*, Carbon 48 (2010), S. 2327-2334.

393) K. Theis-Broehl, C. Hamann, J. McCord, B.P. Toperverg, H. Zabel, *Polarized neutron studies on exchange-bias micro-stripe pattern*, Journal of Physics: Conference Series 211 (2010), S. 12014/1-8.

394) T. Thersleff, K. Iida, S. Haindl, M. Kidszun, D. Pohl, A. Hartmann, F. Kurth, J. Haenisch, R. Huehne, B. Rellinghaus, L. Schultz, B. Holzapfel, *Coherent interfacial bonding on the FeAs tetrahedron in Fe/Ba„Fe1-xCox...2As2 bilayers*, Applied Physics Letters 97 (2010) Nr. 2, S. 22506/1-3.

395) J. Thielsch, D. Hinz, L. Schultz, O. Gutfleisch, *Magnetization reversal in textured NdFeB–Fe composites observed by domain imaging*, Journal of Magnetism and Magnetic Materials 322 (2010) Nr. 20, S. 3208-3213.

396) S. Thirupathaiah, S. de Jong, R. Ovsyannikov, H.A. Duerr, A. Varykhalov, R. Follath, Y. Huang, R. Huisman, M.S. Golden, Y.-Z. Zhang, H.O. Jeschke, R. Valenti, A. Erb, A. Gloskovskii, J. Fink, *Orbital character variation of the Fermi surface and doping dependent changes of the dimensionality in BaFe2-xCoxAs2 from angle-resolved photoemission spectroscopy*, Physical Review B 81 (2010) Nr. 10, S. 104512/1-7.

397) D.J. Thurmer, C.C. Bof Bufon, C. Deneke, O.G. Schmidt, *Nanomembrane-based mesoscopic superconducting hybrid junctions*, Nano Letters 10 (2010) Nr. 9, S. 3704-3709.

398) J. Torrens-Serra, P. Bruna, J. Rodriguez-Viejo, S. Roth, M.T. Clavaguera-Mora, *Effect of minor additions on the glass forming ability and magnetic properties of Fe–Nb–B based metallic glasses*, Intermetallics 18 (2010), S. 773-780.

399) J. Torrens-Serra, P. Bruna, S. Roth, J. Rodriguez-Viejo, M.T. Clavaguera-Mora, *Effect of minor Co additions on the crystallization and magnetic properties of Fe(Co)NbBCu alloys*, Journal of Alloys and Compounds 496 (2010) Nr. 1-2, S. 202-207.

400) C. Tripisciano, M.H. Ruemmeli, X. Chen, E. Borowiak-Palen, *Multi-wall carbon nanotubes - a vehicle for targeted Irinotecan drug delivery*, Physica Status Solidi B 247 (2010) Nr. 11-12, S. 2673-2677.

401) S. Trommler, R. Huehne, K. Iida, P. Pahlke, S. Haindl, L. Schultz, B. Holzapfel, *Reversible shift in the superconducting transition for La1.85Sr0.15Cu04 and BaFe1.8Co0.2As2 using piezoelectric substrates*, New Journal of Physics 12 (2010) Nr. 10, S. 103030/1-6.

402) S. Trommler, R. Huehne, A.D. Rata, L. Schultz, B. Holzapfel, *Growth of strained La1-xSrxCo03 films and multilayers using layer-by-layer growth*, Thin Solid Films 519 (2010) Nr. 1, S. 69-73.

403) S. Trommler, P. Pahlke, R. Huehne, L. Schultz, B. Holzapfel, *Preparation of epitaxial La2-xSrxCu04 thin films for dynamic investigations of epitaxial strain*, Journal of Physics / Conference Series 234 (2010) Nr. 1, S. 12045/1-5.

404) D.M. Trots, A. Senyshyn, B.C. Schwarz, *Low temperature structural variations and molar heat capacity of stolzite, PbW04*, Journal of Solid State Chemistry 183 (2010), S. 1245-1251.

405) K. Tschulik, S. Hoffmann, B.P.T. Fokwa, M. Gillessen, P. Schmidt, *Studies regarding the homogeneity range of the zirconium phosphide telluride Zr2-delta-PTe2*, Solid State Sciences 12 (2010) Nr. 12, S. 2030-2035.

406) K. Tschulik, J.A. Koza, M. Uhlemann, A. Gebert, L. Schultz, *Magnetoelectrochemical surface structuring - Electrodeposition of structured metallic layers in magnetic gradient fields*, ECS Transactions 25 (2010) Nr. 41, S. 149-155.

407) K. Tschulik, R. Sueptitz, J. Koza, M. Uhlemann, G. Mutschk, T. Weier, A. Gebert, L. Schultz, *Studies on the patterning effect of copper deposits in magnetic gradient fields*, Electrochimica Acta 56 (2010), S. 297-304.

408) T.C. Ulbrich, C. Bran, D. Makarov, O. Hellwig, J.D. Risner-Jamtgaard, D. Yaney, H. Rohrmann, V. Neu, M. Albrecht, *Effect of magnetic coupling on the magnetization reversal in arrays of magnetic nanocaps*, Physical Review B 81 (2010) Nr. 5, S. 54421/1-7.

409) J. van den Brink, *What lies between*, nature materials 9 (2010) Nr. 4, S. 291-292.

410) A. Vargov, A. Popov, P. Rapta, B. Sun, L. Zhang, L. Dunsch, *Electrochemical tuning of spin states of the endohedral metallofullerene y@C82 as probed by ESR spectroelectrochemistry*, ChemPhysChem 11 (2010), S. 1650-1653.

411) A. Varykhalov, M.R. Scholz, T.K. Kim, O. Rader, *Effect of noble-metal contacts on doping and band gap of graphene*, Physical Review B 82 (2010) Nr. 12, S. 121101/1-4.

412) A. Vasiliev, O. Volkova, I. Presniakov, A. Baranov, G. Demazeau, J.-M. Broto, M. Millot, N. Leps, R. Klingeler, B. Buechner, M.B. Stone, A. Zheludev, *Thermodynamic properties and neutron diffraction studies of silver ferrite AgFe02*, Journal of Physics: Condensed Matter 22 (2010) Nr. 1, S. 16007/1-6.

413) A.N. Vasiliev, O. Heczko, S. Volkova, T.N. Vasilchikova, T.N. Voloshok, K.V. Klimov, W. Ito, R. Kainuma, K. Ishida, K. Oikawa, S. Faehler, *On the electronic origin of the inverse magnetocaloric effect in Ni-Co-Mn-In Heusler alloys*, Journal of Physics D 43 (2010), S. 55004/1-7.

414) E. Vavilova, Y. Arango, A. Sotnikov, V. Kataev, S.-L. Drechsler, A.S. Moskvin, A. Vasiliev, O. Volkova, B. Buechner, *Frustrated magnet Li2ZrCu04 - paramagnetism meets paraelectricity*, Journal of Physics: Conference Series 200 (2010) Nr. 1, S. 12218/1-4.

415) O. Volkova, I. Morozov, V. Shutov, E. Lapsheva, P. Sindzingre, O. Cepas, M. Yehia, V. Kataev, R. Klingeler, B. Buechner, A. Vasiliev, *Realization of the Nersesyan-Tsvelik model in (NO)[Cu(NO3)3]*, Physical Review B 82 (2010) Nr. 5, S. 54413/1-6.

416) M. Voronov, P. Smid, V. Hoffmann, T. Hofmann, C. Venzago, *Microsecond pulsed glow discharge in fast flow Grimm type sources for mass spectrometry*, Journal of Analytical Atomic Spectrometry 25 (2010), S. 511-518.

417) H. Wang, J.-P. Laval, H. Ehrenberg, H. Fuess, S. Arrii-Clacens, H. Luo, B. Elouadi, *Structural and phase transitions in the high composition domain of the system (1-x)Pb(Mg1/3Nb2/3)O3-xPbTiO3*, Ferroelectrics 400 (2010), S. 362-371.

418) H. Wang, J. Luo, A. Robertson, Y. Ito, W. Yan, V. Lang, M. Zaka, F. Schaeffel, M.H. Ruemmeli, G.A.D. Briggs, J.H. Warner, *High-performance field effect transistors from solution processed carbon nanotubes*, ACS nano 4 (2010) Nr. 11, S. 6659-6664.

419) X. Wang, M. Daghofer, A. Nicholson, A. Moreo, M. Guidry, E. Dagotto, *Constraints imposed by symmetry on pairing operators for the iron pnictides*, Physical Review B 81 (2010) Nr. 14, S. 144509/1-11.

420) X.-B. Wang, C. Chi, M. Zhou, I.V. Kuvychko, K. Seppelt, A.A. Popov, S.H. Strauss, O.V. Boltalina, L.S. Wang, *Photoelectron spectroscopy of C60Fn - and C60Fm 2- (n) 17, 33, 35, 43, 45, 47; m) 34, 46) in the gas phase and the generation and characterization of C1-C60F47 - and D2-C60F44 in solution*, Journal of Physical Chemistry A 114 (2010), S. 1756-1765.

421) J.H. Warner, M.H. Ruemmeli, A. Bachmatiuk, B. Buechner, *Structural transformations of carbon chains inside nanotubes*, Physical Review B 81 (2010) Nr. 15, S. 155419/1-5.

422) J.H. Warner, M.H. Ruemmeli, A. Bachmatiuk, B. Buechner, *Atomic resolution imaging and topography of boron nitride sheets produced by chemical exfoliation*, ACS nano 4 (2010) Nr. 3, S. 1299-1304.

423) J.H. Warner, M.H. Ruemmeli, A. Bachmatiuk, B. Buechner, *Examining the stability of folded graphene edges against electron beam induced sputtering with atomic resolution*, Nanotechnology 21 (2010) Nr. 32, S. 325702/1-6.

424) J.H. Warner, M.H. Ruemmeli, A. Bachmatiuk, M. Wilson, B. Buechner, *Examining Co-based nanocrystals on graphene using low-voltage aberration-corrected transmission electron microscopy*, ACS nano 4 (2010) Nr. 1, S. 470-476.

425) U. Weissker, S. Hampel, A. Leonhardt, B. Buechner, *Carbon nanotubes filled with ferromagnetic materials*, materials 3 (2010), S. 4387-4427.

426) A. Winkler, S.B. Menzel, H. Schmidt, I. Moench, A. Jahn, U. Kuenzelmann, *Novel technology for SAW based microfluidic devices with buried interdigital transducer electrodes*, IOP Conference Series: Materials Science and Engineering 8 (2010) Nr. 1, S. 12012/1-5.

427) K. Wohlfeld, A.M. Oles, G.A. Sawatzky, *t-J model of coupled Cu2O5 ladders in Sr14-xCaxCu24O41*, Physical Review B 81 (2010) Nr. 21, S. 214522/1-7.

428) F. Wolny, T. Muehl, U. Weissker, A. Leonhardt, U. Wolff, D. Givord, B. Buechner, *Magnetic force microscopy measurements in external magnetic fields—comparison between coated probes and an iron filled carbon nanotube probe*, Journal of Applied Physics 108 (2010) Nr. 1, S. 13908/1-4.

429) F. Wolny, T. Muehl, U. Weissker, K. Lipert, J. Schumann, A. Leonhardt, B. Buechner, *Iron filled carbon nanotubes as novel monopole-like sensors for quantitative magnetic force microscopy*, Nanotechnology 21 (2010) Nr. 43, S. 435501/1-5.

430) F. Wolny, U. Weissker, T. Muehl, M.U. Lutz, C. Mueller, A. Leonhardt, B. Buechner, *Stable magnetization of iron filled carbon nanotube MFM probes in external magnetic fields*, Journal of Physics: Conference Series 200 (2010), S. 112011/1-4.

431) R. Xiao, D. Fritsch, M.D. Kuzmin, K. Koepernik, M. Richter, K. Vietze, G. Seifert, *Prediction of huge magnetic anisotropies of transition-metal dimer-benzene complexes from density functional theory calculations*, Physical Review B 82 (2010) Nr. 20, S. 205125/1-13.

432) R. Xiao, M. Kuzmin, K. Koepernik, M. Richter, *CoIr-carbon complexes with magnetic anisotropies larger than 0.2 eV: A density-functional-theory prediction*, Applied Physics Letters 97 (2010) Nr. 23, S. 232501/1-3.

433) Y. Xu, W. Loeser, G. Behr, M. Frontzek, F. Tang, B. Buechner, L. Liu, *Crystal growth of the Pr2PdSi3 intermetallic compound*, Journal of Crystal Growth 312 (2010) Nr. 12-13, S. 1992-1996.

434) Yavaş, H., M. van Veenendaal, J. van den Brink, L.J.P. Ament, A. Alatas, B.M. Leu, M.-O. Apostu, N. Wizent, G. Behr, W. Sturhahn, H. Sinn, E.E. Alp, *Observation of phonons with resonant inelastic x-ray scattering*, Journal of Physics: Condensed Matter 22 (2010) Nr. 48, S. 485601/1-5.

435) M. Yehia, E. Vavilova, V. Kataev, R. Klingeler, O. Volkova, E. Lapsheva, V. Shutov, O. Savelieva, A.N. Vasiliev, B. Buechner, *High field ESR study of the new low dimensional S = 1/2 System: Cu(NO3)2·H2O*, Journal of Low Temperature Physics 159 (2010) Nr. 1-2, S. 96-100.

436) M. Yehia, E. Vavilova, A. Moeller, T. Taetz, U. Loew, R. Klingeler, V. Kataev, B. Buechner, *Finite-size effects and magnetic order in the spin -1/2 honeycomb-lattice compound InCu2/3V1/3O3*, Physical Review B 81 (2010), S. 60414/1-4.

437) L.L. Ying, F. Fan, B. Gao, Y.M. Lu, Z.Y. Liu, C.B. Cai, R. Huehne, B. Holzapfel, *Deposition of Gd2Zr2O7 single buffer layers with different thickness for YBa2Cu3O7-delta coated conductors on metallic substrates*, Physica C 470 (2010), S. 543-546.

438) S.P. Yuan, R.H. Wang, G. Liu, R. Li, J.M. Park, J. Sun, K.-H. Chen, *Effects of precipitate morphology on the notch sensitivity of ductile fracture in heat-treatable aluminum alloys*, Materials Science and Engineering A 527 (2010) Nr. 27-28, S. 7369-7381.

439) K. Zagorodniy, G. Seifert, H. Hermann, *Metal-organic frameworks as promising candidates for future ultralow-k dielectrics*, Applied Physics Letters 97 (2010) Nr. 25, S. 251905/1-2.

440) M. Zaka, J.H. Warner, Y. Ito, J.J.L. Morton, M.H. Ruemmeli, T. Pichler, A. Ardavan, H. Shinohara, G.A.D. Briggs, *Exchange interactions of spin-active metallofullerenes in solid-state carbon networks*, Physical Review B 81 (2010) Nr. 7, S. 75424/1-5.

441) G.S. Zakharova, I. Hellmann, V.L. Volkov, C. Taeschner, A. Bachmatiuk, A. Leonhardt, R. Klingeler, B. Buechner, *Vanadium dioxide nanobelts: Hydrothermal synthesis and magnetic properties*, Materials Research Bulletin 45 (2010), S. 1118-1121.

442) J. Zhang, A. Rastelli, O.G. Schmidt, G. Bauer, *Compositional evolution of SiGe islands on patterned Si (001) substrates*, Applied Physics Letters 97 (2010) Nr. 20, S. 203103/1-3.

443) J.J. Zhang, N. Hrauda, H. Groiss, A. Rastelli, J. Stangl, F. Schaeffler, O.G. Schmidt, G. Bauer, *Strain engineering in Si via closely stacked, site-controlled SiGe islands*, Applied Physics Letters 96 (2010) Nr. 19, S. 193101/1-3.

444) J.J. Zhang, F. Montalenti, A. Rastelli, N. Hrauda, D. Scopece, H. Groiss, J. Stangl, F. Pezzoli, F. Schaeffler, O.G. Schmidt, L. Miglio, G. Bauer, *Collective shape oscillations of SiGe islands on pit-patterned Si(001) substrates: A coherent-growth strategy enabled by self-regulated intermixing*, Physical Review Letters 105 (2010) Nr. 16, S. 166102/1-4.

445) L. Zhang, A.A. Popov, S. Yang, S. Klod, P. Rapta, L. Dunsch, *An endohedral redox system in a fullerene cage: the Ce based mixed-metal cluster fullerene Lu2CeN@C80*, Physical Chemistry Chemical Physics 12 (2010) Nr. 28, S. 7840-7847.

446) L.C. Zhang, M. Calin, F. Paturaud, J. Eckert, *Deformation-induced grain refinement in body-centered cubic Co–Fe alloys upon room temperature compression*, Materials Science and Engineering A 527 (2010) Nr. 21-22, S. 5796-5800.

447) L.C. Zhang, H.B. Lu, M. Calin, E.V. Pereloma, J. Eckert, *High-strength ultrafine-grained Ti-Fe-Sn alloys with a bimodal structure*, Journal of Physics / Conference Series 240 (2010), S. 12103/1-5.

448) N. Zheng, G. Wang, L.C. Zhang, M. Calin, M. Stoica, G. Vaughan, N. Mattern, J. Eckert, *In situ high-energy x-ray diffraction observation of structural evolution in a Ti-based bulk metallic glass upon heating*, Journal of Materials Research 25 (2010) Nr. 12, S. 2271-2277.

449) R. Zinke, J. Richter, S.-L. Drechsler, *Spiral correlations in frustrated one-dimensional spin-1/2 Heisenberg J1-J2-J3 ferromagnets*, Journal of Physics: Condensed Matter 22 (2010) Nr. 44, S. 446002/1-6.

450) M. Zschornak, S. Gemming, E. Gutmann, T. Weissbach, H. Stoecker, T. Leisegang, T. Riedl, M. Traenkner, T. Gemming, D.C. Meyer, *Surface modeling and chemical solution deposition of Sr0(SrTi03)n Ruddlesden - Popper phases*, Acta Materialia 58 (2010) Nr. 14, S. 4650-4659.

451) V.I. Zverev, A.M. Tishin, M.D. Kuzmin, *The maximum possible magnetocaloric delta-T effect*, Journal of Applied Physics 107 (2010) Nr. 4, S. 43907/1-3.

Contributions to conference proceedings and monographs

1) C. Bechthold, J. Buschbeck, A. Lotnyk, B. Erkart, S. Hamann, C. Zamponi, A. Ludwig, L. Kienle, S. Faehler, E. Quandt, *Development towards MSM active FePd thick films*, International Conference and Exhibition on New Actuators and Drive Systems, Bremen, 14.-16.6.10, in: Conference Procceedings, 299-302 (2010).

2) R. Bruenig, M. Weihnacht, G. Guhr, H. Schmidt, *Complex loading and simulation of acoustic thickness shear mode resonator*, Eurosensors XXIV, Linz/ Austria, 5.-8.9.10, in: Procedia Engineering, 5, 476-479 (2010).

3) G. Doerfel, *Roentgens merkwuerdige Bestellung - ein Beitrag zur Entdeckungsgeschichte der Roentgenstrahlen*, in: RoeFo- Fortschritte auf dem Gebiet der Roentgenstrahlen und bildgebenden Verfahren, 182, 879-882 (2010).

4) G. Doerfel, *Der Wettlauf um das weisse Gold - Zur Nacherfindung des europaeischen Porzellans in thueringischen Kleinstaaten*, in: Mitteilungen der Gesellschaft Deutscher Chemiker, Fachgruppe Geschichte der Chemie, 21, 3-32 (2010).

5) J. Eckert, S. Scudino, M. Stoica, S. Kenzari, M. Sales, *Mechanical engineering properties of CMAs*, in: Complex Metallic Alloys: Fundamentals and Applications, Dubois, Jean-Marie ; Belin-Ferre, Esther (Ed.), Weinheim: Wiley-VCH, 273-315 (2010).

6) S. Faehler, *Magnetic shape memory alloys: From better materials towards smarter systems*, International Conference and Exhibition on New Actuators and Drive Systems, Bremen, 14.-16.6.10, in: Conference Procceedings, 295-298 (2010).

7) G. Guhr, R. Bruenig, H. Schmidt, M. Weihnacht, S. Gehrisch, G. Siegert, *Surface acoustic wave resonators as novel tools for multi-parametric blood analysis*, IEEE EMBC2010 (32nd Annual International Conference of the IEEE Engineering in Medicine and Biology Society), Buenos Aires/ Argentinien, 31.8.-4.9.10, in: Proceedings, 3499-3502 (2010).

8) H. Hermann, *Optimization of dielectric and elastic properties of nanoporous ultralow-k dielectric materials*, in: AIP Conference Proceedings, 1300, 153-158 (2010).

9) S. Kaufmann, J. Buschbeck, O. Heczko, L. Schultz, S. Faehler, *Epitaxial growth of Ni-Mn-Ga: Consequences of magnetron configuration on martensitic behavior*, ICOMAT 2008, Santa Fe/ USA, 29.6.-5.7.08, in: Proceedings, 281- (2010).

10) O. Labedz, H. Lange, A. Huczko, M.H. Ruemmeli, T. Gemming, M. Bystrzejewski, *Influence of the iron content in the carbon electrode in arc-discharge on the yield of Fe encapsulates (original in Polish)*, IV Krajowa Konferencja Nanotechnologii, Nano 2010, Poznan/ Poland, 28.6.-2.7.10, in: Proceedings, 267 (2010).

11) M.H. Lee, J.H. Jun, J. Eckert, *Effect of residual stress on mechanical property of monolithic bulk metallic glasses*, 7th Pacific Rim International Conference on Advanced Materials and Processing (PRICM 7), Cairns/ Australia, 1.-5.8.2010, in: Proceedings, J.-F. Nie, A. Morton (eds.), Materials Science Forum, 654-656, 1050 (2010).

12) A. Luedge, H. Riemann, M. Wuenscher, G. Behr, W. Loeser, A. Muiznieks, A. Croell, *Floating zone crystal growth*, in: Crystal Growth Processes Based on Capilarity: Czochralski, Floating Zone, Shaping and Crucible Techniques, T. Duffar (ed.), John Wiley and Sons, Chichester, UK., Chapter 4, 203-275 (2010).

13) T. Marr, J. Freudenberger, A. Kauffmann, J. Scharnweber, C.-G. Oertel, W. Skrotzki, U. Siegel, U. Kuehn, J. Eckert, L. Schultz, *Damaszenleichtmetalle*, International ECEMP Colloquium, 2.-3.12.10, in: Proceedings, 71-79 (2010).

14) N. Mattern, J. Eckert, *Short-range order of Cu-Zr metallic glasses*, 2009 WPI-AIMR Annual Workshop, Miyagi-Zao/ Japan, 1.-6.3.09, in: Proceedings, WPI-AIMR News 10, 104-110 (2010).

15) A. Neudert, Y.W. Lai, R. Schaefer, J. McCord, *Twin boundary motion in NiMnGa upon pulsed field excitation*, International Conference and Exhibition on New Actuators and Drive Systems, Bremen, 14.-16.6.10, in: Conference Procceedings, 762-764 (2010).
16) S. Pfuetzner, J. Meiss, S. Olthof, M.P. Hein, A. Petrich, L. Dunsch, K. Leo, M. Riede, *Improved photon harvesting by employing C70 in bulk heterojunction solar cells*, Photonics for Solar Energy Systems III; Bruessel, 13.-15.4.10, in: Proceedings of SPIE - The International Society for Optical Engineering, 7725, 77250E (2010).
17) M.H. Ruemmeli, P. Ayala, T. Pichler, *Carbon nanotubes and related structures: Production and formation*, in: Carbon nanotubes and related structures: synthesis, characterization, functionalization, and applications, Dirk M. Guldi ; Nazario Martin (eds.), Weinheim: Wiley-VCH, S. 1-17 (2010).
18) S. Scheinert, G. Paasch, I. Hoerselmann, A. Herasimovich, *Low-cost submicrometer organic field-effect transistors*, in: Organic Electronics; Gregor Meller, Tibor Grasser (Volumen-eds.), Serie: Advances in Polymer Science, Springer-Verl., 2010, 223, 155-188 (2010).
19) M. Soszynski, A. Dabrowska, M. Bystrzejewski, M.H. Ruemmeli, T. Gemming, A. Huczko, *Combustion synthesis of one-dimensional silicon carbide*, 5th Wide Bandgap Materials- Progress in Synthesis and Applications and 7th Diamond and Related Films jointly with 2nd International Workshop on Science and Applications of Nanoscale Diamond Materials, Zakopane/ Poland, 28.6.-2.7.10, in: Abstract Proceedings, 173-176 (2010).
20) M. Spindler, S.B. Menzel, J. Eckert, C. Eggs, *Influence of Al on resistance and power durability of Cu-based SAW metallizations*, E-MRS Spring Meeting, Symposium G, Strasbourg/ France, 8.-12.6.2009, in: Proceedings: Fundamentals and Technology of Multifunctional Oxide Thin Films; P. Muralt, M. Kosec, V. Raineri, S. Ravesi (eds.), IOP Publ. Ltd., London. IOP Conf. Series: Materials Science and Engineering, 8, 12013/1-3 (2010).
21) U. Weissker, S. Hampel, A. Leonhardt, B. Buechner, *Carbon nanotubes filled with ferromagnetic materials*, materials 3 (2010), S. 4387-4427.
22) K. Wetzig, *Oberflaechen- und Duennschichtcharakterisierung*, in: Vakuum - Plasma - Technologie, G. Blasek ; G. Braeuer (eds.), Bad Saulgau: E. G. Leuze-Verl., 2010, Band 1, 139-186 (2010).
23) W. Xu, M. Calin, K.B. Kim, J. Das, K. Xia, J. Eckert, *Microscopic deformation behavior and microstructural evolution in Ti-Nb-Ta-M (M = In, Ag, or Cr) beta- alloys*, 2009 WPI-AIMR Annual Workshop, Miyagi-Zao/ Japan, 1.-6.3.09, in: Proceedings, WPI-AIMR News 10, 111-114 (2010).
24) S.R. Yeduru, A. Backen, S. Faehler, A. Diestel, L. Schultz, M. Kohl, *Sacrificial layer technology - a route towards freestanding Ni-Mn-Ga films*, International Conference and Exhibition on New Actuators and Drive Systems, Bremen, 14.-16.6.10, in: Conference Procceedings, 765-768 (2010).
25) A. Zahariev, E. Nazarova, K. Nenkov, T. Mydlarz, V. Kovachev, *Intragranular critical current density in YBCO substituted with Pr or/and Ca*, in: AIP Conference Proceedings, 1203, 367-372 (2010).

Invited Talks

1) A. Bachmatiuk, *Understanding graphitization via SixOy catalyst Systems in CVD*, Invited talk, EMPA St. Gallen/ Switzerland, 13.-14.12.10 (2010).
2) A. Bachmatiuk, *Investigating the graphitisation mechanism with the use of SiO2 nanoparticles in chemical vapor deposition*, Warsaw University, Warschau/ Polen, 4.11.10 (2010).
3) M. Benyoucef, *Quantum-dot single photon sources and strong coupling between resonators*, Seminar, Universitaet Kassel, 8.1.10 (2010).
4) F. Boerrnert, *Early steps towards nano-engineering sp2 carbon with electrons*, Vortrag an der University of Surrey, Guildford/ United Kingdom, 28.5.10 (2010).
5) F. Boerrnert, *Early steps towards nano-engineering sp2 carbon with electrons*, Vortrag an der University of Oxford/ United Kingdom, 14.5.10 (2010).
6) C.C. Bof Bufon, *Energy storage elements based on rolled-up nanomembranes*, Cusanuswerk Fachschaftstagung Physik 2010, Dresden, 16.10.10 (2010).
7) C.C. Bof Bufon, *Hybrid electronics based on rolled-up nanomembranes*, Third International Conference on Telecommunications, Electronics and Informatics (ICTEI), Chisinau/ Republic of Moldova, 20.-23.5.10 (2010).
8) S. Borisenko, *ARPES of iron pnictides*, Workshop on Physics of Complex Oxides, Santorini/ Greece, 14.-17.6.10 (2010).
9) S. Borisenko, *ARPES of iron superconductors*, Seminar, Department of Physics, University of Salerno, Salerno/ Italien, 13.10.10 (2010).
10) S. Borisenko, *ARPES of iron pnictides*, International Conference on Strongly Correlated Electron Systems, Santa Fe/ USA, 27.6.-2.7.10 (2010).
11) S. Borisenko, *Superconductivity without magnetism in LiFeAs*, 9th International Conference on Spectroscopies in Novel Superconductors, Shanghai/ China, 23.-28.5.10 (2010).

12) S. Borisenko, *ARPES of Fe-superconductors*, Edge Topics in Correlated Materials, (ParisEdge2010), Orsay and Paris/ France, 17.-19.5.10 (2010).
13) S. Borysenko, *ARPES of LiFeAs*, HTSC Workshop Munich 2010, Muenchen, 13.-16.4.10 (2010).
14) S. Borysenko, *ARPES investigation of the interplay between the density waves and superconductivity*, Workshop on Emergent Quantum States in Complex Correlated Matter, Dresden, 23.-27.8.10 (2010).
15) S. Borysenko, *ARPES of iron pnictides*, Superstripes 2010, Erice/ Italy, 19.-25.7.10 (2010).
16) S. Borysenko, *Angle resolved photo emission spectroscopy of Fe-based superconductors*, Electronic Structure of Fe-based Superconductors, Stuttgart, 10.-12.5.10 (2010).
17) B. Buechner, *FeAs superconductors*, Workshop Joint Meeting OSU – IFW, Dresden, 23.-25.8.10 (2010).
18) B. Buechner, *From magnetism to superconductivity in iron pnictides*, International Symposium on „Novel States in Correlated Condensed Matter - From Model Systems to Real Materials", Berlin, 2.-4.3.10 (2010).
19) B. Buechner, *Orbital polarons in manganites and colbaltates*, 452. WE-Heraeus-Seminar, Bad Honnef, 15.3.10 (2010).
20) B. Buechner, *Nanoscale electronic order in underdoped iron pnictides*, Workshop on Emergent Quantum States in Complex Correlated Matter, MPI / PkS, Dresden, 23.-27.8.10 (2010).
21) B. Buechner, *Magnetic and electronic properties of iron arsenide superconductors*, Seminarvortrag, Karlsruher Institut für Technologie (KIT), Karlsruhe, 4.2.10 (2010).
22) B. Buechner, *The Iron age of high temperature superconductivity*, Physics at FOM Veldhoven/ Netherlands, 18.1.10 (2010).
23) B. Buechner, *The iron age of high temperature superconductivity*, Kolloquiumsvortrag an der Ernst-Moritz-Arndt Universitaet Greifswald, 3.6.10 (2010).
24) B. Buechner, *Magnetic and electronic properties of iron oxides*, SFB Seminar, Universitaet Koeln, 27.1.10 (2010).
25) B. Buechner, *Magnetic and electronic properties of iron pnictide superconductors*, Focus Session Talk at Physics, FOM Veldhoven, Veldhoven/ Netherlands, 19.1.10 (2010).
26) B. Buechner, *Magnetism meets nanotubes*, Seminarvortrag im LPN-CNRS, Marcoussis/ Frankreich, 22.6.10 (2010).
27) B. Buechner, *Phase diagram of Fe based superconductors*, Superconductivity Explored by Neutron Scattering Experiments (SENSE), Institut Laue-Langevin, Grenoble/ France, 20.-23.10.10 (2010).
28) B. Buechner, *Nanoscale electronic order in underdoped iron pnictides*, Workshop on Principles and Design of Strongly Correlated Electronic Systems, Trieste/ Italy, 2.-13.8.10 (2010).
29) B. Buechner, *The iron age of high temperature superconductivity*, Physik Kolloquium, Universitaet Erlangen, 14.6.10 (2010).
30) M. Calin, *Getting more women in decision-making in materials science (DIVERSITY Project)*, Colloquim - Dipartimento di Chimica I.F.M., Universita di Torino, Turin/ Italy, 24.-25.11.10 (2010).
31) M. Calin, *Improving the gender diversity management in materials research institutions - DIVERSITY FP7 Project*, Balanced Leadership - DIVERSITY Meeting, REPM'10 Workshop, Bled/ Slovenia, 31.8.10 (2010).
32) M. Calin, A. Gebert, *Diversity project out of WomenInNano*, European Workshop 'Leadership positions: how accessible are they for women in materials research?', University of Barcelona/ Spain, 19.-21.5.10 (2010).
33) M. Daghofer, *Multi-orbital models for pnictide superconductors*, Theorie-Kolloquium, TU Dresden, 11.11.10 (2010).
34) M. Daghofer, *Spin-polarized semiconductor induced by magnetic impurities in graphene*, Seminar, University of Alberta/ USA, 7.5.10 (2010).
35) M. Daghofer, *Numerical simulations for the interplay of spins and orbitals in multi-orbital models for pnictides*, Workshop, Lanzarote/ Spanien, 20.-26.6.10 (2010).
36) M. Daghofer, *Multi-orbital models for Pnictide superconductors*, Seminar, KIT Karlsruhe, 18.11.10 (2010).
37) M. Daghofer, *Multi-orbital models for Pnictides: Pairing symmetries and numerical simulations*, Workshop, MPI-PKS, Dresden, 23.-27.8.10 (2010).
38) M. Daghofer, *Correlated two- and three-orbital models for iron-pnictides*, Seminar, MPI-PKS, Dresden, 4.2.10 (2010).
39) C. Deneke, *Hybrid radial superlattices by roll-up of inherent strained films*, Seminar, Universitaet Hamburg, 10.8.10 (2010).
40) C. Deneke, *Fabrication and structure of rolled-up radial hybrid superlattices*, Seminar, Karlsruhe Institute for Technology, KIT Karlsruhe, 12.9.10 (2010).
41) C. Deneke, *Structure of and strain in rolled-up nano-membranes*, Seminar, LNLS Campinas/ Brazil, 22.9.10 (2010).
42) F. Ding, *Engineering the properties of nanostructures by piezoelectric-induced stresses*, Laser Seminar, Quantum Photonics Group, ETH Zurich/ Switzerland, 30.3.10 (2010).
43) F. Ding, *Electro-mechanical control of quantum dot excitonic emission and Raman signal from single layer graphene*, Seminar, Institute of Semiconductors, Chinese Academy of Science, Beijing/ China, 1.3.10 (2010).
44) F. Ding, *Engineering the properties of nanostructures by piezoelectric-induced stresses*, Seminar, IBM Zurich Research Laboratory. Rueschlikon/ Switzerland, 1.4.10 (2010).
45) F. Ding, *Straintronics in semiconductor nanostructures*, Seminar, Ruhr-Universitaet, Bochum, 8.10.10 (2010).
46) K. Doerr, *Strain-dependent ferroelectricity and magnetism in oxide heterostructures*, 452. W.-E. Heraeus-Seminar „Strain in Transition Metal Oxides", Bad Honnef, 14.-17.3.10 (2010).

47) K. Doerr, *Strain tuning the ferroelectric hysteresis of BiFeO3 and the light emission from InGaAs quantum dots*, ICYS Workshop, Minakami/ Japan, 29.1.10 (2010).
48) K. Doerr, *Strain-dependent ferroelectricity and magnetism in oxide heterostructures*, Internationaler Workshop des SFB 672, Martin-Luther-Universitaet Halle-Wittenberg, Irsee, 1.3.10 (2010).
49) K. Doerr, *Explore strain-coupled two-phase multiferroics using piezoelectric substrates*, NIMS, Tsukuba/ Japan, 27.1.10 (2010).
50) K. Doerr, *Nanoskalige Ferroika in den drei Feldern E, H und sigma*, Kolloquium, Universitaet Halle-Wittenberg, 6.7.10 (2010).
51) K. Doerr, *Strain-dependent ferroic properties of doped LaMO3 (M = Mn or Co) and BiFeO3*, Fruehjahrstagung des AK Festkoerperphysik, Symposium Multifunctional Materials, Regensburg, 24.3.10 (2010).
52) K. Doerr, *Reversible strain dependence of ferroic orders in oxide films*, ICMS, Antalya/ Turkey, 29.4.10 (2010).
53) K. Doerr, *Magnetic and ferroelectric orders controlled by reversible epitaxial strain*, MRS Spring Meeting, San Francisco/ USA, 5.-9.4.10 (2010).
54) K. Doerr, *Piezoelectric control of magnetic properties in thin film heterostructures*, CIMTEC, Florenz/ Italy, 6.-11.6.10 (2010).
55) S.-L. Drechsler, *Insights, puzzles and problems in interpreting optical and other experimental data of Fe-pnictides and related materials*, Workshop „New Trends in Strongly Correlated Electron Systems“, Grenoble/ Frankreich, 8.-9.4.10 (2010).
56) S.-L. Drechsler, *Theoretical overview over inchain and interchain couplings in frustrated edge-shared chain cuprate compounds*, Vortrag am MPI-PKS, Einladender: Dr. M. Zhitomirsky, Dresden, 26.5.10 (2010).
57) S.-L. Drechsler, *Inchain and interchain couplings in frustrated chain cuprates*, Workshop „New Trends in Quantum Magnetism“, Einladender: Dr. N. Laflorencie, Orsay/ Frankreich, 2.6.10 (2010).
58) S.-L. Drechsler, *Insights, puzzles and problems in the theoretical interpretation of optical and other experimental data of Fe-pnictides*, Vortrag an der Universitaet Frankfurt/ Theoretische Physik, Einladende: Prof. R. Valenti und Dr. H. Jeschke, Frankfurt, 15.7.10 (2010).
59) L. Dunsch, *Charging of caged systems as studied by spectroelectrochemistry: From empty to endoheral fullerenes*, Instituts-kolloquium, Universitaet Kopenhagen, Chemie Department, Kopenhagen/ Daenemark, 5.11.10 (2010).
60) J. Eckert, *Structure-properties relationship in bulk metallic glasses and bulk metallic glass composites*, International Workshop on Metallic Glasses, Natl. Taiwan University of Science and Technology, Teipei/ Taiwan, 31.5.10 (2010).
61) J. Eckert, *Transformation-mediated plasticity and the role of heterogeneity on improving the deformability of metallic glasses*, Sino-German Workshop „Building the Bridge between Physics and Materials Science in Amorphous Metals“, Beijing/ China, 13.10.10 (2010).
62) J. Eckert, *Plasticity enhancement in bulk metallic glasses*, 17th International Symposium on Metastable, Amorphous and Nanostructured Materials, (ISMANAM 2010), Zuerich/ Switzerland, 6.-9.7.10 (2010).
63) J. Eckert, *Bulk metallic glasses and composites: Development of high performance materials by phase and microstructure design*, National Central University, Jhongli/ Taiwan, 1.6.10 (2010).
64) J. Eckert, *Structure-property relations in bulk metallic glasses*, International Conference on Mechanical Properties of Materials (ICMPM),), Hangzhou/ China, 27.5.10 (2010).
65) J. Eckert, *Transformation-induced plasticity enhancement in metallic glasses: The role of structure and heterogeneity*, Global Research Laboratory Korea - Germany Workshop on Bulk Metallic Glass and Nano-Structured Materials, Gangneung/ Korea, 15.10.10 (2010).
66) J. Eckert, *Materialdesign innovativer metallischer Werkstoffe*, Workshop Nanomaterial - BDLI priority program „Eco-efficient Flying“, EADS, Ottobrunn, 26.2.10 (2010).
67) J. Eckert, *Strengthening of Ti-base glass-forming alloys by microstructure design*, 2010 TMS Annual Meeting & Exhibition, Symposium „Bulk Metallic Glasses (VII)“, Seattle/ USA, 16.2.10 (2010).
68) J. Eckert, *Metallische Glaeser und Komposite - Herstellung, Eigenschaften und Innovationspotenzial*, Workshop / Side Event Innovationspotenzial ausgewaehlter neuer Werkstoffe, Materials Science and Engineering Congress (MSE 2010), Darmstadt, 25.8.10 (2010).
69) J. Eckert, *Metastable metallic materials: Tailoring properties by phase and microstructure design*, 11. ZFM-Festkoerpertag 2010, Zentrum fuer Festkoerperchemie und Neue Materialien, Leibniz Universitaet Hannover, 29.1.10 (2010).
70) J. Eckert, *Metallische Glaeser und Komposite - Materialdesign fuer neue Hochleistungswerkstoffe*, Karlsruher Werkstoffkolloquium, Karlsruhe Institute of Technology, KIT, Karlsruhe, 26.1.10 (2010).
71) J. Eckert, *Tuning the structure for enhancing the plasticity of metallic glasses*, MRS Fall Meeting, Symposium on Bulk Metallic Glasses and their Applications, Boston/ USA, 2.12.10 (2010).
72) H. Ehrenberg, *Lithiumionen-Batterien: Perspektiven und materialwissenschaftliche Herausforderungen*, Vortrag auf der 19. Diskussionstagung Anorganisch-Technische Chemie, Frankfurt, 18.2.10 (2010).
73) H. Ehrenberg, *Elektrodenmaterialien fuer Lithium-Ionenbatterien: Materialwissenschaftliche Herausforderungen und Perspektiven*, Vortrag am Fraunhofer Center Nanoelektronische Technologie CNT in Dresden, 11.3.10 (2010).
74) H. Ehrenberg, *Lithiumionen-Batterien: Perspektiven und materialwissenschaftliche Herausforderungen*, Anorganisch-chemisches Kolloquium, Universitaet Bonn, 1.7.10 (2010).

75) H. Ehrenberg, *Lithiumionen-Batterien: Perspektiven und materialwissenschaftliche Herausforderungen*, Vortrag auf der Klausurtagung des SFB 609 „Elektromagnetische Stroemungsbeeinflussung in Metallurgie, Kristallzuechtung und Elektrochemie" in Schmochtitz, 12.3.10 (2010).
76) H. Ehrenberg, I. Chumak, G. Dmytriv, V. Pavlyuk, H. Pauly, S. Oswald, *New concept for intermetallic composite anodes in Li-ion batteries*, Vortrag auf der XI. International Conference on Crystal Chemistry of Intermetallic Compounds in Lviv/ Ukraine, 2.6.10 (2010).
77) S. Faehler, *Playing lego with martensite*, Seminar, Loughborough University, Loughborough/ UK, 3.12.10 (2010).
78) S. Faehler, *Magnetic shape memory alloys: From bulk to thin films*, TF Colloquium, CAU Kiel, 5.6.10 (2010).
79) S. Faehler, *The role of interfaces in bulk and thin film magnetic shape memory alloys*, Special Workshop on Shape Memory Alloys, Istanbul/ Turkey, 20.-24.6.10 (2010).
80) S. Faehler, *Magnetic shape memory alloys*, 25. Workshop, Novel Materials and Superconductors Computers in Material Sciences, Universitaetssportheim Planneralm, Donnersbach/ Oesterreich, 20.-27.2.10 (2010).
81) S. Faehler, *Interfaces in bulk and thin film magnetic shape memory alloys*, E-MRS 2010 Spring Meeting, Strasbourg/ France, 7.-11.6.10 (2010).
82) S. Faehler, *The role of interfaces in bulk and thin film magnetic shape memory alloys*, SFB 459 Seminar, Universitaet Bochum, 21.7.10 (2010).
83) S. Faehler, *Magnetic shape memory alloys: From bulk to thin films*, KOMET Seminar, Universitaet Mainz, 12.7.10 (2010).
84) S. Faehler, *The role of interfaces in bulk and thin film magnetic shape memory alloys*, SFB 459 Seminar, Universitaet Bochum, 21.7.10 (2010).
85) J. Fink, *Electronic structure studies of Ferropnictide superconductors by angle and timeresolved photoemission spectroscopy*, Symposium on Low-dimensional Magnetism and Multi-band Superconductivity, Dresden, 6.-7.5.10 (2010).
86) J. Fink, *Electronic structure studies of ferropnictide superconductors and their parent compounds by angle and time-resolved photoemission spectroscopy*, Superstripes 2010, Erice/ Italy, 19.-25.7.10 (2010).
87) J. Fink, *Electronic structure studies of ferropnictide superconductors from angle and time resolved photoemission spectroscopy*, Seminarvortrag Universitaet Stuttgart, 2.12.10 (2010).
88) J. Fink, *Angle-resolved photoemission spectroscopy for many-body properties of solids*, Vorlesung an der SLS, Villingen/ Schweiz, 22.4.10 (2010).
89) J. Fink, *Electronic structure studies of ferropnictide superconductors from angle and time resolved photoemission spectroscopy*, Seminarvortrag Universitaet Goettingen, 15.11.10 (2010).
90) J. Fink, *Electronic structure studies of ferropnictides using ARPES*, Seminarvortrag, Universitaet Wuerzburg, 11.2.10 (2010).
91) J. Fink, *Pairing interactions in low-dimensional superconductors studied by angle-resolved photoemission spectroscopy*, The First International Congress of Nanotechnology, Quito/ Equador, 7.-11.6.10 (2010).
92) J. Fink, *Electronic structure studies of the new ferropnictide superconductors*, Seminarvortrag Universitaet Zuerich/ Schweiz, 21.4.10 (2010).
93) J. Fink, *Angle-resolved photoemission spectroscopy for many-body properties of solids*, Winterschool on Photoemission Spectroscopy, Dijon/ Frankreich, 22.-26.2.10 (2010).
94) V.M. Fomin, *Theoretical modelling of the excitonic behaviour in self-assembled quantum rings*, 9th International Conference on Excitonic and Photonic Processes in Condensed and Nano Materials (EXCON'10), Brisbane/ Australia, 11.-16.7.10 (2010).
95) V.M. Fomin, P. Kratzer, *Engineering the electron minibands and transport in arrays of interacting n-type InAs/GaAs quantum dots*, The 2010 Villa Conference on Interaction Among Nanostructures (VCIAN), Santorini/ Greece, 21.-25.6.10 (2010).
96) V.M. Fomin, P. Kratzer, *Enhancement of thermoelectric efficiency due to electronic minibands in InGaAs/ GaAs quantum dot arrays*, Fifth International Conference on Materials Science and Condensed Matter Physics, Chisinau/ Republic of Moldova, 13.-17.9.10 (2010).
97) G. Fuchs, S.-L. Drechsler, N. Kozlova, A. Kauffmann, V. Ginenko, R. Klingeler, G. Behr, S. Wurmehl, S. Aswartham, C. Hess, J. Freudenberger, S. Haindl, F. Onken, K. Nenkov, B. Buechner, L. Schultz, M. Bartkowiak, *Pauli limiting behavior at high fields versus enhanced upper critical fields near Tc in several disordered FeAs-based superconductors*, International Conference on Superconductivity and Magnetism (ICSM 2010), Antalya/ Tuerkei, 25.-30.4.10 (2010).
98) A. Gebert, *Hydrogen reactivity of amorphous and nanocrystalline Mg-based alloys*, International Workshop on Non-crystalline Solids, Barcelona/ Spanien, 21.-23.4.10 (2010).
99) A. Gebert, *Effect of surface finishing and mechanically induced defects on the corrosion of bulk metallic glasses*, 139. TMS Annual Meeting, Seattle/ USA, 14.-18.2.10 (2010).
100) A. Gebert, *Corrosion of bulk metallic glasses: analysis of electrochemical processes at the micro- and nano-scale and their utilization for micro-machining*, MRS Fall Meeting 2010, Boston/ USA, 28.11.-3.12.10 (2010).
101) A. Gebert, *Korrosion von NdFeB-Magnetmaterialien und Einfluss von Magnetfeldern auf Korrosionsprozesse*, Kolloquium Fa. Vacuumschmelze, Hanau, 16.12.10 (2010).
102) J. Geck, *EELS and RIXS studies of La1-xSr1+xMn04*, SLS Seminar, PSI Villigen/ Schweiz, 17.-19.3.10 (2010).

103) J. Geck, *Magnetoresistive manganites*, IFF Ferienschule des Forschungszentrums Juelich, 13.-16.3.10 (2010).
104) J. Geck, *Resonant soft x-ray scattering from charge, spin and orbital order in manganites*, Resonant Spectroscopy Workshop at UBC, Vancouver/ Canada, 11.-20.5.10 (2010).
105) H.-J. Grafe, G. Lang, F. Hammerath, S.-H. Beak, B. Buechner, *NMR studies of the new iron pnictide superconductors*, Recent Advances in Broad-band Solid-state NMR of Correlated Electronic Systems, Trogir/ Kroatien, 5.-10.9.10 (2010).
106) H.-J. Grafe, G. Lang, F. Hammerath, K. Manthey, M. Fuchs, D. Paar, B. Buechner, *NMR studies of the new iron pnictide superconductors*, CIMTEC 2010, 5th Forum on New Materials, Montecatini Terme/ Italien, 13.-18.6.10 (2010).
107) C. Gruenzweig, C. David, O. Bunk, G. Frei, E. Lehmann, J. Kohlbrecher, R. Schaefer, P. Lejcek, H.M.R. Roennow, F. Pfeiffer, *Visualization of magnetic domains and magnetization processes in bulk materials by neutron dark-field imaging*, Magnetic Measurements 2010, Prag/ Tschechien, 12.-15.9.10 (2010).
108) O. Gutfleisch, *Giant magnetocaloric effect in La(FeSi)13 - from fundamentals towards application*, Institutsseminar, Risø National Laboratory for Sustainable Energy, Roskilde/ Denmark, 22.11.10 (2010).
109) O. Gutfleisch, *Materials for energy efficiency*, Cusanus Werk, Fachschaftstagung Physik, Dresden, 16.10.10 (2010).
110) O. Gutfleisch, *Magnetwerkstoffe fuer moderne Kuehltechnik*, Workshop Ideas to Market, Dresdner Materialinnovationen, TU Dresden, 15.1.10 (2010).
111) O. Gutfleisch, *Magnetic materials and hydrides for energy efficient technology*, Seminarvortrag, TU Darmstadt, 2.2.10 (2010).
112) O. Gutfleisch, *Wasserstoff in der physikalischen Metallkunde*, 31. Adelbodener Werkstoffseminar der Universitaet Karlsruhe, Adelboden/ Schweiz, 10.3.10 (2010).
113) O. Gutfleisch, *Magnetic materials and hydrides for energy efficient technology*, Seminarvortrag, Siemens, Erlangen, 19.3.10 (2010).
114) O. Gutfleisch, *Materials for energy applications*, 3rd COSY Young Researchers Workshop on Functional Materials for Energy Applications: Beyond Solid State Hydrogen Storage, Dresden, 9.6.10 (2010).
115) O. Gutfleisch, *Tuning magnets and hydrides on the nanoscale – advanced materials for energy conversion and storage*, Seminarvortrag, Universitaet Konstanz, 16.7.10 (2010).
116) O. Gutfleisch, *Magnetism for energy*, IEEE Magnetics Society Summer School, Dresden, 15.-21.8.10 (2010).
117) O. Gutfleisch, K. Skokov, M. Krautz, J. Liu, J. Moore, *Magnetische Kuehlung: Material-und Prototypenentwicklung*, Dresdener Werkstoffsymposium „Werkstoffe der Energietechnik", Hotel Bellevue, Dresden, 9.-10.10.10 (2010).
118) O. Gutfleisch, K. Skokov, J. Moore, *Challenges for the implementation of magnetocaloric materials*, C-MAC Industry Days, Max Planck Institute for Chemical Physics of Solids Dresden, 15.-16.11.10 (2010).
119) D. Haberer, *Tunable bandgap versus electron localization in hydrogenated quasi-free-standing Graphene*, Vortrag an der University of Surrey, Guildford/ United Kingdom, 25.6.10 (2010).
120) D. Haberer, *Tunable bandgap versus electron localization in hydrogenated quasi-free-standing Graphene*, Vortrag an der Fakultaet fuer Physik Universitaet Wien/ Oesterreich, 10.-13.5.10 (2010).
121) S. Hampel, D. Haase, K. Kraemer, M. Arlt, A. Wolter, A. Elgendy, Y. Krupskaya, R. Klingeler, A. Leonhardt, B. Buechner, *Carbon - nanotube based biomedical agents for heating, sensoring and drug delivery*, Seminar, Universita della Calabria, Rende/ Italy, 20.-22.7.10 (2010).
122) U. Hannemann, K.-H. Mueller, M. Wolf, J. Lyubina, *A two-particle exchange interaction model*, JEMS 2010 Conference, Krakow/ Poland, 23.-28.8.10 (2010).
123) R. Hermann, *Magnetic field controlled floating-zone crystal growth of intermetallic compounds*, Statusseminar AvantSolar, Potsdam, 9.-10.9.10 (2010).
124) V. Hoffmann, *New instrumentation for RF-GD-OES*, International Glow Discharge Spectroscopy Symposium, CUFR Jean Francois Champollion, Albi/ Frankreich, 22.-27.8.10 (2010).
125) V. Hoffmann, *GDOES-Analyse ultraduenner Schichten mit verbesserter Hardware*, Wissenschaftliches Kolloquium des Institutes fuer Werkstoffkunde der TU Darmstadt, 1.7.10 (2010).
126) K. Iida, K. Nenkov, G. Fuchs, G. Krabbes, L. Schultz, B. Holzapfel, *Cost-effective processing: Recycling of large single grain Gd-Ba-Cu-O/Ag bulk superconductors*, PASREG 2010, Washington D.C./ USA, 29.-31.7.10 (2010).
127) V. Kataev, *Magnetic resonance excitations in the heavy fermion compound YbRh2Si2*, Seminar of the Physics Department, Seoul National University, Seoul/ Korea, 7.10.10 (2010).
128) V. Kataev, *Broad band sub-THz ESR spectroscopy at the IFW Dresden: Application to correlated magnetic oxides*, DFG-Rundgespraech: New frontiers in electron spin resonance methodology, Hirschegg/ Oesterreich, 8.-12.9.10 (2010).
129) V. Kataev, *Probing the spin states in magnetically active coordination complexes by multifrequency high field ESR spectroscopy*, Asia-Pacific EPR/ ESR Symposium 2010, Jeju/ Korea, 10.-15.10.10 (2010).
130) V. Kataev, *High field multifrequency electron spin resonance spectroscopy on single molecule magnets*, IV Euro-Asian Symposium „Trends in Magnetism", Ekaterinburg/ Russia, 28.6.-2.7.10 (2010).
131) V. Kataev, *Electron spin resonance spectroscopy: Basic principles and some modern applications*, Seminar of the Physics Department, Chung-Ang University, Seoul/ Korea, 6.10.10 (2010).

132) V. Kataev, *Unveiling spin polarons in the doped LaCoO3 perovskite*, Condensed Matter Seminar, Institute of Physics, RWTH Aachen, 11.2.10 (2010).
133) V. Kataev, *Probing collective spin states in cubic cobaltates by high-frequency ESR spectroscopy*, International Workshop on Terahertz Spectroscopy and its high-field Applications, FZ Dresden-Rossendorf, 14.-15.6.10 (2010).
134) V. Khavrus, E.M.M. Ibrahim, A.A.M. Elgendy, S. Hampel, A. Leonhardt, B. Buechner, *Synthesis, properties and applications of carbon nanostructures*, Optics and High Technology Material Science - SPO 2010, Faculty of Physics of Taras Shevchenko National University of Kyiv, Kiew/ Ukraine, 21.-24.10.10 (2010).
135) S. Kiravittaya, O.G. Schmidt, *Rolled-up resonators for on-chip applications*, Fifth International Conference on Materials Science and Condensed Matter Physics, Chisinau/ Republic of Moldova, 13.-17.9.10 (2010).
136) D. Klemm, U. Kuehn, J. Eckert, *Selektives Laserstrahlschmelzen - generative Fertigung 3dimensional komplex gestalteter Formkoerper*, MBZ Institutsseminar, Dresden, 19.4.10 (2010).
137) D. Klemm, R. Taranczewski, V. Hoffmann, U. Kuehn, J. Eckert, *3D Laserstrahlschmelzen – Technologie fuer die generative Fertigung und Anwendung in der Materialforschung*, Institutsseminar vom Fraunhofer Institut fuer Werkstoff- und Strahltechnik, Dresden, 26.4.10 (2010).
138) R. Klingeler, *Carbon-caged nanomaterials for biomedical applications*, World Conference of Nanomedicine and Drug Delivery, Kottayam/ India, 16.-18.4.10 (2010).
139) R. Klingeler, *Fundamental properties and biomedical applications of carbon-coated nanomagnets*, 4th Seeheim Conference on Magnetism, Frankfurt, 28.3.-1.4.10 (2010).
140) R. Klingeler, *Functional magnetic nanomaterials: From fundamental research towards applications*, The 23rd General Conference of the Condensed Matter Division of the European Physical Society, Warschau/ Polen, 30.8.-3.9.10 (2010).
141) R. Klingeler, *Functional magnetic nanomaterials: From fundamental research towards applications*, Seminar Talk, LMU Muenchen, 24.4.10 (2010).
142) R. Klingeler, *Kathodenmaterialien fuer Lithium-Ionen-Batterien*, Veranstaltung: Ideas to Market - Dresdner Materialinnovationen fuer die Praxis, Dresden, 15.1.10 (2010).
143) A. Kordyuk, *ARPES of 2D metals*, Invited talk at University of Exeter/ UK, 20.-21.4.10 (2010).
144) P. Kratzer, V.M. Fomin, B. Huelsen, M. Scheffler, *Modeling materials with optimized transport properties*, Fifth International Conference on Multiscale Materials Modeling (MMM2010), Freiburg, 4.-8.10.10 (2010).
145) T. Kroll, *Determination of the spin and orbital ground state of transition metal phthalocyanines*, Seminar, Uni Duisburg, AG Wende, Duisburg, 14.-15.6.10 (2010).
146) U. Kuehn, *Herstellung, Eigenschaften und Anwendungen massiver metallischer Glaeser und Komposite*, Symposium „Leichtbauwerkstoffe auf Nanobasis", Erding bei Muenchen, 5.5.10 (2010).
147) G. Lang, *Probing the local properties of correlated electron systems: application to cobaltates and iron pnictides*, Invited Seminar, University of Zagreb/ Croatia, 1.6.10 (2010).
148) J. Liu, *Magnetic shape memory alloys and related phenomena*, Colloquium, The Chair of Magnetofluiddynamics, TU Dresden, 12.5.10 (2010).
149) J. Liu, *Development of new magnetic shape memory alloys*, Peking University, Department of Advanced Materials and Nanotechnology, Beijing/ China, 26.3.10 (2010).
150) J. Liu, S. Weiss, N. Scheerbaum, O. Gutfleisch, *Recent progress of magnetic shape memory composites*, JEMS 2010, Krakow/ Poland, 24.8.10 (2010).
151) W. Loeser, *Solidification of undercooled Al-Ni melts*, Kollquium, Department of Applied Physics, NPU Xian, Xian/ PR China, 7.12.10 (2010).
152) W. Loeser, *Equilibrium and metastable solidification of Ti-Al-Nb intermetallic alloys*, Kollquium, Department of Applied Physics, NPU Xian, Xian/ PR China, 7.12.10 (2010).
153) W. Lorenz, *Dynamics of the frustrated, quasi-one-dimensional model compound Li2Cu02*, Seminar-Vortrag, Institute for Solid State Physics at ETH Zuerich/ Switzerland, 13.12.10 (2010).
154) N. Mattern, U. Vainio, J.M. Park, J.H. Han, A. Shariq, D.H. Kim, J. Eckert, *Liquid-liquid phase separation and structure formation of Cu46Zr47-xAl7Gdx metallic glasses*, 17th International Symposium on Metastable, Amorphous and Nanostructured Materials ISMANAM 2010, Zurich/ Switzerland, 4.-9.7.10 (2010).
155) Y.F. Mei, *Inorganic nanomembranes*, Seminar, Institute of Physics, Humboldt Universitaet Berlin, 17.5.10 (2010).
156) Y.F. Mei, *Inorganic nanomembranes*, Seminar, City University of Hong Kong, PR China, 29.5.10 (2010).
157) Y.F. Mei, *Rolled-up inorganic nanomembranes*, MRS Spring Meeting, San Francisco/ USA, 5.-9.4.10 (2010).
158) Y.F. Mei, O.G. Schmidt, *Shaping nanomembrane technologies*, International Conference on Solid-State and Integrated Circuit Technology (ICSICT), Shanghai/ China, 1.-4.11.10 (2010).
159) Y.F. Mei, O.G. Schmidt, *Shaped nanomembranes: From fundamental perception to new concepts and applications*, IEEE International NanoElectronics Conference, Hong Kong/ China, 3.-8.1.10 (2010).

160) Y.F. Mei, O.G. Schmidt, *Materials science of functional nanomembranes: From flexible magnetoelectronics to world's smallest jet engines*, Shanghai Institute of Microsystem and Information Technology, Chinese Academy of Sciences, Shanghai/ China, 4.11.10 (2010).
161) A. Moebius, *Phenomenological aspects of the metal-insulator transition in disordered systems: So,was Mott right after all?*, Solid State Seminar, University of Minnesota, School of Physics and Astronomy, Minneapolis/ USA, 6.4.10 (2010).
162) A. Moebius, *Remarks on heuristic combinatorial optimisation*, Workshop Energy Landscapes 2010, Chemnitz, 23.6.-3.7.10 (2010).
163) A. Moebius, *Indications for finite-temperature phase transitions connected with the apparent metal-insulator transition in 2D systems*, Conference Out of Equilibrium Quantum Systems, Santa Barbara/ USA, 23.-27.8.10 (2010).
164) A. Moebius, *Coulomb gap numerics*, Workshop Electronic Glasses, Institute of Advanced Studies, Hebrew University Jerusalem/ Israel, 23.-27.5.10 (2010).
165) J. Moore, O. Gutfleisch, *Solid state energy efficient magnetic cooling*, Gordon Research Conference Magnetic Nanostructures, Bates College, ME/ USA, 8.-13.8.10 (2010).
166) T. Muehl, *Magnetische und mechanische Eigenschaften von eisengefuellten Kohlenstoff-Nanoroehren sowie vielversprechende Anwendungen dieser stabilen Nanomagnete*, Institutsseminar, Fraunhofer IWS Dresden, 8.11.10 (2010).
167) S. Nishimoto, *Quasi-1d quantum helimagnets: The fate of multipolar phases*, International Workshop on DMRG and other Advances in Numerical RG Methods, Beijing/ China, 2.9.10 (2010).
168) C. Patschureck, *Beobachtung statischer und dynamischer Magnetisierungsprozesse*, Robert Bosch GmbH, Automotive Electronics (AE/EST1), Reutlingen, 16.2.10 (2010).
169) R. Pfrengle, *Interkulturelles Leben an Leibniz-Einrichtungen*, Verwaltungsausschuss der Leibniz-Gemeinschaft, UFZ Leipzig, 22.-23.4.10 (2010).
170) D. Pohl, F. Schaeffel, E. Mohn, C. Taeschner, M.H. Ruemmeli, C. Kisielowski, L. Schultz, B. Rellinghaus, *Exploring the metal-carbon interface in magnetically terminated carbon nanotubes*, 21. Edgar-Luescher-Seminar, Klosters/ Schweiz, 6.-11.2.10 (2010).
171) A. Rastelli, *Positioning and stressing self-assembled quantum dots*, Seminar, Photonics and Semiconductor Nanophysics, TU Eindhoven/ The Netherlands, 10.6.10 (2010).
172) A. Rastelli, *Looking at self-assembled quantum dots from different perspectives*, The 2010 Villa Conference on Interaction Among Nanostructures (VCIAN), Santorini/ Greece, 21.-25.6.10 (2010).
173) A. Rastelli, *Stress as fabrication and post-fabrication tuning tool for quantum dots*, InfraRed Optical Nanostructure Symposium, Wien/ Austria, 8.-9.4.10 (2010).
174) A. Rastelli, *Fabrication and post-fabrication tuning of quantum dots by stress*, Seminar, Universita di Milano Bicocca, Milano/ Italy, 2.3.10 (2010).
175) A. Rastelli, *Cross-plane thermal conductivity measurements of thin Si layers with embedded Ge dots*, SPP 1386 Workshop on Thermal Conductivity in Reduced Dimensions: 3 Omega method and beyond, Goettingen, 27.-28.5.10 (2010).
176) A. Rastelli, *Making and changing quantum dots by stress*, Transalp Nano 2010, Como/ Italy, 3.-5.6.10 (2010).
177) A. Rastelli, *Scattering phonons and trapping excitons with self-assembled quantum dots*, Colloquium, TU Chemnitz, 14.4.10 (2010).
178) A. Rastelli, *Adding functionalities to quantum dot heterostructures and devices by stress*, Sonderkolloquium, TU Berlin, 22.12.10 (2010).
179) A. Rastelli, O.G. Schmidt, *Thermoelectrics of SiGe: From bulk to nanostructures*, Thermoelectrics Winter School, Bremen, 14.-19.2.10 (2010).
180) B. Rellinghaus, D. Pohl, U. Wiesenhuetter, E. Mohn, F. Schaeffel, U. Queitsch, L. Schultz, *The relevance of surfaces and interfaces for the properties of metallic nanomagnets*, Kolloquium, Leibniz-Institut fuer Neue Materialien, Saarbruecken, 23.6.10 (2010).
181) B. Rellinghaus, D. Pohl, U. Wiesenhuetter, E. Mohn, L. Schultz, *The relevance of surfaces and interfaces for the properties of metallic nanomagnets*, Seminar der Arbeitsgruppen Prof. M. Albrecht und Prof. P. Heussler, TU Chemnitz, 8.6.10 (2010).
182) M. Richter, *Quantitative predictions by electronic structure theory*, Seminar, Department of Condensed Matter Physics, Charles University, Prague/ Tschechien, 1.12.10 (2010).
183) M. Richter, *Quantitative predictions by electronic structure theory: Large magnetocaloric response and huge magnetic anisotropy*, Seminar am Institut de Chimie et des Materiaux Paris-Est/ Frankreich, 14.4.10 (2010).
184) M. Richter, *Relativistic effects in atoms, molecules, and solids: overview and recent applications*, Density Functional Theory and Beyond with Numeric Atom-Centered Orbitals. FHI-aims Developers' and Users' Meeting, Fritz Haber Institut, Berlin, 17.-19.5.10 (2010).
185) U.K. Roessler, A.A. Leonov, A.B. Butenko, A.N. Bogdanov, *Skyrmions in chiral magnets*, DPG Fruehjahrstagung 2010, Hauptvortrag Fachverband Magnetismus, Regensburg, 21.-26.3.10 (2010).
186) U.K. Roessler, A.A. Leonov, A.B. Butenko, A.N. Bogdanov, *Skyrmionic and vortex states in chiral magnetic materials*, Fourth Seeheim Conference on Magnetism, Frankfurt, 28.3.-1.4.10 (2010).
187) M. Ruemmeli, *Rethinking carbon nanotube and graphene growth*, Centre for Applied Physics and Advanced Technology, Queretaro/ Mexico, 9.4.10 (2010).

188) M. Ruemmeli, *Opportunities for Academics and Students in Germany*, National Autonomous University Mexico, Queretaro/ Mexico, 8.-9.4.10 (2010).
189) M. Ruemmeli, A. Bachmatiuk, F. Boerrnert, B. Buechner, *Rethinking carbon nanotube and graphene growth*, Invited Lecture, 1st International Conference on Nantechnology, Quito/ Ecuador, 14.-18.6.10 (2010).
190) M.H. Ruemmeli, *The rise of ceramic catalysts for carbon nanotube and graphene growth*, Conference Trends in Nanotechnology (TNT 2010), Braga/ Portugal, 8.-10.9.10 (2010).
191) M.H. Ruemmeli, *Rethinking carbon nanotube and graphene growth*, Vortrag in Triest/ Italien, 26.3.2010 (2010).
192) M.H. Ruemmeli, *Rethinking carbon nanotube growth*, Edgar Luescher Seminar 2010, Klosters/ Schweiz, 6.-10.2.10 (2010).
193) S. Sanchez, *Wireless control of catalytic microbots for the delivery and assembly of microobjects*, MANA International Symposium, Tsukuba/ Japan, 3.-5.3.10 (2010).
194) S. Sanchez, *Microbots*, SciArt NanoLab 2010, UCLA, Los Angeles/ USA, 30.6.10 (2010).
195) S. Sanchez, *Nanobiochemical applications of nanomembranes: From microbots to on-chip sensors*, Seminar, CIN2, Research Center for Nanoscience and Nanotechnology, Barcelona/ Spain, 12.12.10 (2010).
196) S. Sanchez, *Microbots as nanotechnology tools. Catalytic nanomachines*, Seminar, UCLA, Los Angeles/ USA,15.03.10 (2010).
197) S. Sanchez, *Catalytic and biocatalytic locomotion of rolled-up microbots*, Mini-Workshop on SPM and Bio-Nano, Tsukuba/ Japan, 10.3.10 (2010).
198) S. Sanchez, *Catalytic and biocatalytic tubular microjets*, Seminar, Chemistry Department, Penn State University, Pennsylvania/ USA, 17.3.10 (2010).
199) R. Schaefer, *Die magnetische Mikrostruktur von Elektroblech*, Seminarvortrag am Fraunhofer IWS, Dresden, 14.6.10 (2010).
200) R. Schaefer, *Giant negative domain wall resistance*, 14th Czech and Slovak Conference on Magnetism, Kosice/ Slovakia, 6.-9.7.10 (2010).
201) R. Schaefer, *Magnetische Mikrostrukturen*, Schuelervortrag, Annengymnasium in Goerlitz, 19.4.10 (2010).
202) R. Schaefer, *On the magneto-optical gradient effect*, Workshop Spin and Charge at the nanoscale 2010: 45 Years, Burnaby, British Columbia/ Canada, 1.-4.8.10 (2010).
203) R. Schaefer, D. Elefant, *Giant negative domain wall resistance*, Workshop: Spin and Charge at the Nanoscale, 1010: 45 Years of Magnetism at Simon Fraser University, Burnaby/ Kanada, 1.-4.8.10 (2010).
204) N. Scheerbaum, *Alternative Konzepte fuer die Nutzung des magnetischen Formgedaechtniseffektes*, Institutsseminar, Institut fuer Strukturphysik, TU Dresden, 18.5.10 (2010).
205) O.G. Schmidt, *Nanomembranes: Shaping a new technology*, Tutorial, TU Chemnitz, 23.11.10 (2010).
206) O.G. Schmidt, *Men-made multifunctional micro-/nanoengines*, Symposium on Molecular and Nanoscopic Autonomous Systems, Max-Planck-Institute for Metals Research, Stuttgart, 20.1.10 (2010).
207) O.G. Schmidt, *Ultra-thin membranes: Shaping a new nanoworld*, Seminar, Bio Innovations Center Dresden, 15.11.10 (2010).
208) O.G. Schmidt, *Inorganic and hybrid nanomembranes: From quantum dot photonics to world`s smallest jet engines*, Colloquium, Universitaet Kassel, 26.11.10 (2010).
209) O.G. Schmidt, *Photonics with stretchable and shapeable nanomembranes*, Seminar, Massachusetts Institute of Technology (MIT), Cambridge/ USA, 30.11.10 (2010).
210) O.G. Schmidt, *Chemistry, physics and technology of functional hybrid nanomembranes*, Colloquium, Gesellschaft Deutscher Chemiker e.V., Oldenburg, 11.11.10 (2010).
211) O.G. Schmidt, *Nanostructures under stress: From quantum dots to micro-engines*, Festkolloquium, Johannes Kepler Universitaet, Linz/ Oesterreich, 1.10.10 (2010).
212) O.G. Schmidt, *Hybrid nanomembranes: From quantum dots to nanojet engines*, Seminar, The University of Texas, Austin, Texas/ USA, 27.9.10 (2010).
213) O.G. Schmidt, *Spatial and spectral control of individual quantum dots*, SPIE, Photonics West, San Francisco/ USA, 23.-28.1.10 (2010).
214) O.G. Schmidt, *Kuenstliche Nanomaschinen – auf dem Weg zur „Reise ins Ich"*, 19. Frankfurter Sonderkolloquium – Technik und Gesellschaft im Dialog, Dechema, Frankfurt/ M., 28.1.10 (2010).
215) O.G. Schmidt, *Catalytic microtube engines*, IEEE International Conference on Robotics and Automation (ICRA), Anchorage, Alaska/ USA, 3.-8.5.10 (2010).
216) O.G. Schmidt, *Elastic nanomembranes for interdisciplinary research*, Seminar, University of Wisconsin, Madison/ USA, 23.6.10 (2010).
217) O.G. Schmidt, *Quantum dots and smart tubes for on- and off-chip applications*, Colloquium, Leibniz-Institut fuer Innovative Mikroelektronik Frankfurt (Oder), 9.3.10 (2010).
218) O.G. Schmidt, *Nanoraketen*, Nano erleben, Nanotechnologie - Demonstrationsversuche fuer die Oberstufe, Marburg, 11.3.10 (2010).
219) O.G. Schmidt, *The physics of inorganic and hybrid nanomembranes*, Physics Colloquium, The University of Utah, Salt Lake City/ USA, 2.12.10 (2010).

220) O.G. Schmidt, *Inorganic nanomembranes for photonic, electronic, fluidic and robotic applications*, Seminar, Helmholtzzentrum, Berlin, 22.4.10 (2010).
221) O.G. Schmidt, *Hybrid nanomembranes fo photonics, electronics, and robotics*, SFG Meeting "From local constraints to macroscopic transport", Dresden, 28.4.10 (2010).
222) O.G. Schmidt, *Stretchable, flexible, and shapeable nanomembranes for interdisciplinary research*, Seminar, The University of Utah, Salt Lake City/ USA, 26.8.10 (2010).
223) O.G. Schmidt, *Planar and vertical ring resonators: From physics to optofluidic studies*, 3rd Asian-German Workshop on Optical Microcavities: Quantum Chaos in Open Systems Meets Optical Resonators, Dresden, 17.-21.5.10 (2010).
224) O.G. Schmidt, *Multifunctional „lab-in-a-tube" systems and self-propelled micro- / nanoengines*, Seminar on New Developments in Biological Physics, University of Gothenburg/ Sweden, 20.5.10 (2010).
225) O.G. Schmidt, *Strained nanostructures for interdisciplinary research*, Sonderkolloquium, Walter-Schottky-Institut, Muenchen, 14.12.10 (2010).
226) O.G. Schmidt, *Physics and technology of inorganic and hybrid nanomembranes*, Seminar, Johannes Kepler Universitaet Linz/ Austria, 9.6.10 (2010).
227) O.G. Schmidt, *Selected scientific aspects of inorganic and hybrid nanomembranes*, Seminar, Universitaet Konstanz, 7.6.10 (2010).
228) O.G. Schmidt, *Physics and technology of stressed quantum dots*, MRS Fall Meeting, Boston/ USA, 29.11.-3.12.10 (2010).
229) O.G. Schmidt, *Engineering autonomous systems at the micro-/nanoscale*, Graduate Seminar, The University of Utah, Salt Lake City/ USA, 27.8.10 (2010).
230) O.G. Schmidt, *Physics, materials science and applications of nanomembranes*, Fifth International Conference on Materials Science and Condensed Matter Physics, Chisinau/ Republic of Moldova, 13.-17.9.10 (2010).
231) O.G. Schmidt, *Quantum dots and smart tubes: From artificial atoms to artificial machinery*, Sonderkolloquium, Universitaet Wuerzburg, 20.12.10 (2010).
232) O.G. Schmidt, *Fabrication, manipulation and properties of 3D quantum dot crystals*, 30th International Conference on the Physics of Semiconductors (ICPS), Seoul/ Korea, 25.-30.7.10 (2010).
233) R. Schoenfelder, *Synthesis, purification and characterisation of SWCNT, diameter control and growth mechanism*, Yucatan Centre for Scientific Research, Yucatan/ Mexico, 27.10.10 (2010).
234) L. Schultz, *Vom Schweben auf Magnetfeldern: Die wundersame Welt der Supraleiter*, Science Slam, Festsaal der TU Dresden, 22.11.10 (2010).
235) L. Schultz, *Vom Schweben auf Magnetfeldern: - Spur-gebundene Verkehrssysteme*, Cusanuswerk - Fachschaftstag Physik, Dresden, 16.10.10 (2010).
236) L. Schultz, *Contactless levitation systems using bulk superconductors*, Plenarvortrag, ICEC 23 - ICMC 2010, Wroclaw/ Polen, 20.7.10 (2010).
237) L. Schultz, *Vom Schweben auf Magnetfeldern: Die wundersame Welt der Supraleitung*, Festvortrag, Hoersaaleinweihung des Instituts fuer Werkstoffwissenschaften, Universitaet, Erlangen-Nuernberg, 15.7.10 (2010).
238) L. Schultz, *Vom Schweben auf Magnetfeldern - Die wundersame Welt der Supraleitung*, Oeffentlicher Abendvortrag, Semper-Salon Dresden, 23.6.10 (2010).
239) L. Schultz, *Supraleitende Systeme*, Dresdner Werkstoffsymposium, Dresden, 9.-10.12.10 (2010).
240) L. Schultz, *Vom Schweben auf Magnetfeldern: Die wundersame Welt der Supraleitung*, Ferienschule „Theoria cum Praxi", Dresden, 11.-14.10.10 (2010).
241) L. Schultz, *Riding on magnetic fields - the miraculous world of superconductors*, Plenarvortrag, Junior EUROMAT 2010, Lausanne/ Schweiz, 26.-29.7.10 (2010).
242) J. Schumann, M. Stordeur, *Potenziale thermoelektrischer Generatoren zur Elektroenergieerzeugung*, Abschlusspraesentation zur Thermoelektrik-Trendstudie, EnBW Energie Baden-Wuerttemberg AG, Karlsruhe, 14.7.10 (2010).
243) U. Siegel, U. Kuehn, J. Eckert, *Metallische Glaeser und Komposite - Herstellung, Eigenschaften und Applikationen*, Material Forum des Materials Valley e.V., Vacuum Schmelze Hanau, 15.3.10 (2010).
244) K. Skokov, J. Liu, M. Krautz, J. Moore, O. Gutfleisch, *Adiabatic temperature change and magneto-volume effect in La-Fe-Si bulk, melt-spun and hydrogenated compounds*, MRS Fall Meeting 2010, Boston/ USA, 28.11.-2.12.10 (2010).
245) E.J. Smith, S. Schulze, S. Kiravittaya, Y.F. Mei, S. Sanchez, O.G. Schmidt, *Towards Lab-in-a-Tube: Individual cell manipulation and detection in a single on chip microtube optical ring resonator*, NanoBioTech, Montreux/ Switzerland, 15.-17.11.10 (2010).
246) K. Tschulik, J.A. Koza, M. Uhlemann, A. Gebert, L. Schultz, *Influence of magnetic gradient fields on the electrodeposition of metallic layers*, Gastvortrag am Institut für Stroemungsmechanik und Aerodynamik der Uni der Bundeswehr Muenchen, 18.3.10 (2010).
247) K. Tschulik, M. Uhlemann, A. Gebert, J. Koza, R. Sueptitz, L. Schultz, *Effects of magnetic fields on electrochemical processes*, Institutsseminar, University of Virginia, Charlottsville/ USA, 19.7.10 (2010).
248) M. Uhlemann, *Magnetoelectrochemistry*, Graduiertenkolleg MHD, TU Ilmenau, 1.6.10 (2010).
249) J. van den Brink, *Elementary excitations probed by resonant inelastic X-ray scattering*, Physics Seminar, Rijksuniversiteit Groningen/ The Netherland, 29.4.10 (2010).

250) J. van den Brink, *Resonant x-rays on correlated matter*, Theory Colloquium TU Dresden, 15.4.10 (2010).
251) J. van den Brink, *Resonant x-rays on correlated matter*, Antrittsvorlesung, TU Dresden, 18.5.10 (2010).
252) J. van den Brink, *Elementary excitations probed by resonant inelastic X-ray scattering*, Physics Colloquium, University of Dortmund, 11.5.10 (2010).
253) J. van den Brink, *Iron superconductors: Breaking the high Tc rules*, FOM Meeting, Iron Pnictide Focus Session, Veldhoven/ The Netherlands, 19.1.10 (2010).
254) J. van den Brink, *Resonant x-rays on correlated matter*, Physics Seminar, Max Planck Institute Stuttgart, 30.6.10 (2010).
255) J. van den Brink, *Elementary magnetic excitations probed by RIXS*, Physics Seminar, Nat. Synchrotron Radiation Research Center, Hsinchu/ Taiwan, 30.7.10 (2010).
256) J. van den Brink, *Resonant x-rays on correlated matter*, Meeting of the Swiss Physical Society, Basel/ Switzerland, 21.6.10 (2010).
257) J. van den Brink, *The role of correlations in iron pnictide superconductors*, Edgar Luescher Seminar, Klosters/ Switzerland, 7.2.10 (2010).
258) J. van den Brink, *Resonant inelastic X-ray scattering*, 1st Summer School on X-ray Science, Sun-Moon Lake/ Taiwan, 2.8.10 (2010).
259) J. van den Brink, *Elementary magnetic excitations probed by RIXS*, VUV/X Satellite Meeting on RIXS, Saskatoon/ Canada, 9.7.10 (2010).
260) J. van den Brink, *Multiferroicity due to charge ordering*, CIMTEC 2010, 5th Forum on New Materials, Montecatini Terme/ Italy, 10.6.10 (2010).
261) K. Wetzig, *Application of Ion beams in materials science*, Vortragsreihe an der Slovakischen TU Bratislava/ Slovakische Republik, 31.5.-4.6.10 (2010).
262) K. Wetzig, *50 Jahre Elektronenmikroskopie in Dresden - Von den Wurzeln bis zur Gegenwart*, Physikalisches Kolloquium, TU Dresden, 23.11.10 (2010).
263) N. Wizent, G. Behr, W. Loeser, B. Buechner, *Challenges in the crystal growth of Li2CuO2 and LiMnPO4*, International Crystal Growth Conference, Beijing/ China, 8.-15.8.10 (2010).
264) T.G. Woodcock, G. Hrkac, T. Schrefl, N.M. Dempsey, D. Givrod, O. Gutfleisch, *Novel approaches to microstructural characterisation in NdFeB materials*, 21st Workshop on Rare Earth Permanent Magnets and their Applications (REPM'10), Bled/ Slovenia, 29.8.-2.9.10 (2010).
265) S. Wurmehl, *Heusler compounds for spintronics*, Vortrag an der Universitaet Koeln, 19.5.10 (2010).

Patents

Issues of Patents 2010

DE 103 39 865 Temperaturstabiler Oszillator auf der Basis akustischer Oberflächenwellen
Inventors: G. Martin, M. Weihnacht

DE 103 57 264 Einrichtung zur Erzielung von Fahrtrichtungsänderungen für supraleitende Magnetschwebesysteme
Inventors: O. de Haas, C. Beyer, L. Schultz

DE 10 2005 005 706 Magnetschwebevorrichtung
Inventors: C. Beyer, O. de Haas, T. Riederich, L. Schultz

DE 10 2005 005 704 Verwendung von Partikeln für die Ermittlung der lokalen Temperatur in organischen und nichtorganischen Körpern
Inventors: B. Büchner, R. Klingeler, A. Leonhardt, J. Haase et. al.

DE 10 2006 016 229 Verfahren und Vorrichtung zur simultanen Ermittlung von Höhenunterschieden und Zusammensetzungen mittels Glimmentladungsspektroskopie
Inventor: V. Hoffmann

DE 10 2007 038 280 Aktuator und Verfahren zu seiner Herstellung
Inventors: S. Menzel, H. Schmidt

DE 10 2008 000 292 Röhrenförmiger Multifunktionssensor in Flüssigkeiten, Verfahren zu seiner Herstellung und Verwendung
Inventors: O. G. Schmidt, E. Bermudez, Y. Mei

DE 10 2008 040 930 Verfahren zur Herstellung von dotierten Vanadiumoxid-Nanoröhren
Inventors: G. Zakharova, C. Täschner, A. Leonhardt et. al.

DE 10 2008 026 009 Verfahren zur Bestimmung der Viskosität und Elastizität von viskoelastischen Medien
Inventors: R. Brüning, M. Weihnacht, H. Schmidt

Patent Applications 2010

11002 Verfahren und Anordnung zur Manipulation von in einem magnetischen Medium gespeicherten Domäneninformationen
Inventor: R. Schäfer

11003 Elektrodenmaterial und seine Verwendung zur Herstellung von elektrochemischen Zellen
Inventors: H. Ehrenberg, F. Scheiba, M. Herklotz et. al.

11006 Wandler mit natürlicher Unidirektionalität für akustische Oberflächenwellen
Inventor: G. Martin, S. Biryukov et. al.

11007 Verfahren und Anordnung zur Anregung von Spinwellen in magnetischen Festkörpern
Inventor: R. Schäfer

11009 Hochfeste, bei Raumtemperatur plastisch verformbare und mechanische Energie absorbierende Formkörper aus Eisenlegierungen
Inventors: U. Kühn, J. Eckert, U. Siegel, J. Hufenbach et. al.

11010 Neues Lithium-metall-phosphat
Inventors: H. Ehrenberg, F. Scheiba, M. Herklotz et. al.

21011 Kurbelarm
Inventors: D. Klamm, R. Taranczewski

11012 Magnetisches Speichermedium
Inventors: M. Richter

11013 Production Method of Rare Earth Magnet
Inventors: T. Woodcock, O. Gutfleisch et. al.

11014 Atomic-Layer-Deposition (ALD) für mikroakustische Bauteile
Inventors: S. Menzel, M. Spindler et. al.

11015 Bauelement auf der Basis akustischer Oberflächenwellen
Inventor: G. Martin et. al.

11016 Verwendung eines seltenerdmetallfreien Stoffes als magnetokalorisch aktives Material
Inventors: M. Richter, M. Kuz'min

11017 Verfahren zur Wärmebehandlung von hochfesten Eisenlegierungen
Inventors: J. K. Hufenbach, J. Eckert, U. Kühn, S. Kohlar

11018 Oberflächenstrukturierte metallische Gläser und Verfahren zur Herstellung
Inventors: B. Jerliu, J. Eckert, S. Scudino, K.- B. Surreddi, S. Pauly

Habilitations, PhD and diploma theses 2010

Habilitation

Prof. Dr. Jürgen Eckert	Metastabile Phasen in mehrkomponentigen Systemen, TU Dresden

PhD theses

Glen Guhr	Mikroakustische und elektrische Charakterisierung komplexer biologischer Fluide
Tetyana Shapoval	Local imaging of magnetic flux in superconducting thin films
Roman Schuster	Electron Energy-Loss Spectroscopy on Underdoped Cuprates and Transition-Metal Dichalcogenides
Markus Löffler	Nanomanipulation and In-situ Transport Measurements on Carbon Nanotubes
Mohammed El Bahrawy	High field electron magnetic resonance in complex correlated spin systems
Olga Shuleshova	Equilibrium and metastable solidification in Ti-Al-Nb and Al-Ni systems
Cristina Bran	Domain structure and magnetization processes of complex multilayers
Jörg Buschbeck	Stabilisierung martensitischer Strukturen mittels epitaktischen Wachstums ungeordneter Eisen-Palladium Schichten und deren magnetische Eigenschaften
Martina Cornelia Dekker	Phase-separated manganites - The effect of reversible elastic lattice strain on the electronic properties
Alexander Gaganov	Hochfeste und hochleitfähige Cu-Ag-Leitermaterialien
Julia Lyubimova	Einfluss thermomechanischer Behandlung auf die Struktur-Eigenschaftsbeziehung von CuAgZr-Legierungen
Jacub Adam Koza	Electrocrystallization of CoFe Alloys under the Influence of External Homogeneous Fields
Tetyana Shapoval	Local imaging of magnetic flux in superconducting thin filmsKatarzyna Werniewicz: Fe-based composite materials with advanced mechanical properties
Liran Wang	Thermal Expansion and Magnetostriction Studies on Iron Pnictides
Nikolai Kyselov	Phenomenological theories of magnetic multilayers and related systems
Jorge E. Hamann Borrero	X-ray studies of magnetism and electronic order in Fe-based materials
Christine Hamann	Magnetische Hybridschichten - Magnetische Eigenschaften lokal austauschgekoppelter NiFe/IrMn-Schichten
Ute Queitsch	Nanopartikel – Substrat – Wechselwirkungen
Tim Niemeier	Supraleitung in biaxial texturierten Seltenerd-Nickel-Borkarbidschichten
Claudia Apetrii	YBa2Cu3O7-x thin films prepared by Chemical Solution Deposition
Julia Lyubimova	Einfluss thermomechanischer Behandlung auf die Struktur-Eigenschaftsbeziehungen von CuAgZr-Legierungen
Katarzyna Werniewicz	Fe-based composite materials with advanced mechanical properties
Uwe Siegel	Strukturelle thermische und mechanische Charakterisierung von amorphen Eisenbasislegierungen und Glasmatrixkompositen
Valentin Kokotin	Polyhedra-based analysis of computer simulated amorphous structures
Simon Pauly	Phase formation and mechanical properties of metastable Cu-Zr-based alloys
Narendirakumar Narayanan	Physical properties of double perovskites La2-xSrxCoIrO6 ($0 \leq x \leq 2$)

Diploma, master and bachelor theses

Mariann Banki	Hybridmaterialien aus Übergangsmetalloxiden und metallischen Schäumen zur elektrochemischen Energiespeicherung, HTW Dresden
Christian Behler	Fe-Pt-Schichten als Modellsystem für magnetisches Schalten und magnetokristalline Anisotropie, TU Dresden
Björn Bieniek	Oberflächennahe Gitterstruktur von Übergangsmetall-Nanopartikeln, TU Dresden
Juliana Brunzlaff	Konstruktion eines Rastertunnelmikroskops, TU Dresden
Daniel Eichner	Mikrostrukturelle und mechanische Charakterisierung von hochfesten Aluminium-Basislegierungen hergestellt über Pulvermetallurgie, TU Dresden
Jan Engelmann	Herstellung und Charakterisierung von nbN/SmCo5 Bilagen, TU Dresden
Andy Fiedler	Untersuchungen zur elektrokatalytischen Bildung von Li2O2 an Kohlenstoff-basierten Elektroden (Bachelor), Hochschule Lausitz
Kathleen Fischer	Einfluss von strukturellen Merkmalen von CAE PVD beschichteten Werkzeugen auf die Schneidleistung, TU Dresden
Felix Fleischhauer	Koerzitivfeldstärkemechanismus in gekoppelten SmCo5/PrCox Schichten, TU Dresden
Gerd Friemel	Transportmessungen an 122-Eisenarsenid-Supraleitern, TU Dresden

Ronald Gärtner	Entwicklung einer biaxial texturierten Pufferschichtarchitektur für metallische Substrate auf der Basis von IBAD-TiN, TU Dresden
Christian Geipel	$Mg_{0.69}Ni_{0.26}Ti_{0.05}$ for Solid State Hydrogen Storage: from Thin Film to Bulk, TU Dresden
Colin Georgi	Mn-Fe-Oxide als Konversionselektrode in Lithium-Ionen-Batterien, TU Dresden
Stefan Giron	Entwicklung und Aufbau eines Kerrmikroskops mit getrennten Strahlengängen, TU Dresden
Anna Grushina	Electron spin resonance spectroscopy on magnetically active polynuclear molecular complexes, TU Dresden (Master)
Arne Helth	Untersuchung zum Einfluss von Bor und Sauerstoff auf die mechanischen und strukturellen Eigenschaften der Legierung Ti66Nb13Ni6.8Al6.2Cu8, TU Dresden
Maik Hensel	Katalysatorentwicklung für die Synthese von SW/DWCNT s durch CVD, Hochschule Zittau/Görlitz
Julia Hufenbach	Mikrostrukturelle und mechanische Charakterisierung von Fe88,9Cr4,3V2,2C4,6 (at. %), TU Bergakademie Freiberg
Diana Iselt	Herstellung und Charakterisierung von FeGa Legierungsschichten, TU Dresden
Stefan Kaufmann	Epitaktische Schichten als Modellsystem für adaptiven Martensit in Ni-Mn-Ga, TU Dresden
Stefanie Kohlar	Mikrostrukturelle und mechanische Charakterisierung von Fe(CrMoVWC), TU Dresden
Julia Köhler	Untersuchungen der strukturellen und mechanischen Eigenschaften hochverformter Ti60Nb40-Legierungen, TU Dresden
Andreas König	Charge Density Waves and Plasmon Dispersion in the Transition-Metal Dichalcogenide 2*H*-$TaSe_2$, TU Dresden
Lukas Löber	Mechanische und thermische Charakterisierung einer rascherstarrten Fe84.3Cr4.3Mo4.6V2.2C4.6-Legierung, TU Dresden
Konrad Löwe	Investigation of the thermal decomposition reaction in the magnetocaloric system $La(Fe,Si,Co)_{13}$, TU Dresden
Benjamin Mahns	Elektronische Anregungen in dotiertem Mangan-Phthalocyanin, TU Bergakademie Freiberg
Katarina Manthey	NQR-Messungen an FeAs-Supraleitern, TU Dresden
Robert Niemann	Magnetostrukturelle Transformation in epitaktischen Ni-Co-Mn-In-Schichten, TU Dresden
Sven Partzsch	Structural and Magnetic Properties of Multiferroic Iron-doped Yttrium Manganate $YMn_{2-x}Fe_xO_5$, TU Dresden
Heike Pfau	Aufbau eines Systems für thermische Transportmessungen bis 300 mK, TU Dresden
Carmen Powik	Mikrostrukturelle und mechanische Charakterisierung von Fe84.4Cr4.3Mo4.6V2.2C4.6 und
Martin Queck	AlCuFe(Sn) quasicrystals as reinforcing agents for Al-based metal matrix composites: preparation, structure and mechanical properties, TU Dresden
Andreas Reisner	Herstellung und Charakterisierung von $NbFe_2$-Schichten, TU Dresden
Tobias Ritschel	Druckabhängige Untersuchung der elektronischen Ordnung 1T-TaS2, TU Dresden
Jan Romberg	Untersuchungen von geometrischen Einflussfaktoren auf die thermomechanischen Eigenschaften von Ni-Mn-Ga polykristallinen magnetischen Formgedächtnislegierungen, TU Dresden
Lotta Römhildt	Exploring novel concepts for magnetic hardening mechanisms of NdFeB, TU Dresden
Simon Sawatzki	Maximierung der Energiedichte magnetisch austauschgekoppelter SmCo5/Fe-Vielfachschichten mittels statistischer Prozessführung, TU Dresden
Thomas Schied	Phasenbildung und Magnetismus dünner Eisen-Palladium-Schichten auf amorphem Siliziumoxid, TU Dresden
Ronny Schlegel	Aufbau und Inbetriebnahme eines Eintauch-Rastertunnelmikroskops, TU Dresden
Christian Schmidt	Photoemissionsspektroskopie an Übergangsmetall-Phthalocyaninen, TU Dresden
Wolf Schottenhamel	Weiterentwicklung und Kalibrierung eines höchstauflösenden Dilatometers zur Messung der Magnetostriktion, FH Mittweida
Matthias Schrade	Elektronen-Energieverlust-Spektroskopie an $La_{1-x}Sr_{1+x}MnO_4$, TU Dresden
Michael Schulze	Synthese und Charakterisierung von supraleitenden Proben im System Eisen-Selen-Tellur, FH Jena
Christian Stieler	AC losses in superconducting YBCO double-pancake coils, TU Dresden
Evelyn Stilp	Bestimmung des Anisotropiefeldesvon SmCo5 in gepulsten Magnetfeldern bis 50T, TU Dresden
Robert Taranczewski	3D-Laserstrahlschmelzen – verfahrensgerechte Gestaltung, Burg Giebichenstein Hochschule für Kunst und Design Halle
Alexander Thomas	Untersuchung zur Synthese und den elektrochemischen Eigenschaften von Li3Ti(MO4)3, (M=Mo,W), HTW Dresden
Uwe Treske	Photoelektronenspektroskopie an hochgeordneten Phthalocyaninschichten, Friedrich-Schiller-Universität Jena
Henning Turnow	Mikrostruktur und mechanische Eigenschaften von FeCr(Mo)VC-Gusslegierungen, TU Dresden
Sandra Weiß	Ni2MnGa-Polymer-Komposite, TU Dresden
Susi Wintz	Photoelektronenspektroskopie an Grenzflächen zwischen $SrTiO_3$ und Metallen, TU Bergakademie Freiberg
Martin Zier	Ermüdung von Elektrodenmaterialien in unter Druck verbauten Lithium-Ionen-Batterien, TU Dresden

Calls and Awards 2010

Calls on Professorships

Dr. Yongfeng Mei	Fudan Univ. Shanghai
Prof. Dr. Bernd Büchner	Univ. Köln
Dr. Helmut Ehrenberg	Karlsruhe Institute of Technology
Dr. Helmut Ehrenberg	TU München (appointment offer)
Dr. Kathrin Dörr	Univ. Bonn
Dr. Kathrin Dörr	Univ. Halle

Appointments as Guest and Honorary professorships

Prof. Dr. Ludwig Schultz	Univ. Ulsan, South Korea (Fellow Professorship)
Dr. Oliver Gutfleisch	Imperial College London (Visiting Professorship)
Dr. Helmut Ehrenberg	TU Bergakademie Freiberg (Guest Professorship)
Dr. Bernhard Holzapfel	TU Bergakademie Freiberg (Guest Professorship)

Awards

Dr. Jens Freudenberger	Georg-Sachs-Preis der Deutschen Gesellschaft für Materialkunde
Dr.-Ing. Franziska Schäffel	Bertha Benz-Preis für junge Ingenieurinnen 2010
Dr. Simon Pauly	DGM Nachwuchspreis
Robert Taranczewski	Eurobike Award Students Category
Dr. Oliver Gutfleisch	IEEE Magnetics Society 2011 Distinguished Lecturer
Prof. Dr. Oliver G. Schmidt	Sachsen ASSE 2010, category Science
Prof. Dr. Ludwig Schultz	Thornton Medal (incl. Clerk Maxwell Award), The Institute of Materials, Minerals & Mining (IOM3)
Prof. Dr. Ludwig Schultz	Ehrennadel der Deutschen Physikalischen Gesellschaft
Dr. h. c. Rolf Pfrengle	Memorial Eurocoin Aurel Stodola TU Bratislava
IFW Dresden	"Baupreis Plauen 2010" for the high pressure depot for liquid Helium

Publication and poster awards

Ferdinand Lipps	Nature publishing group prize for best student poster, 6th International Conference on Quantum Dots, Nottingham, UK, 26-30 April 2010
Johannes D. Plumhof	Quantum Dot 2010 Runner up Poster Prize, 6th International Conference on Quantum Dots, Nottingham, UK, 26-30 April 2010
Varvara Efimova	Best presentation award – second price, International Glow Discharge Spectroscopy Symposium, 22.-27.08.2010, Albi
Fatemeh A. Javid	Best Poster Award, ISMANAM 2010, 17th International Symposium on Metastable, Amorphous and Nanostructured Materials, 4.-9. Juli, Zürich

IFW Awards

Dr. Annett Gebert	IFW Research Award 2010
Dr. Simon Pauly	Deutsche Bank Junior Award 2010 for the best PhD thesis
Dr. Hans-Joachim Grafe	IFF Research Award 2010
Dr. Bernd Rellinghaus	IMW Research Award 2010
Prof. Dr. Mariana Calin	IKM Research Award 2010
Dr. Carlos Cesar Bof Bufon	IIN Research Award 2010

Scientific conferences and IFW colloquia 2010

Conferences

Symposium on Low-dimensional Magnetism and Multi-band Superconductivity	Dresden, Germany May 6 – 7, 2010 Chairperson: Dr. M. Richter (IFW Dresden)
Third annual IEEE Magnetics Society Summer School	IFW Dresden, Germany August 16 – 20, 2010 Chairperson: Dr. O. Gutfleisch (IFW Dresden)
Joint Meeting Ohio State University - IFW Dresden	IFW Dresden, Germany 23. – 25. August 2010 Chairperson: Prof. Dr. B. Büchner (IFW Dresden)
Workshop: Biomedical applications of functionalised carbon nanotubes	Dresden, Germany September 6 – 9, 2010 Chairperson: Dr. R. Klingeler (IFW Dresden)
126. Versammlung der Gesellschaft Deutscher Naturforscher und Ärzte	Dresden, Germany September 17 – 21, 2010 Chairperson: Prof. Dr. L. Schultz (IFW Dresden) 1200 Participants

IFW colloquia

Prof. Theo H. M. Rasing, Radboud University of Nijmegen, Controlling Magnetism by light, 14.01.2010

Prof. Hans Hilgenkamp, Univ. of Twente, Conductance and magnetic effects at interfaces between insulating perovskite oxides, 21.01.2010

Prof. Joel Mesot, PSI-Institute, Switzerland, Combined neutron and ARPES studies of cuprate superconductors: What have we learned? 28.1.2010

Prof. Jasper Knoester, Zernike Institute for Advanced Materials, Univ. of Groningen, Spectroscopy of complex molecular systems: Physics on an exciton cake-walk, 4.2.2010

Prof. Horst Biermann, TU Bergakademie Freiberg, TRIP-Matrix-Composite - neue Hochleistungs-Verbundwerkstoffe, 25.2.2010

Prof. Paul M. Koenraad, Eindhoven Univ. of Technology, Semiconductor nanostructure formation and doping studied at the atomic scale by cross-sectional scanning tunneling microscopy, 15.4.2010

Prof. Hidenori Takagi, Univ. of Tokyo, Japan Phase Sensitive Imaging of Complex Electrons in High Temperature Superconductors, 22.4.2010

Prof. David J. Singh, Oak Ridge National Laboratory Electronic Structure, Chemistry and Physical Properties of Iron-Based Superconductors, 6.5.2010

Prof. Dr. Gustaaf van Tendeloo, Univ, of Antwerp, EMAT research group Advanced electron microscopy and applications to inorganic materials, 20.5.2010

Prof. Markus Braden, Univ. Köln, Itinerant magnetism in layered ruthenates, 27.5.2010

Prof. Peter Fratzl, MPI of Colloids and Interfaces Biological materials with mechanical function, 3.6.2010

Prof. David Cahen, Weizmann Institute of Science, Israel, Towards Molecular Modulation of Electronic Devices, 10.6.2010

Prof. Gunther Eggeler, Ruhr-Univ. Bochum, Gitterdefekte, Mikrostrukturen und Phasenumwandlungen in NiTi-Formgedächtnislegierungen, 1.7.2010

Prof. Achim Rosch, Univ, zu Köln, Ultracold fermions in optical lattices: Mott transitions and non-equilibrium states, 15.7.2010

Prof. Thomas Palstra, Zernike Institute for Advanced Materials, Univ, of Groningen Multiferroic Behavior in Transition-Metal and Hybrid Systems, 28.10.2010

Prof. Alberto Morpurgo, Univ. of Geneva, Organic single-crystal field-effect transistors, 04.11.2010

Prof. Dieter Weiss, Univ, Regensburg, Semiconductor Spintronics, 11.11.2010

Prof. Jan Zaanen, Univ. Leiden, Quantum criticality, high Tc superconductivity and the AdS/CFT correspondence of string theory, 16.12.2010

IFW Winterschool on superconductivity in Oberwiesenthal, Jan. 10-13, 2010

Honorary colloquium on the occasion of the 70th birthday of Prof. Klaus Wetzig, Oct. 7, 2010

Opening of the IFW Colloquium in the winter terms with talks of the prize winners of the Research Awards 2010 of the IFW's Institutes, Oct. 14, 2010

Guests and Scholarships

Guest scientists (stay of 4 weeks and more)

Name	Home Institute	Home country
Azar Aliabadi	Sharif Univ. of Technology	Iran
Luuk Ament	Leiden Univ.	Netherlands
Dr. Mircea-Odin Apostu	Cuza Univ.Tazi	Rumania
Prof. Dr. Victor Aristov	Institute of Solid State Physics, Moscow	Russia
Prof. Dr. Ernest Arusanov	Institute for applied physics Kishiniew	Rep. Moldavia
Artur Ascherov	Moldova State Univ.	Rep. Moldavia
Bassem Assfour	TU Dresden	Syria
Dr. Alicja Bachmatiuk	Szczecin Univ. of Technology	Poland
Dr. Seung Ho Baek	Los Alamos Laboratory	South Korea
Dr. Nilam S. Barekar	Indian Institute of Technology Kharagpur	India
Dr. Maria Bendova	TU Wien	Slovakia
Valentina Bisogni	Politecnico di Milano	Italy
Dr. Cordula Braun	TU Dresden	Germany
Dr. Pedro M. F.J. da Costa	CICEDO-Univ. of Averio	Portugal
Dr. Alexander Darinskiy	Institute for Crystallography Moscow	Russia
Martina C. Dekker	Leiden Univ.	Netherlads
Dr. Fei Ding	MPI Stuttgart	China
Hryhoriy Dmytriv	Lviv National Univ.	Ukraine
Dr. Roger Domenech Ferrer	Univ. Autonoma de Barcelona	Spain
Dr. Sesegma Dorzhieva	Baikal Institute of Nature Management	Russia
Prof. Dr. Ilgiz Garifullin	Zavoisky Phys.-Techn. Institute Kazan	Russia
Florian German	Daimler AG Stuttgart	Germany
Dr. Romain Giraud	CNRS, Lab. de Photoique et de Nanostructures	France
Dr. Luminita Harnagea	Univ. Paris	Rumania
Dr. Oleg Heczko	Institute of Physics, Prague	Czech Rep.
Alexanne Holcombe	Ohio State Univ., Columbus	USA
Felix Jasenek	Univ. Stuttgart	Germany
Dr. Steven Johnston	Lorentz-Institute, Leiden Univ.	Canada
Dr. Martin Kalbac	Heyrovski Institute of Physical Chemistry Prague	Czech Rep.
Dr. Olga Kataeva	Arbuzov Inst. of Organic and Physical Chemistry Kazan	Russia
Prof. Dr. Konstantin Kikoin	School of Physics and Astronomy, Tel-Aviv Univ.	Russia
Dr. Xianghua Kong	Institute of Chemisty, Peking	China
Natalia Kuratyeva	Nikolaev Inst. of Inorganic Chemistry, Novosibirsk	Russia
Dr. Roman Kuzian	Institute for Materials Sc. Kiew	Ukraine
Dr. Min Ha Lee	Iowa State Univ., USA	South Korea
Caiju Li Kunming	Univ. of Science and Technology	China
Ran Li Bejing	Univ. of Aeronautics and Astronautics	China
Angela Llavona	Univ. Complutense de Madrid	Spain
Dr. Libo Ma	Shandong Normal Univ. Jinan	China
Dr. Jiri Malek	Univ. Prague	Czech Rep.
Dr. Daria Mikhailova	TU Darmstadt	Russia
Dr. Hector Mireles	California State Polytechemei Univ.	USA
Dr. Igor Morozov	Lomonosov Univ. Moscow	Russia
Narendirakumar Narayanan	TU Darmstadt	Germany
Denis Nica	Moldova State Univ.	Rep. Moldavia
Dr. Kristian Nikolowski	TU Darmstadt	Germany
Dr. Satoshi Nishimoto	MPI PKS Dresden	Japan
Dr. Jin Man Park	Yonsei Univ. Seoul	South Korea

Oleksiy Perevertov	Institute of Physics, ASCR, Prague	Ukraine
Dr. Fabio Pezzoli	Universita Di Milano-Bicocca	Italy
Katja Pinkert	TU Dresden	Germany
Dr. Ashim Kumar Pramanik	UGC-DAE Consortiu, Univ. Indore	India
Carine Rongeat	INRS Université du Québec, Canada	France
Dr. Vanishri Saligrama	Indian Institute of Science	India
Maria Grazia Salvaggio	Univ. of Messina	Italy
Wenping Si	TU Chemnitz	China
Dr. Surjeet Singh	Univ. de Paris-Sud	India
Sung Woo Sohn	Yonsei Univ. Seoul	South Korea
Dr. Liudmila Syurakshina	LIT JINR, Moscow	Russia
Arthur Westphal Taylor	TU Dresden	Brazil
Dr. Rinaldo Trotta	Univ. Rom	Italy
Chih-Yen Tseng	National Univ. of Tainan	China
Dr. Thomas Vad	TU Dresden & HASYLAB DESY Hamburg	Germany
Oleksii Vakaliuk	Institute for Metal Physics NASU	Ukraine
Prof. Alexander Vasiliev	Moscow State Univ.	Russia
Dr. Evgeniya Vavilova	Physical Technical Institute Kazan	Russia
Dr. Olga Volkova	Moscow State Univ.	Russia
Dr. Maxim Voronov	Univ. Greifswald	Russia
Dr. Guojiang Wan	Southwest Jiaotong Univ.	China
Dr. Wang Xi	Univ. of Oxford	China
Masao Yamazaki	Aichi Steel Cooperation	Japan
Liping Yang	FOM, Lorentz-Institute, Leiden Univ.	China
Dr. Shangfeng Yang	Univ. of Science and Technology of China	China
Dr. Victor Yushankhai	Laboratory Theoretical Physics Russia	Russia
Dr. Galina Zakharova	Institute of Solid State Chemistry Yekaterinburg	Russia
Yue Zhang	TU Darmstadt	China
Prof. Dr. Zhe-Feng Zhang	Institute of Metal Research Shenyang	China
Dr. Honglou Zhen	Institute of Metal Research Shenyang	China

Scholarships

Name	Home country	Donor
Dr. Qiang Luo	China	Alexander von Humboldt-Stiftung
Dr. Yuri Naidyuk	Ukraine	Alexander von Humboldt-Stiftung
Dr. Hengxing Ji	China	Alexander von Humboldt-Stiftung
Dr. Surendran K. Peethambharan	India	Alexander von Humboldt-Stiftung
Dr. Guillaume Manilal Lang	France	Alexander von Humboldt-Stiftung
Dr. Daoyong Cong	China	Alexander von Humboldt-Stiftung
Dr. Alexey Popov	Russia	Alexander von Humboldt-Stiftung
Dr. Teng Qiu	China	Alexander von Humboldt-Stiftung
James B. Whitaker	USA	Alexander von Humboldt-Stiftung
Dr. Krzysztof Wohlfeld	Poland	Alexander von Humboldt-Stiftung
Dr. Peter Rapta	Slovakia	Alexander von Humboldt-Stiftung
Dr. Gang Wang	China	Alexander von Humboldt-Stiftung
Sami A. Mahmoud Makharza	Palestine	DAAD
Maria Dimitrakopoulou	Greece	DAAD
Dr. Sesegma Dorzhieva	Russia	DAAD
Anil Kumar Chaubey	India	DAAD
Fedor Fedorov	Russia	DAAD
Hyo Yun Jung	South Korea	DAAD

Roman Rezaev	Russia	DAAD
Santosh Kumar Pal	India	DAAD
Kumar Babu Surreddi	India	DAAD
Cristiano da Silva Teixeira	Brazil	Erasmus Mundus External Cooperation
Dr. Saisamorn Niyomsoan	Thailand	Erasmus Mundus External Cooperation
Karolina Wyszynska	Poland	Erasmus Mundus External Cooperation
Anna Efimenko	Russia	Erasmus Mundus FAME
Claudia Patschureck	Germany	Studienstiftung des deutschen Volkes
Marietta Seifert	Germany	Studienstiftung des deutschen Volkes
Maria Sparing	Germany	Studienstiftung des deutschen Volkes
Silvia Vock	Germany	Cusanuswerk
Dr. Simon Pauly	Germany	Cusanuswerk
Franziska Thoss	Germany	Deutsche Bundesstiftung Umwelt
Grzegorz Parzych	Poland	ECEMP Internat. Graduiertenschule
Alexey Alfonsov	Russia	Int. Max Planck Research School
Anupama Parameswaran	India	Int. Max Planck Research School
Shasha Zhang	China	Int. Max-Planck Research School
Martin Philipp	Germany	Saint-Gobain Recherche Frankreich
Peng Li	China	China Scholarship Council / DAAD
Shilong Li	China	China Scholarship Council
Jun Tan	China	China Scholarship Council
Kaikai Song	China	China Scholarship Council
Yiku Xu	China	China Scholarship Council
Yang Zhang	China	China Scholarship Council
Na Zheng	China	China Scholarship Council
Jun-Wie Cui	China	China Scholarship Council
Lin Zhang	China	China Scholarship Council
Zhi Wang	China	China Scholarship Council
Ruitao Qu	China	China Scholarship Council
Dr. Chien-Hung Lin	Taiwan	National Science Council Taiwan
Fahad Ali	Pakistan	PIEAS Islamabad
Ahmed A. Mahmoud Elgendy	Egypt	Egypt Government
Mahmoud Abdel-Hafez Mohamed	Egypt	Egypt Government
Abdelwahab Hamdy Hassan	Egypt	Egypt Government
Dr. Alexander Grüneis	Austria	APART Austria
Cristina Liliana Iordache	Rumania	Rumania SOPHRD

Guest stays of IFW members at other institutes

Dr. Kathrin Dörr	Oak Ridge National Laboratory, Tennessee, USA, May and Oct./Nov. 2010, CNMS user project on ferroelectric switching
Christian Stieler	Niigata Univ., Japan, Feb./March 2010, Guest scientist at the Faculty of Engineering
Christina Bran	Institute of Physics, Uppsala Univ., Sweden, March - May 2010, Guest scientist in the magnetic force microscopy laboratory
Kristina Tschulik	Univ. of Virginia, Charlottesville, USA, May – July 2010, Guest scientist at the Faculty Materials Science and Engineering
Dr. Rudolf Schäfer	Simon Fraser Univ., Burnaby, Canada, July – Aug. 2010, Guest scientist in the Kerr microscopy laboratory
Phillip Grohmann	Institute of Physics, Uppsala Univ., Sweden, Oct./Nov. 2010, Preparation and magnetic measurements on magnetic particles
Arnulf Möbius	Univ. of California, Santa Barbara, USA, Aug. – Oct. 2010, participation in the guest program „Electron glasses“
Thomas Kroll	The Solomon Laboratory, Stanford Univ. Stanford, USA, Oct.-Dec. 2010, research cooperation
Claudia Nacke	Univ. Paris-Sued Paris, France, Oct.-Nov. 2010, research cooperation
Sven Partzsch	Brookhaven National Laboratory New York, USA, May-Nov. 2010 research cooperation
Ronny Schönfelder	Centro de Investigacion Cientifica de Yucatan Merida, Mexico, Sept. 2010 – July 2011
Roman Schuster	Univ. de Fribourg, Switzerland, May – Sept. 2010, measurement stay
Laura Steller	Univ. of Crete und IMBB (Institute of Molecular Biology & Biotechnology), Forth Heraklion, Crete, Greece, March-May 2010, research cooperation
Andreas Winkler	Micro/Nanophysics Research Laboratory (MNRL) of the Monash Univ. Melbourne, Australia, Oct. 2010 – Jan. 2011 research cooperation
Katarzyna Werniewicz	Univ. di Torino, Dept. of Chemistry, Italy, Feb./March 2010, DAAD financed stay on Ti-based amorphous alloys
Na Zheng	Institute of Metal Research, Chinese Academy of Sciences (IMR CAS), Shenyang, China Sept./Oct. 2010, DAAD financed research cooperation on metallic glasses
Jin Young Kim	Korea Institute for Rare Metals, Korea Institute of Industrial Technology, Incheon/Korea, Nov. 2010 – Feb. 2011, research cooperation on porous materials
Uwe Gaitzsch	Boise State Univ., Idaho, USA, Oct. 2010 – Feb. 2011 DAAD financed stay on magnetic shape memory alloys

Board of trustees

Joachim Linek, Saxonian Ministry of Science and Art - Head -
Dr. Herbert Zeisel, Federal Ministry of Education and Research
Prof. Dr. Bernd Kieback, TU Dresden
Prof. Dr. Konrad Samwer, Univ. Göttingen

Scientific Advisory Board

Prof. Dr. Reiner Kirchheim, Univ. Göttingen, Germany - Head -
Prof. Dr. Dominique Givord, Laboratoire Louis Néel, Grenoble, France
Prof. Dr. Alan Lindsay Greer, Univ. of Cambridge, U.K.
Prof. Dr. Rudolf Gross, Walter Meißner Institute Garching, Germany
Prof. Dr. Rolf Hellinger, Siemens AG Erlangen, Germany
Prof. Dr. Max Lagally, Univ. of Wisconsin-Madison, U.S.A.
Prof. Dr. Xavier Obradors Berenguer Univ. Autònoma de Barcelona, Spain
Prof. Dr. Stuart Parkin, IBM Almaden Research Center, San Jose, USA
Prof. Dr. Eberhardt Umbach, Karlsruhe Institute of Technology, Germany
Prof. Dr. Gertrud Zwicknagl, TU Braunschweig, Germany

IFW's Research Program 2011

1. Superconductivity and superconductors
1.1 Electronic structure and fundamentals
1.2 Superconducting materials
1 P1 Superconducting transport systems and magnetic bearings
1 P2 YBCO tape conductors
1 P3 Nanoscaled inhomogeneities in superconductors (Pakt 2009)

2. Magnetism and magnetic materials
2.1 Theoretical and experimental fundamentals
2.2 Magnetic materials
2.3 Magnetic microstructures
2.4 Phase equilibria and single crystal growth
2 P1 Pulsed high magnetic fields
2 P2 Magnetic shape memory alloys
2 P3 Energy efficient cooling with magnetocaloric materials (Pakt 2010)

3. Molecular nanostructures and molecular solids
3.1 Nanotubes and fullerenes
3.2 Conducting polymers and organic molecular solids
3.3 Molecular Magnets
3 P1 Manipulation of nanoscaled magnets (Pakt 2007)

4. Metastable alloys
4.1 Solidification and crystallization
4.2 Corrosion and hydrogen
4.3 Bulk amorphous metals and composite materials
4.4 Lithium-ion batteries
4 P1 Cluster materials with competing properties (Pakt 2008)

5. Stress-driven architectures and phenomena
5.1 3D micro/nanoarchitectures
5.2 Quantum dots
5.3 Ferroic oxid films
5.4 SAW systems